Spring 1-1-2014

Use of Fluorescence Spectroscopy to Characterize Dissolved Organic Matter

Julie Ann Korak
University of Colorado at Boulder, julie.korak@colorado.edu

Use of Fluorescence Spectroscopy to Characterize Dissolved Organic Matter

by

Julie Ann Korak
B.S. Chemical Engineering, University of Colorado at Boulder, 2009
B.S. Environmental Engineering, University of Colorado at Boulder, 2009
M.S. Civil Engineering, University of Colorado at Boulder, 2013

A thesis submitted to the
Faculty of the Graduate School of the
University of Colorado in partial fulfillment
of the requirements for the degree of
Doctor of Philosophy
Department of Civil, Environmental and Architectural Engineering
2014

This thesis entitled:
Use of Fluorescence Spectroscopy to Characterize Dissolved Organic Matter

written by Julie A. Korak
has been approved for the
Department of Civil, Environmental and Architectural Engineering

Fernando Rosario-Ortiz (chair)

R. Scott Summers

Diane M. McKnight

Karl Linden

Date:

The final copy of this thesis has been examined by the signatories, and we find that both the content and the form meet acceptable presentation standards of scholarly work in the above mentioned discipline.

ABSTRACT

Korak, Julie Ann (PhD, Civil Engineering)

Use of fluorescence spectroscopy to characterize dissolved organic matter

Thesis directed by Assistant Professor Fernando L. Rosario-Ortiz

Dissolved organic matter (DOM) is a heterogeneous mixture of organic molecules derived from a variety of sources (plant and microbial) and is ubiquitous to all natural water sources. DOM removal is a core treatment objective for water treatment plants to prevent the formation of disinfection byproducts (DBPs). Due to its complex nature, current understanding of DOM and its effects on drinking water quality relies on bulk characterization methods, such as fluorescence spectroscopy. Fluorescence measures a fraction of DOM that is optically active and has the potential to absorb and reemit light. This thesis investigated how the optical properties of DOM can be used to understand and monitor drinking water treatment processes.

After a critical analysis of commonly-used fluorescence metrics, the use of fluorescence to characterize DOM removal by coagulation was investigated. Coagulation of DOM isolates demonstrated the advantages and disadvantages of following different fluorescence metrics. The results provided evidence that the association of different peak regions (A and C) with distinct DOM fractions (humic and fulvic acids) is unsupported. The study was then extended to cover 22 different waters with diverse water quality characteristics. Robust, universal relationships were developed between optical surrogates and DOM removal. Both UV absorbance and fluorescence intensities (Peaks A and C) were found to perform equally as DOM surrogates when compared on a relative basis. In contrast, specific UV absorbance (SUVA) was a better

predictor of DBP yields than fluorescence compositional metrics. These differences were attributed to heterogeneity amongst non-fluorescing moieties.

Finally, fluorescence was evaluated as a potential surrogate for metabolite (e.g. Microcystin-LR, MIB and geosmin) release from cyanobacteria cells during oxidation processes within a treatment plant. Characterization of intracellular organic matter (IOM) isolates determined that IOM has a unique fluorescence signature compared to DOM, but it also shows compositional differences between species. Parallel Factor Analysis (PARAFAC) identified compositional difference in phycobiliproteins between species. Cell oxidation studies found that fluorescence index (FI) and FDOM intensity (Ex 370 nm, Em 460 nm) better capture the loss of viable cells and release of metabolites compared to absorbance and are promising monitoring tools for utilities.

DEDICATION

To those who taught me to love, respect and strive to understand nature

ACKNOWLEDGEMENTS

Pursuing a doctorate degree is not an individual endeavor but one that requires support from many people on different levels. I have been very fortunate to have two great advisors (Fernando Rosario-Ortiz and Scott Summers) who have pushed me to be the best researcher I can be and to never shy away from the tough problems. I may have never embarked on this journey if it was not for Scott's receptiveness and flexibility when I randomly stopped by the department to inquire about graduate studies after a job interview on-campus. Since that fateful afternoon, I have had more opportunities than I could have imagined at the outset. Fernando and Scott have given me the opportunity to work on many different projects, even ones that seem a bit off the wall. They have also taught me to balance the engineering and chemist perspectives in environmental research. I thank Fernando for supporting me to attend national and local conferences to present work and meet others in the field. I am also grateful for the opportunities he has given me to teach classes and the encouragement to pursue teaching and professional development opportunities.

I am thankful for the members of my committee (Diane McKnight, Karl Linden, Aaron Dotson and Eric Dickenson) who willingly gave their time and energy to provide constructive feedback and encouragement.

Thanks to National Science Foundation, who funded my studies through the Graduate Research Fellowship Program, I had the flexibility to research a number of diverse topics related to natural organic matter. That opportunity, however, would not have been possible without the support of Aaron Dotson, who helped me develop the proposal and taught me about fluorescence methods before ever having the opportunity to touch a spectrofluorometer.

I would not have learned to love research if it were not for the other graduate students. I came into the lab with very little research experience and many apprehensions. From my first day, I could not ask for a better mentor than Tom Zearley, who had the patience and enthusiasm to teach me everything from how to use a pipet to how to run a pilot-scale reverse-osmosis system. I have to thank the entire Summers' lab that first summer (Anthony Kennedy, Janet Cardenas, Chris Corwin Josh Kearns and Dorothy Noble) for welcoming me into the lab and making it such a positive learning experience. It gave me the confidence and enthusiasm to embrace the next four years. As the next generation of Summers' students moved into the offices, I am ever grateful for the positive energy and light-heartedness that filled the space deep in the bowels of the engineering center, where there are no windows and lots of fluorescent lighting. I thank Dorothy Noble, Dave Kempisty, Eli Townsend, Anthony Kennedy, Kyle Shimabuku, Tyler Dougherty and Leigh Gilmore for the good conversation and team atmosphere.

As my research transitioned towards the Rosario-Ortiz lab group, I had the fortunate experience of learning from many people along the way. Mei Mei (Vivy) Dong taught me to roll up my sleeves, learn the mechanics of every instrument I use and be able to troubleshoot them effectively. I am grateful to Mandi Hohner, Kate Dowdell, Dorothy Noble and Jennifer Moutinho for their contributions to the coagulation project (Chapter 5). I thank Simón Mostafa, Kyle Shimabuku and Caitlin Glover for teaching me all about ultrafiltration and other aspects of photochemistry, even though it did include filtering 80 L of wastewater effluent, 500 mL at a time. Finally, I thank Eric Wert and Fernando for bringing me on board for the cyanobacteria project and the Water Research Foundation for funding the work to give me the opportunity to expand my horizons.

Outside the lab, I am thankful for the unconditional love and support that my family has given me. My parents (Greg and Carol Korak) have pushed me to follow my dreams and explore the world. They have always been positive role models in my life and have taught me the importance of balancing work and play. I have the best sister (Kathryn) in the entire world. Even from afar, she always finds the time to reach out, and her drive to chase her own goals inspires me. I thank my Colorado parents (Joe Villa and Debby Blair) for taking me in as one of their own and giving me more love and support than I deserve. Last but not least, I thank the love of my life, Jacob Villa, for being by my side every step of the way. He was the one who encouraged me to stop by the department to inquire about graduate school. Somehow, he knew where I was headed before I even knew myself. He is my rock who has stood by me through all the ups and downs of graduate school and helps me keep it all in perspective.

TABLE OF CONTENTS

LIST OF TABLES

LIST OF FIGURES

Chapter 1 Introduction

1.1 Motivation

Dissolved organic matter (DOM) has been an active area of research since at least the 1950s with the study of yellow organic acids (Shapiro, 1957). Since then, researchers have strived to understand the complex role that it plays in natural and engineered systems. DOM is a heterogeneous mixture of organic molecules that are derived from a number of sources within the environment and that vary in composition both spatially and temporally. In most environments, DOM is a mixture of allochthonous material derived from degraded plants (i.e. lignin, cellulose etc.) and autochthonous material derived from microbial processes (Steinberg, 2003). Aside from varying source materials, DOM in any given water body is continually being transformed through environmental processes, such as photochemical reactions, microbial activity and DOM fluxes from other sources. As a result, DOM cannot be characterized to any level of detail, such as molecular structure modeling.

DOM plays a significant role in the global carbon cycle, particularly for carbon fluxes from continents to oceans (Perdue, 2009). Its concentration and composition control the fate and transport of contaminants, such as metals and organic compounds (e.g. pesticides, chlorinated solvents) (Chiou et al., 1986; Reuter and Perdue, 1977). When a normally insoluble compound sorbs to DOM, it becomes soluble as a complex and has the ability to be transported and affect the health of end users. The unique chemical sub-structures within DOM, particularly quinone-like moieties, give DOM the ability to mediate oxidation-reduction reactions within the environment that would not normally occur in its absence (Dunnivant and Schwarzenbach, 1992). DOM also controls photochemical reactions within a water source by either acting as a source or

sink for reactive species (Mostafa et al., 2014; Sharpless, 2012). In other words, DOM plays a critical role in all ecosystems.

From an engineering perspective, DOM removal is desirable, because it improves the efficiency of engineered systems, improves water aesthetics and protects human health. Early research within the drinking water field strived to remove DOM from drinking water to remove the colored material and improve aesthetics (Hall and Packham, 1965). Removing DOM through coagulation prior to filtration also improved the efficiency of filter beds, requiring back flushing less often. In the 1970s, landmark studies discovered that chlorinating DOM generates trihalomethanes, a class of disinfection byproducts (DBPs) (Rook, 1977; Rook, 1976). Since then, over 600 different DBP compounds have been identified (Richardson, 2012). Currently, two different DBP classes, trihalomethanes and haloacetic acids, are regulated by the USEPA through the Stage 1 and Stage 2 Disinfection Byproduct Rules (USEPA, 2006). The more that is learned about DOM, the more questions that have yet to be answered.

To better understand the relationships between DOM and processes of interest, many characterization tools have been developed (Leenheer, 2009). Some methods fractionate the heterogeneous mixture based on hydrophobicity (e.g. XAD), size (e.g. ultrafiltration, SEC, field flow fractionation) or polarity (e.g. PRAM). Others measure bulk characteristics of DOM. Examples include its optical properties (e.g. absorbance and fluorescence), bulk chemical characteristics (e.g. ^{13}C NMR, elemental analysis, and mass spectroscopy), acidic functional groups, and its ability to form reactive species (e.g. hydroxyl radical, triplet states and singlet oxygen). Each method characterizes DOM based on specific chemical properties, and no single method can provide a complete characterization. Some methods are more sample- and time-intensive than others.

Recently, fluorescence has gained particular attention, because it is neither sample volume nor time intensive. Unlike many other characterization methods, fluorescence also has the potential to be incorporated into rapid or real-time monitoring programs at water utilities or deployed as probes in source waters. Water managers are constantly faced with the challenge of understanding and adapting to changing source water quality. Changes may occur gradually, such as DOC increases in a water source (Beggs et al., 2013) and vegetation changes due to invasive species (Beggs and Summers, 2011), or they may occur rapidly in the case of cyanobacteria proliferation (Zamyadi et al., 2013) and wildfires (González-Pérez et al., 2004). Developing readily accessible absorbance and fluorescence based tools for characterizing these dynamic processes would be a valuable tool for anyone responsible for managing water sources and delivering safe drinking water to consumers.

1.2 Research Objectives

The overarching goal is to develop methods using fluorescence to better understand and predict DOM behavior in engineered systems. This thesis considers two specific applications. The first is the removal of DOM by coagulation. The second is the release of organic matter from cyanobacteria cells in a water treatment plant. Throughout these projects, I have tried to approach these problems from the perspectives of both an engineer and an environmental chemist. As an engineer, the overarching question to answer is, "How can fluorescence be used to design, monitor and control drinking water processes? Does fluorescence offer advantages over more traditional UV measurements?" From the perspective of an environmental chemist, the question is, "What can studying DOM fluorescence within engineered systems reveal about its fundamental behavior, composition and photophysics?" More specific objectives are the following:

1) Evaluate the contemporary methods of fluorescence data analysis in order to strategically analyze and provide interpretations of observed fluorescence behaviors
2) Investigate the use of fluorescence as an optical surrogate for DOM and DBP precursor removal by coagulation
    a. Determine the advantages and disadvantages of fluorescence tools compared to UV absorbance.
    b. Compare the utility of fluorescence- and absorbance-based measurements to predict DOM reactivity, as quantified by disinfection byproduct formation
3) Evaluate the viability of employing fluorescence as a monitoring tool to detect the release of cyanobacteria intracellular organic matter (IOM) during preoxidation processes
    a. Characterize the optical properties of isolated IOM and determine the feasibility of detecting its optical indicators after release into a water source
    b. Evaluate if the identified IOM fluorescence characteristics are viable surrogates for IOM and metabolite release during bench-scale oxidation of cyanobacteria cells

1.3 Dissertation Organization

The dissertation has five main chapters, and each is written as a stand-alone publication. A few chapters have already been published; citations are provided at the beginning of each chapter. Chapter 2 provides an overview of the instrumentation and data processing for fluorescence analysis. Chapter 3 includes a critical analysis of contemporary fluorescence data analysis methods. Chapters 4 and 5 both cover the use of fluorescence for DOM removal by coagulation. Chapter 4 investigates the fluorescence response during the coagulation of DOM isolates (humic and fulvic acids). Chapter 5 compares absorbance and fluorescence as a surrogate for DOM removal and DBP formation across diverse water sources. Chapters 6 and 7 evaluate

fluorescence for the purpose of detecting organic matter release during cyanobacteria blooms in source waters. Chapter 6 characterizes the fluorescence signatures of isolated intracellular organic matter, and Chapter 7 evaluates the suitability of using fluorescence as a surrogate for metabolite release during simulated cell oxidation experiments. Conclusions and future work are provided in Chapter 8. There are three appendices with supplemental information for select chapters.

Chapter 2 Fluorescence Spectroscopy

2.1 Introduction

This chapter provides an overview of the fluorescence phenomenon from both a qualitative and quantitative perspective. The objective is to synthesize relevant information that is currently scattered among the literature yet is important for quantitative fluorescence analysis. An overview of photophysical mechanisms (i.e., absorption and fluorescence) is provided including quantitative theory. Two sections are devoted to instrumentation and describe key spectrofluorometer components and how method parameters impact quantitative analysis. Instrument-specific information is provided for a John Yvon Horiba Fluormax-4 (F4) instrument, which was used exclusively for the original research presented in latter chapters. The final section provides an overview of spectral correction procedures including the derivation for primary and secondary inner filter effects. A comparison of Raman normalization procedures is also provided to determine any systematic biases between contemporary normalization methods.

2.2 Fluorescence Fundamentals

Fluorescence is an optical phenomenon where molecules emit light. The wavelengths at which a molecule (or moiety within a larger molecule) absorbs and emits light is unique to the chemical structure (and its environmental conditions) and can be used as a characterization tool.

Before fluorescence can occur, an organic molecule must absorb energy (i.e., photons). To absorb energy, electrons are promoted from the ground state configuration to unoccupied antibonding orbitals (Figure 2.1). The energy required to promote an electron depends largely on the type of orbital and the presence of electron delocalization or conjugation. The absorption

wavelength represents the energy difference between the ground and excited states. Excitation of an electron in a σ bond has the largest energy gap and exhibits absorption in the far UV region (Valeur, 2002). A π bond occurs where molecules have a double bond. As the extent of π bond conjugation increases, electrons are delocalized, and the energy difference between ground and excited states decreases (increasing the wavelength of absorption). Non-bonding elections, n electrons, are lone pairs on atoms such as oxygen or nitrogen. The energy required to promote an n electron is generally less than σ or π bond electrons. The energy gap for the latter two transitions ($n \rightarrow \pi^*$ and $\pi \rightarrow \pi^*$) is smaller and occurs at longer wavelengths (Valeur, 2002). In the region where dissolved organic matter (DOM) is typically characterized (UV and visible), the important transitions are the promotion of π and n electrons.

Once excited, a molecule can undergo several processes, one of which yields fluorescence (Figure 2.1). Within each electronic state, several vibrational energy levels exist. A molecule first undergoes vibrational relaxation (v_r) to the lowest vibrational level of the excited state (S_1) (Kasha, 1950). From that point, fluorescence can occur releasing a photon (i.e., light) with the same energy as the energy gap between electronic states (S_1-S_0). Fluorescence always occurs at emission wavelengths longer than the absorption wavelength (Stokes Shift) due to the energy lost during vibrational relaxation. Relaxation back to the ground state can also occur through a non-radiative mechanism called internal conversion (IC). Finally, an excited electron can undergo intersystem crossing (ISC) to a triplet state (T_1), where the multiplicity (or electron spin) changes. While this process involves a forbidden transition, the efficiency of this process is greater for $n \rightarrow \pi^*$ transitions and when heavy atoms, such as halides, are present (Valeur, 2002). From a triplet state, relaxation can occur through radiative (i.e., phosphorescence) or non-radiative (i.e., IC) processes (Figure 2.1).

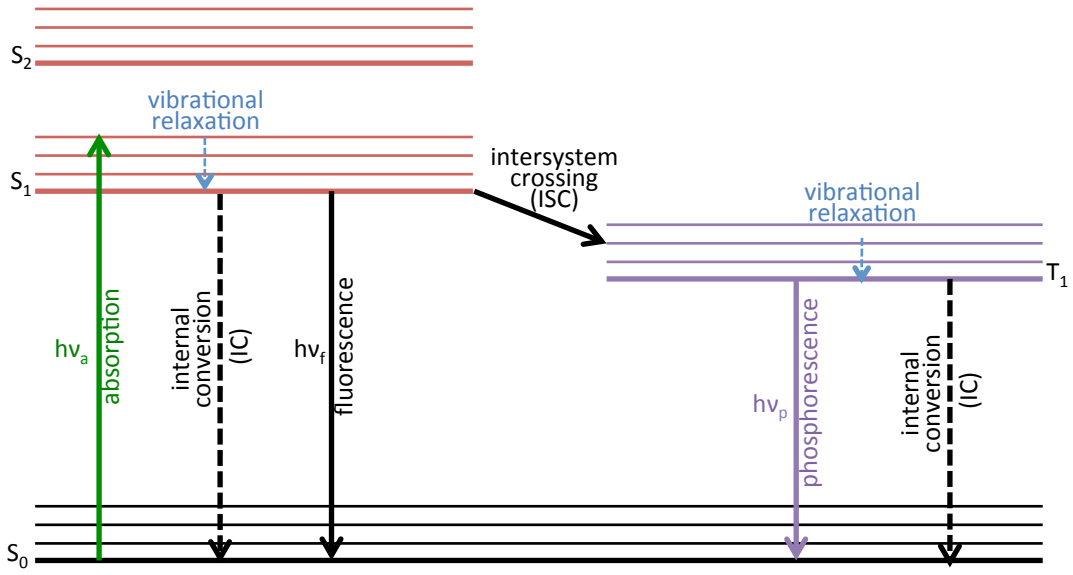

Figure 2.1 Jablonski Diagram depicting absorption, fluorescence and phosphorescence

2.2.1 Quantitative Theory of Light Absorption

Beer-Lambert law is the fundamental relationship that describes how light intensity decreases as a function of distance across a sample cell. Eqns 1 through 6 derive the Beer-Lambert relationship yielding a general equation for light intensity at any distance (x) in a sample. The local intensity at any point depends on the initial intensity (I_0), the extinction coefficient (a property of the chromophores) and the concentration of the chromophores. To simplify the math in the following steps, the variable α, representing the product of extinction coefficient and concentration, is used throughout. It is important to note that α quantifies all chromophores, even if only a subset actually fluoresces. Eqn 6 shows that intensity decays exponentially with distance.

$$dI = -I\alpha dx \qquad (1)$$

$$\frac{dI}{I} = -\alpha dx \qquad (2)$$

I_0: Initial intensity entering cell
I_x: Intensity at position x in cell
I: Intensity
x: distance from incident edge

$$\int_{I_0}^{I_x} \frac{dI}{I} = -\alpha \int_0^x dx \quad (3)$$

$$ln\frac{I_x}{I_0} = -\alpha x \quad (4)$$

$$\frac{I_x}{I_0} = e^{-\alpha x} \quad (5)$$

$$I_x = I_0 e^{-\alpha x} \quad (6)$$

α = a c
a: Naperian extinction coefficient
c: Concentration

When the sample absorbance is measured in a spectrophotometer, the distance term in Eqn 6 becomes the pathlength of the sample cell. When the pathlength (d) is substituted into Eqn 5, it becomes Eqn 7. The quantity I_d/I_0 is equivalent to the sample transmittance (T) shown in Eqn 8. While absorbance is more commonly measured in the lab, the derivation for the inner filter corrections will utilize T to simplify the math before converting to absorbance at the end.

$$\frac{I_d}{I_0} = e^{-\alpha d} \quad (7)$$

T=Sample transmittance
d=cell pathlength

$$T = \frac{I_d}{I_0} \quad (8)$$

$$T = e^{-\alpha d} \quad (9)$$

$$lnT = -\alpha d \quad (10)$$

$$\frac{lnT}{d} = -\alpha \quad (11)$$

Rearranging Eqn 9 for α and substituting it into Eqn 4 yields Eqn 12. This equation represents the intensity of light at a distance x, based on the measured transmittance of the sample.

$$ln\left(\frac{I_x}{I_0}\right) = \frac{x}{d} * ln\,(T) \quad (12)$$

$$I_x = I_0 e^{\left(\frac{x}{d}\right) ln(T)} \quad (13)$$

$$I_x = I_0 T^{\frac{x}{d}} \quad (14)$$

The expression x/d represents the fractional distance with respect to the entire pathlength. A new variable, w, is defined to represent this quantity (Eqn 15). With this new variable, Eqn 14 simplifies to Eqn 16.

$$w = \frac{x}{d} \qquad (15)$$ w= fractional distance

$$I_w = I_0 T^w \qquad (16)$$

2.2.2 Quantitative Fluorescence Theory

This section derives the fundamental expression relating fluorescence intensity to system and sample parameters as published in various sources (Rendell, 1987; Valeur, 2002). Figure 2.2 depicts a simplified fluorescence schematic where light enters a sample cell at an initial intensity (I_1), a portion of the light is absorbed according to Beer-Lambert law and the exiting intensity (I_2) is less than I_1. The fluorescence intensity (F) is measured at a 90° angle relative to the excitation beam. The fluorescence intensity (F) depends on the intensity absorbed (I_a) and the quantum yield (Q) as dictated by Eqns 17 and 18. Photons absorbed are the difference between I_1 and I_2 leading to Eqn 19. The fraction in Eqn 19 is equivalent to the sample transmittance, which can be represented by the Beer-Lambert Law and Eqn 9.

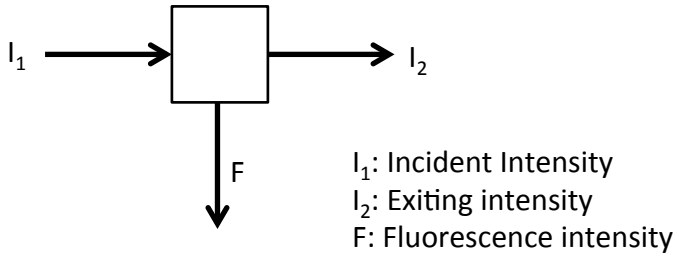

Figure 2.2 Simplified fluorescence schematic

$$F = QI_a \qquad (17)$$ F: Fluorescence intensity

$$Q = \frac{photons\ emitted}{photons\ absorbed} = \frac{F}{I_a} \qquad (18)$$ Q: Quantum yield

I_a: Intensity absorbed

$$F = Q(I_1 - I_2) = QI_1\left(1 - \frac{I_2}{I_1}\right) \quad (19)$$

$$F = QI_1(1 - e^{-\alpha d}) \quad (20)$$

Eqn 20 shows that the fluorescence intensity is not proportional to concentration due to the exponential term. When the exponential term is small, however, a linearizing approximation can be made. The exponential function can be approximated using the series expansion in Eqn 21. When the product (αd) is small, the higher order terms can be neglected. When the first two terms are substituted back into Eqn 20, the equation dictating fluorescence intensity simplifies to Eqn 23 and represents the case when fluorescence intensity is proportional to concentration. This linear approximation is useful for analytical and engineering applications, but it is only valid when the αd term is small.

$$e^{-\alpha cd} \approx 1 - \alpha d + \frac{(\alpha d)^2}{2} - \frac{(\alpha d)^3}{6} + \cdots \quad (21)$$

$$F = QI_1\big(1 - (1 - \alpha d)\big) \quad (22)$$

$$F = QI_1\alpha d \quad (23)$$

2.3 System Hardware Components

2.3.1 Lamp

Optical measurements require a light source to excite chromophores in dissolved organic matter. The light source in an F4 spectrofluorometer is an ozone-free 150 W Xenon arc lamp. This lamp emits light continuously, as opposed to pulsed lamps that are used for unsteady state and phosphorescence analyses. The lamp emits light across a wide range of wavelengths that can be selected to excite a sample. A lamp scan measures the lamp output at the reference detector as a function of wavelength. A characteristic of Xenon arc lamps is that they have a peak intensity

output at 467 nm, as shown in Figure 2.3. At higher and lower wavelengths, the lamp output is lower.

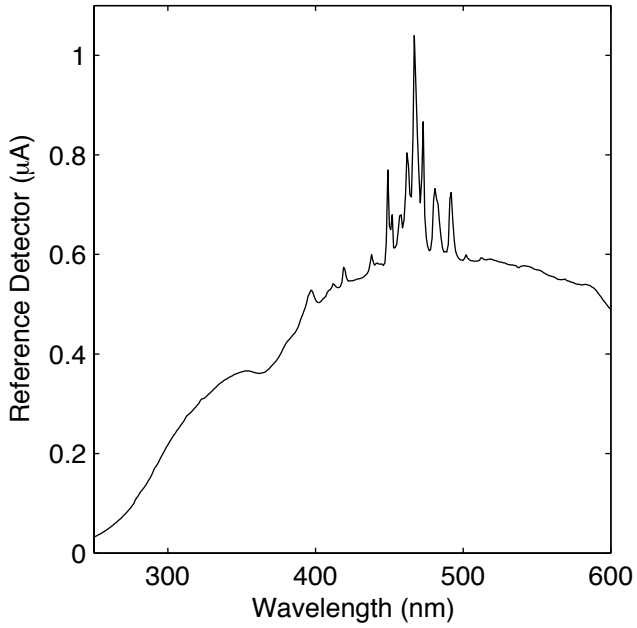

Figure 2.3 Lamp output as a function of wavelength

2.3.2 Monochromator

Monochromators are optical components that select specific wavelengths of light from a broad spectrum. Fluorometers have two monochromators to select excitation and emission wavelengths to analyze. One monochromator is located between the lamp and the sample to select one wavelength of light from the broad spectrum emitted by the lamp to pass into the sample. Another monochromator is located between the sample compartment and signal detector to select one wavelength from the spectrum emitted by the sample to analyze for intensity. Both monochromators in the F4 are Czerny-Turner monochromators that are designed to maintain good resolution over the spectral range.

Each monochromator has two key subcomponents that affect the fluorescence analysis of DOM samples. Gratings are grooved surfaces that diffract a spectrum of incident light. Both

excitation and emission monochromators in an F4 have 1200 grooves mm^{-1}. Eqn 24 defines the relationship between the wavelength of light and the angle at which it is diffracted. By rotating the grating, specific wavelengths are allowed to be collimated by the concave mirror and passed through the monochromator. While the gratings can be rotated to select different wavelengths, they are etched (or blazed) to produce the maximum reflection efficiency at specific wavelengths. The excitation grating in an F4 is blazed at 330 nm and the emission grating is blazed at 500 nm. At wavelengths above or below the blazing wavelength, efficiency can drop to about 40% (Jack Sawicki, personal communication). As a result, the fluorometer is designed to have the most efficient light transmission at excitation wavelengths in the UV regions and emission wavelengths in the high-UV to near-IR range.

$$d(sin\theta_i + sin\theta\_r) = m\lambda \qquad (24)$$

d: distance between reflecting surfaces
θ_i: angle of incidence
θ_r: angle of diffraction
m: diffraction order (m=0, 1, 2…)
λ: wavelength

The other monochromator component that affects fluorescence analysis is the slit width. Each monochromator has an entrance and exit slit, and the size of the slit affects the light bandpass. Bandpass is a measure of the wavelength distribution that actually exits the monochromator when it is set at a particular wavelength. The effective bandwidth is defined as the wavelength range at one-half the peak maximum as illustrated in Figure 2.4.

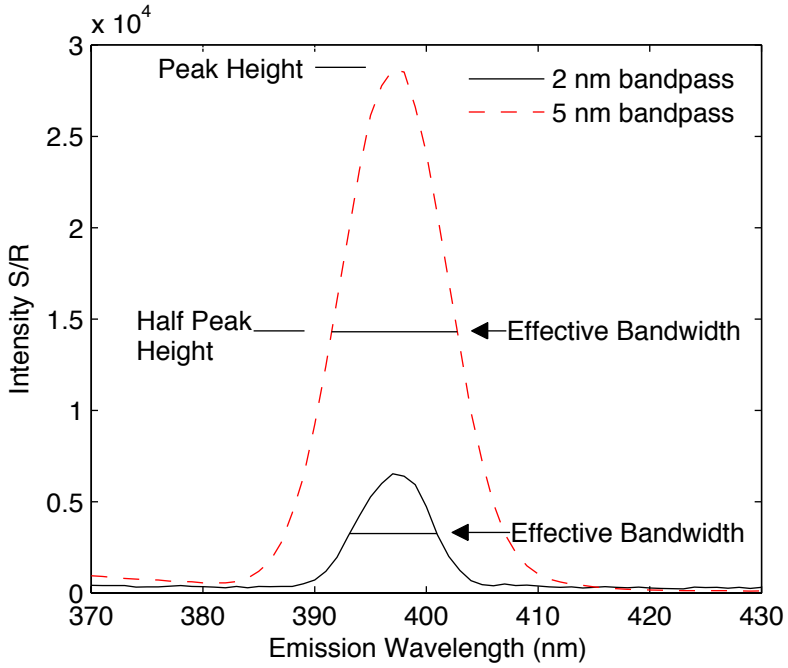

Figure 2.4 Raman scans of lab-grade water with different bandpass settings.

The bandpass of light exiting a monochromator depends on the slit width and the linear dispersion of the grating based on Eqn 25. In the F4, the grating dispersion is 4.25 nm mm^{-1} (Horiba Scientific, 2009). Table 2.1 provides some examples of slit widths and their corresponding spectral bandpasses for the F4. Since dispersion is not adjustable, the spectral bandpass is adjusted by changing the instrument slit width.

$$bandpass = slit\ width \times dispersion \quad (25)$$

With the following units
bandpass: [nm]
slit width: [mm]
dispersion: [nm mm^{-1}]

Table 2.1 Example conversions between slit width and bandpass for the F4. Reproduced from Horiba Scientific (2009).

Slit Width (mm)	Bandpass (nm)	Rounded bandpass (nm)
0.50	2.125	2
1.175	4.994	5
2.00	8.50	8.5

In adjusting the slit width, there is a tradeoff between spectral resolution and signal. Increasing the slit width increases the amount of light reaching the detector and improves the signal to noise ratio, but the spectral resolution (through the bandpass) decreases. As a result, it is more difficult to resolve peaks accurately. The relationship between slit width and signal is non-linear (Eqn 26) (Horiba Scientific, 2009; Skoog et al., 2006). Doubling the slit width (or bandpass) increases the signal by a factor of 4. This relationship becomes important when selecting method settings such that signal levels are within the linear operating range of the detector.

$$signal \propto (slit\ width)^2 \qquad (26)$$

2.3.3 Detectors

The F4 has two detectors: signal detector (S) and reference detector (R). The signal detector measures the light emitted from the sample; the reference detector measures the light output of the lamp using a beam splitter that diverts about 8% of the excitation light after the excitation monochromator (Horiba Scientific, 2009). The purpose of the detector is to convert the radiant energy (photons) into an electrical signal that can be recorded. The signal detector is a photomultiplier tube (PMT) with a working linear range up to 2 million counts per second (cps). Between 2 and 4 million cps, the detector may either still exhibit a linear response or attenuate the peak 5 to 10% depending on the unit (Jim Mattheis, personal communication). For optimal accuracy, it is recommended to keep the signal below 2 million cps. The reference detector is a UV-enhanced silicon photodiode that measures the intensity in units of μA. Compared to the PMT detector, the reference detector maintains linearity better and will saturate around 10-12 μA (Jack Sawicki, personal communication). While most standard methods record the fluorescence intensity in ratio mode (S/R), it is important to check sample response of the S and R detectors

separately to ensure that the signal is in the linear range of the detector. This can be accomplished rapidly with real-time control.

2.4 Method Parameters

2.4.1 Excitation and Emission Wavelengths

When measuring the fluorescence intensity at fixed wavelengths, the user must specify the excitation and emission wavelength in order for the instrument to position the two monochromators to select for these wavelengths. When running a two-dimension emission scan, the user selects a constant excitation wavelength and then a range of emission wavelengths. In collecting three-dimensional excitation-emission matrices (EEMs), a range for both excitation and emission wavelengths are specified.

The wavelength range depends on both experimental objectives and instrument capabilities. Most DOM analyses probe the fluorescence behavior from the UV range (Excitation 240 nm, Emission 300 nm) through the visible range (Excitation 450 nm, Emission 560-600 nm). Analyses for photosynthetic components (chlorophyll and phycobiliproteins) require wavelengths far into the visible range. The range at which an instrument can measure depends largely on the lamp source and efficiency of the optical components. On an F4, the lamp emits light down to 200 nm, but the instrument does not have reliable correction factors below 240 nm, largely due to the low intensity emitted at the lowest wavelengths. Therefore, samples should not be analyzed at excitation wavelengths below 240 nm.

2.4.2 Bandpass

The spectral bandpass quantifies the wavelength distribution that is permitted to pass through a monochromator when set to a specific wavelength. This parameter affects the spectral

resolution (the ability to resolve peaks accurately). The bandpass is determined by setting the slit width. Care must be taken when setting the bandpass in the F4 instrument with respect to the nomenclature and units. The bandpass value is set in the Experimental Set-up on "Monos" tab in the box labeled "Slit, nm." This description is a little misleading. Slit width (the actual spacing in the monochromator) has units of millimeters and is related to the actual bandpass based on the grating dispersion factor. The units for the "Slit" value are specified on the "Units" tab. The default unit is "Bandpass, nm." Therefore, the value entered into the "Slit" field is actually the spectral bandpass and not the physical slit width.

2.4.3 Scan Increment

The scan increment setting dictates the wavelength step size for the excitation and/or emission wavelength range. Typical values range from 1 to 10 nm. The smaller the step size is, the smoother the spectrum appears. A smaller step size also requires a longer analysis time and more lamp usage. While the increment does affect the spectral resolution, it plays a smaller role than spectral bandpass. If the bandpass is too large to resolve peaks, decreasing the step size will have little effect on resolution or will not reveal additional spectral features.

2.4.4 Integration Time

Integration time is the amount of time that the detector spends counting photons at each wavelength setting. Increasing the integration time improves the signal to noise ratio according to the relationship in Eqn 27. Doubling the integration time increases the signal to noise ratio by about 42%. When optimizing experimental settings to ensure the fluorescence signals fall within the linear range of the detector, adjusting the bandpass will have a larger effect on the signal compared to the integration time. For example, to decrease the signal by a factor of two, the

bandpass would have to be decreased by 30% whereas the integration time would have to be decreased by 75%.

$$\frac{S}{N} \propto t^{\frac{1}{2}} \quad (27)$$

S: signal
N: noise
t: integration time

2.4.5 Detector Parameters

Most commercial fluorometers have two detectors (S and R) in order to measure the light intensity both before and after the sample and adjust for fluctuations in lamp intensity over both time and excitation wavelength. Lamps do not emit at the same intensity across all wavelengths as shown in Figure 2.3. To compare fluorescence measurements at different excitation wavelengths, it is important to account for differences in lamp output at each wavelength. Additionally, lamp output decreases over time. Figure 2.5 plots the lamp peak intensity as a function of usage hours for two different lamps. In order to compare fluorescence data collected at two different times, the measurements have to take into account changes in lamp output between analyses.

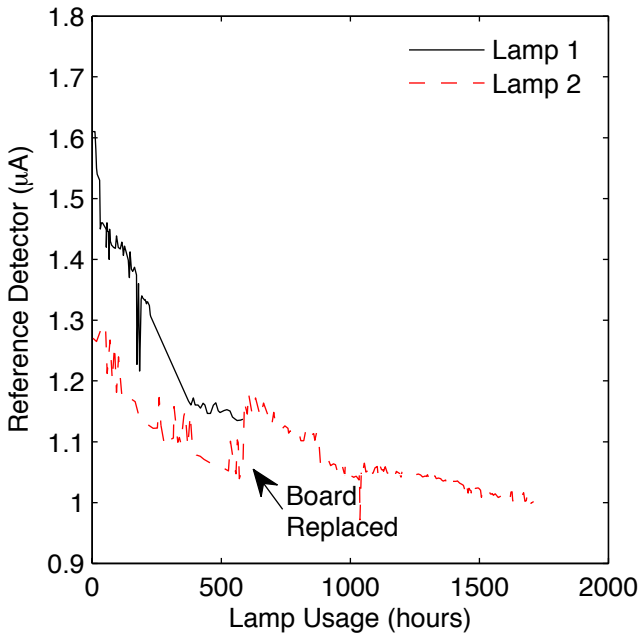

Figure 2.5 Reference detector response at 467 nm excitation as a function of lamp usage.

By measuring both intensities in tandem, the light emitted from a sample (S) can be normalized to the intensity of light that actually entered a sample (R) by dividing the two signals (S/R). This process is normally done within the instrument software in real-time by setting the method to measure both signals (S and R) and to calculate the ratio between the two.

2.4.6 Spectral Correction Factors

While operating in ratio mode (S/R) can account differences in lamp output, spectral correction factors account for differences in optics that are unique to each instrument. The efficiency of the monochromators depends on the wavelength, and there may be differences in other optical components between instruments. Each instrument has a set of correction factors that are applied to both S and R detector signals. Example correction factors are provided in Figure 2.6. The F4 correction factors are multiplied by the signal, but other instruments use a division operator (Cory et al., 2010). Most newer instruments have these correction factors built into the data acquisition software, or they can be applied during post processing. On the F4, the

correction factors are automatically applied in the detectors settings with the designations Sc and Rc for signal and reference, respectively.

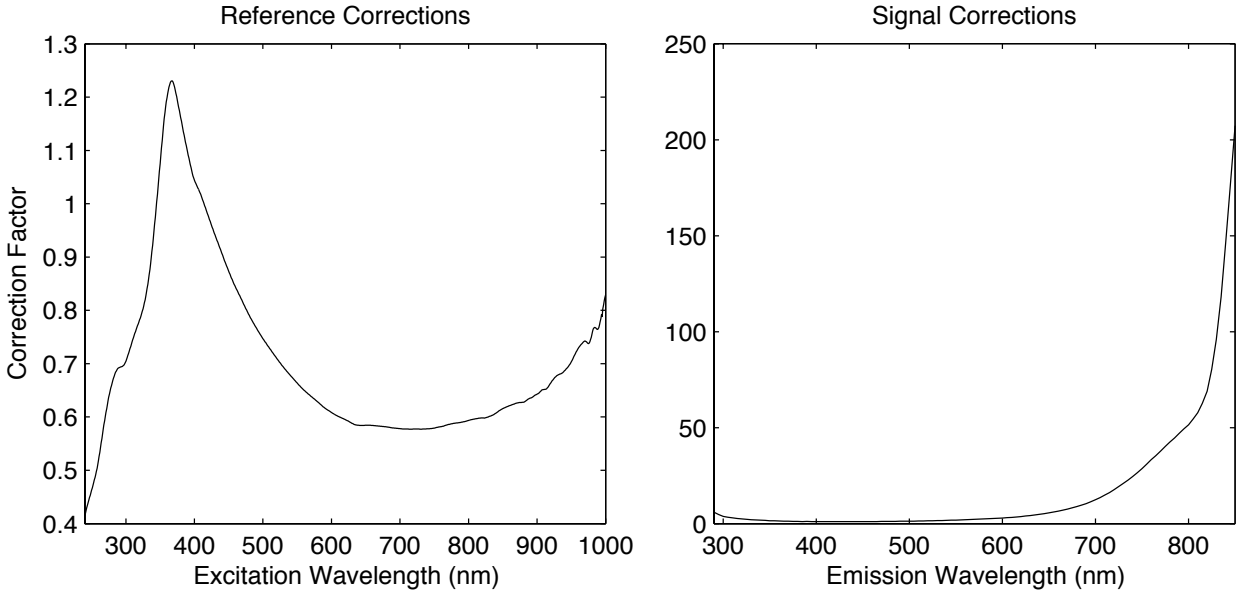

Figure 2.6 Example excitation and emission correction factors for a Fluoromax-4

2.5 Fluorescence Data Post Processing

2.5.1 Rayleigh Masking

Rayleigh scattering is an effect of the solvent and does not represent sample fluorescence. When light enters the cuvette, the solvent (water in most environmental samples) scatters the light. As a result, light intensity is measured at the same wavelength as the excitation wavelength. In excitation-emission matrices (EEMs), this appears as a diagonal line of intensity at points where the excitation wavelength equals the emission wavelength (Figure 2.7). When light is diffracted by the monochromator grating at a given angle, the wavelengths occur in multiples according to the diffraction order in Eqn 24. As a result, when the excitation monochromator passes 250 nm light into the sample compartment, there will also be some 500 nm light entering the sample at the same time. This phenomenon leads to second order Rayleigh scattering, which

appears in EEMs at locations where the emission wavelength equals two times the excitation wavelength (Figure 2.7).

Since these intensity readings do not represent sample fluorescence, they are removed through masking. Intensities in these regions are commonly replaced with either zero values or missing values (NaN in Matlab®) (Figure 2.7). There are also numerical methods that will interpolate the values within this region (Murphy et al., 2013; Zepp et al., 2004). Based on the spectral bandpass values around 5 nm, masking usually removes the intensity within 10 to 12 nm of the scattering peak. Since fluorescence emission always occurs at wavelengths greater than the excitation wavelength, the region where $\lambda_{em}<\lambda_{ex}$ is normally replaced with zeros as well. Removing data in this region can speed up statistical modeling techniques, such as parallel factor analysis (PARAFAC) (Stedmon and Bro, 2008).

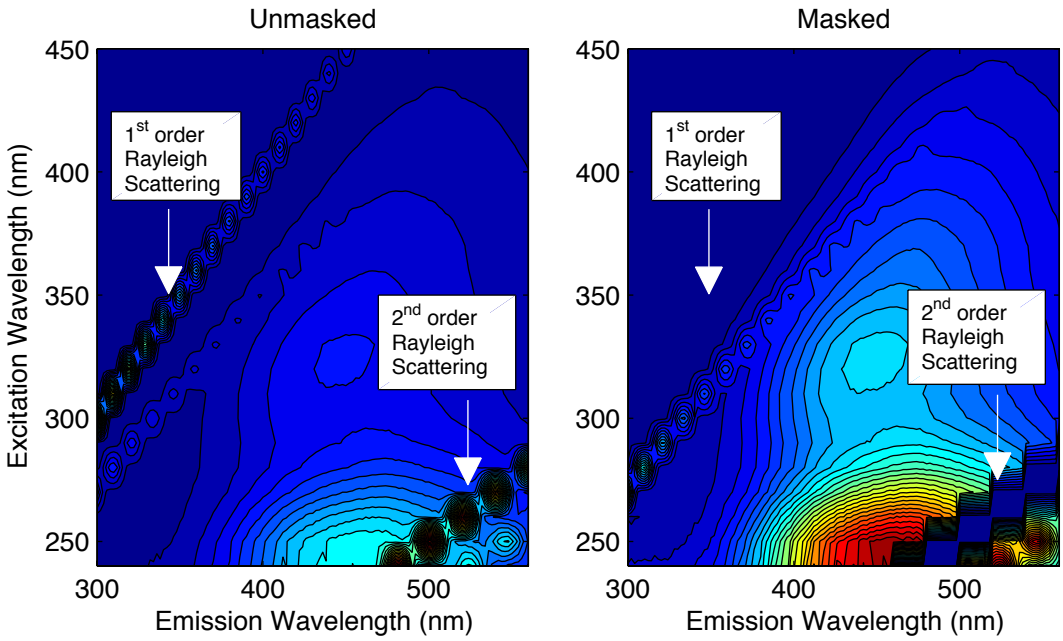

Figure 2.7 Example of masking to eliminate 1st and 2nd order Rayleigh scattering

2.5.2 Inner Filter Corrections

For the measured fluorescence intensity to be representative of the true fluorescence, the samples must be corrected for sample absorbance. While a sample cuvette may be 1 cm wide, the size of the excitation light beam that passes through the sample cuvette is narrow and only illuminates a small cross section of the sample. Likewise, the emission monochromator is focused to only detect a narrow cross section of light exiting the sample cuvette. Where these two cross sections intersect is termed the interrogation zone, and this is the region where sample fluorescence is actually measured (Figure 2.8).

Inner filtering occurs when the inherent absorbance of the sample attenuates light traveling to and from the interrogation zone. Primary inner filtering refers to the loss of light intensity of the excitation beam entering the sample. Secondary inner filtering occurs when light emitted as fluorescence is re-absorbed by the sample between the interrogation zone and cuvette edge (Figure 2.8). In many applications, only primary inner filtering is important, because absorbance at the emission wavelength is negligible. For DOM analysis, both primary and secondary inner filter effects are important, because DOM absorbs light well into the visible wavelength range.

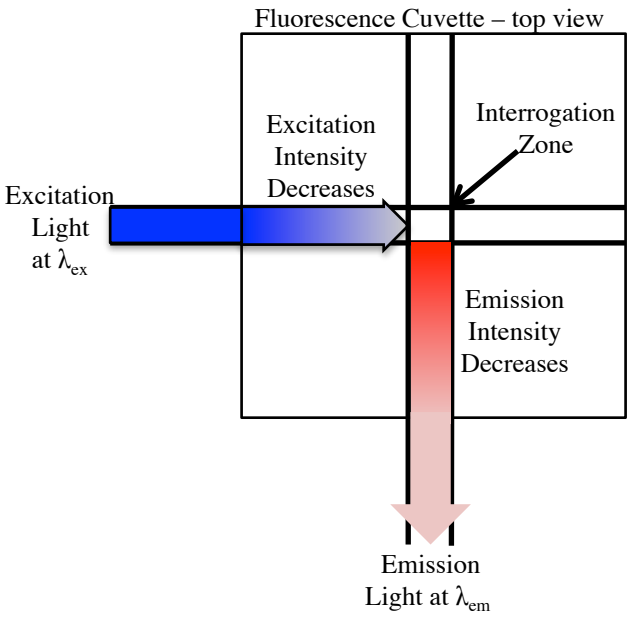

Figure 2.8 Schematic of fluorescence interrogation zone and conceptual representation of inner filter effects.

A number of studies have explored the development and use of inner filter corrections (Gu and Kenny, 2009; Holland et al., 1977; Kothawala et al., 2013; Kubista et al., 1994; Luciani et al., 2009; MacDonald et al., 1997; Parker and Barnes, 1957; Tucker et al., 1992; Yappert and Ingle, 1989). The first method published by Parker and Barnes (1957) provided a formula for correcting primary inner filtering effects using the sample absorbance, but no derivation was provided. Holland et al (1977) was the first study to derive the correction factor presented by Parker and Barnes, and MacDonald et al (1997) derived the small bandwidth approximation. There have also been several other correction methods published, including cell-shift methods (Christmann et al., 1981; Gu and Kenny, 2009) and controlled dilution approaches (Luciani et al., 2009). A recent study compared absorbance based approaches to the controlled dilution approach and concluded that the accuracy of each method depends on the wavelengths corrected, but

absorbance-based approaches perform sufficiently up to absorbance values of 1.5 (Kothawala et al., 2013).

Since absorbance-based methods are commonly used, the following sections derive the absorbance–based inner filter correction formulas following the derivations presented in several studies (Holland et al., 1977; MacDonald et al., 1997; Yappert and Ingle, 1989). The derivation for primary inner filter corrections is presented in its entirety. Since the secondary inner filter corrections are analogous and applied independently of primary corrections, a full derivation will not be shown for secondary correction factors. The notation used in the derivation follows the nomenclature in Figure 2.9.

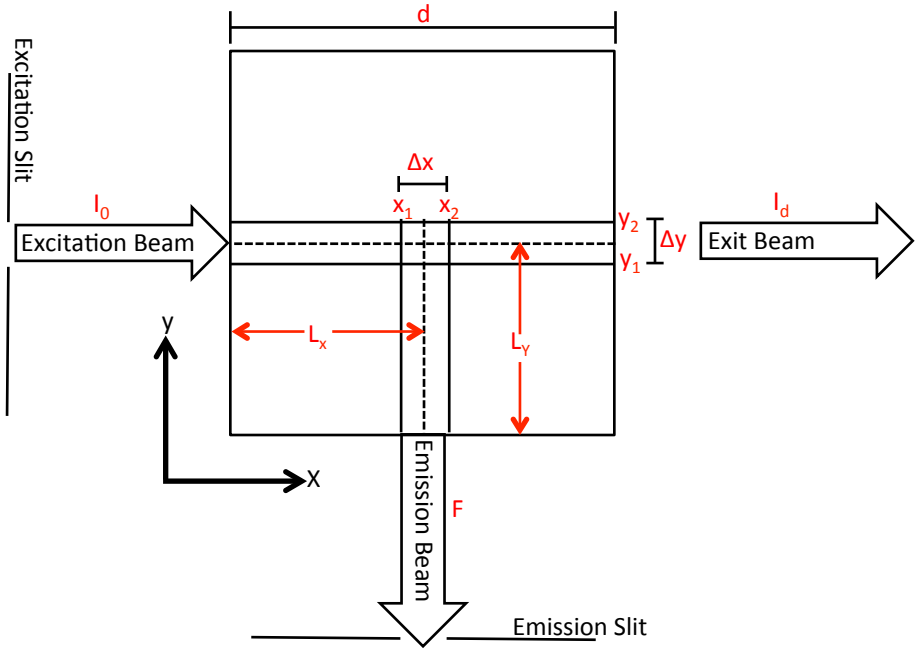

Figure 2.9. Cuvette dimensions and variable definitions for inner filter correction derivation

2.5.2.1 Derivation of Primary Inner Filter Corrections

In the absence of inner filter effects, fluorescence intensity is proportional to the intensity of the excitation source (I_0), the size of the interrogation zone ($\Delta x \Delta y$) and other constants related

to the fluorophore according to Eqn 28. Here, the absorption term (α_f) quantifies the absorption characteristics of the fluorescing species, not all chromophores. Based on the bandpass of the instrument, the excitation light is focused through a narrow width of the cuvette that extends from y_1 to y_2 in Figure 2.9. The emission monochromator is focused to measure fluorescence emitted across a narrow cross section, marked x_1 and x_2 in Figure 2.9. Therefore, the fluorescence that is measured by the detector originates from photons absorbed between x_1 and x_2.

$$F_{ideal} = k\phi\alpha_f I_0 \Delta x \Delta y \qquad (28)$$

F_{ideal}: Fluorescence observed without inner filtering
k: proportionality constant
Φ: quantum yield
α_f: Naperian extinction coefficient multiplied by concentration for fluorophore
Δx: width of interrogation zone for excitation beam
Δy: width of interrogation zone for emission beam

If fluorescence is measured, then there was some light absorbed across the pathlength. This absorption decreases the intensity that is observed in the interrogation zone compared to I_0. Therefore, fluorescence is no longer proportional to I_0 but some value less than I_0. Correcting for primary inner filter effects takes into account the overall decrease in light intensity compared to I_0 and the variation in light intensity across the interrogation zone. For example, excitation light is more intense on the left boundary of the interrogation zone (x_1) and less intense at the right boundary of the zone (x_2). Between these two points, light intensity decreases exponentially according to Beer-Lambert Law.

Holland et al (1977) rationalized that the ratio between ideal fluorescence and the excitation intensity (F_{ideal}/I_0) is equal to a set of constants ($\alpha_f\Phi\Delta x\Delta y$) according to Eqn 28. In the presence of excitation attenuation, those same constants would also be equal to the ratio of the observed fluorescence to the average excitation intensity across the interrogation zone (F_{obs}/I_{avg}).

Therefore, these two ratios could be equated to each other yielding Eqn 29. With some variable rearranging, a primary correction factor (f_p) can be defined as the ratio of the source intensity and the average intensity in the zone (Eqn 31). Since I_{avg} is less than the I_0, corrected fluorescence will be greater than the observed fluorescence.

$$\frac{F_{ideal}}{I_0} = \frac{F_{obs}}{I_{avg}} \quad (29)$$

$$F_{ideal} = \frac{I_0 F_{obs}}{I_{avg}} = F_{obs} * f_p \quad (30)$$

$$f_p = \frac{I_0}{I_{avg}} \quad (31)$$

F_{obs}: Observed fluorescence due to inner filtering
I_{avg}: Average excitation intensity across interrogation zone Δx

The average intensity (I_{avg}) across the zone can be determined by integrating the intensity (I_w) across the region and dividing it by the length of the interrogation zone (Eqn 32). By substituting the analytical expression for intensity (Eqn 16) in for I_w and integrating, I_{avg} can be written in terms of the sample transmittance and the fractional distance across the cuvette. When the expression for I_{avg} is substituting back in to the correction factor equation, I_0 cancels out leading to Eqn 33.

$$I_{avg} = \frac{\int_{w_1}^{w_2} I_w \, dw}{w_2 - w_1} = \frac{\int_{w_1}^{w_2} I_0 T^w \, dw}{w_2 - w_1} = \frac{\left.\frac{I_0 T^w}{lnT}\right|_{w_1}^{w_2}}{w_2 - w_1} = \frac{I_0 (T^{w_2} - T^{w_1})}{lnT \, (w_2 - w_1)} \quad (32)$$

$$f_p = \frac{I_0 lnT \, (w_2 - w_1)}{I_0 (T^{w_2} - T^{w_1})} = \frac{lnT \, (w_2 - w_1)}{(T^{w_2} - T^{w_1})} \quad (33)$$

Decadic absorption is more commonly measured and reported than transmittance. The correction factor can be converted to an absorbance basis and transformed back into absolute distance terms (x) through a series of substitutions and simplifications yielding Eqn 35.

$$f_p = \frac{ln(10^{-A})\left(\frac{x_2}{d} - \frac{x_1}{d}\right)}{\left((10^{-A})^{\frac{x_2}{d}} - (10^{-A})^{\frac{x_1}{d}}\right)} = \frac{\frac{-A}{d} ln(10)\ (x_2 - x_1)}{\left(10^{-\frac{A}{d}x_2} - 10^{-\frac{A}{d}x_1}\right)} \quad (34)$$

Equations to substitute
$T = 10^{-A}$
$w_2 = \frac{x_2}{d}$
$w_1 = \frac{x_1}{d}$

$$f_p = \frac{\frac{A}{d} ln(10)\ (x_2 - x_1)}{\left(10^{-\frac{A}{d}x_1} - 10^{-\frac{A}{d}x_2}\right)} \quad (35)$$

This form of the correction factor is close the one originally reported by Parker and Barnes (1957). That study used the optical density per centimeter (D) as a variable, which is equivalent to the absorbance divided by the pathlength (Eqn 36). With this convention, Eqn 37 is the same as the original correction factor presented without derivation.

$$D = A/d \quad (36)$$ D: Optical density per unit length

$$f_p = \frac{D\ ln(10)\ (x_2 - x_1)}{(10^{-Dx_1} - 10^{-Dx_2})} \quad (37)$$

There is another form in which the correction factors can be presented. The following steps convert Eqn 33 into the form used by MacDonald et al (1997). Converting to this form is necessary for developing an approximation for small bandpass settings. Rather than define the interrogation zone by x_1 and x_2, the convention is changed to defining x_1 and Δx. Transmittance is also converted to the exponential expressions using Eqns 9 and 10. The end product is an expression that quantifies the correction factor in terms of α, x_1, and Δx. Here, α is used to account for all chromophores, including non-fluorescing species.

$$f_p = \frac{lnT\ (w_2 - w_1)}{(T^{w_2} - T^{w_1})} \quad (38)$$

Equations to substitute
$w_2 = \frac{x_2}{d}$ (39)

$$w_1 = \frac{x_1}{d}$$
$$x_2 = x_1 + \Delta x$$
$$f_p = \frac{lnT\left(\frac{x_2}{d} - \frac{x_1}{d}\right)}{\left(T^{\frac{x_2}{d}} - T^{\frac{x_1}{d}}\right)} = \frac{lnT\left(\frac{x_1 + \Delta x}{d} - \frac{x_1}{d}\right)}{\left(T^{\frac{x_1+\Delta x}{d}} - T^{\frac{x_1}{d}}\right)} \quad (40)$$

Convert from T to exponential form

$$T = e^{-\alpha d} \quad (41)$$
$$lnT = -\alpha d \quad (42)$$
$$f_p = \frac{-\alpha d\ (\Delta x)}{d\left(e^{-\alpha d\frac{x_1+\Delta x}{d}} - e^{-\alpha d\frac{x_1}{d}}\right)} = \frac{-\alpha(\Delta x)}{(e^{-\alpha(x_1+\Delta x)} - e^{-\alpha x_1})} \quad (43)$$
$$f_p = \frac{-\alpha(\Delta x)}{(e^{-\alpha x_1}e^{-\alpha\Delta x} - e^{-\alpha x_1})} = \frac{\alpha\ (\Delta x)}{e^{-\alpha x_1}(1 - e^{-\alpha\Delta x})} \quad (44)$$

2.5.2.2 Approximation for small Δx values

For most practical applications, this correction factor (Eqns 33, 35 or 44) is not convenient, because it is often unknown what the dimensions of the actual interrogation zone (x_1, x_2) are for a given instrument. There have been several studies that demonstrate how to determine these variables for a specific instrument using cell-shift methods (Christmann et al., 1981; Gu and Kenny, 2009). Kubista et al (1994) demonstrated that the interrogation zone size (Δx, Δy) is not important for most practical applications. The size of the interrogation zone is a function of the bandpass, and the location of the interrogation center (L_x and L_y) is unique to the instrument. Kubista et al (1994) found that an empirically fitted primary correction factor could be approximated with a simplified function (Eqn 45). The same relationship was valid for a range of bandpass values between 0.5 and 15 nm, and the coordinate of the zone center (L_x) could be fitted empirically for a particular instrument using a known fluorophore to calibrate. These results demonstrated that the width of the interrogation zone becomes less important at

small bandpass settings, but this study provided no rationale why this approximation is reasonable mathematically.

$$f_p \approx 10^{AL_x} \qquad (45)$$

A latter study by MacDonald derived the inner filter corrections and justified the commonly-used approximation in Eqn 45 and Lakowicz (2006). The mathematical simplification for small bandpass settings begins with the inner filter correction factor in the form of Eqn 46. The exponential term in parentheses can be approximated by a series expansion (Eqn 47). After substituting the series back into Eqn 46, simplifying and factoring out αΔx, the correction factor can be simplified to Eqn 50.

$$f_p = \frac{\alpha\,\Delta x}{e^{-\alpha x_1}(1 - e^{-\alpha\Delta x})} \qquad (46)$$

Series Expansion on term $e^{-\alpha\Delta x}$

$$e^{-\alpha\Delta x} \approx 1 - \alpha\Delta x + \frac{(\alpha\Delta x)^2}{2} - \frac{(\alpha\Delta x)^3}{6} + \cdots \qquad (47)$$

Substitute back into Eqn 33 and simplify

$$f_p = \frac{\alpha\,\Delta x}{e^{-\alpha x_1}\left(1 - \left(1 - \alpha\Delta x + \frac{(\alpha\Delta x)^2}{2} - \frac{(\alpha\Delta x)^3}{6} + \cdots\right)\right)} \qquad (48)$$

$$f_p = \frac{\alpha\,\Delta x}{e^{-\alpha x_1}\left(\alpha\Delta x - \frac{(\alpha\Delta x)^2}{2} + \frac{(\alpha\Delta x)^3}{6} + \cdots\right)}$$

$$f_p = \frac{\alpha\,\Delta x}{e^{-\alpha x_1}(\alpha\Delta x)\left(1 - \frac{\alpha\Delta x}{2} + \frac{(\alpha\Delta x)^2}{6} + \cdots\right)} \qquad (49)$$

$$f_p = \frac{1}{e^{-\alpha x_1}\left(1 - \frac{\alpha\Delta x}{2} + \frac{(\alpha\Delta x)^2}{6} + \cdots\right)} \qquad (50)$$

The series in parentheses in Eqn 50 is close to the series expansion in Eqn 51. The first two terms are the same, but the denominators in the quadratic term differ. When Δx is small, the higher order terms become negligible, and the series can be approximated with the new

exponential term leading to Eqn 52. The term in parenthesis ($x_1+\Delta x$) represents the center of the interrogation zone as indicated in Figure 2.9 leading to Eqn 54.

$$e^{-\frac{\alpha\Delta x}{2}} \approx \left(1 - \frac{\alpha\Delta x}{2} + \frac{(\alpha\Delta x)^2}{8} + \cdots\right) \quad (51)$$

$$f_p = \frac{1}{e^{-\alpha x_1} e^{-\frac{\alpha\Delta x}{2}}} = \frac{1}{e^{-\alpha\left(x_1+\frac{\Delta x}{2}\right)}} \quad (52)$$

Define

$$L_x = x_1 + \frac{\Delta x}{2} \quad (53)$$

$$f_p = \frac{1}{e^{-\alpha L_x}} = e^{\alpha L_x} \quad (54)$$

The simplified correction factor in Eqn 54 can be converted back to absorbance units yielding Eqn 56. It is commonly assumed that the interrogation zone lies in the center of the cuvette. If this assumption is made, then the correction factor reduces Eqn 58, which is the same form reported in Lakowicz (2006).

$$f_p = e^{\alpha L_x} = e^{\frac{-lnTL_x}{d}} = T^{-\frac{L_x}{d}} = 10^{-A*-\frac{L_x}{d}} \quad (55)$$

Substitute in Equations

$$\alpha = \frac{-lnT}{d}$$

$$T = 10^{-A}$$

$$f_p = 10^{\frac{AL_x}{d}} \quad (56)$$

$$If\ \frac{L_x}{d} = 0.5 \quad (57)$$

$$Then\ f_p = 10^{0.5A} \quad (58)$$

2.5.2.3 Secondary Inner Filter Corrections

The previous sections derived the equations for primary inner filter effects where the excitation intensity is attenuated. Secondary inner filter effects are analogous but occur along the y-axis in Figure 2.9. Photons emitted at side of the interrogation zone opposite the detector (y_2) will be attenuated more than photons emitted at the opposite boundary (y_1). While primary correction factors determine the fraction of photons that reach the interrogation zone from the

sample surface at x=0, secondary correction factors (f_s) account for the fraction of photons emitted in the interrogation zone that reach the sample surface at y=0. The attenuation of emitted photons follows the same principles of Beer-Lambert law, and the correction factors are analogous to each other, as shown in Eqns 59 and 60. The excitation and emission wavelengths are independent of each other. In primary correction factors, the absorbance values are at the excitation wavelength. For secondary corrections, the absorbance used is at the emission wavelength. This distinction is made in Eqns 59 and 60.

$$f_s = \frac{lnT_{em}(v_2 - v_1)}{(T_{em}{}^{v_2} - T_{em}{}^{v_1})} = \frac{\frac{A_{em}}{d} ln(10)\ (y_2 - y_1)}{\left(10^{-\frac{A_{em}}{d}y_1} - 10^{-\frac{A_{em}}{d}y_2}\right)} \quad (59) \qquad v_2 = \frac{y_2}{d}$$

$$f_s = \frac{\alpha_{em}(\Delta y)}{e^{-\alpha_{em}y_1}(1 - e^{-\alpha_{em}\Delta y})} \quad (60) \qquad v_1 = \frac{y_1}{d}$$

Starting with Eqn 60, the same series expansions and approximations can be made for small Δy values, which simplifies the correction factor to Eqn 61. If is assumed that the interrogation zone falls in the center of the cuvette, then secondary correction simplifies to Eqn 63.

$$f_s = 10^{A_{em}\left(\frac{L_y}{d}\right)} \quad (61)$$

If $\frac{L_y}{d} = 0.5$ (62)

Then $f_s = 10^{0.5A_{em}}$ (63)

When fluorescence data is corrected for both primary and secondary inner filter effects, Eqn 30 is expanded to Eqn 64. The final form shows that the corrections are applied independently to each other. When the small bandpass correction factors are used, the resulting equation is identical to Lakowicz (2006) and many publications on DOM fluorescence.

$$F_{ideal} = F_{obs} * f_p * f_s \quad (64)$$

$$F_{ideal} = F_{obs} * 10^{\frac{A_{ex}+A_{em}}{2}} \quad (65)$$

It is important to note that Eqn 65 is specific to one excitation wavelength and one emission wavelength. To correct EEMs, there is a different correction factor for each excitation and emission wavelength combination. These corrections are easily performed by generating a matrix of correction factors representing each wavelength combination. The correction matrix is then multiplied in an element-wise manner with the sample EEM matrix.

2.5.3 Blank Subtraction

While Rayleigh scattering can be removed by masking, Raman scattering occurs in regions where DOM fluoresces, especially in the Peak B region (Coble, 1996). These peaks can be largely removed by subtracting a blank EEM from the sample EEM. Inner filter corrections should always be performed on the sample EEM prior to the blank subtraction step. The Raman peak intensities are attenuated by sample absorbance (especially at the lower wavelengths). If inner filter corrections are not performed first, it is possible to have negative fluorescence intensities at lower wavelengths after blank subtraction. Subtracting the blank fluorescence intensity also helps ensure that the final corrected fluorescence signal is only do to the sample and not other instrument artifacts. This correction step is accomplished by simply subtracting the two matrices of data, either in Excel® or Matlab®.

2.5.4 Intensity Normalization

The final step in correcting fluorescence data is to normalize the measured intensities to a reference standard. The intensities measured (typically in units of CPS) are dependent on the instrument used in the analysis. Optical components and detectors vary. By calibrating the intensity to a standard, it provides a reference point for samples to be easily compared. There are

two predominant methods throughout DOM literature: quinine sulfate normalization and water Raman normalization.

2.5.4.1 Quinine Sulfate Normalization

Quinine sulfate (QS) is a standard that is used throughout fluorescence analysis and was the first fluorescence standard reference material from the National Institute of Standards and Technology (Velapoldi and Mielenz, 1980). QS has an absorption peak at 348 nm, a fluorescence maxima at 452 nm and a quantum yield of 0.54 (Birks, 1970; Velapoldi and Mielenz, 1980). This standard can be used to not only calibrate instrument intensity but also to standardize spectra and develop instrument correction factors.

When normalizing intensities to QS, the intensities are normalized based on the intensity response of 1 ppb (1 µg/L) of quinine at excitation 350 nm and emission 450 nm (Jaffe et al., 2004; Murphy et al., 2010). Since it is difficult to accurately generate a standard at 1 ppb, a standard dilution curve is used. At low concentrations, the fluorescence response is proportional to the concentration, and the slope of a fitted line represents the change in intensity per unit (i.e. ppb) of QS (Eqn 66). When the measured fluorescence intensities are divided by the standard curve slope, the normalized intensity is referred to as quinine sulfate equivalents (QSE) or quinine sulfate units (QSU). The slope of the QS standard curve is used to normalize the sample intensities at all wavelengths according to Eqn 67, where F_{samp} and $F_{samp,norm}$ represent a matrix of data. The intensity units [Int] in Eqn 66 and 67 may vary between instruments depending on the detector. On an F4 instrument, the units for samples measured in S/R mode are [CPS/µA]. Data can also be normalized to Raman Units (RU) prior to conversion to QSE (Murphy et al., 2010).

$$F_{QS} = m \times C_{QS} + b \qquad (66)$$

F_{QS}: fluorescence intensity (Ex 350 nm, Em 450 nm) [Int]
m: slope of regression [Int/ppb]

$$\boldsymbol{F}_{samp,norm} = \frac{\boldsymbol{F}_{samp}}{m} \quad (67)$$

C_{QS}: QS concentration [ppb]
b: Regression intercept [Int]
F_{samp}: Measured sample intensity matrix [Int]
$F_{samp,norm}$: Normalized sample intensity matrix [Int]

When developing the standard curve through dilutions, it is important to ensure that the concentrations chosen fall in the linear range. From a theoretical standpoint, the range in which fluorescence intensity is proportional to concentration depends on whether the linear approximation in Eqn 21 is valid. Since quinine sulfate has a high quantum yield, the instrument detector may play a more important role in determining the range of linearity. When quinine sulfate is measured using a fluorescence method commonly used for DOM analysis on an F4 (5 nm excitation and emission bandpass settings and 0.25 s integration time), the signal detector can easily exceed the linear range of operation. Even though the NIST standard for quinine sulfate is 1 mg/L as quinine sulfate dihydrate, this concentration yields a signal response of 12.6 million CPS, far beyond the recommended 2 million CPS threshold. To operate within the linear range of the detector, it is necessary to run a much lower quinine sulfate concentration (0.1 mg/L). As a result, normalization using a quinine sulfate dilution curve requires diluting low concentrations that may be susceptible to more error.

2.5.4.2 Water Raman Normalization

Another normalization method that alleviates the use of low concentration standards and the need for dilution is Raman normalization. Where Rayleigh scattering represents inelastic scattering of light, Raman scattering represents elastic scattering of light. It occurs at a wavelength longer than the excitation light and is a characteristic of the solvent. For lab-grade water, excitation at 350 nm leads to a Raman peak at 397 nm. As mentioned in Section 2.3.2, this

characteristic peak is used to ensure proper calibration of the emission monochromator. The intensity of the peak can also be used to calibrate the sample intensity.

Figure 2.10 shows that the Raman peak intensity depends on instrumental settings. A larger bandpass leads to greater water Raman peak uncorrected intensity S1 (Figure 2.10a). When both excitation and emission bandpass values are 2 nm, the intensity is much lower than when both are set to 5 nm. When one bandpass is set to 3 nm and the other 5 nm, the signals are similar to each other regardless of which monochromator is set to the larger bandpass. A different trend emerges when the S1c/R1c responses are compared, as would be done during sample analysis. Regardless of excitation bandpass, the peak intensity is greater for larger emission bandpass settings (Figure 2.10b). While the peak intensity can take into account the differences in overall intensity reaching the detector due to changes instrumental settings, it does not account for changes in peak shape. Figure 2.10c shows that when the Raman peaks are normalized to the maximum peak intensity, the breadth of the peak changes. A wider bandpass leads to a broader peak. These differences in the water Raman signature due to bandpass settings also affect DOM fluorescence.

A study by Lawaetz and Stedmon (2009) demonstrated that integrating the area under the Raman peak yields a better correction compared to normalizing to peak intensity (Holbrook et al., 2006). Figure 2.11 repeats the Lawaetz and Stedmon experiment with quinine sulfate and compares peak height and peak area normalization methods. The unnormalized quinine sulfate intensities (S1c/R1c) are highly dependent on instrument bandpass. The large emission bandpass intensity is a factor of 3 greater than the small emission bandpass intensity (Figure 2.11a). When the quinine spectra intensities are normalized to the height of the Raman peak, the differences are smaller (Figure 2.11b). The relative percent difference between quinine sulfate peak intensities is

15%. When the quinine sulfate intensities are normalized to the Raman peak area, the three spectra overlay each other (Figure 2.11c) demonstrating that this normalization method best accounts for differences in instrumental bandpass settings.

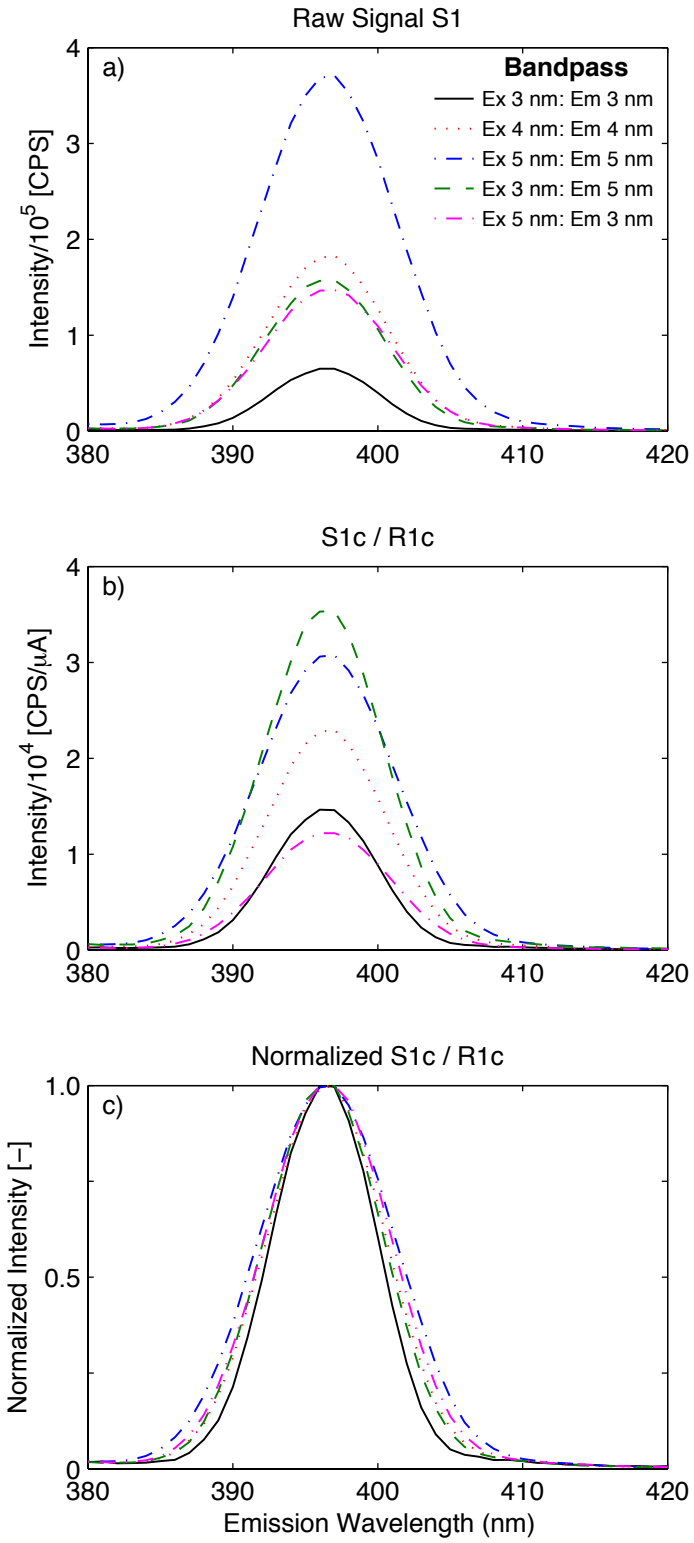

Figure 2.10 Raman peak of lab-grade water at excitation 350 nm measured with different instrumental settings plotted as a) Signal S1, b) Signal S1c/R1c and c) Normalized S1c/R1c.

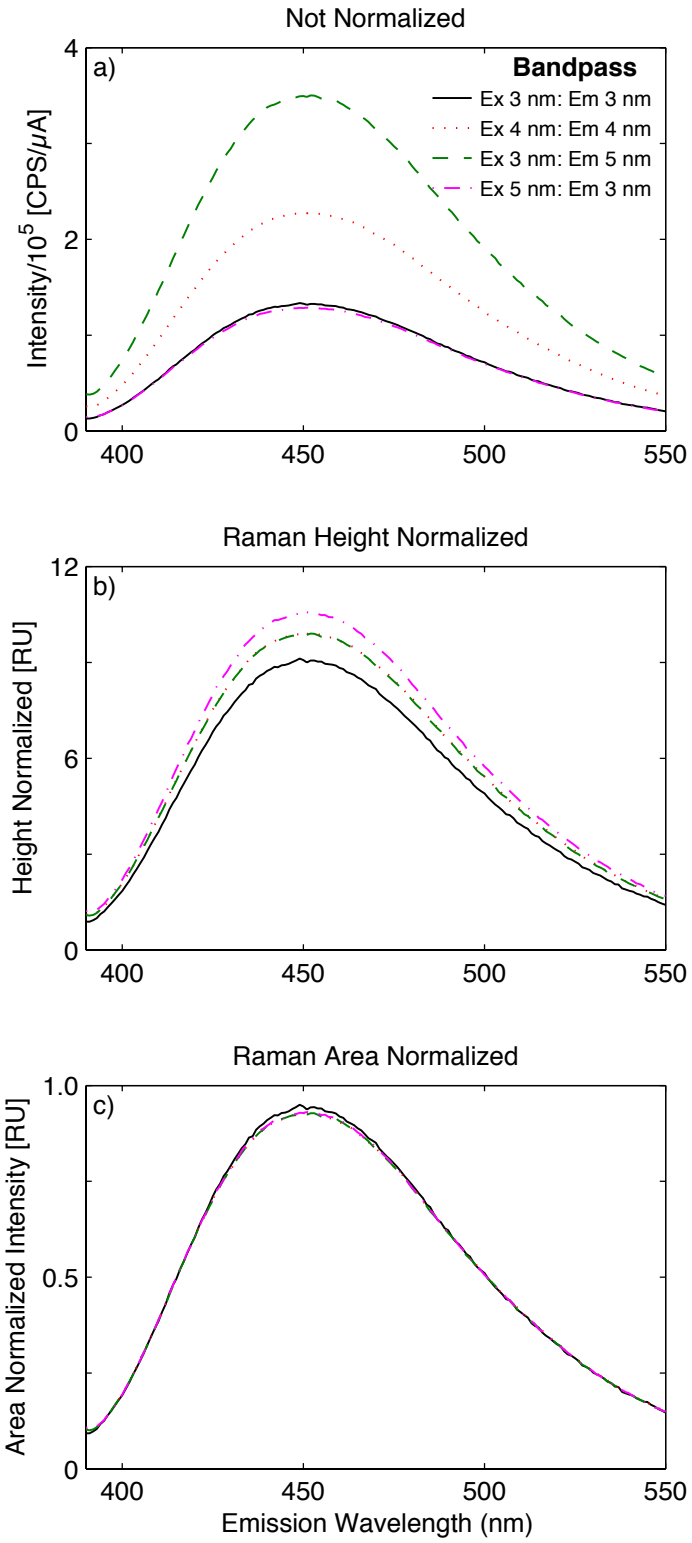

Figure 2.11 Emission spectra of quinine sulfate at excitation 340 nm plotted as a) S1c/R1c b) Normalized to Raman peak intensity of lab-grade water and c) Normalized to the Raman peak area of lab-grade water

Several different methods have been used to integrate the Raman peak area, because it can be difficult to define the upper and lower limits of the peak. In the Lawaetz and Stedmon (2009) study, the Raman peak at excitation 350 nm was integrated from 371 nm to 428 nm based on the theoretical position of the water Raman peak at that excitation wavelength. The MATLAB® code distributed at the Institute of Alpine and Artic Research (INSTAAR) fluorescence workshop (2011) integrates the Raman peak from 365 nm to 450 nm and subtracts the baseline area between endpoints. Finally, a more recent study determined the extent of the water Raman peak systematically by determining where the derivative of the Raman spectra changes (Murphy, 2011). Figure 2.12 compares the three methods. All methods successfully normalize the data such that the effects of different instrumental settings are removed; all emission spectra overlay each other. Maximum normalized intensities calculated using the Lawaetz and Stedmon method are about 10% lower than those calculated using the INSTAAR and Murphy methods, because the baseline area is not subtracted from the peak area. The INSTAAR and Murphy methods yield intensities that are within 1.2% of each other.

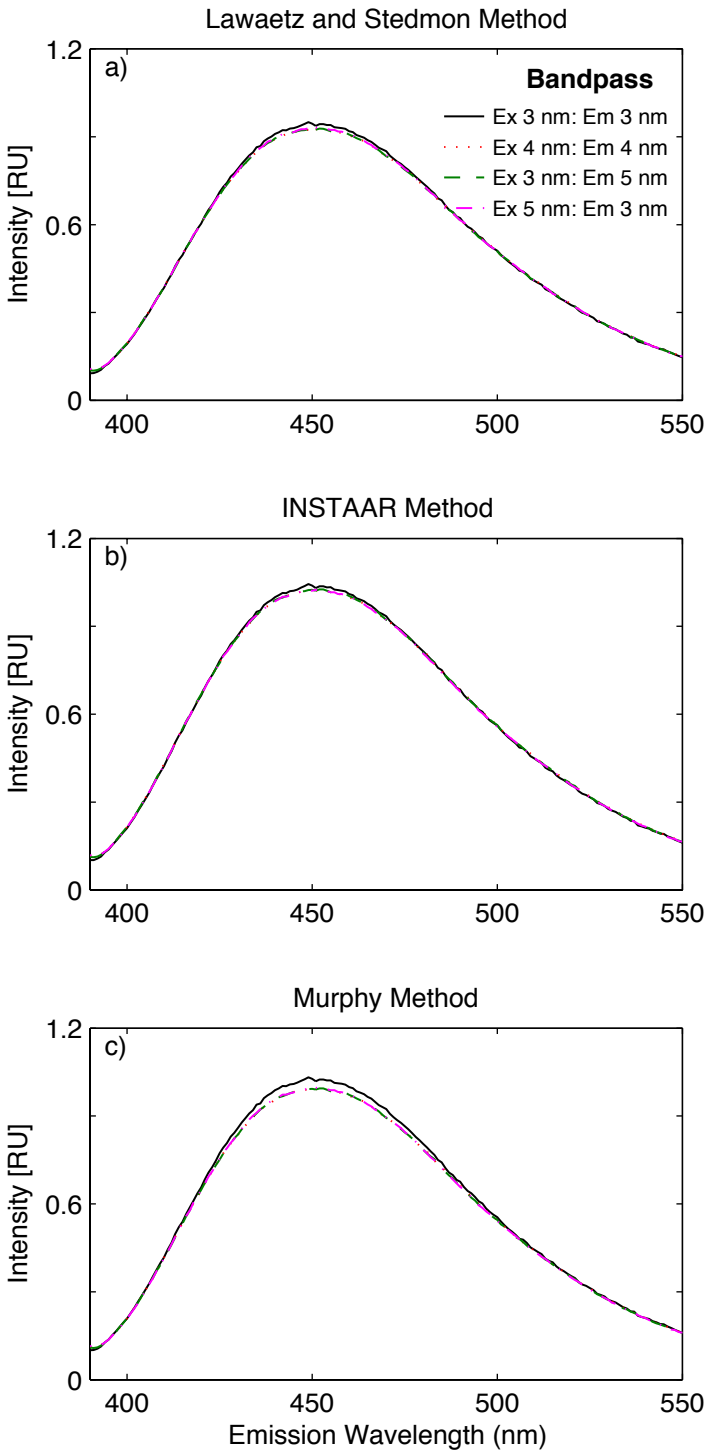

Figure 2.12 Comparison of Raman area normalization methods a) Lawaetz and Stedmon method b) INSTAAR method and c) Murphy method

Chapter 3 Critical analysis of commonly used fluorescence metrics to characterize dissolved organic matter

The work in this chapter has been published as:
Korak, J.A., Dotson, A.D., Summers, R.S., Rosario-Ortiz, F.L., 2014. Critical Analysis of Commonly Used Fluorescence Metrics to Characterize Dissolved Organic Matter. Water Research 49, 327–338.

3.1 Abstract

The use of fluorescence spectroscopy for the analysis and characterization of dissolved organic matter (DOM) has gained widespread interest over the past decade, in part because of its ease of use and ability to provide insight of bulk DOM chemical characteristics. However, the lack of standard approaches for analysis and data evaluation has complicated its use. This study utilized comparative statistics to systematically evaluate commonly used fluorescence metrics for DOM characterization to provide insight into the implications for data analysis and interpretation such as peak picking methods, carbon-normalized metrics and the fluorescence index (FI). The uncertainty associated with peak picking methods was evaluated, including the reporting of peak intensity and peak position. The linear relationship between fluorescence intensity and dissolved organic carbon (DOC) concentration was found to deviate from linearity at environmentally relevant concentrations and simultaneously across all peak regions. Comparative analysis suggests that the loss of linearity is composition specific and likely due to non-ideal intermolecular interactions of the DOM rather than the inner filter effects. For some DOM sources, Peak A deviated from linearity at optical densities a factor of 2 higher than that of Peak C. For carbon-normalized fluorescence intensities, the error associated with DOC measurements significantly decreases the ability to distinguish between compositional differences. An in-depth analysis of FI determined that the metric is mostly driven by peak emission wavelength and less

by emission spectra slope. This study also demonstrates that fluorescence intensity follows property balance principles, but the fluorescence index does not.

3.2 Introduction

Dissolved organic matter (DOM) is comprised of a wide range of compounds that originate from terrestrial or aquatic sources as well as from anthropogenic inputs, such as wastewater effluent (Leenheer, 2009). Composition is spatially and temporally dependent and associated with source material variation and environmental transformation processes (e.g., redox and photochemical processing). DOM is highly heterogeneous and is often characterized by bulk parameters (e.g., dissolved organic carbon (DOC), light absorption/fluorescence, aromaticity, hydrophobicity and functional groups) (Leenheer, 2009).

Fluorescence spectroscopy measures the fraction of DOM that both absorbs and emits light, and the fluorescent DOM fraction is often associated with aromaticity (Senesi et al., 1991). Observed fluorescence can be a function of individual fluorophores contributing superimposed signals or a function of intramolecular charge-transfer mechanisms between interacting fluorophores (Del Vecchio and Blough, 2004).

3.2.1 Application of Fluorescence Spectroscopy for DOM Characterization

Fluorescence spectroscopy has been used extensively to characterize differences in DOM signatures in natural systems (Fellman et al., 2010; Hudson et al., 2007). Recently, fluorescence has been applied to engineered treatment systems to characterize DOM changes (Allpike et al., 2005; Baghoth et al., 2011b; Beggs et al., 2013; Beggs and Summers, 2011; Beggs et al., 2009; Bieroza et al., 2011; Cheng et al., 2004; Dwyer et al., 2009; Kraus et al., 2010; Swietlik and Sikorska, 2004; Win et al., 2000). Early applications of fluorescence included two-dimensional emission, excitation and synchronous scans and focused on spectral peak intensity and positions.

Analysis of two-dimensional scans also led to the development of indices such as the fluorescence index (FI) and humification index (HIX) (McKnight et al., 2001; Ohno, 2002; Zsolnay et al., 1999). Recent analysis of DOM fluorescence has focused on the use of three dimensional excitation-emission matrices (EEMs), as illustrated in Figure 3.1. Peak picking methods have driven a significant portion of quantitative fluorescence analysis (Coble, 1996). Furthermore, parallel factor analysis (PARAFAC) has been used to decompose EEMs into components, but relies on collecting large datasets of EEMs (Murphy et al., 2013; Stedmon et al., 2003; Stedmon and Bro, 2008).

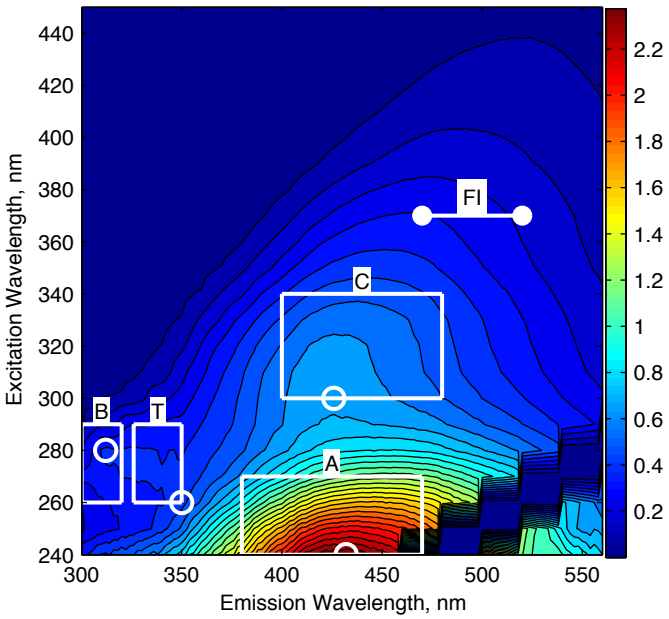

Figure 3.1 Excitation emission matrix for BEM. Intensity is presented in Raman units (RU). Boxes outline the four peak regions (A, B, C and T) with labels above. Hollow circles indicate the location of the peak intensity in each region. The two points used in the I470/I520 Fluorescence Index (FI) metric are represented by filled circles connected by a line at an excitation of 370 nm

A wide range of metrics has been used to analyze EEMs. The simplest EEM characterization method is qualitative observation of the presence or absence of regional intensity (Bu et al., 2010). A fluorescence regional integration (FRI) method was developed that sums all intensities within a region (Chen et al., 2003; Zhou et al., 2013). Peak picking is a quantitative method that records the peak intensities within pre-defined regions of interest. Common peak regions relevant to freshwater include two humic-like (A, C) and two heterocyclic nitrogen/polyphenolic/protein-like peaks (B, T) and are outlined in Table 3.1 (Coble, 1996; Leenheer, 2009). Peak picking has been executed using two distinct methods. The first method reports the intensity of a stationary point (fixed wavelength) within each region of interest (Leenheer, 2009; Lønborg et al., 2010; Murphy et al., 2010; Romera-Castillo et al., 2011). The second approach is to define a region of interest and systematically extract the maximum intensity within the region even though the location of maximum may vary between samples and replicates (Beggs and Summers, 2011; Bieroza et al., 2011; Esparza-Soto et al., 2011; Guéguen and Cuss, 2011; Senesi et al., 1991; Wang et al., 2009; Yang et al., 2013). This method will be referred to as an "algorithm-based" approach herein. Many studies that employ this method also record the excitation and emission wavelength at which the maximum is located and use this information to infer changes in DOM composition (Bieroza et al., 2011; Del Vecchio and Blough, 2004; Esparza-Soto et al., 2011; Wang et al., 2009; Yang et al., 2013). Furthermore, much in the same way as specific UV absorbance (SUVA) has been used to characterize DOM (Weishaar et al., 2003), carbon-normalized peak intensities (intensity divided by DOC), have been used to characterize fluorescence per unit DOC, often termed specific intensities (Alberts et al., 2002; Alberts and Takács, 2004; Allpike et al., 2005; Beggs and Summers, 2011; Cheng et al., 2004;

Cumberland and A. Baker, 2007; Dwyer et al., 2009; Fellman et al., 2010; Fleck et al., 2013; Hudson et al., 2007; Jaffe et al., 2004; Wu et al., 2007).

FI has been correlated to DOM aromaticity and is often used as a surrogate for DOM origin, i.e., allochthonous or autochthonous (Allpike et al., 2005; Baghoth et al., 2011b; Beggs et al., 2013; 2009; Beggs and Summers, 2011; Bieroza et al., 2011; Cheng et al., 2004; Dwyer et al., 2009; Kraus et al., 2010; McKnight et al., 2001; Swietlik and Sikorska, 2004; Win et al., 2000). FI was originally defined for fulvic acids isolated from a range of DOM sources, but has since been applied to whole water analyses (Beggs et al., 2009; Beggs and Summers, 2011; Kraus et al., 2010; McKnight et al., 2001). FI was initially defined as a ratio of emission intensities at 450 nm and 500 nm when excited at a wavelength of 370 nm (Coble, 1996; McKnight et al., 2001). The 450 nm point was chosen because it was between the peak emission for Pony Lake and Suwannee River end members. The 500 nm index represented the point where emission intensity for microbial end members was half of its maximum intensity. Due to instrument specific corrections that shift the emission maxima to longer wavelengths by about 15 nm (red-shifted), the indices for FI were modified to the ratio of 470 nm to 520 nm (Cory et al., 2010).

Past work has made great advances in standardizing the procedures by which EEMs are collected, corrected and normalized (Lawaetz and Stedmon, 2009; Murphy et al., 2010). Murphy et. al., (2010) focused on the use of instrument-specific correction factors, correcting for inner filter effects and a comparison of Raman and quinine sulfate normalization methods. The study also compared the reproducibility of single intensities and intensity ratios through an inter-laboratory comparison. These, however, are only a few of the commonly used metrics that have been employed, and the literature lacks a thorough discussion of metric limitations and a validation of underlying assumptions.

Many metrics rely on an underlying assumption that fluorescence intensity and DOC concentration are linearly related. Using this assumption, fluorescence can be used as a surrogate for DOC concentration in monitoring applications by developing site-specific correlations (Bergamaschi et al., 2012; Carpenter et al., 2012; Goldman et al., 2012). Online monitoring is one application where there are limitations inhibiting the use of inner filter corrections (IFCs), which in turn affects linearity assumptions. Identifying metrics that do not require IFCs would benefit such applications. To illustrate another example, for the ratio of two intensities (i.e., peak C/ peak T, FI) to be an intrinsic, compositional metric over a range of DOC concentrations, the peak intensities must vary proportionally across the range of concentrations. Fundamental theory supports a linear response between fluorescence intensity and DOC concentration given a number of constraints described herein (Kubista et al., 1994; Parker and Rees, 1962). According to the Beer-Lambert law, at low concentrations absorption is directly proportional to concentration when the composition (decadic molar extinction coefficient) and cell path length are constant (Lakowicz, 2006). Non-linear absorption behavior often occurs in the presence of scattered light from turbidity, fluorescing species, and molecular aggregation (Lakowicz, 2006). Once organic molecules are in the excited singlet state, the fluorescence quantum yield dictates the fraction of absorbed energy that is released through a radiative fluorescing mechanism versus non-radiative or phosphorescing energy dissipation mechanisms. The quantum yield is dependent on the fluorophore composition and surrounding environment. The presence of quenchers, enhancers, or the formation of excimers can all impact the quantum yield (Lakowicz, 2006). Past research has demonstrated that DOM behaves as a complex mixture where charge transfer interactions play an important role (Del Vecchio and Blough, 2004).

For a given application, a variety of metrics have been used to investigate the same process. For example, across a range of DOM coagulation studies, some report changes in peak intensities (Afcharian et al., 1997; Baghoth et al., 2011b; Bieroza et al., 2011; 2009; Cheng et al., 2004; Dwyer et al., 2009; Gone et al., 2009; Kraus et al., 2010; Swietlik and Sikorska, 2004), some report specific intensities (Allpike et al., 2005; Beggs and Summers, 2011; Cheng et al., 2004; Dwyer et al., 2009), and others use indices such as the FI (Beggs et al., 2009; Beggs and Summers, 2011; Kraus et al., 2010). With the increasing use of EEMs to study DOM, the literature lacks a comprehensive study on metric sensitivity and applicability. This study utilized comparative statistics to systematically evaluate the commonly used fluorescence metrics to provide insight into the implications for data analysis and interpretation such as peak picking methods, carbon-normalized metrics and the fluorescence index (FI). The intent is to aid researchers in understanding limitations and pitfalls of different DOM fluorescence data analysis tools. Application of the concepts described here will provide a strong foundation for future experimental design and data analysis to allow for more consistent practices and better comparison across literature. While this study relied on well-characterized DOM standards and some surface waters, the results highlight important considerations for any DOM analysis by evaluating spectral features common to many DOM samples. Metrics were evaluated both with and without IFCs. The article will highlight metrics where inner filter effects can be considered negligible with the remaining analysis documented in the Supplemental Information.

3.3 Materials and Methods

3.3.1 DOM Sources

Four DOM isolates provided by the International Humic Substance Society and four surface waters were used in this study. The DOM isolates include: Suwannee River NOM

(SRNOM, 1R101N), Suwannee River Fulvic Acid (SRFA, 1S101F), Suwannee River Humic Acid (SRHA, 2S101H), and Pony Lake Fulvic Acid (PLFA, 1R109F). One surface water, Big Elk Meadows Lake (BEM), was used throughout the study and is from a mountain lake in Colorado located at about 7500 feet above sea level that naturally has a high DOC concentration, low conductivity and low alkalinity. The other four waters, Boulder Reservoir, Betasso Water Treatment Plant influent, Barr Lake and Boulder Wastewater (WW) effluent, were analyzed to augment the FI discussion. All samples were filtered with GF/F 0.7μm filters (Whatman) that were muffled at 550°C for 4 hours and rinsed with 250 mL of 18MΩ-cm lab-grade water (LGW). The DOM isolates and BEM sources were dissolved/diluted with 10 mM, pH 7.5 phosphate buffer using LGW to 8 different concentrations targeting the linear absorbance range according to the Beer-Lambert law (Lakowicz, 2006). The final pH of the dilutions was 7.5±0.15.

After dilution, the solutions had DOC concentrations that ranged from 0.83-40.5 $mg_C\ L^{-1}$, as measured by high-temperature combustion in the presence of platinum catalyst and non-dispersive infrared detection using a non-purgeable organic carbon method (TOC-V_{CSH}, Shimadzu, MD). Samples were analyzed with repeated injections with the criteria that the peak area coefficient of variation was less than 2% or the standard deviation is less that 0.2, which ever was less. The instrument was calibrated with potassium hydrogen phthalate and the study-wide accuracy and precision of 5 $mg_C\ L^{-1}$ standards were both within 5%. The minimum reporting limit was 0.16 $mg_c\ L^{-1}$ following EPA method 415.3.

3.3.2 Fluorescence Spectroscopy Analysis.

Fluorescence EEMs were collected using a spectrofluorometer (John Yvon Horiba FluoroMax-4, NJ). All samples were measured in triplicate with a new sample aliquot for each EEM. Fluorescence intensity was measured during emission scans (300 nm to 550 nm every 2

nm) at set excitation wavelengths in 10 nm increments from 240 nm to 500 nm. A 5 nm bandpass for excitation and emission wavelengths and 0.25 s integration time were used. Fluorescence data were corrected following published methods (Murphy et al., 2010). The EEMs were collected in signal divided by reference mode and incorporated instrument-specific correction factors. Unless specifically stated otherwise for the parallel metrics analysis, all EEMs were corrected for primary and secondary inner filter effects using a UV-Vis absorbance spectrum collected in a quartz cell with a 1 cm path length (Cary-100, Agilent Technologies, CA) (Lakowicz, 2006). EEMs were blank subtracted and Raman normalized based on the Raman peak area for LGW collected at an excitation wavelength of 350 nm (Lawaetz and C. A. Stedmon, 2009). Corrected EEMs are presented in Raman Units (RU). Lamp scans to verify monochromator calibration and cuvette contamination checks with LGW were performed daily. EEMs were corrected and analyzed using MATLAB (Mathworks, MA) software. Specific fluorescence intensities were calculated by dividing the fluorescence intensity by the DOC (RU L mg_c^{-1}). FI was calculated as the ratio of emission intensities at 470 nm and 520 nm at an excitation of 370 nm (Cory et al., 2010). Local total optical density (OD_{Total}) was defined as the sum of absorbance measurements at a fluorescence peak excitation and emission wavelengths, because this quantity determines the magnitude of inner filter corrections applied to the measurements.

3.3.3 Statistical Methods

Coefficient of variation (CV) was used as a comparative metric when triplicate reproducibility was evaluated. For carbon-normalized fluorescence metrics, error propagation using the root mean square approach for the quotient of two measurements was carried out to account for the uncertainty of both measurements (Taylor, 1997). Fluorescence in the Peak B

region for the three Suwannee River isolates was not evaluated due to a lack of local intensity; fluorescence intensity was less than 0.02 RU and did not increase with concentration. Regression and ANOVA analyses were performed at a 95% confidence level. Model adequacy was judged by evaluating the significance of model terms and a residuals analysis. The coefficient of determination, R^2, was not used to judge model adequacy because it cannot identify systematic residuals or curvature.

3.4 Results and Discussion

3.4.1 Method Comparison for Peak Intensity Reproducibility

An intra-laboratory comparison was performed to compare the reproducibility of both peak picking methods to determine if the algorithm-based approach introduced greater uncertainty compared to the fixed wavelength approach. The fixed wavelength method evaluated the CV between triplicates at a fixed point at the center of each peak region Table 3.1.

Table 3.1 Defined peak regions and the coordinates for the center of each region.

Peak	Range	Center Points (Ex, Em) nm	Type
A	Ex: 240-270 nm Em: 380-470 nm	(260, 426)	Humic-like
B	Ex: 260-290 nm Em: 300-320 nm	(280, 310)	Tyrosine-like
C	Ex: 300-340 nm Em: 400-480 nm	(320 440)	Humic-like
T	Ex: 260-290 nm Em: 326-350 nm	(280 338)	Tryptophan-like

Intensities at the center of Peak A and C regions (Table 3.2) were the most reproducible with CVs less than 1% for most samples. As concentration and fluorescence intensity decreased (<1 RU), the CVs increased up to 5% (Figure A.1). Peak T center intensities had more variability with CVs around 3%. These values are in agreement with published fixed point reproducibility

data (Murphy et al., 2010). Intensities at the center of the Peak B region exhibited the worst reproducibility. Samples with ample signal, PLFA and BEM, had an average CV of 9.6%. CVs for the Suwannee River isolates were not analyzed due to insufficient signal in the region. The poor reproducibility in the Peak B region could be attributed to the coincidence with Raman scattering and an inability to remove all scattering effect through blank subtraction. Reproducibility worsened with decreasing concentration (Figure A.1). Analysis of CVs for the algorithm-based method found no appreciable differences in reproducibility for Peaks A, C and T compared to regional center intensities (Table 3.2). Peak B reproducibility improved for PLFA and BEM using an algorithm-based method. The algorithm-based Peak B location lies in the lower right corner of the peak region away from Raman scattering. Therefore, employing the algorithm-based peak picking approach does not impart additional variability that would affect data interpretation.

Table 3.2 Reproducibility of peak intensity based on a fixed wavelength center point and an algorithm-based approach that picks the highest intensity within each peak region based on the average coefficients of variance (CV) for triplicate measurements. Peak B analysis only included PLFA and BEM samples.

	Peak Center Approach		Algorithm-based Approach	
Peak	**Location**	**CV**	**Range**	**CV**
A	(260nm, 426nm)	1.0%	Ex: 240-270 nm Em: 380-470 nm	0.82%
B*	(280nm, 310nm)	9.6%	Ex: 260-290 nm Em: 300-320 nm	2.1%
C	(320nm, 440nm)	0.78%	Ex: 300-340 nm Em: 400-480 nm	0.93%
T	(280nm, 338nm)	2.9%	Ex: 260-290 nm Em: 326-350 nm	4.0%

These observations have implications for how instrument stability and accuracy are evaluated. Quinine sulfate is the most common fluorescence standard used, but it does not fluoresce in the B or T regions. If quantifying fluorescence at the lower wavelengths is a research

objective, then it suggests that an additional standard could be used. Some DOM sources have strong fluorescence intensities in the B and T regions, but many terrestrially-impacted sources do not. Since the coincidence of Raman scattering appears to affect the reproducibility of DOM fluorescence, it would be important for the fluorescence intensity of any standard to be representative of the samples to be analyzed in order to quantify the variability due to Raman scattering effects. The amino acids tyrosine and tryptophan seem like a logical choice for standards that fluoresce in this region, but their high molar absorptivity and quantum yields would lead to problematically low concentrations in order to be representative of DOM fluorescence.

3.4.2 Deviations from the Fluorescence-DOC Linearity Assumption

For a limited concentration range, a linear model adequately describes the relationship between fluorescence peak intensity and DOC concentration with a 95% confidence level and random residuals with respect to the fitted value that are normally distributed (Figure 3.2 and Table A.2). Figure 3.2 illustrates this relationship for the subset of samples with a UV_{254} absorbance less than 0.2 cm^{-1}. Peak B was not included for the three Suwannee River isolates. The slope is dependent on DOM composition. In the humic regions A and C, the two fulvic acid isolates exhibited the highest fluorescence intensity per unit carbon, and the SRHA and BEM isolates had the lowest fluorescence intensity per unit carbon. In the protein-like regions, illustrated in Figure 3.2 for Peak T, PLFA and BEM fluorescence were more sensitive to changes in DOC (steeper slope) compared to terrestrial DOM sources. Regression intercepts were near or below 0.02 RU and most were statistically insignificant.

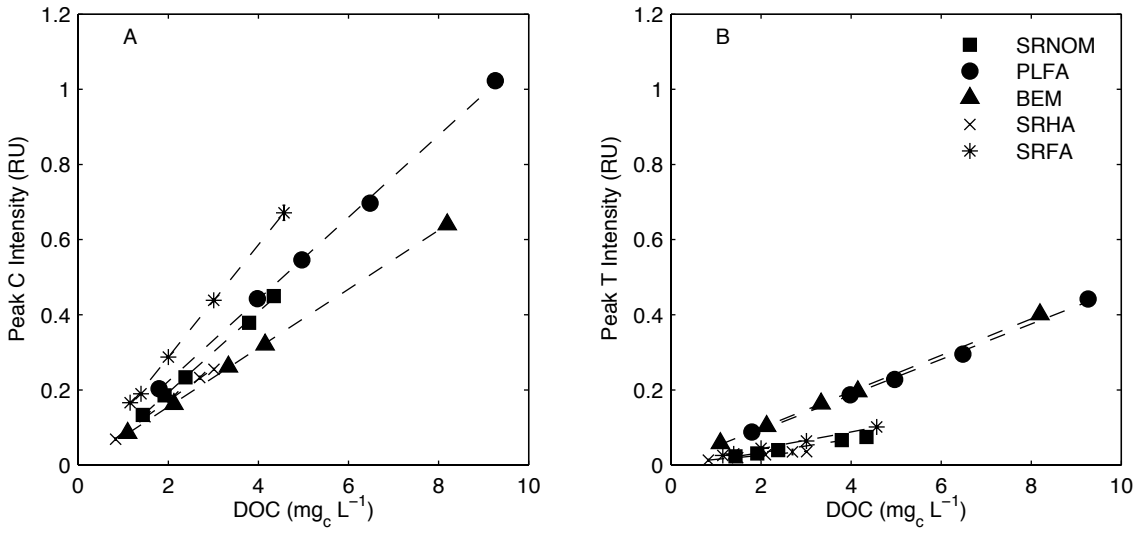

Figure 3.2 Peaks C (a) and T (b) intensity as a function of DOC for five DOM sources. Data is IFC corrected and error bars representing the standard deviation are smaller than marker size.

When higher concentrations are included in the model in a stepwise fashion, the linearity assumption is violated and a non-linearity threshold was identified where residuals showed signs of systematic deviations. All DOM sources showed concave down curvature with the inclusion of increasingly higher concentrations, indicated by a linear model that systematically overestimates the high and low concentrations while underestimating intermediate concentrations. The linearity threshold range was defined by the highest measured concentration that yielded random residuals and the next highest measured concentration with curvature. When a non-linear behavior is first observed, intensity deviations are between 5-10% (Figure 3.3). As higher concentrations are added to the regression, deviations for the lowest concentrations exceed 20% for many DOM sources (Figure A.2 and Figure A.3), and the inclusion of high concentrations acts as a leverage point that skews the predictability at low concentrations. In this study, almost all R^2 values were greater than 0.99 regardless if the regression was fit to 5 low concentrations or across 9 concentrations spanning 40 mg_C L^{-1} with systematic deviations exceeding 30% (Table A.2) and is therefore an inappropriate metric. It was confirmed that UV

absorbance was linearly related to DOC with random residuals at a 95% confidence level throughout the concentration range indicating that there were no deviations from Beer-Lambert law.

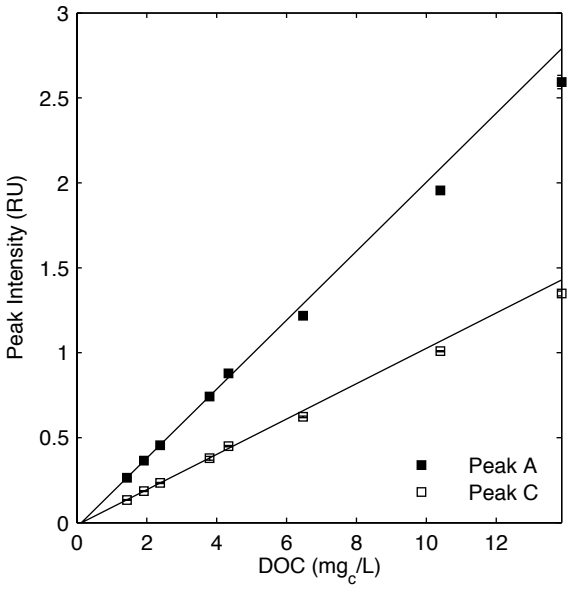

Figure 3.3 Peak A and C intensity as a function of DOC concentration for SRNOM. All data are inner filter corrected and the lines represent a linear model fit to the lowest 5 DOC concentrations. Error bars representing the standard deviation between triplicate measurements may be smaller than the marker.

Comparing the thresholds for each DOM source suggests that deviations occur due to a change in fluorescence quantum yield with increasing concentration. No threshold was found for BEM within the concentration range evaluated, because the sample was not concentrated beyond its environmental DOC concentration. While Peaks A and C demonstrated curvature for SRHA, Peak T never deviated from linearity. Aside from these few exceptions, the results found that all peaks lost linear integrity simultaneously within the same DOC range as summarized in Table 3.3. The lower limit of the DOC threshold range varied between DOM sources (4.3 mg L^{-1} for SRNOM and 13.7 mg L^{-1} for PLFA). Using PLFA and SRNOM as two samples with different absorption behaviors, the local total optical density range that each peak deviated did not overlap

with one another. For PLFA, Peak A deviations occurred with an optical density range of 0.36-0.53 cm^{-1}. SRNOM Peak A deviations occurred in the optical density range of 0.18-0.25 cm^{-1}.

Table 3.3 Thresholds for deviations from linearity for inner filter corrected peak intensities. The lower limit is defined as the highest measured sample with random residuals from linear regression, and the upper limit is the next highest measured sample. OD_{Total} is the sum of the absorbances at excitation and emission wavelengths at the peak center in units of cm^{-1}.

DOM	DOC mg L^{-1}	Peak A OD_{Total}	Peak B OD_{Total}	Peak C OD_{Total}	Peak T OD_{Total}
SRNOM	4.3-6.5	0.18-0.25	BQL	0.09-0.13	0.20-0.28
PLFA	13.2-20.7	0.36-0.53	0.45-0.66	0.18-0.26	0.39-0.58
SRFA	7.1-9.6	0.29-0.40	BQL	0.14-0.20	0.31-0.43
SRHA	4.7-6.0	0.33-0.41	BQL	0.20-0.25	>1.90
BEM	>8.2	>0.18	>0.13	>0.07	>0.17

This observation suggests that absorbance and inner filtering is not the only factor controlling non-linearity as suggested previously (Miller et al., 2010). Comparing Peaks A and C for each DOM source, optical density ranges did not overlap and differed by about a factor of two from each other when linearity is lost. Furthermore, the optical density where SRHA deviates from linearity is almost twice that of SRNOM. These observations suggest that loss of linearity is not solely due to the integrity of inner filter corrections, but that other phenomena contribute. As the concentration increases, the molecular environment and intermolecular interactions, such as electrostatic interactions or collisional quenching, may lead to decreased apparent fluorescence quantum yield by favoring other non-radiative decay mechanisms. Previous results have shown that fluorophores in the A and C regions to be related to one another by exhibiting multiple excitation wavelengths for a single emission wavelength (Li et al., 2013) and support the hypothesis that a change in fluorescence quantum yield could affect the fluorescence across

multiple regions simultaneously. These results suggest that deviations may be insignificant when UV_{254} absorbance is less than 0.2 cm^{-1}.

Many different thresholds have been published regarding fluorescence DOM analysis. The most common ones cited pertain the need for IFCs. Studies have cited a wide absorbance range from 0.05 up to 0.4 for a 1 cm path length below which inner filter effects result in negligible deviations (Baddi et al., 2013; Baker, 2001; Murphy et al., 2013). Inner filter effects are an absorption phenomena that can be calculated using Beer-Lambert Law (Lakowicz, 2006). A total optical density of 0.05 leads to a 6% attenuation of fluorescence, whereas a total optical density of 0.4 leads to 58% reduction in fluorescence. Therefore, any rationalization that IFCs are unnecessary at optical densities above 0.05 cannot be mathematically justified, because the deviations are greater than analytical error. Other studies have cited DOC thresholds between 1 to 20 mg/L below which inner filter effects are said to be negligible (Hudson et al., 2007). Since the specific absorbance differs between DOM, Figure A.8 shows that DOC is a poor predictor of when inner filter effects become important. It is always best to evaluate the need for IFCs using the sample absorbance at the fluorescence wavelengths of interest rather than rely on published heuristics. In addition to these thresholds, Miller et al. (2010) has suggested an absorbance at 254 nm of 0.3 above which samples should not be analyzed *even with inner filter corrections* applied due to an observed non-linear behavior. While these authors attributed the deviations to sample absorbance, the work presented here suggests that there are composition-specific interactions that affect the fluorescence behavior. Table 3.3 also suggests that a more conservative general threshold of 0.2 cm^{-1} may be more appropriate.

The composition-specific, non-linear behavior has implications for both the interpretation of published data and the design of future experiments. It is important to consider how experimental

design affects underlying assumptions and the implications for quantitative results presented. Since only a limited range of isolates was analyzed, an evaluation of DOM-specific concentration effects should be performed prior to quantitative fluorescence work as some DOM may exhibit non-linear behaviors at optical densities less than 0.2 cm^{-1} at 254 nm. These results can also be extended to studies using PARAFAC and FRI. Concentration effects in the raw EEMs will also be apparent in any methods that process them.

3.4.3 Specific Peak Intensity

Several studies have normalized fluorescence intensity by the DOC concentration (or diluted all samples to the same concentration) in an attempt to draw conclusions about compositional differences from a concentration-independent metric but different concentration ranges (and IFC procedures) have been employed (Alberts et al., 2002; Alberts and Takács, 2004; Allpike et al., 2005; Baker et al., 2008; Beggs et al., 2009; Beggs and Summers, 2011; Kalbitz et al., 1999; Miano et al., 1988; Wu et al., 2007). Applications have ranged from fundamental compositional comparisons, estuary studies, relationships with molecular size and applied studies such as the evaluation of chlorine reactivity and DBP formation. Specific peak intensity effectively measures the slope of the line relating fluorescence intensity to DOC concentration. Loss of linearity in this relationship can negate the benefits of a concentration-independent metric.

Fulvic acids had the highest specific intensities in the humic-like regions A and C, consistent with previous studies. Alberts and Takács (2004) demonstrated that humic acids have the lowest specific humic-like intensity and whole water samples have intermediate specific peak intensities. In the protein-like regions, PLFA and BEM had the highest specific fluorescence

intensity indicating that fluorophores in these regions contribute more fluorescence per unit DOC than the other DOM sources (Figure A.5, Figure A.6 and Table A.2).

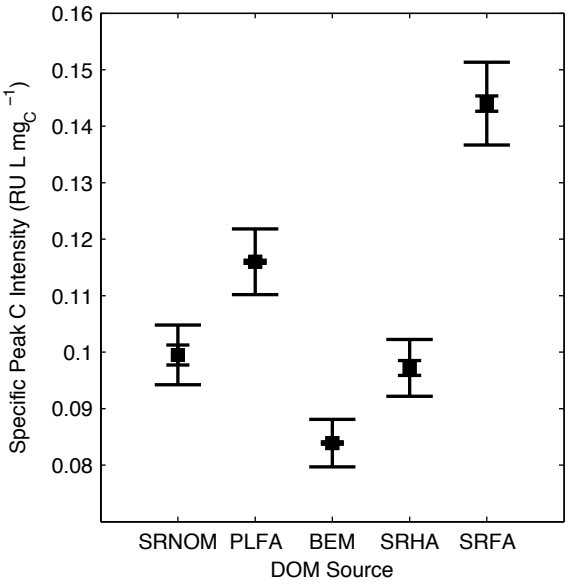

Figure 3.4 Specific Peak C intensity for 5 DOM sources within linear concentration range with IFCs applied. The inner (shorter) error bar represents the uncertainty associated with only fluorescence. The outer (wider) error bar is the uncertainty associated with both fluorescence and DOC measurements.

Before the non-ideal effects are addressed, the reproducibility of specific peak intensity based on the uncertainty of both the fluorescence intensity and DOC concentration was determined. Triplicate measurements in this study found that the uncertainty in the fluorescence measurement is about 1% within the humic-like regions (A and C). Duplicate DOC measurements had relative percent differences between 2-5%. Using a DOC error estimate of 5%, error propagation analysis found that the uncertainty associated with specific peak intensity is driven almost entirely by the uncertainty associated with the DOC measurement for the humic-like peaks (Figure 3.4). When the fluorescence reproducibility is poor, as was the case for BEM in the B region due to the coincidence of the identified peak with Raman scattering (CV=8%), then the associated error is driven by the error in the fluorescence measurement (Figure A.9).

For the humic-like peaks A and C, a change in specific peak intensity that is smaller than the DOC error is most likely due to error and not a change in composition.

Inclusion of DOC uncertainty decreases the ability of specific peak intensity to distinguish compositional differences between most DOM sources (Figure 3.4). When only the fluorescence uncertainty is considered, the specific peak C intensities of SRNOM and SRHA are statistically different from each other ($p=0.04$). With the DOC measurement uncertainty, however, differences in the two specific peak intensities become statistically insignificant ($p=0.11$). Evaluation and clear reporting of error associated with both measurements is important to determine statistically significant changes in specific peak intensity.

Specific peak intensity is sensitive to deviations from linearity. At concentrations above the linearity threshold, specific peak intensity decreases with increasing concentration and may no longer be considered a compositional metrics. Fluorescence intensity deviations increase from about 5% upwards. Initially, the deviation may be indistinguishable from the DOC error contribution but differences become more severe with increasing concentration (Figure 3.5A). For metrics that rely on an underlying linearity assumption, any source of deviation can skew data, impact interpretations and make data between studies incomparable without more information. Diluting samples to the same concentration (say 10 $mg_C\ L^{-1}$) does not negate the need to consider concentration effects (or apply IFCs) because the magnitude of deviations depends on both composition and concentration.

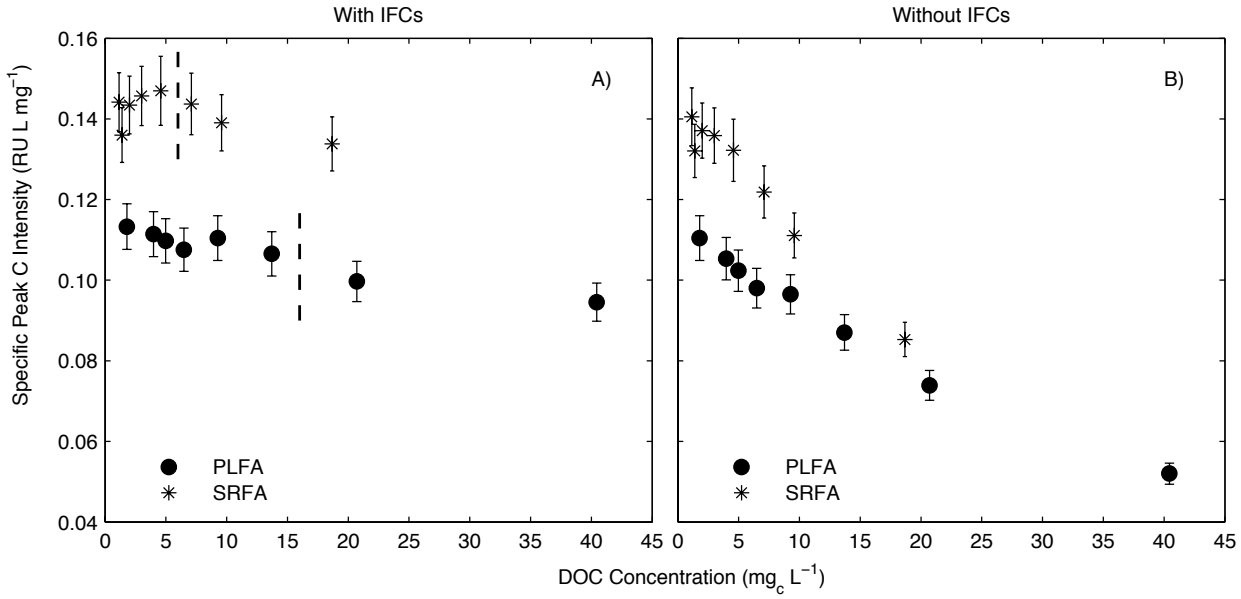

Figure 3.5 Specific Peak C intensity across the full range of concentrations for SRFA and PLFA. Error bars represent the combined error associated with DOC and fluorescence error. The linearity threshold for each DOM is indicated by the dashed line in subplot A.

If IFCs are not applied, then specific peak intensity cannot be considered a compositional metric at any reasonable concentration. Figure A.7 showed that the same 5% deviations arising from concentrated solutions also occur at a UV_{254} absorbance greater than about 0.05 cm^{-1}. As a result, there is a strong correlation between specific peak intensity and concentration throughout the entire applicable range for most freshwater samples (Figure 3.5B).

Specific peak intensity and peak ratios are both compositional metrics that are commonly used but each has their own advantages and disadvantages. Since fluorescence generally has better reproducibility than DOC, the ratio of peak intensities will likely have less uncertainty and be more sensitive to changes in composition compared to carbon-normalized metrics. Peak ratios, however, only have the ability to characterize compositional changes within the small fraction of DOM that actually fluoresces. Specific intensities provide additional insight by describing the

fluorescence behavior relative to the total amount of organic matter in the system, fluorescing and non-fluorescing.

3.4.4 Peak Location Analysis

Reproducibility was evaluated for peak location measurements identified using the algorithm-based approach. Since the excitation scan increment was large (10 nm), the standard deviation between identified peak excitation wavelengths was small due to a lack of resolution. The emission scan increment was 2 nm, which is smaller than the emission bandpass of 5 nm. A Bandpass greater than the emission increment has been commonly applied in literature for DOM characterization (Goldman et al., 2012; Kraus et al., 2010; McKnight et al., 2001; Sanchez et al., 2013). With these settings, it is difficult to resolve peak emission wavelength, which leads to variation in peak location between samples and is tabulated in Table 3.4. The error associated with peak emission wavelength is important for interpreting results, especially for developing quantitative relationships or identifying compositional differences as has been done based on Peak C emission wavelength (Baker et al., 2008; Senesi et al., 1991). The range of Peak C emission wavelengths across DOM end members (PLFA and SRHA) is about 50 nm. Some papers examining rather homogenous waters report ranges of emission wavelengths closer to 10-20 nm (Alberts et al., 2004; Bieroza et al., 2011; 2009; Glover et al., 2005; Jaffe et al., 2004). With an average sample standard deviation of 2.5 nm, the confidence interval for triplicate measurements is ± 6nm at a 95% confidence level (Type I error), which may limit interpretation if samples are not statistically different. The uncertainty and low resolving power associated with using large bandpasses may also affect component spectra in PARAFAC models.

Table 3.4 Peak location as determined by an algorithm-based approach that picks the maximum intensity in each region. Only samples below linearity threshold with IFCs were used for each water (n=15).

	Peak A		Peak B	
Water	**Ex (nm)**	**Em (nm)**	**Ex (nm)**	**Em (nm)**
SRNOM	250.0 ± 0.0	461.5 ± 5.0	BQL	
PLFA	250.0 ± 0.0	446.4 ± 4.5	270.0 ± 0.0	315.3 ± 4.8
SRFA	250.0 ± 0.0	455.9 ± 6.7	BQL	
SRHA	250.0 ± 0.0	465.7 ± 2.1	BQL	
BEM	250.0 ± 0.0	434.9 ± 4.4	278.7 ± 3.5	313.5 ± 2.8

	Peak C		Peak T	
Water	**Ex (nm)**	**Em (nm)**	**Ex (nm)**	**Em (nm)**
SRNOM	322.0 ± 4.1	450.3 ± 3.3	260.0 ± 0.0	349.9 ± 0.5
PLFA	300.0 ± 0.0	426.1 ± 2.9	260.0 ± 0.0	349.9 ± 0.5
SRFA	320.0 ± 0.0	448.3 ± 2.8	260.0 ± 0.0	349.8 ± 0.6
SRHA	300.0 ± 0.0	477.5 ± 2.4	260.0 ± 0.0	349.2 ± 1.7
BEM	300.0 ± 0.0	424.5 ± 2.2	260.7 ± 2.6	348.8 ± 3.6

If peak emission wavelength is to be used as a metric for detecting changes in DOM composition, sample size and the prevalence of Type II error become important. Type II error is the failure to detect a change in a parameter. For this scenario, it is the risk associated with failing to recognize a shift in emission wavelength when a change in composition has shifted the peak emission. Operating characteristic curves are commonly used to determine the sample size necessary to be able to detect parameter differences with a small probability of Type II error. To illustrate, with a significance level of 0.05 (α) and power of 0.9 ($1-\beta$), the number of replicates required to detect a difference between two samples can be determined using an estimated standard deviation of 2.5 nm. The operating characteristic curves, Figure A.10, show that to detect a shift of 5 nm (equal to the bandpass), 6 replicates need to be collected. If duplicate EEMs are collected, only a shift of 12 nm is detectable with any certainty. These results

emphasize the need to understand how the error associated with fluorescence metrics impact interpretations.

Since DOM generally has a broad, featureless fluorescence spectra, many DOM sources do not exhibit an absolute peak maximum in the regions outlined by Coble (1996). The peak location relative to the region boundary was evaluated to determine the validity of reporting peak location and its implications for algorithm-based peak picking methods. Only samples below the linearity threshold were included in the analysis. For the Peak T region, 99% of the identified peaks occurred along the region's boundary, specifically the corner adjacent to the Peak A region. Regardless of DOM composition, Peak A fluorescence was dominant and inhibits the ability of extracting useful information about Peak T from its location. For DOM sources that lack significant signal in the Peak B region (SRNOM, SRHA and SRFA), algorithm-based peak picking approaches yield maximum intensities that lie along on boundary near the lower right corner for 98% of samples, indicating the heavy influence from the Peak A region. For BEM and PLFA with strong fluorescence in this region, only 33% of the peaks fall along the region's boundary. For a quantitative analysis of intensities in the B and T regions to be representative of the region as a whole, a static point in the center of each region or regional integration approach may yield a more representative intensity.

For the humic-like peaks, the maximum intensity in Peak A region occurred on a boundary less than 10% of the time. Peak C maxima occurred on boundaries in 61% of EEMs. PLFA, SRHA and BEM maxima fell along the 300 nm excitation boundary that is illustrated by the presence of a broad shoulder instead of a local maximum. Past work has indicated that there is often a correlation between Peak C excitation wavelength and emission wavelength that is attributed to the charge transfer interactions between donor and acceptor groups (Boyle et al.,

2009; Del Vecchio and Blough, 2004). As a result, the user-defined region, especially the lower excitation boundary, can bias the reported results for peak emission wavelength between studies.

The results in this section are important for both the direct application of reporting peak position but also for reporting peak intensities using the algorithm approach. Since many of the algorithm-identified peaks fall on a region boundary, it is important to report the region boundaries and provide a perspective as to how the boundaries may introduce bias into the reported peak intensities. Additionally, some methods define a single excitation wavelength and range of emission wavelengths to identify peaks (Cottrell et al., 2013). These methods are also biased by the subjectivity of selecting the excitation wavelength when there is no absolute maximum in the EEM.

3.4.5 Fluorescence Index

FI has been correlated to DOM aromaticity and is often used as an indicator of DOM origin (McKnight et al., 2001). PLFA and BEM had the highest FIs around 1.45, indicating lower aromaticity, and SRHA had the lowest FI around 1.06, indicating higher aromaticity, with the other Suwannee River samples falling in between (Figure 3.6). When applied to the linear concentration range, FI had the best reproducibility of any of the fluorescence metrics examined with CV values between triplicate measurements at about 1% (σ=0.02), consistent with past research (Murphy et al., 2010).

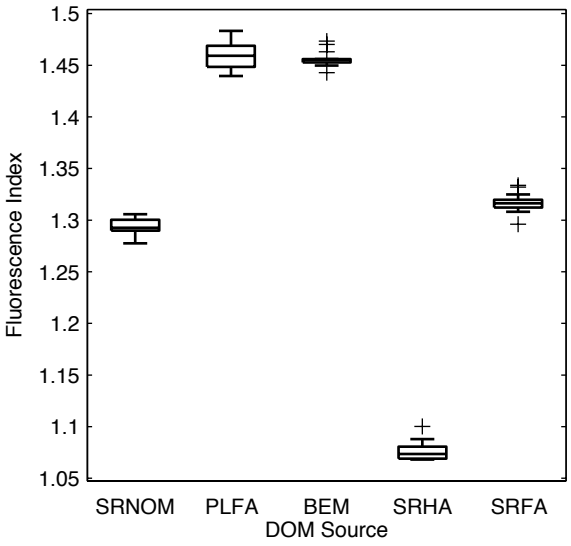

Figure 3.6. FI for different DOM sources using the I_{470}/I_{520} at an excitation of 370 nm for samples within the linear regime. All data is inner filter corrected. Box edges define the 25th and 75th percentiles. The centerline marks the median and the whiskers mark ±2.7σ.

Regression analysis found that there is a negative correlation between FI and DOC concentration ($p<0.01$) for SRNOM, PLFA, SRHA and SRFA with slopes around $5x10^{-3}$ (Figure 3.7 and Table A.3). While the ratio of two fluorescence or absorbance measurements is generally applied as a concentration-independent metric, past work on other optical ratios, such as the E4:E6, has shown a concentration dependence at low concentrations (Summers et al., 1987). The FI-DOC slope is small with respect to typical FI values. If the concentration dependence is ignored, the CVs between all samples across the linear range were about 1.3%. This result implies that over a narrow range of concentrations, the correlation with DOC may be insignificant compared to experimental random error. Application over a wide range of concentrations would limit the sensitivity of this metric and its ability to track compositional changes.

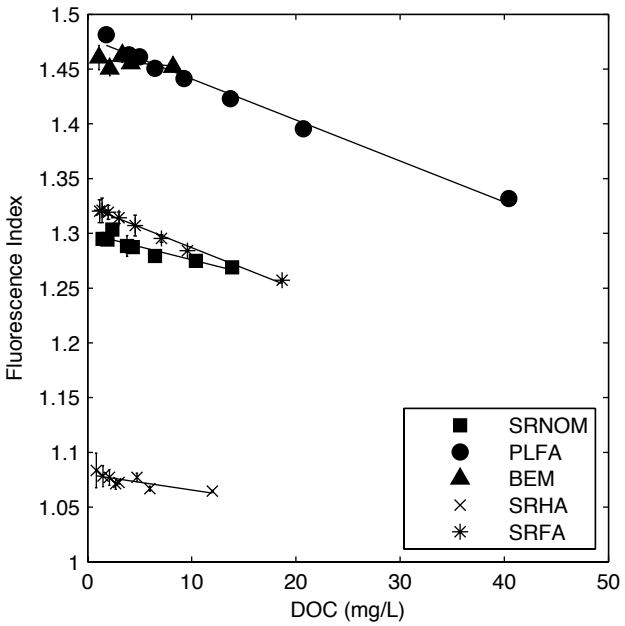

Figure 3.7. Fluorescence index as a function of DOC concentration with inner filter corrections applied.

If IFCs are not applied, there is a systematic decrease in fluorescence index across all concentrations due to the small differences in optical density at each emission wavelength. At the lowest measured concentrations, the shift is smaller than the experimental error between replicate measurements. The decrease due to IFCs exceeds the replicate standard deviation of 0.02 at concentrations above the linear threshold where there is also evidence of non-ideal interactions. When the UV_{254} absorbance is below about 0.2 cm^{-1}, FI may be applied without inner filter corrections with little bias, which may be important for online monitoring applications. On-line measurements have additional experimental artifacts to correct for because sample absorbance, turbidity and temperature are variable and require additional corrections (Downing et al., 2012). Probes monitoring FI could monitor compositional changes and eliminate the need to measure and correct for absorbance.

The FI for SRHA is low because the emission peak falls almost equidistant between the two indices Figure A.11. While FI has been described as the slope of an emission curve, past work has reported fulvic acid maximum emission wavelengths less than 470 nm leading to indices that lie on either side of the emission maximum (Cory et al., 2010). The effect of index location relative to the emission peak was explored. Figure 3.8 shows that FI depends on both the slope of the emission curve and the position of the emission peak. For a given DOM, FI increases as the points used to calculate it shift to longer wavelengths away from the peak (spaced 50 nm apart). The concept of using the ratio of two emission intensities as a surrogate for peak emission location has also been suggested before for a different application (Perrette et al., 2005). If FI were calculated in the same location relative to the peak maximum (i.e., distance = 0 nm), microbially dominated waters (high FI) would have a steeper sloped emission curve compared to terrestrial end members (low FI). Using a one-way ANOVA analysis for local curvature calculated at a range of locations relative to the emission peak, however, SRFA and PLFA are indistinguishable based on local curvature alone. If the emission peaks are overlaid with peak maxima set at 0 nm, the FI indices can fall within a relatively large range of emission wavelengths delineated in Figure 3.9 and still yield slopes that are statistically the same. SRFA's lower FI using the I_{470}/I_{520} metric is caused by the red-shifted peak and the difference in relative location where FI is measured. Conversely, Figure 3.8 also shows that the slope of Boulder WW effluent 's emission curve is shallower than that of Barr Lake, but its I_{470}/I_{520} FI is greater due to the blue-shifted (lower wavelength) peak emission.

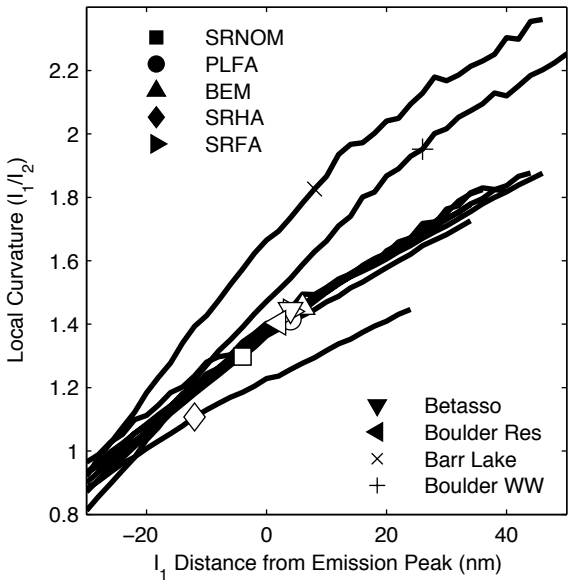

Figure 3.8 Local curvature as a function of location relative to the peak emission. Local curvature is the ratio of two intensities (I_1/I_2) spaced 50 nm apart with I_1 occurring at the lower wavelength. The x-axis refers to the position of I_1 relative to the emission peak. A distance of 0 nm means that the I_1 is located at the peak and the second is located 50nm higher. The markers indicate where FI is calculated using the I_{470}/I_{520} ratio according to Cory et. al.. All FIs are measured at an excitation wavelength of 370 nm.

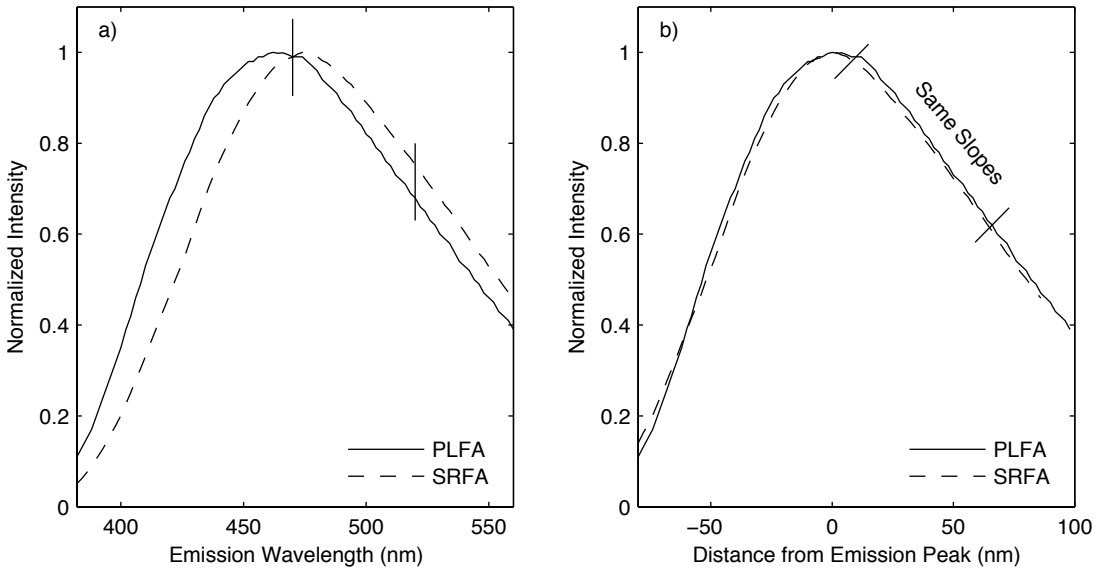

Figure 3.9 Normalized emission spectra at an excitation of 370 nm plotted according to a) emission wavelength and b) relative to peak emission wavelength. The lines in plot a) indicate the location of the I_{470} and I_{520} and in b) the range of emission wavelengths where the slopes calculated 50 nm apart are statistically the same.

Peak emission wavelength as the driver for FI is in agreement with the published relationship between FI and aromaticity (McKnight et al., 2001). Comparing the peak emission wavelength to published aromatic carbon data for the IHSS standards (Thorn et al., 1989), DOM isolates with higher degrees of aromaticity have emission peaks shifted to longer wavelengths (Table A.1). This shift decreases the FI regardless of local curvature.

These results demonstrate that FI is an intrinsic metric with good reproducibility but its application effectively measures changes in both peak emission wavelength and to a lesser degree local curvature. Since there are numerous combinations of peak position and curvature that can yield the same FI, peak position should be compared alongside FI before concluding that there is no change in FI or composition.

The analysis of how both peak position and spectral shape affect the reported ratio of emission intensities can be extended to other similar metrics. The biological index (BIX)

evaluates the ratio of two intensities on either side of the emission maxima at an excitation of 310 nm and has been described as representing the breadth of an emission peak (Huguet et al., 2009). The spectral features at 310 nm are similar to those at 370 nm in that there is a single broad emission peak (Huguet et al., 2009). The general relationship depicted in Figure 3.8 shows that both emission peak position and width would also contribute to BIX.

3.4.6 Fluorescence Metrics and Property Balance Principles

A composite scenario was tested to highlight some of the advantages and disadvantages of metric selection. PLFA and SRHA were mixed together in a series of ratios ranging from 0% PLFA to 100% PLFA and at values below a UV_{254} of 0.2 cm^{-1}. Figure 3.10 shows that peak intensity varies linearly with composition ratio, and that these ratios could be predicted using a property balance. It is important to note that this relationship is true only because neither SRHA nor PLFA exceeded its threshold for concentration effects, and there are no additional interactions affecting the fluorescence quantum yields. The DOC error associated with specific peak intensity is large with respect to the difference between end members reducing its sensitivity as depicted by the large error bars in Figure A.12. FI does not follow property balance principles, because both peak emission wavelength and local curvature vary simultaneously (Figure 3.8). The rate at which these parameters change is not proportional to the composite ratio like the other metrics. Figure A.13 shows a large decrease in peak emission wavelength and increase in curvature occurred between 0% PLFA (100% SRHA) and 25% PLFA, but only incremental changes were observed as the proportion of PLFA is increased from 25% up to 100%. Due to the similar spectral features, BIX likely does not follow property principles either. These results show that peak intensity or specific peak intensity may be a more appropriate

metric for composite ratio studies, such as the confluence of two rivers, compared to fluorescence index.

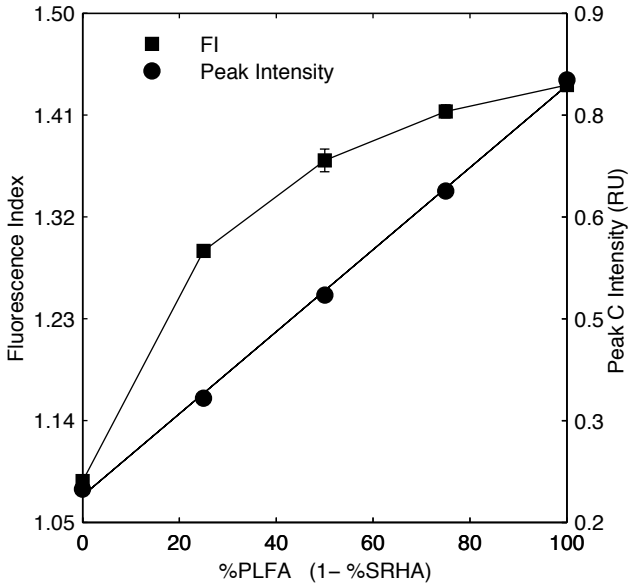

Figure 3.10 Fluorescence index and Peak C intensity as a function of composite ratio between SRHA and PLFA. Error bars representing the standard deviation may be smaller than the marker.

3.5 Conclusions and Recommendations

Fluorescence spectroscopy can be a valuable tool for characterizing DOM in natural and engineered systems but careful consideration for analysis and data interpretation is necessary. There was no appreciable difference in reproducibility between the different peak picking methods commonly used, except in the analysis of the Peak B Region, likely due to the coincidence with Raman scattering. As a result, when reporting intensities in this region, regional uncertainty should be evaluated with DOM-representative samples. The linear relationship between fluorescence and concentration is only valid across a narrow concentration range and is composition-specific. For metrics that depend on an underlying linearity assumption, validation of this assumption should be established, especially for studies that span a wide concentration range or involve high optical densities where deviations are likely to be greater. Specific peak

intensity can provide information about DOM compositional changes as an intrinsic metric but the error associated with DOC measurements limits its sensitivity. Interpretation of compositional differences should include an evaluation of DOC concentration uncertainty.

Care must be taken in interpreting the peak position within predefined peak regions as they may be heavily influenced by the presence of dominant neighboring fluorophores and the user-defined regions. The boundaries for algorithm-based peak picking methods should be reported as well as their impact on both peak intensity and position results. Fluorescence index is largely driven by the location of the indices relative to the emission maxima. Quantitative interpretation of FI should consider that FI does not follow conservative property balance principles, and the change in FI may not be representative of the degree to which the mass composition has changed.

Chapter 4 Fluorescence characterization of humic substance coagulation: Application of new tools to an old process

The work in this chapter has been published as:
Korak, J.A., Rosario-Ortiz, F.L., Summers, R.S., 2014. Fluorescence characterization of humic substance coagulation: Application of new tools to an old process, in: Rosario-Ortiz, F.L. (Ed.), Advances in the Physiochemical Characterization of Dissolved Organic Matter. American Chemical Society. In Press.

4.1 Abstract

A classic process, the coagulation of humic and fulvic acids, is revisited in this chapter using contemporary fluorescence methods to characterize dissolved organic matter (DOM) removal. Different fluorescence metrics are explored and their insights into DOM behavior highlighted. Peak picking and fluorescence regional integration methods are compared and suggest that integrated data does not provide additional insight beyond simple peak picking approaches. The limitations of analyzing only fluorescence intensities are highlighted, because it is difficult to separate changes in DOM quantity, quality, and other interactions. While all methods captured the interactions between DOM and aluminum species before physical removal, quantum yields and fluorescence index (FI) offer more information regarding compositional changes. Finally, this study also provides evidence that ascribing the chemical significance of humic acid-like and fulvic acid-like is flawed and unsupported for aquatic DOM.

4.2 Background

The coagulation of humic substances has been an area of active research since the early 1960s. The earliest endeavors were motivated by the removal of color from drinking water sources. With the discovery of haloforms in drinking water (Rook, 1976) and the eventual link between disinfection byproducts and humic materials established (Rook, 1977), the motivation for dissolved organic matter (DOM) removal shifted from aesthetic purposes to public health protection. Research ensued investigating the removal of humic and fulvic acids by coagulation.

Two comprehensive research reviews with identification of knowledge gaps were published in 1979 and 1988 (AWWA Research Committee on Coagulation, 1979; Randtke, 1988).

When this process was initially investigated, the analytical methods for characterizing the processes were limited compared to today's capabilities. The main surrogate parameters for water quality analyses were turbidity, color, total organic carbon, total trihalomethane formation potential and UV absorbance at 254 nm (UV_{254}) (Edzwald et al., 1985). The quantification of DOM often relied on absorption measurements coupled with calibration curves rather than direct organic carbon measurements (Edzwald, 1978; Hall and Packham, 1965).

Analytical methods have improved dramatically since then providing new tools for DOM characterization. Fluorescence spectroscopy started to gain popularity in the late 1980s/early 1990s to characterize soil derived organic matter (Senesi et al., 1991; 1989). The use of excitation-emission matrices (EEMs) to characterize DOM was introduced in 1990 and demonstrated that these heterogeneous mixtures show general similarities in their fluorescent material (Coble et al., 1990). Methods for analyzing fluorescence EEMs have developed over the past 30 years yielding techniques such as peak picking (Coble, 1996), calculation of quantum yields (Green and Blough, 1994), fluorescence regional integration (FRI) (Chen et al., 2003), and DOM-specific indices, such as fluorescence index (FI) (McKnight et al., 2001) and humification index (HIX) (Zsolnay et al., 1999).

4.3 What are Humic and Fulvic Acids?

Since DOM is a heterogeneous mixture, its fractionation based on chemical characteristics has been widely used to better understand the complex behaviors of whole waters by attributing certain behaviors to distinct fractions. Thus, humic and fulvic acids have been at the center of DOM research for decades. Whether the process of interest is a water treatment unit

operation or the fate and transport of contaminants in the environment, DOM research has a pattern of investigating specific topics using well-characterized fractions and then extrapolating analyses to whole water samples in the environment. This chapter will only discuss aquatic DOM, humic acids and fulvic acids. It should be noted that soil organic matter and aquatic organic matter, while still containing humic and fulvic acids, exhibit different characteristics. The interpretation and discussions herein should not be extrapolated to soil-derived humic and fulvic acids.

Aquatic humic and fulvic acids have been defined using a variety of criteria. One of the simplest definitions is that a humic acid is soluble in basic conditions but insoluble in mineral acid, whereas a fulvic acid is soluble in both (AWWA Research Committee on Coagulation, 1979; Edzwald, 1978). Other methods define humic substances (humic and fulvic acids combined) as organic matter that adsorbs onto an XAD-8 resin and desorbs with sodium hydroxide. Once eluted, the humic acid fraction precipitates at pH 1 while the fulvic acid fraction remains soluble (Leenheer, 2009). The International Humic Substances Society (IHSS) has adopted an XAD-8 method with cation exchange, but explicitly states that they do not endorse their own method as "the best" in the hope that research will continue.

In any case, it is important to note that these operationally defined DOM fractions are based on differences in chemical characteristics. Humic and fulvic acids, which elute together as hydrophobic acids before precipitation, account for about 60% of the DOC in a freshwater sample, but the mass ratio of fulvic acids to humic acids is about 3:1 (Perdue and Ritchie, 2009). The average molecular weight of humic acids is larger than that of fulvic acids and unfractionated DOM (Perdue and Ritchie, 2009). While the range of aromatic carbon content can vary greatly across waters (Perdue and Ritchie, 2009), within one water the humic acid fraction

typically has a higher percentage of aromatic carbon compared to fulvic acids and unfractionated DOM (Thorn et al., 1989). The increased aromaticity in humic acids is manifested as a higher specific UV_{254} compared to fulvic acids and unfractionated waters (Weishaar et al., 2003). While humic acids absorb more light per unit carbon, fulvic acids fluoresce more light per unit carbon (Alberts and Takács, 2004; Korak et al., 2014a). The fluorescence quantum yield, fraction of light emitted relative to the light absorbed, of fulvic acids is greater than the quantum yield of humic acids (Del Vecchio and Blough, 2004). Therefore, these fractions have different chemical characteristics and would be expected to behave differently.

In this chapter, we revisit a classic drinking water treatment process, the coagulation of humic and fulvic acids, but characterize DOM removal using contemporary fluorescence spectroscopy methods. We investigate three questions: What insight do fluorescence techniques give to the DOM coagulation process? How do these methods of analyzing fluorescence data reveal different aspects of the process? And what light does this classic process shed on prevailing interpretations of fluorescence data?

4.4 Materials and Methods

4.4.1 Materials

Three IHSS standards were used in the study: Suwannee River Natural Organic Matter (SRNOM, 2R101N), Suwannee River Fulvic Acid (SRFA, 1S101F) and Suwannee River Humic Acid (SRHA, 2S101H). Each isolate was dissolved in de-chlorinated tap water. Divalent cations and other inorganics can affect coagulation (Randtke, 1988); so de-chlorinated tap was used in order to have a naturally occurring balance of inorganic ions and alkalinity. The water was prepared by passing Boulder, CO municipal drinking water through a 200 L barrel of granulated activated carbon (Norit 1240, 12×40 US standard mesh size, bituminous) with an empty bed

contact time of 10 minutes followed by a 25 μm cartridge filter (Pentek DGD-7525-20) to remove particles. The finished water has a dissolved organic carbon (DOC) concentration less than 0.1 mg_C/L, UV_{254} absorbance less than 0.001, and no detectable fluorescence. Absorbance values are reported as unitless numbers. The water had an alkalinity of 29 mg/L as $CaCO_3$ and conductivity of 136 μS. The water quality values after the isolates were dissolved in the de-chlorinated tap water are shown in Table 4.1. The initial UV_{254} absorbance values of the dissolved isolates were below 0.2 to minimize non-ideal, concentration-dependent fluorescence behaviors (Korak et al., 2014a).

4.4.2 Coagulation Methods

Coagulation studies were performed using a programmable jar tester (Phipps & Bird) in 1L volumes with alum (aluminum sulfate, Al_2SO_4-$16H_2O$) at doses of 5, 10, 14, 18 and 20 mg/L as alum. Mixing conditions included a rapid mix period (1 minute at 290 rpm), two flocculation phases (10 minutes at 55 rpm and 10 minutes at 20 rpm) and a sedimentation period (30-minutes with no mixing). The supernatant was filtered through pre-combusted (500°C for 4 hours in a muffle furnace) and rinsed 0.7 μm GF/F filters (Whatman) prior to DOC, UV and fluorescence analyses. All samples were stored in pre-combusted amber bottles, refrigerated until use and analyzed within 7 days.

Table 4.1 Summary of initial water quality characteristics for each isolate in solution

DOM	pH	Alkalinity mg/L as $CaCO_3$	DOC mg_C/L	UV_{254}
SRNOM	7.6	27	3.4	0.133
SRHA	7.6	26	3.0	0.197
SRFA	7.5	28	3.7	0.157

4.4.3 Analytical Methods

Alkalinity was measured using a Hach digital titrator (Model 16900-01) with manufacturer specified methods. pH was measured on a Fisher Scientific Accumet AB15 meter. DOC was analyzed on a Shimadzu TOC-V_{CSH} using a high temperature combustion non-purgeable organic carbon method. Duplicates were measured on 7 of the 19 samples (37%). For samples with a DOC greater than 1 mg_C/L, the differences in concentration were less than 0.2 mg_C/L. For samples with a DOC less than 1 mg_C/L, the difference in duplicates was less than 0.1 mg_C/L. UV absorbance was measured on a Cary Bio 100 (Agilent Technologies, CA) from 200 to 600 nm in a 1 cm path length quartz cuvette and baseline corrected to deionized water. Replicate UV_{254} measurements had coefficient of variance values less than 1%.

Fluorescence excitation-emission matrices (EEMs) were collected on a spectrofluorometer (Fluoromax-4, John Yvon Horiba, NJ). Excitation wavelengths were incremented from 240 to 450 nm in 10 nm steps. Emission scans were collected from 300 to 560 nm in 2 nm increments. Both excitation and emission bandpass settings were set to 5 nm, and the integration time was 0.25 s. Intensities were collected in ratio mode (signal divided by reference), and instrument-specific correction factors were applied. All EEMs were blank subtracted, corrected for primary and secondary inner filter effects and normalized to the Raman area of deionized water at 370 nm. Lamp scans, cuvette contamination checks and Raman scans were performed daily to ensure proper operation. The average relative percent difference (RPD) between duplicate peak intensities (A and C) and normalized integrated fluorescence volumes (V_{III} and V_V) were 3.3% and 2.7%, respectively. The average RPD between FI values and maximum quantum yields were 0.3% and 4.6%, respectively.

4.5 Results and Discussion

4.5.1 DOC and UV_{254} Removal

Using the classic assessment with DOC and UV measures, the coagulation of the SRHA, SRFA and SRNOM as a function of coagulant dose is shown in Figure 4.1. At low coagulant doses (alum $\leq$ 14 mg/L), there is little change in both DOC and absorbance. At a dose of 18 mg/L, there is a large and abrupt removal of both UV and DOC from solution, which is similar to that previously observed with other humic substances (Dempsey et al., 1984; Edzwald, 1978; Narkis and Rebhun, 1977; Randtke and Jepsen, 1981). In general, UV absorbance is removed to a greater extent with 55 to 90% removal compared to DOC with 40 to 70% removal (Babcock and Singer, 1979). At the same dose, SRHA is more amenable to removal compared to SRFA or SRNOM (Hall and Packham, 1965).

The pattern of removal depicted in Figure 4.1 has been referred to as Type I coagulation as opposed to Type II, which elicits a more regular dose response behavior (Randtke, 1988). The mechanisms for removal are complex and depend on not only the DOM present but also if it behaves as a truly dissolved species or more like a colloid. Other factors that affect removal mechanisms include turbidity, pH and background water constituents (Randtke, 1988). If it is assumed that the material is predominantly dissolved, then removal was likely a combination of aluminum-humate/fulvate precipitation and adsorption, where humic substances adsorb onto aluminum hydroxide particles, based on the study pH range of 7.3-7.6 (Randtke, 1988).

DOC and UV measurements only provide a narrow glimpse into this process. They provide little insight into the interactions between DOM and aluminum species at low coagulant doses where there is no apparent change in either measurement.

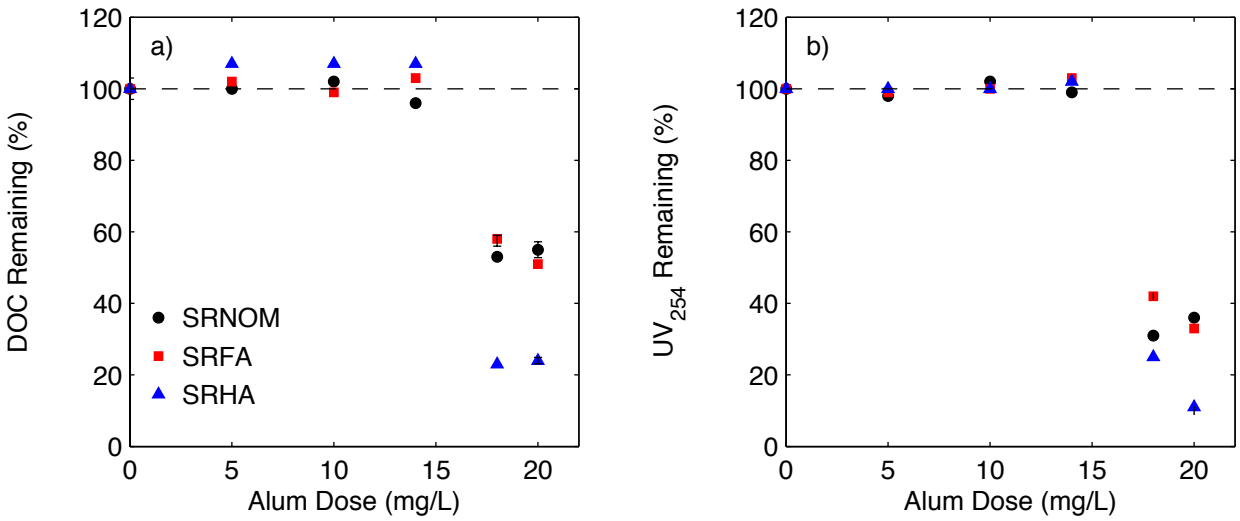

Figure 4.1 Relative remaining amount of a) DOC and b) UV254 as a function of alum dose. Error bars represent the standard deviation between duplicates but most are smaller than the marker size.

4.5.2 Fluorescence Analysis

Many different methods have been developed for analyzing fluorescence data for DOM characterization. Table 4.2 presents initial water quality fluorescence measures using several different methods. In the following sections, we will explore these methods for analyzing fluorescence data with respect to this process and identify how each method provides different insight into the process.

Table 4.2 Summary of initial fluorescence metrics for the isolates in solution including peak intensities (A and C) in Raman units (RU), regional integration areas (III and V), FI and maximum quantum yields.

DOM	Intensity (RU)		FRI Volume (RU nm^2)			
	A	C	V_{III}	V_V	FI	Φ_{max}
SRNOM	1.47	0.46	44780	14353	1.34	0.014
SRHA	0.97	0.34	30010	10606	1.14	0.0048
SRFA	1.71	0.57	52842	17154	1.35	0.015

4.5.3 Fluorescence Intensities

One of the most common ways to analyze fluorescence data is to track how the fluorescence intensity changes. There are two prevailing methods. The first includes peak picking approaches where regions of interest are identified and then a single intensity from each region is extracted. Most peak picking methods follow the peak regions identified by Coble, because each region has been associated with a particular chemical significance (Coble, 1996). Peaks A and C, outlined in Figure 4.2a, have been associated with humic-like fluorescence. Coble states, "The overall similarity between the humic substance XAD extract and the other samples is the basis for referring to both peaks as humic-like" (Coble, 1996). The authors interpret this to refer to humic substances in general and not the humic acid fraction because no further distinction is made in that study. Peaks B and T (not shown) have been associated with the phenolic and indolic functional groups in the amino acids tyrosine and tryptophan, respectively (Coble, 1996). In this study, the reported peak intensities are the maximum from each region, many of which fall on a region boundary due to the shape of the EEM contours.

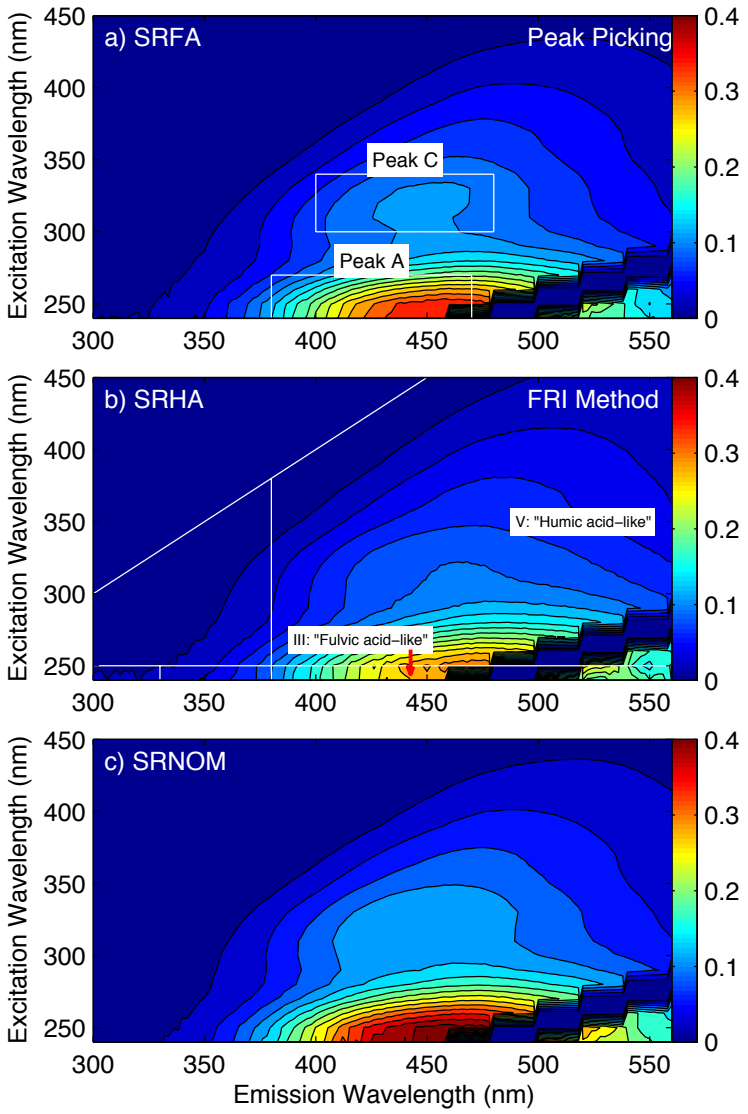

Figure 4.2. EEMs for a) SRFA, b) SRHA and c) SRNOM. Intensities are normalized to DOC concentration in units of RU L/mg$_C$. Peak picking regions A and C are outlined in a). The FRI regions are outlined in b) with the commonly ascribed chemical significance of humic acid-like and fulvic-acid like.

Chen et al realized that extracting a couple intensities from an entire EEM only provides a limited view, because it cannot capture how the contours are changing, and developed the fluorescence regional integration (FRI) method (Chen et al., 2003). This method slices the EEM into five regions (Figure 2b) and integrates each region yielding fluorescence volumes. To account for differences in region size and wavelength increments, the data is normalized based

on the fractional projected areas. The results can either be presented on a magnitude basis ($V_{i,n}$) or on a percent basis compared to the total integrated volume ($P_{i,n}$). The Greek capital letter phi is normally used to indicate the integrated volume (Chen et al., 2003). The letter V is used here as to not confuse this notation with quantum yield notation that also uses the same letter.

If both approaches are applied to this example, fluorescence reveals a more complex behavior compared to DOC or UV_{254} absorbance alone. Figure 4.3a and Figure 4.3b depict Peaks A and C intensities as a function of alum dose and show that there is a monotonic decrease in fluorescence intensity across the entire dose range. Figure 4.3c and Figure 4.3d present the same behavior in terms of the normalized integrated volumes ($V_{III,n}$ and $V_{V,n}$). At low alum doses, where DOC and UV showed little change, fluorescence decreases indicating that the interactions between DOM and aluminum species cause a quenching of fluorescence intensity. This phenomenon has been well documented elsewhere (Cabaniss, 1992; Elkins and Nelson, 2002; C. Sharpless and McGown, 1999). One notable difference is the pH. Most studies investigating the interactions between aluminum species and humic substances hold the pH in the 4 to 5 range to limit the analysis to free aluminum in solution (Elkins and Nelson, 2002; Luster et al., 1996; Ohno et al., 2008; Sharpless and McGown, 1999). At pH values between 7.3 and 7.6 measured during this study, the aluminum equilibrium is dominated by aluminum hydroxide species ($Al(OH)_3$) (Elkins and Nelson, 2002). Cabaniss (1992) demonstrated similar quenching of fulvic acid fluorescence at pH 7.5 and concluded that the quenching is due to static interactions between the aluminum species and fulvic acid.

Had fluorescence been used in isolation without other complimentary analytical methods, it would be tempting to interpret the data as a removal of fluorescent material across the entire dose range, but the DOC and UV data prove otherwise. From these data alone, it is also very

difficult to determine the alum dose at which DOM removal occurs as the relationship between fluorescence and alum dose appears continuous. This observation highlights that peak intensity or FRI volumes may not be the most informative tools for characterizing this process.

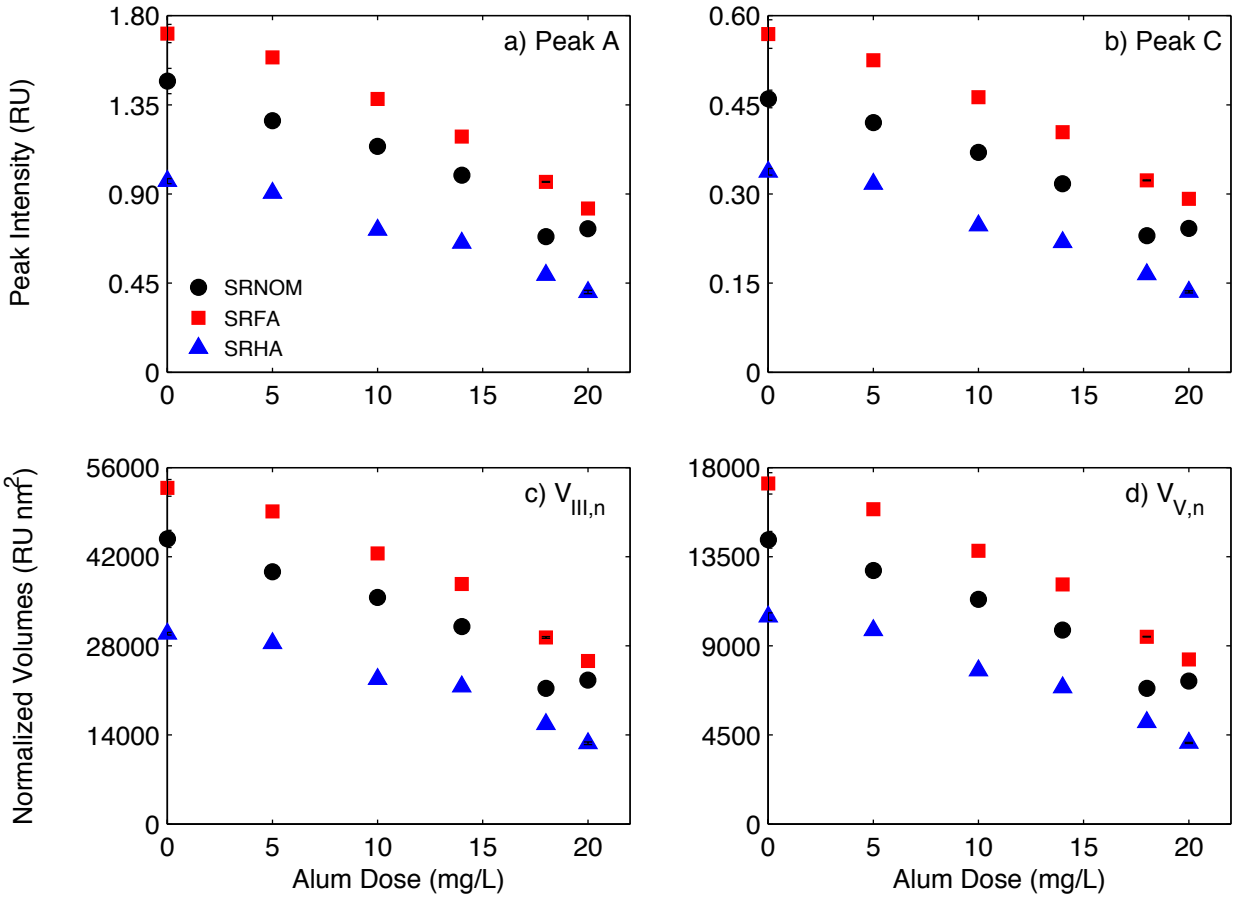

Figure 4.3 Fluorescence intensities (Peak A (a) and Peak C (b)) and normalized fluorescence volumes ($V_{III,n}$ (c) and $V_{V,n}$ (d)) as a function of alum dose.

Comparing the peak picking and FRI methods, the data do not suggest that one method offers obvious advantages over the other for this dataset. The magnitudes differ, but in each case the relative relationships between the isolates and coagulant doses are similar. For example, at an alum dose of 20 mg/L, Peak A and Region $V_{III,n}$ for SRFA decrease by 51% compared to both starting values (Table 4.4). Peak C and Region $V_{V,n}$ decrease by 47% and 50%, respectively. While FRI has the potential to better capture region heterogeneity and fluorescence behaviors

that occur away from peak intensities, it does not appear to capture any differences in this system that peak picking cannot capture.

Table 4.3. Percent removals of DOC, peak intensities and normalized fluorescence volumes for select alum doses.

DOM	Alum Dose (mg/L)	pH	Percent Removals (%)				
			DOC	Peak		FRI Volume	
				A	C	$V_{III,n}$	$V_{V,n}$
SRNOM	14	7.4	<10	34	33	32	33
	18	7.4	47	55	51	53	53
	20	7.5	45	52	48	51	51
SRFA	14	7.3	<10	29	27	27	28
	18	7.4	42	43	42	43	44
	20	7.3	49	51	47	51	50
SRHA	14	7.3	<10	33	36	28	34
	18	7.4	77	50	52	48	51
	20	7.4	76	58	60	57	61

4.5.4 Quantum Yields

While peak intensities and integrated volumes are straightforward calculations, they are difficult to interpret directly. In an application such as coagulation, both DOM quantity and quality change. With intensities alone, it is hard to determine whether the observed decrease in intensity is due to a reduction in organic matter concentration or a change in the organic matter composition. Analyzing quantum yields provides a perspective that helps separate differences in quality and quantity.

Quantum yields (Φ) quantify the fluorescence efficiency relative to non-radiative decay mechanisms. By comparing the fluorescence intensity to the amount of light absorbed, quantum yields offer a compositional parameter to compare differences in DOM before and after coagulation. Quantum yields for DOM have been determined by comparing DOM behavior against a known standard like quinine sulfate (QS) in dilute (0.1 N) sulfuric acid using Equation 1 (Birks, 1970; Del Vecchio and Blough, 2004; Green and Blough, 1994; Lakowicz, 2006).

Quantum yields are calculated at specific excitation wavelengths (λ_{ex}) by integrating the fluorescence intensity (F) across all emission wavelengths (λ_{em}) and dividing it by the absorption coefficient (a) at the same excitation wavelength. By comparing the DOM values to the known standard QS, which has a well-characterized Φ_{QS} of 0.51 (Birks, 1970), the Φ of DOM is calculated. It is normally assumed that the refractive indexes of DOM and quinine sulfate are equal (terms not shown in Equation 1).

$$\frac{\Phi_{DOM}(\lambda_{ex})}{\Phi_{QS}(\lambda_{ex})} = \frac{\int F_{DOM}(\lambda_{ex},\lambda_{em})\delta\lambda_{em}}{a_{DOM}(\lambda_{ex})} \times \frac{a_{QS}(\lambda_{ex})}{\int F_{QS}(\lambda_{ex},\lambda_{em})\delta\lambda_{em}} \quad (1)$$

DOM Φs are dependent on excitation wavelength as shown in Figure 4.4. This trend of increasing Φ to 350 nm excitation followed by a decrease in Φ with increasing excitation wavelengths has been attributed to the different mechanisms for long wavelength fluorescence emissions, such as charge transfer interactions (Boyle et al., 2009; Del Vecchio and Blough, 2004). Figure 4.4 shows that the quantum yields of SRFA and SRNOM are similar to each other and are about a factor of three greater than SRHA. Even though humic acids typically absorb more light per unit carbon, they have a higher molecular weight, which has been shown to lead to a decrease in fluorescence in favor of internal conversion, a non-radiative decay pathway (Boyle et al., 2009; Richard et al., 2004; Stewart and Wetzel, 1981; Wang et al., 1990).

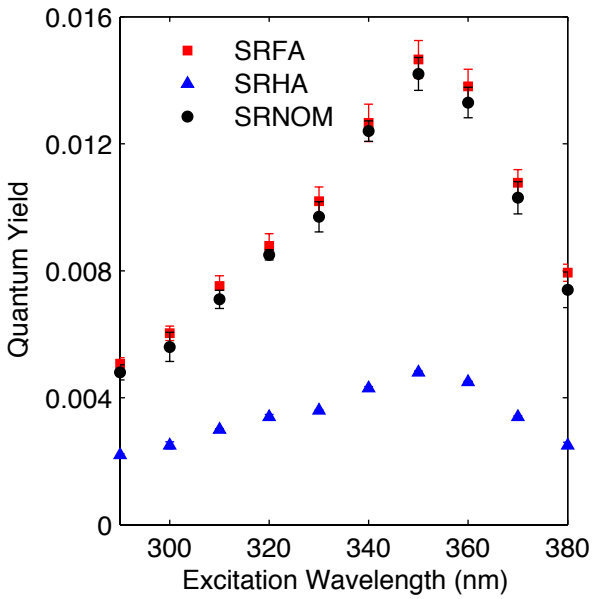

Figure 4.4 Fluorescence quantum yield as a function of excitation wavelength for SRNOM, SRFA and SRHA. Error bars represent the standard deviation between duplicates.

To characterize the changes in DOM optical properties during coagulation, the maximum quantum yield, which consistently occurs around 350 nm, was compared between coagulant doses as shown in Figure 4.5. During coagulation, the quantum yield decreases up to an alum dose of 14 mg/L and then increases dramatically. At 14 mg/L, the quantum yields of all three isolates has decreased by 33-35% compared to the initial value, but the difference appears larger for SRFA and SRNOM because of the higher initial values. Between these doses, the maximum observed increase in absorbance was only 6% at 350 nm (SRFA), so absorbance alone cannot explain the decrease in fluorescence efficiency. However, fluorescence intensity, as quantified by Peak C intensity, decreases 27-36% compared to the controls (Figure 4.3b) and accounts for the decrease observed in the quantum yield. Presenting the fluorescence results in this manner also confirms the quenching behavior observed in Figure 4.3.

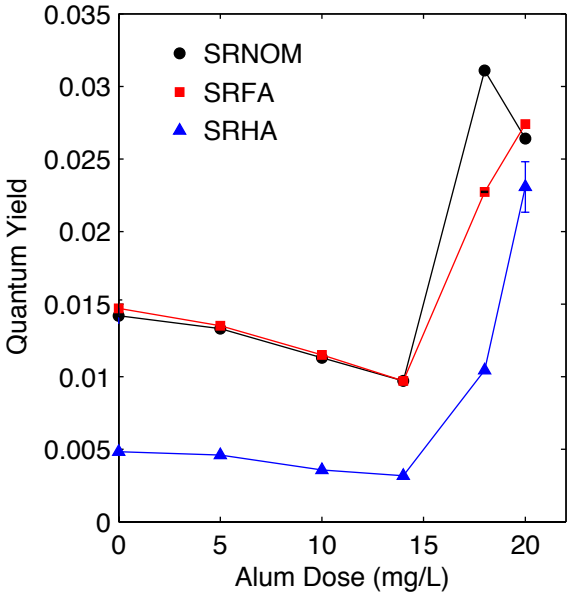

Figure 4.5 Maximum fluorescence quantum yields for each isolate as a function of alum dose. The maximum consistently occurred between 350 and 360 nm excitation wavelengths.

At alum doses of 18 and 20 mg/L, where there is a large removal of both UV_{254} and DOC, the quantum yield increases significantly relative to that at 14 mg/L alum where little UV_{254} and DOC removal occurred. Even though the fluorescence intensity decreases after coagulation, the fluorescence efficiency increases in the remaining organic matter. It is well established that coagulation preferentially removes the hydrophobic and large molecular weight fractions of DOM (Randtke, 1988) leaving organic matter that is more hydrophilic and lower in molecular weight. Quantum yields and fluorescence per unit absorbance have also been shown to be greater in lower molecular weight fractions (Boyle et al., 2009; Richard et al., 2004; Stewart and Wetzel, 1981; Wang et al., 1990). At 18 mg/L of alum, the quantum yields of both SRFA and SRHA increase by a factor of 2 (relative to the 14 mg/L dose), and the quantum yield of SRNOM increases by a factor of 3. SRFA and SRNOM exhibit similar quantum yields in the uncoagulated control samples and at the lower coagulant doses, but they have different quantum yields after a fraction of the DOM is removed by coagulation. These differences indicate that the

organic matter has different affinities for removal (Figure 4.1) and the remaining DOM has compositional differences that result in different fluorescence efficiencies. Finally, at 20 mg/L alum, the quantum yields of all three fractions converge at similar values. This behavior suggests that the fraction of each DOM pool that is least amenable to coagulation shares similar chemical characteristics. However, it must be noted that it is unknown whether or not residual aluminum in the system is still interacting with the remaining DOM and affecting its fluorescence signature. At the experimental pH values, it is unlikely that there is free aluminum (Al^{3+}), but the dominant aluminum speciation would include $Al(OH)_3(s)$ and negatively charged hydrolysis products, such as $Al(OH)_4^-$ (Elkins and Nelson, 2002). Interactions between negatively charged NOM and $Al(OH)_4^-$ are unlikely, but there may be stable aluminum-fulvate/humate complexes in solution. Complexed aluminum will likely result in a static quenching of the associated DOM (Cabaniss, 1992). Revisiting this classic process demonstrates the utility of moving past fluorescence intensities and analyzing fluorescence data from the perspective of quantum yields.

4.5.5 Fluorescence Index

Fluorescence index (FI) is another metric that provides insight into compositional differences between organic matter samples. This ratio has been correlated to aromatic carbon content, which is also associated with differences in DOM origin (allochthonous vs. autochthonous). Typical values range from 1.2 for allochthonous, higher aromaticity DOM to over 2 for autochthonous, lower aromaticity sources (McKnight et al., 2001). Originally developed in 2001 and then modified in 2010, FI is the ratio of emission intensities (470 nm divided by 520 nm) collected at an excitation wavelength of 370 nm (Cory et al., 2010; McKnight et al., 2001).

FI provides an additional level of insight to the coagulation behavior and a message of caution. Comparing the bulk isolates, the FI values for SRFA and SRNOM are greater than that of SRHA (Figure 4.6). These differences suggest that SRHA is composed of organic matter that is more enriched in aromatic moieties, which can be confirmed with IHSS published aromaticity data (Thorn et al., 1989). From a fluorescence perspective, these differences are manifested as a red-shift (to longer wavelengths) of the emission peak and (to a lesser degree) a broadening of the emission spectra (Korak et al., 2014a). As alum is added to the system, the fluorescence index increases. At doses less than or equal to 14 mg/L, there was no change in DOC or UV_{254} yet FI increased for all isolates. Since there was no change in the mass of organic matter in solution, this increase cannot be interpreted as a change in DOM composition but rather a change in how the DOM is interacting. The increase in FI is an indication that interactions with the coagulant are not quenching all intensities uniformly but preferentially targeting longer wavelength fluorescence. Non-uniform quenching was previously demonstrated at a lower pH (Sharpless and McGown, 1999). If long wavelength fluorescence is due to charge transfer interactions (Del Vecchio and Blough, 2004), it suggests that interactions with aluminum species preferentially disrupt the population and/or radiative decay of lower energy states. The FI for SRHA increased more in magnitude compared to SRFA and SRNOM suggesting the degree to which the DOM is interacting with the aluminum species is different between isolates.

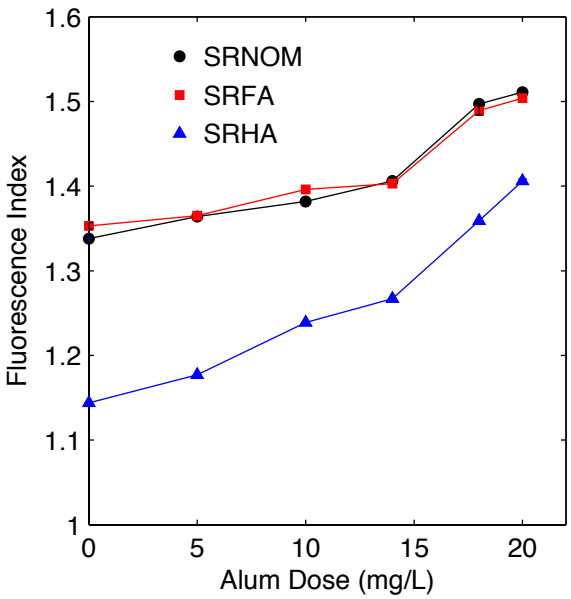

Figure 4.6 Fluorescence index (FI) as a function of alum dose

At the highest alum doses (18 and 20 mg/L) where DOM is removed through coagulation processes, Figure 4.6 shows that the FI exhibited a discontinuous increase that is greater than what would have been predicted by the trends at lower coagulant doses. By preferentially removing the larger molecular weight, more hydrophobic and presumably more aromatic material, the remaining DOM is less aromatic and has a higher FI.

This work demonstrates that FI, which is almost exclusively discussed in the context of DOM composition, is affected by the presence of other inorganic species (e.g., metal hydroxides). These complex effects need to be explored and understood, if FI is used to determine compositional differences across systems with varying background constituents that impact the DOM fluorescence.

4.5.6 Interpretations of Fluorescence Chemical Significance

Fluorescence is an appealing analytical method because of its ease of use, small sample volumes, and limited preparation required. Difficulties arise in trying to relate fluorescence data

to DOM chemical characteristics. Both peak picking and FRI methods have been prescribed chemical characteristics at some point in their application. While Coble defined Peaks A and C as related to humic substances in general, some have assigned more specific designations to the different peak regions. Some fluorescence, such as Peak C, has sporadically been referred to as fulvic-like fluorescence (Bieroza et al., 2009; Hudson et al., 2007), but it is more common for interpretations of the FRI method to include chemical characteristics. When the method was introduced, Region III was associated with fulvic acids and Region V with humic acids (Chen et al., 2003). This interpretation has become very popular and is commonly applied, especially in water treatment applications (Ayache et al., 2013; Jiang et al., 2013; Zhang et al., 2013).

By visual inspection alone, Figure 4.2 shows that both aquatic humic acids and fulvic acids fluoresce in both regions (A vs C and III vs V). Even though humic acid fluorescence occurs at longer wavelengths, both peak picking and the FRI methods would still capture the signal within the same prescribed area as the fulvic acids. In all three Suwannee River samples, the Peak A/Region III area has a higher fluorescence intensity compared to Peak C/Region V. Soil derived humic acids show a distinctly different fluorescence signature compared to aquatic humic acids, and this discussion is only limited to aquatic organic matter (Alberts and Takács, 2004).

If both operationally defined DOM fractions fluoresce in the same regions, is there evidence to suggest that one region is associated with one fraction over another? Comparing the ratio of intensities or regional integration volumes provides insight into how the fluorescence in one region is changing relative to another. Table 4.4 summarizes the ratio of three different quantitative methods: ratio of Peak A to Peak C intensities, ratio of fluorescence volumes ($V_{III,n}$:$V_{V,n}$) and ratio of volumetric percentages ($P_{III,n}$:$P_{V,n}$). Regardless of which ratio method is

used, all three isolates (before coagulation) have ratios near 3. The ratio for SRHA is slightly lower near 2.85, whereas the ratios for SRNOM and SRFA are greater near 3.10. These values are still within 8% of each other. In the FRI method, Region V is attributed to the humic-like fraction, but the ratio of regions shows only a 10% enrichment of Region V fluorescence in SRHA compared to SRFA. These results suggest that there is not much difference in the distribution of fluorescence signals between humic and fulvic acids.

If fluorescence regions were associated with chemically distinct fractions of DOM, then it would be expected that the ratio between regions would change after coagulation. If coagulation is more efficient at removing humic acid-like material relative to fulvic acid-like material, then the region associated with humic acids should be removed with greater efficiency than fulvic acid fluorescence. Figure 4.3 summarizes the relative removal of each peak and integrated region for the 18 and 20 mg/L alum doses compared to the controls. Each type of fluorescence was removed in roughly equal amounts, and there is no region that showed more than 5% additional removal relative to the other. For example, at 18 mg/L of alum, Peaks A and C were both removed by 42% and 43%, respectively, for SRFA. If the regions are compared on a relative basis to each other, the ratio of intensities or integrated volumes stays relatively constant around 3 as shown in Figure 4.4. The range of ratios for each isolate is within 10% of the average, indicating that there is little change in one region relative to the other after coagulation. In other words, coagulation removes fluorescing material in each region in equal proportion and does not preferentially remove fluorescing material in one region over another.

Table 4.4 Summary of fluorescence ratios for peak picking (A:C), normalized fluorescence volumes ($V_{III,n}$:$V_{V,n}$) and normalized region percentages ($P_{III,n}$:$P_{V,n}$).

Alum Dose (mg/L)	Peaks A:C			$V_{III,n}$:$V_{V,n}$			$P_{III,n}$:$P_{V,n}$		
	SRNOM	SRFA	SRHA	SRNOM	SRFA	SRHA	SRNOM	SRFA	SRHA
0	3.21	3.04	2.85	3.12	3.10	2.83	3.12	3.10	2.83
5	3.02	3.04	2.86	3.09	3.09	2.90	3.09	3.09	2.90
10	3.09	2.99	2.91	3.14	3.08	2.95	3.14	3.08	2.95
14	3.14	2.94	2.97	3.17	3.12	3.13	3.17	3.12	3.13
18	2.97	2.97	2.98	3.10	3.11	3.05	3.10	3.11	3.05
20	2.99	2.84	3.01	3.13	3.08	3.13	3.13	3.08	3.13
Range/Mean	8%	7%	5%	2%	1%	10%	2%	1%	10%

Based on these observations, it seems like there is little basis to associate one fluorescing region with either humic or fulvic acids exclusively. Both regions behave similarly to each other during coagulation. For these isolates, which were all collected from the same location, the fluorescence is distributed between regions in constant proportion. Other work has also demonstrated that the A and C regions are likely related to each other. Many parallel factor analysis (PARAFAC) models identify dominant components that have dual excitation maxima with one occurring in each region (Cory and McKnight, 2005; Ishii and Boyer, 2012; Pifer and Fairey, 2012), providing evidence that the fluorescence in both regions vary together in a set proportion to each other. Another study found that increasing DOM concentrations affect the apparent quantum yield in both regions simultaneously (Korak et al., 2014a). Li et al also provided evidence for dual excitation fluorophores using size exclusion chromatography (Li et al., 2013). These results suggest that each region is not associated with one operationally defined DOM fraction over another but are related to each other.

If any descriptor were to be used beyond general ‘humic substances’, the only reasonable interpretation would be that both regions (A/Region III and C/Region V) are most representative of the fulvic acid fraction compared to humic acids. Fulvic acids have higher quantum yields and

higher fluorescence per unit carbon (Alberts and Takács, 2004; Korak et al., 2014a). In a typical aquatic DOM sample, fulvic acids contribute three times as much mass as humic acids (Perdue and Ritchie, 2009). More likely, fluorescence analysis of natural DOM samples would be more representative of fulvic acids compared to humic acids due to their greater abundance and higher fluorescence efficiency.

If fluorescence were to be used to differentiate the differences in humic and fulvic acid fractions, methods that can quantify subtle differences in EEMs would be more powerful. Both methods, peak picking and FRI, lump a wide range of fluorescence wavelengths into one number. Although humic acids have peak emissions shifted to longer wavelengths compared to fulvic acids, the fluorescence contribution of fulvic acids will overlap and likely out fluoresce the humic acids. Neither peak picking nor FRI can effectively capture this heterogeneity if fulvic acids dominate the local fluorescence at lower emission wavelengths. Statistical methods, like PARAFAC, that can simultaneously capture differences in fluorescence intensity and position would be more powerful in discerning differences between DOM fractions.

4.6 Conclusions

Fluorescence spectroscopy is a powerful analytical tool but data interpretation is difficult due to the complexity of the fluorescence phenomena. In this study, we revisited a classic process to compare the behavior of humic and fulvic acid fractions. Fluorescence offered insight into the complexity of the coagulation process that DOC concentration and UV_{254} absorbance could not. At low coagulant doses (less than or equal to 14 mg/L), there was no change in either parameter. Changes in fluorescence revealed the complex interactions between DOM and aluminum species before any physical removal occurs. Fluorescence intensity is quenched and quantum yields decreased. Increases in FI demonstrate that fluorescence is not quenched

uniformly, but preferentially quenched at the longer emission wavelengths. The preferential change in the longer wavelength fluorescence compared to shorter wavelengths could not be captured following peak intensities, integrated regions or quantum yields alone. This work also illustrates that not all fluorescence indicators are equal, and it is important to explore multiple ones to gain a wider perspective of system behaviors.

The appealing aspects of fluorescence do not come without disadvantages. Fluorescence is impacted by a number of experimental factors, because intensity is a measure of not only the fluorescent material but also how that material interacts with its surroundings. This point was illustrated by analyzing the changes in fluorescence without any change in DOC concentration or UV_{254} absorbance.

Finally, revisiting the fundamentals of humic and fulvic fluorescence suggest that the practice of relating fluorescing regions to either humic acids or fulvic acids is flawed. There is little evidence to suggest that regional DOM fluorescence is specific to different operationally defined fractions. For DOM analysis, specification beyond general humic substances should be approached cautiously and would likely require more complex data analysis than peak picking or FRI.

Chapter 5 Evaluation of Optical Surrogates for the Characterization of DOM an DBP Precursor Removal by Coagulation

5.1 Abstract

The use of optical properties for characterizing the removal of dissolved organic matter (DOM) and disinfection byproducts (DBP) precursors has potential monitoring advantages and as such, has been of recent interest. In this study, 22 different surface waters with dissolved organic carbon (DOC) concentrations ranging from 2.3 to 12 mg/L and a wide range of DOM characteristics were coagulated using bench scale jar tests. UV absorbance (UV_{254}) and fluorescence excitation-emission matrices (EEMs) were measured for all coagulant doses, and selected samples were chlorinated for DBP analyses with the objective of examining the advantages and disadvantages of these optical properties as surrogates for DOC and DBP precursor removal. There were strong linear relationships between relative DOC removal and both relative UV and relative fluorescence peak intensity removal that was valid across multiple waters and coagulation levels. Contrary to other studies, neither UV nor fluorescence peak intensities performed better than the other as a predictive tool for DOC removal. The relative removal of peaks A and C had the same linear relationships with DOC removal demonstrating that these EEM regions are chemically similar to each other. There was also a strong relationship between the relative increase of the fluorescence index and DOC removal. Specific UV absorbance (SUVA) was a better optical surrogate for predicting DBP molar yields. Fluorescence compositional metrics had statistically significant relationships but with significant scatter that decreases the predictive power. SUVA is more robust as a predictor of DBP yields across diverse DOM sources compared to fluorescence. The results suggest that UV absorbance

and fluorescence are effectively measuring different subsets of DOM, and thus impacting the relative power of each optical measure as a predictive tool for DOM or DBP precursor removal.

5.2 Introduction

The removal of dissolved organic matter (DOM) is an important treatment objective for drinking water utilities in order to meet disinfection byproduct (DBP) regulations, as DOM serves as a DBP precursor (Belzile and Guo, 2006; Cavani et al., 2009; Chin et al., 1994; Traina et al., 1990; USEPA, 2006). As a heterogeneous mixture of organic molecules, the characterization and quantification of DOM is commonly achieved through surrogate measurements of bulk characteristics. Some example surrogates that have been used include dissolved organic carbon (DOC), color and UV-Vis absorbance at 254 nm (UV_{254}) (Edzwald et al., 1985; USEPA, 2006; Weishaar et al., 2003). DOC is the most direct measure of DOM by quantifying DOM mass in the form of carbon (DOM is roughly 50% carbon). Unlike color and absorbance, DOC does not depend on DOM chemical composition or its ability to absorb light.

Absorbance and fluorescence both measure the fraction of the DOM that is optically active. Generally, the optical activity of DOM has been associated with aromatic content and sp^2 hybridized functional groups. UV-Vis absorbance measures the capacity of a chromophore to absorb light and produce an excited state as a function of wavelength, or energy level. Fluorescence is a phenomenon where a portion of the absorbed energy is emitted in the form of light and can be quantified. Excitation-emission matrices (EEMs) are contour plots representing the intensity of light emitted as a function of wavelength absorbed (excitation wavelength) and wavelength emitted as depicted in Figure 5.1.

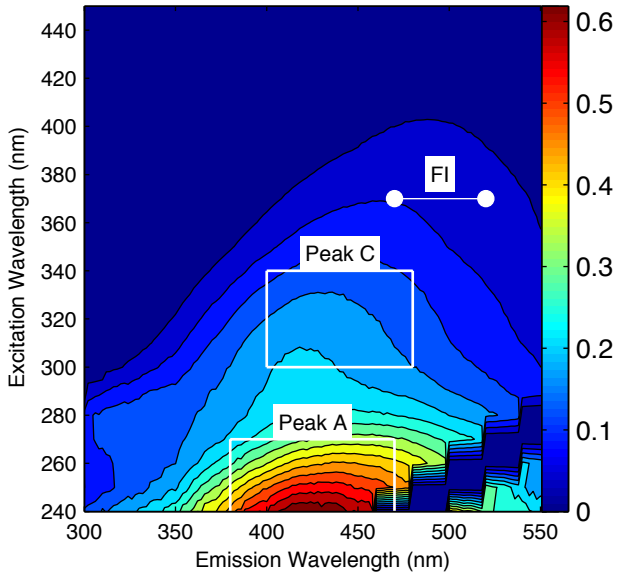

Figure 5.1 Example EEM of Source 6 raw water. Peak regions A and C are outlined. The two points used to calculate the FI are indicated by the markers.

While both absorbance and fluorescence measure fractions of DOM that could be similar in nature, it is important to note that there are some differences in the material that absorbs light efficiently compared to material that fluoresces efficiently. DOM with greater aromaticity absorbs more light per unit mass, which is commonly quantified by the normalization of absorbance to the DOC, specific UV absorbance (SUVA) (Weishaar et al., 2003). Higher SUVA values are associated with greater molecular weight fractions (Belzile and Guo, 2006; Cavani et al., 2009; Chin et al., 1994; Traina et al., 1990; USEPA, 2006), greater DBP formation (Edzwald et al., 1985; USEPA, 2006; Weishaar et al., 2003) and greater affinity for removal by coagulation (Edwards, 1997; Weishaar et al., 2003). Fluorescence, on the other hand, measures a subset of UV-Vis absorbing moieties that return to ground state via a radiative process, but it tends to occur more efficiently in lower molecular weight fractions on a per unit absorbance basis (Boyle et al., 2009; Mostafa et al., 2014; Richard et al., 2004; Stewart and Wetzel, 1981; Wang et al., 1990). Compared to absorbance, the fraction of emitted light is estimated to be small, less than

5% of the light absorbed (Boyle et al., 2009; Bruccoleri et al., 1993; Del Vecchio and Blough, 2004; Mostafa et al., 2014; Power and Langford, 1988). Since efficient absorbing and fluorescing moieties could be dominant in different DOM pools (with some overlap), it is expected that the capacity of each surrogate to predict DOM removal and DBP formation would be different.

Optical properties, that is absorbance (or optical density) and fluorescence, have been used to characterize humic substances since the late 1950s (Shapiro, 1957) as surrogates for DOM concentration and removal in treatment systems. UV-Vis absorbance, particularly UV_{254}, has been used extensively to monitor DOM removal by coagulation (Edzwald, 1978; Edzwald et al., 1985; Hall and Packham, 1965). Fluorescence spectroscopy has been used to investigate DOM removal during coagulation (Baghoth et al., 2011b; Bieroza et al., 2011; 2009; Cheng et al., 2004; Gone et al., 2009; Pifer and Fairey, 2014; 2012; Sanchez et al., 2013; Shutova et al., 2014). Of these studies, many have investigated fluorescence surrogates in tandem with UV surrogates to critically evaluate the benefit of one optical surrogate over another (Baghoth et al., 2011b; Bieroza et al., 2011; 2009; Cheng et al., 2004; Pifer and Fairey, 2014; 2012; Shutova et al., 2014), but only two studies evaluated the surrogates with respect to THM formation (Pifer and Fairey, 2014; 2012). In all these cases, however, there have been shortcomings within the study that limits the ability to apply the results to multiple water sources or treatment levels.

Most fluorescence studies have a trade-off between analyzing multiple waters at a single coagulant dose or individual waters at multiple doses. For example, several studies collected raw and treated water from full-scale plants (Baghoth et al., 2011b; Bieroza et al., 2011; 2009; Sanchez et al., 2013; Shutova et al., 2014). Full-scale studies are limited in that plant operation and source water vary between sampling events, and only one coagulant dose can be investigated

at a time. Bench scale studies have either examined different degrees of treatment limited to a few waters (Cheng et al., 2004; Gone et al., 2009) or studied only one coagulant dose across multiple samples from the same water body (Pifer and Fairey, 2014; 2012). Additionally, most studies have also been limited by a lack of diversity in the water quality characteristics examined. Full-scale sampling is also often limited to local facilities, and the dataset can only be as diverse as the raw water allows. Most studies have not incorporated a wide range of DOM compositions as indicated by SUVA, which is an important factor for determining DOM removal efficiency (Edwards, 1997). Comparing recent full-scale studies, one study did not include any low SUVA waters with values less than 2.9 L mg_C^{-1} m^{-1}, which would be representative of many lakes and reservoirs in the US (Bieroza et al., 2011). Another had two similar SUVA waters with intermediate values (Baghoth et al., 2011a). Others studies only had waters with SUVA values less than about 3 (Baghoth et al., 2011b; Johnstone et al., 2009), which would not be applicable to water sources with large terrestrial inputs. Others did not report any SUVA values (Bieroza et al., 2009; Sanchez et al., 2013) to give perspective into DOM composition. Without investigating a wide range of waters within the same study, it is impossible to critically compare different optical surrogates as predictors for DOM removal that would be applicable across multiple water sources and treatment levels.

The objective of this study is to systematically compare UV_{254} and fluorescence as optical surrogates for DOC removal and DBP precursor reduction across multiple waters and coagulation levels. One goal was to identify relationships that are water specific or universal across multiple waters. Methods for analyzing fluorescence EEMs were peak picking, Peak C/UV and FI, all of which can be directly extracted and have the potential to eventually be incorporated into real-time monitoring systems.

5.3 Experimental Methods

5.3.1 Source waters

Twenty-two water samples were collected to provide a sample set that represents a wide range of water qualities and DOM character as listed in Table 5.1. Five samples were collected at locations outside Colorado and the remainder came from sources within Colorado. Samples 1-4 were sampled from the Boulder-Lakewood influent to the Betasso Water Treatment Plant. Sampling occurred over the course of two months to capture the effects of spring run-off where the DOM is terrestrially dominated with minimal reservoir attenuation. Boulder Reservoir was sampled three times throughout the summer and was experiencing a taste and odor episode during the September sampling. Barr Lake and Jackson Reservoir are in the South Platte River watershed in eastern Colorado and are more than 75% impacted by point sources of nutrients as calculated using the SPARROW model. Barr Lake had an algal mat covering the surface at the sampling point. Sources 10-14 were sampled from water utilities around the country to expand the data set to include a wide variety of water qualities. Sources 15-22 are from water sources all associated with municipal water utilities across Colorado.

5.3.2 Coagulation Methods

Jar tests were performed using a 6-jar programmable jar tester (Phipps&Bird model 7790-901) with 2 liter jars (Phipps&Bird B-KER^2). Aluminum sulfate ($Al_2(SO_4)_3 \cdot 16H_2O$, Mallinckrodt Chemicals, 3208-04) was used as the coagulant. Mixing conditions included a rapid mix phase (1 minute, 290 rpm), two flocculation phases (10 minutes at 55rpm and 10 minutes at 20 rpm) and a sedimentation period (30-minute with no mixing). Turbidity and pH measurements were recorded directly after sedimentation. The supernatant was filtered through a muffled (550°C for 4 hours) and rinsed 0.7 μm Whatman GF/F filters to isolate the dissolved

fraction for DOC, UV absorbance, fluorescence, and DBP analyses. Samples were coagulated and analyzed for DOC, absorbance and fluorescence within a week. Raw water samples were also analyzed for the same water quality parameters (Table 5.1). Samples were stored in muffled amber bottles in the dark at 4°C.

The number of coagulant doses utilized varied between water sources depending on the quantity of water available and is listed in Table 5.1. For readily available source waters, a series of jar tests were performed targeting the point of diminishing coagulant returns. For water sources where only one coagulant dose could be applied, the alum dose was estimated using the EPA Water Treatment Plant Model to meet Stage 1 Disinfection Byproduct total organic carbon removal requirement (USEPA, 2006).

5.3.3 Chlorination and DBP Formation

For each jar test, the source water and one jar were chlorinated according to uniform formation conditions (UFC) targeting a chlorine residual of 1 mg/L (± 0.4) at 24 hours and a pH of 8 (Summers et al., 1996). The jar test that yielded a DOC concentration that best represented the DOC removal dictated by enhanced coagulation under the Stage 1 Disinfection Rule was selected for chlorination. After 24 hours, the chlorine residual was quenched with ammonium chloride according to EPA Method 551.1.

5.3.4 Analytical Methods

Initial water quality conditions are listed in Table 5.1. Alkalinity of all source waters was determined by using a Hach digital titrator (Model 16900-01) and the manufacturer's standard method. pH measurements were collected using a Fisher Scientific Accumet AB15 for all raw water and coagulated samples prior to filtration. A Hach 2100N turbidimeter was used for all turbidity measurements on raw and coagulated samples, which are reported in nephelometric

units (NTUs). DOC was measured with a Shimadzu TOC-V_{CSH} with autosampler using a non-purgeable organic carbon method. The accuracy and precision of a 5 mg_C/L potassium hydrogen phthalate standard were both within 5% throughout the study. UV absorbance from 200 to 600 nm was measured using a spectrophotometer (Varian Cary Bio 100, Agilent Technologies, CA) with a 1 cm path length quartz cell. SUVA was calculated by dividing the UV_{254} by the DOC concentration and reported in units of L mg_C^{-1} m^{-1}.

Fluorescence EEMs were measured for all raw and coagulated samples (Fluoromax-4, John-Yvon Horiba, Edison, NJ) for a total of 98 EEMs. Excitation wavelengths ranged from 240 nm to 450 nm in 10 nm increments with emission scans collected from 300 to 560 nm in 2 nm increments. The bandpass for both excitation and emission monochromators was set at 5 nm and the integration time was 0.25 s. Data was corrected following published methods (Murphy et al., 2010) and is presented in Raman Units (RU). Briefly, measured intensities incorporated instrument-specific correction factors, were corrected for primary and secondary inner filter effects, blank subtracted and normalized to the Raman area of LGW at an excitation of 370 nm. Past method development work on this instrument has determined that the analytical error of the fluorescence metrics used in this study are less than 3% for peak intensities and less than 2% for FI. For carbon-normalized metrics, the error associated with both fluorescence and DOC measurements stipulates that changes less than 6% are likely not statistically justified.

EEMs were analyzed only using methods that allow for the direct analysis individual EEMs rather than models that rely on large datasets (i.e., PARAFAC). Peak picking was used to methodically extract regional intensities from the EEM based on the regions defined by Coble (1996). Regions A and C have been associated with humic substances (Coble, 1996), and the peak is defined as the maximum intensity within each region. Peak A is defined as the maximum

intensity within the region extending from excitation wavelengths 240 to 270 nm and emission wavelengths 380 to 470 nm. Likewise, Peak C is the maximum intensity in the region that extends from excitation wavelengths 300 to 340 nm and emission wavelengths 400 to 480 nm. Due to the nature of the EEMs measured, 65% of the Peak C maximum intensities identified (out of 98) lie along the 300 nm excitation region boundary, because there is no absolute maximum as depicted in Figure 5.1. Specific peak intensity is defined at the fluorescence intensity divided by the DOC concentration yielding units of RU L mg_C^{-1} and provides perspective into the fluorescence intensity relative to the mass of DOM present. Fluorescence index (FI) is defined as the ratio of emission intensities at 470 nm and 520 nm at an excitation wavelength of 370 nm (Cory et al., 2010) and has been correlated to sample aromaticity (McKnight et al., 2001). Peak C/UV is the ratio of the Peak C intensity and the absorbance at the corresponding excitation wavelength where the maximum was located. This ratio has been used as a surrogate for quantum yield to quantify the amount of light emitted relative to the amount of light absorbed and has been correlated to molecular weight (Baker et al., 2008; Beggs et al., 2013; Stewart and Wetzel, 1981). Any sample with a UV_{254} greater than 0.2 cm^{-1} was diluted prior to analysis to minimize concentration-based quenching effects (Korak et al., 2014a).

Samples were also analyzed for haloacetic acids (HAA) and trihalomethanes (THM) with according to EPA methods 552.2 and 551.1, respectively. DBPs are reported as HAA_5 (sum of monochloro-, dichloro-, trichloro-, monobromo-, and dibromoacetic acids) and total THM (TTHM) (sum of chloroform, bromoform, bromodichloromethane, and dibromochloromethane) on a molar basis. The relative percent difference between duplicates was 2% for TTHM and 4% for HAA_5.

5.4 Results and Discussion

5.4.1 Range of Coagulation Behaviors.

This study examined twenty-two waters with a wide range of water quality characteristics, especially for SUVA and alkalinity that are listed in Table 5.1. Bromide levels were less than the detection limit (0.0031 mg/L) for all waters except for Barr Lake (0.1 mg/L), Fort Collins (0.01 mg/L) and Arvada (0.03 mg/L). Jackson reservoir had detectable bromide levels but was not chlorinated. For source waters with TOC values greater than 2 mg_C/L, the Stage 2 DBP Rule dictates required TOC removal based on a 3x3 matrix according to raw water TOC and alkalinity. Of the nine possible bins, this data set includes waters from seven bins, including both extremes.

The differences in water quality characteristics translated into a wide range of coagulation behaviors as depicted in Figure 5.2. Coagulation doses of 5 to 120 mg/L were used resulting in DOC removals between 5 to 70%. The observed removal of each water agreed with those predicted by the Edwards coagulation model using the "General Low DOC" parameters (Edwards, 1997). For 85% of the coagulated waters, the predicted DOC removal based on SUVA and pH was within 15% of the experimental data (Figure 5.3). The model under predicted the DOC removal for the high SUVA, low alkalinity waters by about 20% (Sources 1-3). The general agreement between the data set in this study and the model helps substantiate that this data not only covers a wide range of coagulation behaviors but also conforms to the fundamental behaviors reported elsewhere. Therefore, the dataset used in this study overcomes some of the shortcomings of past studies by investigating a wide range of source water qualities at multiple degrees of treatment. The results can be considered broadly applicable to other surface water sources.

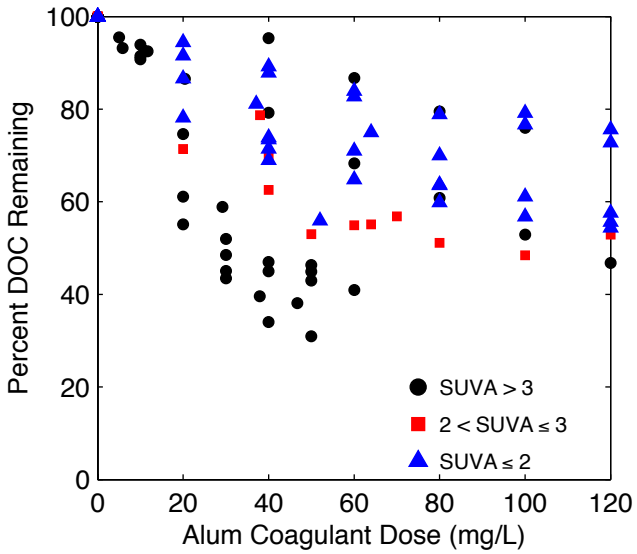

Figure 5.2 Relative DOC removal as a function of alum dose for all waters divided by raw water SUVA.

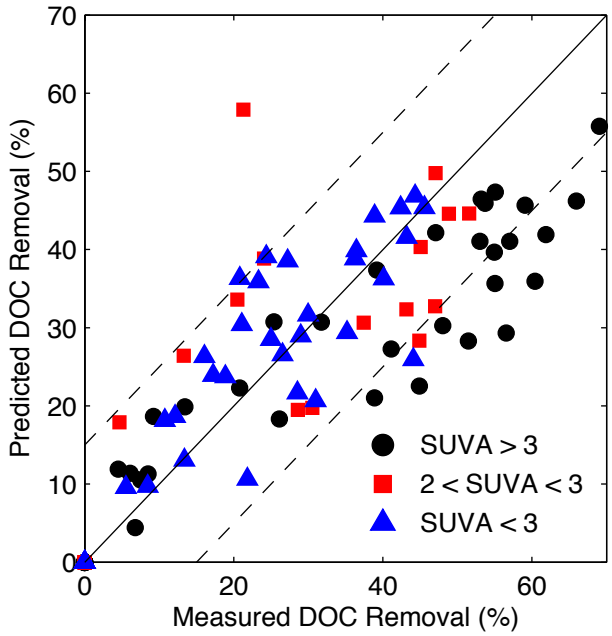

Figure 5.3 Measured DOC removal compared to predicted DOC removal based on Edwards' Model.

Table 5.1 Summary of source water quality parameters

No.	Source	DOC (mg/L)	UV_{254} (cm^{-1})	SUVA (L/mg_C-m)	FI	Alkalinity (mg/L as $CaCO_3$)	pH	Turbidity (NTU)	No. of Coagulant Doses
1	Betasso WTP	7.1	0.28	4.0	1.36	--	6.52	1.5	6
2	Betasso WTP	7.7	0.30	4.0	1.34	17	5.67	1.5	6
3	Betasso WTP	2.7	0.10	3.6	1.34	--	7.21	0.9	6
4	Betasso WTP	2.3	0.08	3.5	1.38	57	7.32	1.7	6
5	Boulder Reservoir	3.5	0.07	2.0	1.40	40	7.8	22.5	6
6	Boulder Reservoir	3.8	0.07	1.9	1.45	70	7.72	20.2	6
7	Boulder Reservoir	3.7	0.07	2.0	1.46	45	7.58	13.2	3
8	Barr Lake*	6.2	0.11	1.8	1.83	94	8.68	50.0	6
9	Jackson Reservoir*	8.1	0.11	1.3	1.67	90	7.77	9.3	6
10	Lake Mead, NV	2.6	0.05	1.9	1.51	134	7.8	0.2	1
11	Danville, KY	3.1	0.08	2.6	1.56	84	7.2	4.6	6
12	Red River, ND	10.1	0.32	3.2	1.49	160	7.6	92.0	4
13	Red Lake, MN	12.4	0.42	3.4	1.45	95	7.52	51.0	5
14	Lake Erie, OH	2.2	0.02	1.0	1.58	63	8.02	1.1	1
15	Arvada	3.0	0.05	1.5	1.46	48	7.88	7.1	1
16	Boulder	3.2	0.06	2.0	1.45	80	8.2	7.6	1
17	Evergreen	3.7	0.14	3.7	1.40	28	7.62	39.2	1
18	Fort Collins	4.0	0.11	2.6	1.39	30	7.85	3.6	1
19	Grand Junction	2.6	0.06	2.2	1.44	69	8.23	2.5	1
20	Greely-Loveland	5.6	0.13	2.3	1.43	46	7.95	5.6	1
21	Greely-Seaman	7.1	0.17	2.4	1.42	80	8.23	1.3	1
22	Pueblo	2.6	0.06	2.2	1.46	80	8.15	5.0	1

*indicates wastewater impacted sources
Sources 1-4 and 15-22 are from Colorado
Sources 1-4 were sampled at four different times between June-July 2011 capturing the spring run-off
Sources 5-7 were collected at different times between June-September 2010

5.4.2 Water-specific Relationships

Surrogates, such as DOC and UV_{254}, are often used to assess the DOM removal by coagulation, and fluorescence spectroscopy is another potential surrogate given its capacity to elucidate a spectrum of DOM characteristics. All three parameters are compared side-by-side for select water sources in Figure 5.4. Water source 2 (Figure 5.4a) represents a water with efficient DOM removal at relatively low coagulant doses with 70% DOC removal at an alum dose of 40 mg/L. Source 5 represents a water with moderate DOM removal, 25% DOC removal at an alum dose of 40 mg/L; and Source 8 represents a water that is wastewater impacted with inefficient DOM removal with the maximum DOC removal of only 25% at an alum dose of 120 mg/L.

Figure 5.4 highlights the general trend observed for all waters. In general, all three surrogates (DOC, UV_{254} and Peak C) track each other with increasing coagulant doses, which demonstrates that the removal of these optical signatures is strongly correlated to DOC removal. Strong correlations between both optical parameters and DOM removal are supported by physiochemical properties of DOM. Coagulation has been shown to preferentially remove the more hydrophobic and aromatic fractions of DOM (Edzwald, 1993; Liang and Singer, 2003; White et al., 1997). Optically active moieties in DOM are associated with aromatic and sp^2 hybridized functional groups because their electron structure is conducive to the absorption of light (Birks, 1970).

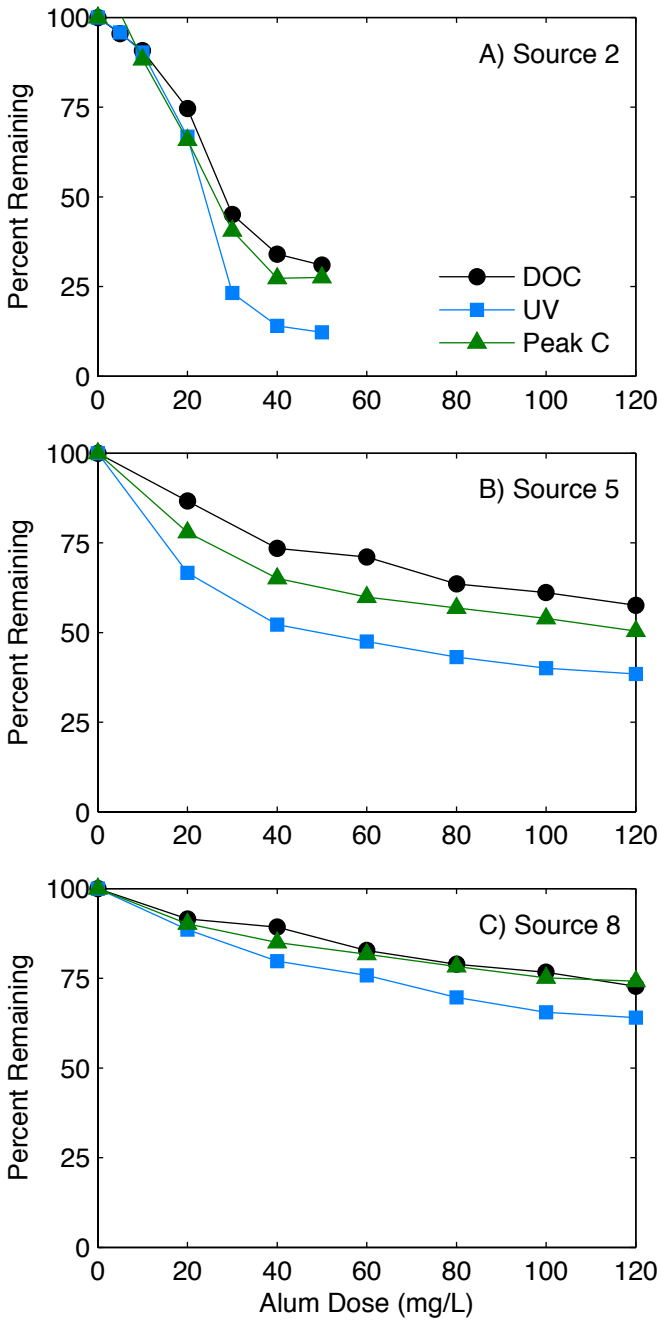

Figure 5.4 Relative amount of DOC, UV_{254}, and Peak C remaining as a function of alum dose for three waters representing a range of behaviors

FI also showed a consistent trend between all of the waters; it increased with increasing coagulant doses (Figure 5.5). Since FI has been correlated to sample aromaticity (McKnight et al., 2001), an increase would be expected, because coagulation preferentially removes high

SUVA moieties (Edzwald, 1993; Liang and Singer, 2003; White et al., 1997). After coagulation, the remaining DOM has a lower SUVA, presumably less aromaticity and thus have a higher FI, as shown before (Beggs and Summers, 2011). Figure 5.5 shows that the degree to which FI increases varies between the source waters. The waters that had the most efficient DOM removal (i.e. Source 2) showed the greatest increases in FI, whereas the waters with less efficient removal (i.e. Source 8) showed smaller increases in FI. Even though FI is typically used to measure compositional differences in DOM, these results suggests that the relative change in FI is related to the relative DOM removal.

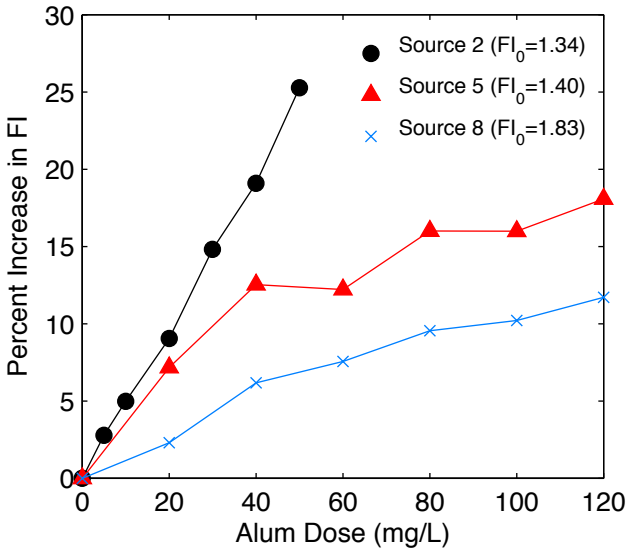

Figure 5.5 Relative increase in FI as a function of alum dose for three source waters exhibiting a range of DOC removal behaviors. FI values for the raw water are listed in the legend.

In general, care must be taken in interpreting fluorescence measurements as a function of alum dose as in Figure 5.4 and Figure 5.5. Past work has demonstrated that the fluorescence signature (as quantified by intensities, FI and other metrics) can be affected by the presence of aluminum even when there is no physical removal of DOC (Korak et al., 2014b). As a result, it is important to confirm that changes in the fluorescence response are actually accompanied by

DOC removal. For the remainder of the paper, relationships between optical surrogates and DOC removal are investigated directly. It is important to note that there is still a possibility that residual aluminum after filtration can affect the measured DOM fluorescence, and the effects of changing DOM quantity, composition and metal interactions are difficult to separate. The purpose, however, is to investigate relationships that provide utility and predictive capabilities for municipal and monitoring applications regardless of the complex interactions.

5.4.3 Optical Surrogate Relationships for DOC Removal

In this section, the use of both optical surrogates is compared directly to DOC removal to evaluate the effectiveness of optical surrogate compared to the other across the entire dataset. Fluorescence analysis follows Peak A intensity, Peak C intensity and FI. Relative changes were calculated with respect to the raw water values. The relative removals of UV_{254} absorbance and both fluorescence peak intensities are linearly related to the relative DOC removal, as shown in Figure 5.6. While this relationship has been shown before for constrained data sets (Bieroza et al., 2011; 2009; Gone et al., 2009), this study demonstrates that the same relationship is valid across multiple source waters, multiple coagulation levels and does not exhibit site-specific variations.

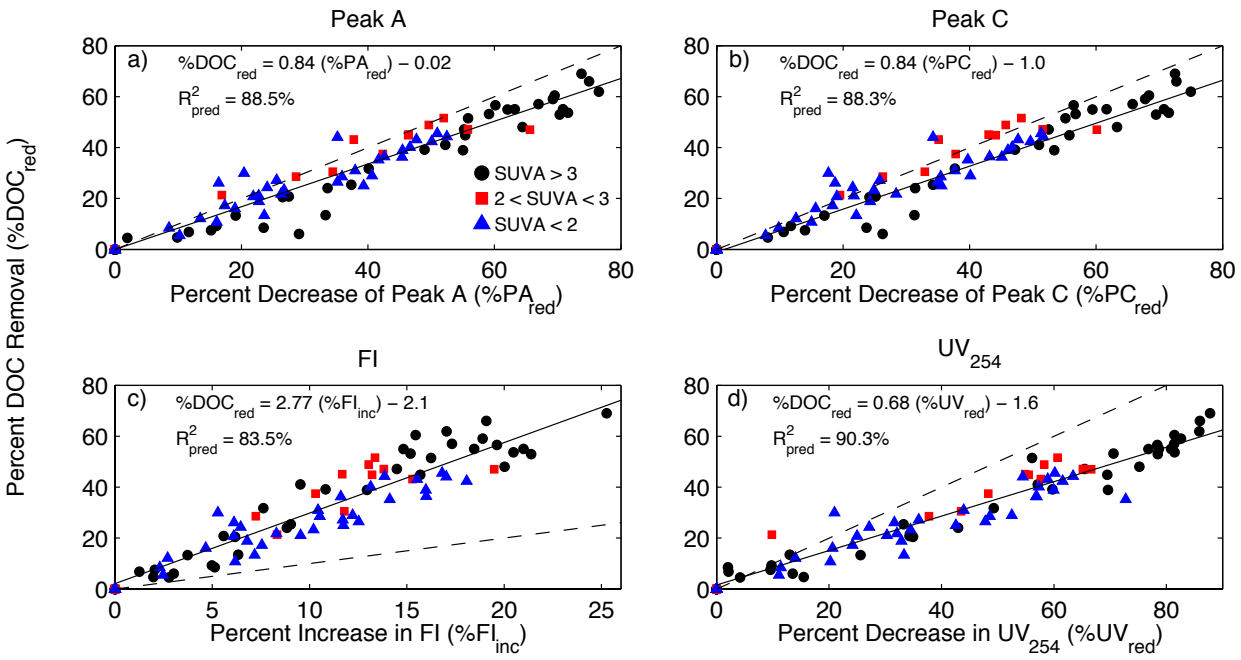

Figure 5.6 Relative percent change in optical properties as a predictor for DOC removal for a) Peak A, b) Peak C, c) FI and d) UV_{254}. The solid line represents the best-fit line (excluding repeated points at the origin). The equation and R^2_{pred} values are provided. The dashed line represents the 1:1 line.

Linear regressions were fit to each of the optical surrogates, excluding the points at the origin, and the equations are listed in Figure 5.6. Peaks A and C both had statistically indistinguishable slopes, based on the confidence intervals of the slope parameter, and fall just below the 1:1 line. Gone et al (2009) showed that Peaks A and C had similar slopes (0.86-0.88) for one water. The slopes determined in this study match in good agreement and confirm that the regression is not water-specific. The slope between UV removal and DOC removal falls further below the 1:1 line, indicating that the relative removal of absorbing species is always greater than the DOC removal, which has been shown before (Babcock and Singer, 1979; Edzwald, 1993; Volk et al., 2000). While both UV and fluorescence are removed to a greater extent than DOC, the higher removal rate for absorbance relative to fluorescence suggests that there is a subset of DOM removed that absorbs light but does not fluoresce. Given that fluorescence and

UV-Vis are known to measure different DOM pools, this fraction is likely high molecular weight DOM that has been shown to have high SUVA values but low fluorescence efficiencies (Belzile and Guo, 2006; Cavani et al., 2009; Chin et al., 1994; Mostafa et al., 2014; Stewart and Wetzel, 1981; Wang et al., 1990).

A strong linear relationship was also found between the relative increase in FI and DOC removal (Figure 5.6c). Peak emission wavelength at 370 nm excitation shifted to lower wavelengths (blue-shifted) with increasing DOC removal (Figure 5.7). Peak location has been shown to be an important factor in determining FI (Korak et al., 2014a), but the scatter in Figure 5.7 suggests that local curvature is also playing an important role in the strong relationship in Figure 5.6c. Despite differences in water quality characteristics or DOM composition, FI quantifies the removal of a DOM fraction that appears to be common across multiple water sources, because the relationship between degree of compositional change and DOC removal is consistent across multiple waters. The relationship between change in FI and change in DOC has a slope of 2.8 (±0.28), which indicates that small changes in FI yield large changes in DOC. Measuring FI has an advantage over measuring single fluorescence intensities. Fluorescence intensities are attenuated by the inherent sample absorbance and should be corrected for inner filter effects when the total optical density exceeds 0.05. As the ratio of two emission intensities at the same excitation wavelength, the difference in attenuation between the two points is small and FI can be calculated without inner filter corrections in many applications (Korak et al., 2014a). For the online-measurements or to rapidly determine DOC removal, FI may be operationally simpler than measuring peak intensities.

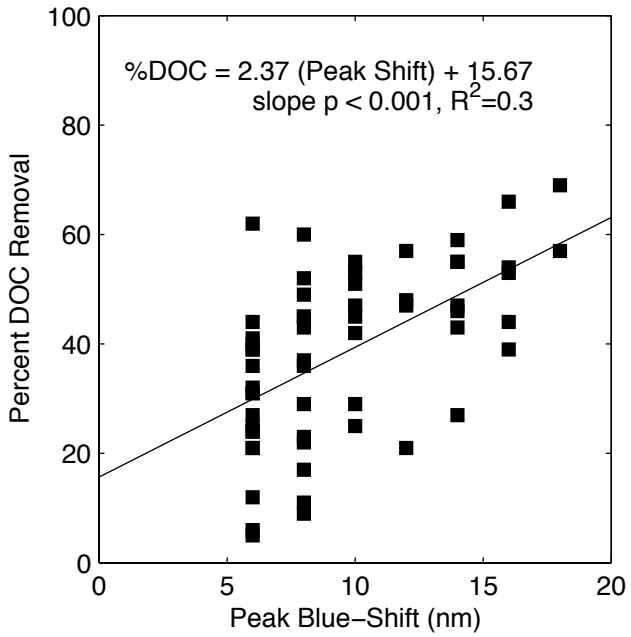

Figure 5.7 Percent DOC removal as a function of peak blue-shift (to lower wavelengths) at excitation 370 nm. Shifts less than 6 nm not shown due to poor accuracy when desired shift is less than emission bandpass.

The ability of optical parameters to predict DOC removal was evaluated by comparing the R^2 predicted values (R^2_{pred}) from linear regressions fit to each data set. This statistic evaluates the ability of the model to predict new data and is generally more conservative than R^2. The R^2_{pred} value is marginally greater for the correlation with UV_{254} (0.903) compared to Peak A and C (0.885 and 0.883, respectively). The R^2_{pred} value for the correlation with FI is slightly lower (0.835) and the wider distribution of values is evident in Figure 5.6c. These results demonstrate that there is little difference in the use of UV_{254} or fluorescence peak intensities to represent DOC removal, and it cannot be concluded that one surrogate is definitively better than the other to predict DOC removal.

These results contrast past work that has also presented strong correlations between the relative changes in both Peak C and UV and relative DOC removal. Bieroza et al (2009) states that the strength of a Peak C-DOC relative removal relationship is site-specific, but the data

presented here suggest that the relationship holds up well across multiple waters and conditions. Another study suggests that the relative reduction in Peak C fluorescence is a better predictor of TOC removal than the reduction of UV_{254} (Bieroza et al., 2011), but this contrasting conclusion may be more associated with differences in experimental methods. Another study concluded that the raw water composition by fluorescence offers a better predictor of DOC removal than SUVA for optimized systems (Shutova et al., 2014). The results presented here demonstrate that DOC removal can be predicted equally by UV_{254} and fluorescence intensity by comparing influent and clarified water regardless of plant optimization or local treatment objectives.

If fluorescence efficiency is typically less than 5%, it is interesting that there are such strong correlations between fluorescence intensity removal and DOC removal when the bulk of the material removed is weakly fluorescent. Fluorescence is likely an effective surrogate for DOC removal because the fluorescing material seems to be consistently removed in similar proportions to DOC across multiple waters. The affinity for removal of the fluorescent material is representative of the affinity of the bulk DOM. In that case, the removal of fluorescent material is acting more as a tracer for all DOM removed by coagulation.

The similar removal behavior in the Peak A and C regions presents evidence that challenges the assertion that each region corresponds to a chemical distinct fraction of DOM. In interpreting fluorescence data, some interpretations relate the each region of the EEM to either humic acid-like or fulvic acid-like organic matter fractions by either relating peak regions (Bieroza et al., 2009) or fluorescence regional integration regions (Chen et al., 2003) to specific DOM fractions. Past research coagulating humic and fulvic acid fractions directly has shown that not only do both fractions fluoresce in each region, but fluorescence in each region is removed in equal proportion to each other despite differences in chemical characteristics, quantum yields

and removal efficiencies (Korak et al., 2014b). The removal behavior in this study differ from those investigating only organic matter isolates, because there is particulate material and a more heterogeneous distribution of DOM characteristics within each water that promote more gradual DOC removal (Letterman and Yiacoumi, 2011). Even with different removal behaviors, statistically equivalent slopes for the Peak A and Peak C regressions indicate that the material contributing to the fluorescence in these regions are chemically similar to each other and have similar affinities for removal by coagulation. This observation provides additional evidence that these regions of an EEM should not be considered chemically distinct from one another but are related.

5.4.4 Optical properties as predictor of DBP Yield

Compositional indicators (SUVA, specific peak C intensity, FI and Peak C/UV) were evaluated to assess potential relationships with DOM reactivity as expressed by DBP yields. This approach is different from those explored in other recent publications. The more common approach has been to search for correlations between DBP concentrations and either fluorescence intensities or PARAFAC component loadings (Fmax values) (Pifer and Fairey, 2014; 2012). This comparison relates two extrinsic (mass-dependent) parameters to one another. In this study, intrinsic (compositional) fluorescence parameters are investigated to be analogous to the relationships developed between SUVA and DBP yields (Weishaar et al., 2003; Yang et al., 2008).

Figure 5.8a and Figure 5.8b show that SUVA has a positive relationship with both TTHM and HAA_5 molar yields. For TTHM, a strong linear relationship (slope $p<0.001$, $R^2_{adj}=0.81$) was found throughout the entire SUVA range. Strong relationships between SUVA and TTHM yields have been shown before (Ates et al., 2007; Liang and Singer, 2003; Roccaro and Vagliasindi,

2009; Weishaar et al., 2003; Yang et al., 2008). There is a statistically significant positive relationship between HAA_5 yields and SUVA ($p<0.001$), as has been shown before (Ates et al., 2007; Roccaro and Vagliasindi, 2009; Yang et al., 2008), but the relationship shows signs of non-linearity. At SUVA values less than 2 L mg_C^{-1} cm^{-1}, HAA5 yields are less sensitive to SUVA compared to greater SUVA values. Past research has demonstrated that in low SUVA waters (less than 2 L mg_C^{-1} cm^{-1}) the hydrophilic fraction plays a more important role for both THM and HAA formation and can lead to weaker relationships with SUVA (Ates et al., 2007; Hua and Reckhow, 2007).

Even though fluorescence also measures a subset of DOM with similar characteristics, the relationships between fluorescence properties and DBP yields are much weaker and do not have the same strength across multiple waters as SUVA. Specific Peak C intensity, a fluorescence analogy to SUVA, has a positive correlation HAA5 yields ($p<0.01$) and TTHM yields ($p<0.01$) as shown in Figure 5.8c and Figure 5.8d. These relationships, however, have more scatter compared to the relationships with SUVA and lower predictive power. For a specific peak C intensity of 0.10 RU L mg_C^{-1}, the HAA5 yield differs by more than a factor of 2. For the TTHM molar yields, there is a distinct break in the dataset between the raw and coagulated waters. The raw waters have a much higher TTHM yields compared to coagulated samples with similar specific peak C intensities. This break indicates that there are distinct DOM pools that have similar fluorescence efficiencies but different reactivities.

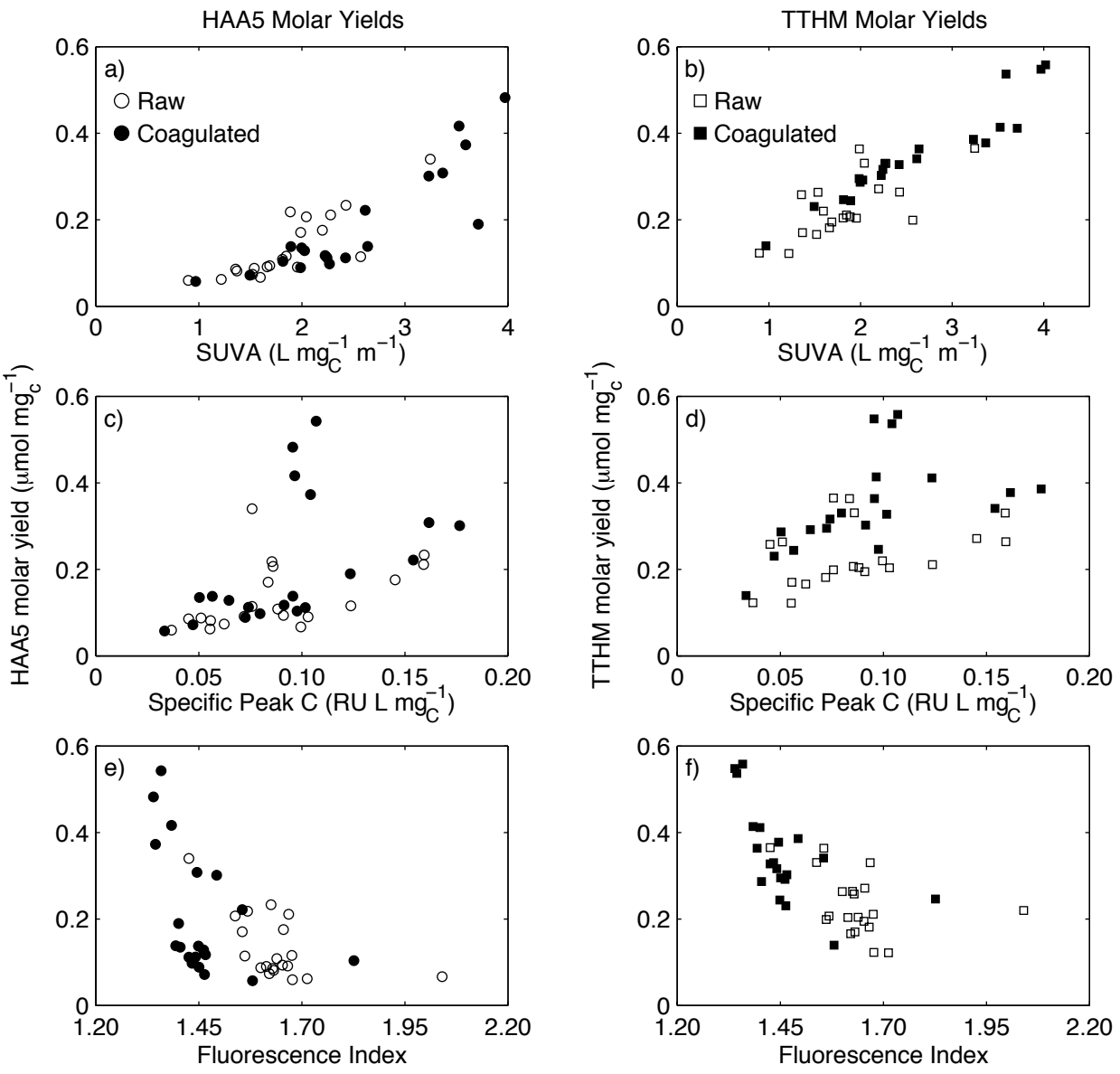

Figure 5.8 Relationships between optical compositional metrics and C-DBP molar yields

FI and Peak C/UV, two metrics used to evaluate DOM compositional differences, were also evaluated to determine if they have the ability to predict DBP yields. Figure 5.8e and Figure 5.8f show that FI is also a poor predictor of DBP yields across multiple waters. While the slope of a general regression fit to both DBP classes would yield significant slopes ($p<0.01$), the relationship is mostly driven by the extreme end members within the dataset. If the Betasso

samples (lowest FI samples) and Barr Lake samples (highest FI samples) are removed from the regressions, there is no longer a statistically significant relationship between FI and HAA yields ($p=0.19$). There is still a significant relationship between TTHM yield and FI ($p<0.001$), but there is significant scatter that does not allow FI to be a useful predictive tool. For Peak C/UV, there was no strong relationship between either TTHM yields ($p=0.03$, $R^2=0.10$) or HAA yields ($p=0.17$).

Past work has demonstrated that fluorescence compositional properties can correlate well with TTHM yields within a watershed or close geographical area. Beggs et al. (2013) characterized the reactivity of DOM from neighboring watersheds from the Rocky Mountains of Northern Colorado. That study found good correlations between the same three fluorescence measures (Specific Peak C intensity, FI, and Peak C/UV) and TTHM yields. The results in this study demonstrate that when the dataset is expanded to include a more heterogeneous DOM sources, these correlations are less robust. It suggests that the application of fluorescence to predict DBP reactivity should only be used for constrained systems and not to compare highly diverse DOM samples.

While both UV and fluorescence intensity surrogates performed equally as well as each other to predict DOC removal, the differences in DBP predictability reaffirms that UV and fluorescence do not quantify the same subset of DOM. Although SUVA and FI have both been correlated with aromaticity (McKnight et al., 2001; Weishaar et al., 2003), they are not direct measurements of same chemical characteristics within a DOM sample. Figure 5.9 shows that while there is a statistically significant relationship between SUVA and FI ($p<0.001$), there is still substantial scatter. At FI values between 1.4-1.7 (typical range for many surface waters), SUVA can range by more than a factor of 2. The stronger correlations between SUVA and DBP

yields compared to fluorescence metrics suggest that fluorescence is measuring only a small fraction of the possible DBP precursors, and there is significant heterogeneity among the non-fluorescing precursor material. In other words, there is better overlap between the subset of DOM that absorbs light efficiently and the pool of DBP precursor materials across a diverse set of water sources compared to fluorescence.

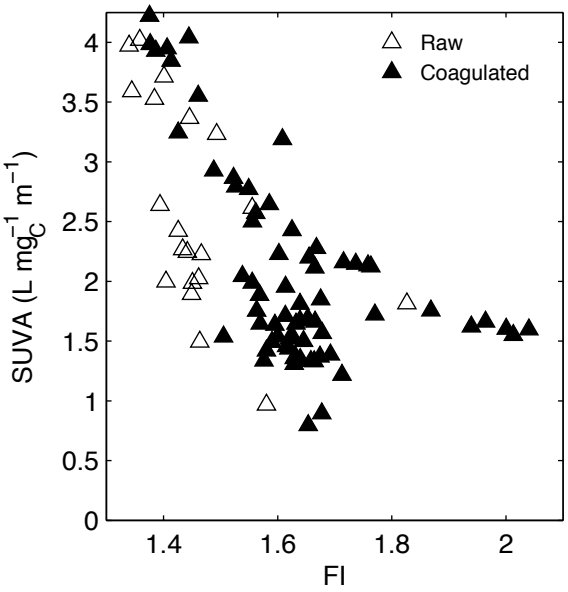

Figure 5.9 Relationship between SUVA and FI for all source waters (hollow) and coagulated waters (filled)

5.5 Conclusions

UV absorbance and fluorescence spectroscopy were evaluated for their effectiveness in characterizing DOM removal by coagulation. Both UV_{254} absorbance and Peak C fluorescence performed equally as a surrogate for DOC removal by relating the relative removal of DOC to the relative change of the optical measurement. A single linear relationship between DOC removal and the decrease in the optical surrogate was found to be valid across a diverse range of water sources tested up to 80% DOC removal. These results demonstrate that either UV or fluorescence metrics (i.e., Peak C and FI) could be used for a rapid assessment of DOM removal

by coagulation. The relative increase in FI was also linearly related to DOC removal, but the relationship less accurate than following fluorescence peak intensities. On the other hand, FI may be operationally easier to rapidly assess because inner filter effects are less important for FI compared to peak intensities.

Peaks A and C fluorescence intensities were removed in equal proportion to each other by coagulation. This result indicates that the DOM fluorescing in each region is chemically similar to each other, because it has similar affinities to removal by coagulation. This result along with other evidence suggests that the assignment of different chemical characteristics (i.e. humic acid-like and fulvic acid-like) to each EEM region is not supported.

Finally, compositional metrics were compared to DBP molar yields. There was a strong correlation between SUVA and DBP yields across chemically diverse water sources. While strong relationships between fluorescence compositional metrics have been shown in the past for localized watersheds, these relationships show more variability across diverse water sources. Therefore, fluorescence could be a valuable tool for predicting DBP formation on a local scale, but SUVA is a more universal predictor of reactivity between dissimilar water sources.

This study demonstrates that the utility of different optical measurements depends on the scale of interest. This study explored universal trends between optical measurements and DOM removal between a diverse set of water sources rather than provide an in-depth characterization of one watershed or one utility's water source. Despite some of the weaker regressions in this study, relationships between fluorescence and DBPs are likely to be more robust and informative on a local scale.

Chapter 6 Evaluating fluorescence spectroscopy as a tool to characterize cyanobacteria intracellular organic matter upon simulated release and oxidation in natural water

6.1 Abstract

The fluorescence characteristics of intracellular organic matter (IOM) extracted from three cyanobacteria species were evaluated to determine the feasibility of using fluorescence as a surrogate for IOM release during oxidation processes. Multiple fluorescence data analysis methods were explored to determine which IOM indicators provide unique fluorescence signatures even under oxidizing conditions and show minimal interactions with background dissolved organic matter (DOM). The three cyanobacteria showed similar fluorescence signatures in the Humic Region (Ex 250-450 nm, Em 300-560 nm). Parallel Factor Analysis (PARAFAC) identified 9 components in the Pigment Region (Ex 450-700 nm, Em 550-700 nm) specific to cyanobacteria with compositional differences observed between species. Interactions between IOM-specific fluorescence and DOM were found to be important and can greatly affect the design and calibration of fluorescence methods. Cyanobacteria protein-like fluorescence was quenched by 20-30% in the presence of DOM. Fluorescence at excitation 370 nm and emission 460 nm was enhanced or quenched from DOM interactions depending on the specie. For phycobiliproteins, no interaction effect was observed between DOM and phycocyanin or phycoerythrin standards. However, pigment fluorescence was severely quenched when IOM and DOM are mixed and new fluorescence peaks are also observed. Fluorescence intensity in all regions decreased with exposure to ozone, free chlorine, and chlorine dioxide, but the fluorescence index still indicated compositional differences compared to DOM. Chloramine oxidation had little effect in the Humic Region but decreased pigment fluorescence. While bulk changes in TOC or other cyanobacteria metabolites may be difficult to quantify in real-time, the

fluorescence signature of IOM, specifically compositional indicators, may provide a useful surrogate to assess release during oxidative processes.

6.2 Introduction

Cyanobacteria blooms are an area of concern for watershed management and protecting drinking water source quality. Some cyanobacteria produce cyanotoxins, such as microcystin-LR, that may present a human health risk (Hitzfeld et al., 2000; Latifi et al., 2008; Pearson et al., 2010; Sinclair and Hall, 2008; WHO, 2003). Other species produce the metabolites geosmin and 2-methylisoborneol (MIB) that create taste and odor episodes (Juttner and Watson, 2007; Smith et al., 2008; Watson, 2004; 2003). Some drinking water treatment plants apply oxidants upstream of physical removal processes to meet various treatment objectives, which has the potential to damage cell integrity and release metabolite-containing intracellular organic matter (IOM) (Ding et al., 2009; Latifi et al., 2008; Wert et al., 2013; 2014; Wert and Rosario-Ortiz, 2013; WHO, 2003; Zamyadi et al., 2012a). The release of cyanobacteria-derived organic matter is difficult to quantify, because it is likely found at low concentrations compared to NOM and may be biodegradable in the environment (Wert and Rosario-Ortiz, 2013). Monitoring the fluorescent components of IOM may be a valuable surrogate of interest for water utilities.

Phycocyanin and phycoerythrin are two fluorescent phycobiliproteins in cyanobacteria phycobilisomes that are commonly used to characterize cyanobacteria populations in natural systems (Brient et al., 2008; Izydorczyk et al., 2009; 2005; McQuaid et al., 2011; Watras and Baker, 1988). On-line fluorescence monitoring of cyanobacteria have mainly focused on probes that measure *in vivo* fluorescence of chlorophyll *a* and phycocyanin that is correlated to cell concentrations or biomass (Bastien et al., 2011; Brient et al., 2008; Gregor et al., 2007; Heaney, 1976; Stewart and Farmer, 1984; Watras and Baker, 1988; Zamyadi et al., 2012c). The ratio of

chlorophyll *a* and phycocyanin *in vivo* fluorescence has been related to the abundance of cyanobacteria compared to other algal phyla (Watras and Baker, 1988). *In vivo* measurements have also been correlated to total extractable chlorophyll *a* and phycocyanin (Zamyadi et al., 2012c). Since phycobiliproteins are predominantly limited to cyanobacteria, they are important for distinguishing cyanobacteria from other algae such as green algae.

Phycobilisomes are light harvesting complexes attached to the thylakoid membrane that expand the range of wavelengths the organism can utilize for photosynthesis. They absorb light in the visible range predominately from 550 to 650 nm, where chlorophyll *a* cannot absorb light (Bryant, 1994). The supramolecular assembly of phycobiliproteins absorbs light and then transfers the energy through the complex by predominately Förster resonance energy transfer to chlorophyll *a* (MacColl, 1998). The fluorescent behavior of phycobiliproteins is complex. Each chromophoric bilin has a unique absorbance and fluorescence spectra. The fluorescent signature of the phycobiliproteins (i.e. phycocyanin) depends on the aggregation state (monomer, trimer or hexamer) in addition to interactions with linker proteins (Bryant, 1994; MacColl, 1998). For a thorough discussion, refer to Appendix B.1. These unique fluorescent signatures occur in a wavelength region where DOM does not fluoresce strongly and may be good candidates to detect the release of cyanobacteria-derived organic matter under oxidizing conditions. No investigations have been done to evaluate if fluorescence probes designed to measure *in vivo* phycocyanin fluorescence are also suitable to detect IOM released into natural waters during water treatment operations such as oxidation processes.

The objective of this study was to evaluate the feasibility of using fluorescence spectroscopy as a surrogate for IOM in a heterogeneous DOM matrix. An ideal fluorescence surrogate should exhibit several key characteristics: it has unique fluorescence signature different

background DOM, its fluorescence signature is not impacted by interactions with background DOM, and its unique signature is not lost upon oxidation in order to act as a conservative tracer. This study investigated each of these three characteristics for IOM extracted from three cyanobacteria species in ultrapure and natural water matrices. PARAFAC was used to decompose the phycobiliprotein fluorescence, and the resulting components were compared to known fluorescing species in the literature. IOM fluorescence responses were evaluated following ozone, chlorine, chlorine dioxide, and chloramine oxidation in ultrapure water.

6.3 Methods

6.3.1 Cell Cultures and IOM Extraction

Microcystis aeruginosa (MA) (LB 2385, Culture Collection of Algae at the University of Texas, Austin, TX), *Oscillatoria* sp. (OSC) (LM 603d, Metropolitan Water District of Southern California (MWDSC), La Verne, CA), and *Lyngbya* sp. (LYG) (SDC 202d, MWDSC, La Verne, CA) were selected for the study based upon their occurrence in source water supplies, availability of an axenic culture, ability to produce odorous or toxic metabolites, and different cell morphology. Each cyanobacteria was cultured using a batch method. Details regarding the culturing methods, growth medias and growth curves can be found elsewhere (Wert et al., 2013).

MA, OSC, and LYG cells were harvested during the late exponential growth phase (28 days). The cells were separated from the growth media by centrifugation (1900 rpm, 14 min). The supernatant containing the growth media and the EOM was discarded. The remaining cell pellet was rinsed with 10 mM phosphate buffered Milli-Q water (pH = 7.5), centrifuged and the supernatant discarded with any residual growth media and/or EOM. For OSC and LYG, a mortar and pestle was used to grind the cell pellet to improve the extraction of IOM from these filamentous cyanobacteria. Three freeze-thaw sequences (-77 °C freezer, 35 °C water bath) and

sonication (60 min in an ice bath) were used to release the IOM from the cells. Filtration was used to separate the cell debris from the dissolved IOM (0.7 μm GF/F, Whatman). The filtrate was used as the extracted IOM standard for each MA, OSC, and LYG.

Phycocyanin (#P2172, Sigma Alrich, St. Louis, MO) and phycoerythrin (#52412, Sigma Aldrich, St. Louis, CO) standards were acquired to characterize the fluorescence interactions with DOM and oxidation behaviors. The phycocyanin standard was a 40% w/w lyophilized powder from *Spirulina* sp. preserved with sucrose, dithilerythritol and sodium azide. The phycoerythrin standard was dissolved in 150 mM sodium phosphate with 60% ammonium sulfate, 1 mM EDTA and 1 mM sodium azide.

6.3.2 Experimental Methods

IOM standards were diluted in lab grade water with 10 mM phosphate buffer (pH=7.5) to concentrations of 2 mg_c/L for MA and 1 mg_c/L for OSC and LYG. IOM was also spiked into filtered Colorado River Water (CRW) at varying concentrations. Similarly, phycocyanin and phycoerythrin standards were both prepared in phosphate buffer for oxidation studies and spiked to CRW in increasing concentrations.

The oxidation methods have been published in more detail elsewhere (Wert et al., 2014; 2013). Briefly, the three IOM isolates in phosphate buffer and the CRW sample were exposed to four oxidants: ozone, free chorine, chlorine dioxide and chloramines as batch processes at room temperature (20-25°C). Ozone stock solutions were prepared by dissolving gaseous ozone at a concentration of 80 mg/L (Standard Methods 4500-O3) (APHA et al., 1998) into deionized water at 2°C and adding an aliquot to the sample (Wert et al., 2009). Chlorination experiments used a 5.6% liquid sodium hypochlorite (NaOCl, Fisher Scientific, USA). Chloramination experiments used a preformed chloramine solution by first adding ammonia (29% ammonium hydroxide

solution, J.T. Baker, USA) followed by sodium hypochlorite (5.6% sodium hypochlorite, NaOCl, Fisher Scientific, USA) using a chlorine:ammonia ratio of 3:1. The pH of the preformed chloramine solution was above 10 favoring monochloramine at the time of addition. Chlorine dioxide experiments were performed using a 3,000 mg/L solution (CDG Environmental, Bethlehem, PA, USA). For the IOM, ozone and chlorine dioxide were dosed at oxidant to DOC ratios between 0 and 1. Free chlorine and chloramine were dosed at ratios between 0 and 2. Residual ozone decayed after 30 minutes and no quenching agent was required. Samples with chlorine-based oxidants and their accompanying controls were quenched with 80 mg/L of sodium thiosulfate after 120 min. The effects of quenching agents on fluorescence are discussed where appropriate.

6.3.3 Analytical Methods

A UV-VIS absorbance spectrum for each sample was measured from 200 to 800 nm (Cary 100, Agilent Technologies, CA) in a quartz cell with a 1 cm path length. Spectra were baseline corrected to the lab grade water. The average relative percent difference between duplicate absorbance measurements at 254 nm was 2%. Dissolved organic carbon (DOC) was measured using a TOC analyzer (Shimadzu, Columbia, MD) following SM5310B. The coefficient of variance (CV) between all 2 mg_C/L standards throughout the study was 2.4% (n=58).

Fluorescence excitation-emission matrices (EEMs) were collected on a spectrofluorometer (Fluoromax 4, John Yvon Horiba, NJ). EEMs were collected as a series of emission scans (300 nm to 800 nm in 2 nm increments) at set excitation wavelengths (250 nm to 700 nm in 10 nm increments). A 5 nm bandpass was used for both excitation and emission monochromators, and the integration time was 0.25 s. All EEMs were collected in ratio mode

(signal divided by reference) and incorporated instrument-specific correction factors. All EEMs were corrected and normalized following published methods and presented in Raman units (RU) (Murphy et al., 2010). EEMs were blank subtracted to minimize Raman scattering, inner filter corrected and normalized to the Raman area of 18.2MΩ lab-grade water at an excitation of 370 nm. All samples had an optical density less than 0.2 at 254 nm. All samples were stored filtered at 4°C in the dark and analyzed within 10 days.

Several fluorescence metrics were used to analyze the fluorescence data in the Humic Region (Excitation 250-450 nm, Emission 300-560 nm). Peak P intensity is the maximum in the region extending from 260 to 290 nm excitation wavelengths and 300 to 350 nm emission wavelengths. Fluorescent dissolved organic matter (FDOM) intensity is a fixed wavelength intensity located at excitation 370 nm and emission 460 nm to follow the wavelength pairs commonly used in FDOM sensors for online monitoring applications (Downing et al., 2012; Fleck et al., 2013; Kraus et al., 2010; Saraceno et al., 2009). Specific peak intensity is the peak intensity normalized to the DOC concentration presented in the units RU L mg_C^{-1}. The fluorescence index (FI) is defined as the ratio of intensities at 470 nm and 520 nm at an excitation of 370 nm and has been correlated to sample aromaticity (Cory et al., 2010; McKnight et al., 2001). These metrics are depicted in Figure 6.1.

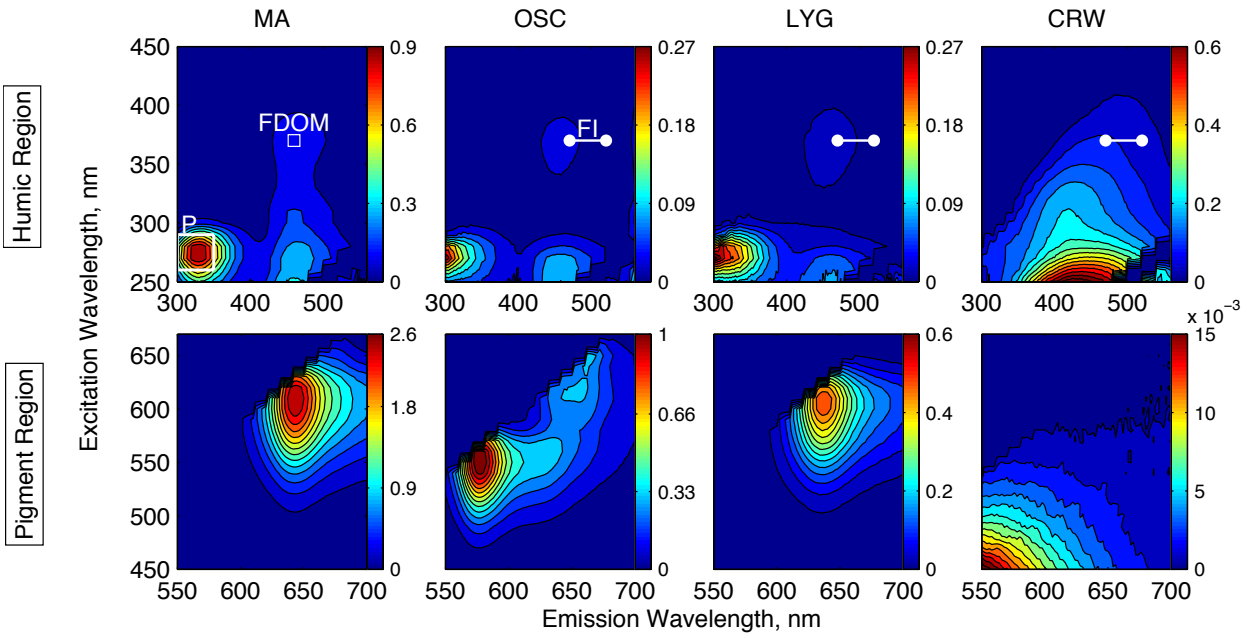

Figure 6.1 EEMs of three cyanobacteria IOM and CRW. The DOCs for each sample are 2, 1, 1, and 2.5 mg_C/L for MA, OSC, LYG and CRW, respectively. Note the wavelengths and intensity scales are different between rows. The top row is the Humic Region and the bottom row in the Pigment Region. Each column represents a different IOM species or CRW. Between the cyanobacteria IOM, the intensity in the Pigment Region is much greater than the Humic Region, and CRW fluorescence in the Pigment Region is two orders of magnitude less than the IOM. The location of the intensities used to calculate FI in the humic region are indicated with points connected by a line. The Peak P region is outlined and FDOM intensity location is marked for MA.

A parallel factor analysis (PARAFAC) model was developed for the pigment region (Ex 450-700nm, Em 550-700nm) using the DOMFluor toolbox and published tutorial (Stedmon and Bro, 2008). A PARAFAC model was not built for the Humic Region because there was not enough statistical variation in the CRW samples. Attempts yielded a model that repeatedly identified the same cyanobacteria components but was not robust in consistently identifying DOM components during random initialization. The Pigment PARAFAC Model dataset includes IOM in phosphate buffer, IOM in phosphate buffer exposed to oxidants and IOM samples spiked into CRW (n=78). The EEMs from the IOM characterization and oxidation studies spanned over four orders of magnitude. Isolated IOM samples had very strong fluorescence signal in the

pigment region exceeding 2 RU. The CRW samples had lower signals near 10^{-3} RU, and some oxidized IOM samples showed random noise around 10^{-4} RU. To adequately capture the range fluorescence signatures with a PARAFAC model and not favor the samples with the highest intensities, samples with a maximum fluorescence greater than 0.1 RU were normalized to have a maximum intensity of 0.1 RU. Samples with a maximum less than 0.1 RU were not scaled as to not inflate spectroscopic noise. After the model was fit, the resulting Fmax values were scaled up for the normalized EEMs. The order of the EEMs was also randomized using the random number generator in Excel before building the data matrix to be used in the DOMFluor toolbox. The final model has 10 components, depicted in Figure 6.2.

Full details regarding the model validation are provided in Appendix B.3. Four different validation methods were explored: sum squared error, split half analysis, random initialization and residuals analysis. Sum squared error showed little difference between 9 and 10 component models (Figure B.2). Residuals analysis justified the addition of the 10^{th} component, and the model was confirmed to be a robust minimum after 10 random initializations (Appendix B.3.2 and B.3.3, Figure B.3 to Figure B.7). Although it found similar components, split half analysis was not successful because the model is limited by the number of samples (Murphy et al., 2013) and the uneven distribution in phycoerythrin containing cyanobacteria (Figure B.8 and Figure B.9). Although split half analysis failed, the authors believe that the model is still valid given the limited pool of fluorescing pigments found in cyanobacteria cells versus the complexity of DOM and the limited number of samples in the dataset.

6.4 Results and Discussion

6.4.1 Isolation IOM Fluorescence Characterization

EEMs of each isolated IOM in phosphate buffer showed two main regions with strong fluorescence signals (Figure B.1). Figure 6.1 breaks the full EEM apart displaying each region separately. The top row in Figure 6.1 shows that IOM has a distinct fluorescence signature in the Humic Region (Excitation 250-450 nm, Emission 300-560 nm) that differs from typical DOM fluorescence, as represented by CRW. The IOM fluorescence signature is distinct compared to other studies that examined extracellular organic matter (EOM) in that EOM shows a continuum of fluorescence in the Humic Region (Qu et al., 2012). IOM, on the other hand, appears to be a much more homogeneous mixture of fluorescing compounds. The bottom row of Figure 6.1 shows that IOM has a strong fluorescence signal in the Pigment Region (Ex 450-700 nm, Em 550-700 nm) that is several orders of magnitude more intense than CRW. For the IOM, the intensity in the Pigment region is much greater than that of the Humic Region.

Since the fluorescence intensity differs significantly between the two regions, each region was analyzed separately. The remainder of the results and discussion will follow each region in parallel by referring to them as Humic Region and Pigment Region.

6.4.1.1 Humic Region Characterization

Figure 6.1 shows that the humic region, where DOM is commonly analyzed, has two different fluorescence signatures. There is strong fluorescence at the lower wavelengths, denoted as Peak P in this study. Additionally, there is a band of fluorescence at a 460 nm emission wavelength.

Fluorescence in the Peak P region has been commonly associated with protein-like functional groups because the phenolic functional group in tyrosine and the indolic functional

group in tyrptophan both fluoresce in this region (Coble, 1996; Lakowicz, 2006). Humic-associated polyphenolic compounds have also been shown to fluoresce in this region (Hernes et al., 2009; Maie et al., 2007). Given that IOM is of microbial origin and has been shown to contain fewer phenolic functional groups compared to allochthonous organic matter (Nguyen et al., 2005), it is likely that the fluorescence in this region is mainly associated with proteinaceous material. Figure 6.1 and Table 6.1 highlight some compositional differences between species. The Peak P location in MA IOM shows one peak at longer wavelengths that also corresponds more closely with the indolic functional group tryptophan (Lakowicz, 2006; Reynolds, 2003). The peak in OSC and LYG is blue-shifted to lower wavelengths with a shoulder that extends to the longer emission wavelengths. The peak fluorescence location in OSC and LYG is consistent with the presence of the phenolic functional group in tyrosine (Lakowicz, 2006), and the shoulder may be representative of overlapping signals with indolic functional groups. Even though tyrosine is less commonly measured by fluorescence because it readily participates in efficient energy transfer to tryptophan (Lakowicz, 2006), distinct contributions from the phenolic functional group is evident. Free tyrosine amino acids have been measured in MA IOM (Fang et al., 2010) and several phycobiliproteins have more tyrosine residues relative to tryptophan (Glazer and Bryant, 1975; Glazer and Fang, 1973; Ong and Glazer, 1991).

Table 6.1 Summary of fluorescence metrics for the Humic Region for isolated cyanobacteria IOM in phosphate buffer and CRW. The average and standard deviations are listed for the specific Peak P intensities and FI (n=4). Peak positions are rounded to the nearest integer. IOM specific FDOM intensities are for the unpreserved control sample.

Source	Peak P (Ex, Em) (nm)	Peak P Sp. Intensity (RU L mg_C^{-1})	FI	FDOM Sp. Intensity (RU L mg_C^{-1})
MA IOM	280, 330	0.49 ± 0.04	2.32 ± 0.02	0.081
OSC IOM	270, 302	0.29 ± 0.02	2.65 ± 0.06	0.052
LYG IOM	270, 301	0.27 ± 0.02	2.39 ± 0.05	0.021
CRW	260, 350	0.16 ± 0.01	1.50 ± 0.01	0.039 ± 0.002

Table 6.1 quantitatively compares differences in fluorescence signatures between species. MA has more fluorescent material per unit carbon compared to OSC and LYG. Preservation with sodium thiosulfate had no systematic effect on Peak P fluorescence, so specific intensity presented include all control samples, with and without preservative. These compositional differences affecting both fluorescence maxima and specific intensities are important to develop strategic monitoring strategies to detect the release of IOM.

All species have a common fluorescence emission around 460 nm with excitation maxima near 250 and 370 nm suggesting that the fluorescence may be related to each other by Kasha's rule (Kasha, 1950). The major intrinsic fluorophores in cells are nicotinamide adenine dinucleotide (NADH or NAD(P)H) and flavins (Lakowicz, 2006). NADH has a characteristic fluorescence emission at 460 nm whereas flavins emit around 525 nm (Lakowicz, 2006). This fluorescence may be associated with the presence of (NADH), a coenzyme that is important to all cell metabolism. Pure NADH in water has absorption maxima at 260 and 340 nm (Wolfbeis, 1985), but the differences observed here may be due to interactions with other constituents that can affect optical signatures (Lakowicz, 2006; Wolfbeis, 1985). While there are other naturally occurring fluorescing compounds that fluoresce around 460 nm like flavones, chormones and coumarins, most occur in plants and are not well documented to occur in cyanobacteria (Wolfbeis, 1985). Figure 6.1 shows that MA also has additional fluorescence at higher excitation wavelengths near 300 nm, which indicates compositional differences from OSC and LYG.

Figure 6.1 shows that the fluorescence signal where FI is measured in the humic region is common to all three species characterized. Table 6.1 shows that the FI of the three IOM was high compared to CRW. Values above 2 are high compared to the microbially derived fulvic acids, but FI values greater than 2 have been attributed to nonhumic organic matter released directly

from algae (McKnight et al., 2001). Sample preservation did not lead to any systematic change in FI.

All three species exhibited fluorescence maxima at excitation wavelengths of 370 nm and emission wavelengths ranging from 456 to 462 nm, which coincides with the wavelengths used in some FDOM sensors (Downing et al., 2012). Table 6.1 presents the specific intensities for samples without preservatives. Adding preservative decreased the FDOM fluorescence specific intensity for MA and LYG by 0.02 and 0.14 RU L mg_C^{-1}, respectively, while slightly increasing the specific intensity for LYG by 0.005 RU L mg_C^{-1}. The reproducibility among the three preserved FDOM specific peak intensities had CV values between 6 and 10%, including DOC error. Since FI did not change, it suggests that the fluorescence is quenched uniformly across those emission wavelengths. Only the unpreserved samples are tabulated, because the investigation of IOM-DOM effects relied on unpreserved samples. Table 6.1 shows that the amount of fluorescing material in this region varies between species with MA containing the most fluorescent material per unit carbon followed by OSC and LYG. While both OSC and LYG had similar specific Peak P intensities, specific FDOM intensities differed between the two species. Differences in specific fluorescence intensity highlight compositional differences between cyanobacteria species and suggest that the sensitivity for detecting IOM-specific fluorescence varies between species. The relationship between fluorescence and mass of IOM is also varies between species.

Comparing the cyanobacteria fluorescence to CRW demonstrates some of the disadvantages related to monitoring fluorescence in this region. The cyanobacteria-derived fluorescence overlaps with regions of strong fluorescence in CRW and other natural waters. The Peak P specific intensity is greater in cyanobacteria compared to CRW, suggesting that this

region would have greater fluorescence sensitivity for capturing increases in IOM concentration. The specific FDOM intensity for CRW falls in between LYG and OSC and is about half as high as MA. This result suggests that it may be easier to detect species such as MA and more difficult to detect IOM from less fluorescent ones like LYG with FDOM sensors. The consistent differences in FI, however, indicate that FI could be a useful tool for detecting the release of IOM during preoxidation because it is very different in magnitude compared to CRW and all species behave similarly. Most surface waters have FI values less than about 1.6, so these results would be applicable across most surface waters.

6.4.1.2 Pigment Region PARAFAC Model

The PARAFAC model identified 10 components of which 9 are associated with the cyanobacteria and 1 is associated with DOM fluorescence. The components are summarized in Table 6.2 and depicted in Figure 6.2. All model components are denoted with the letter P before the component number.

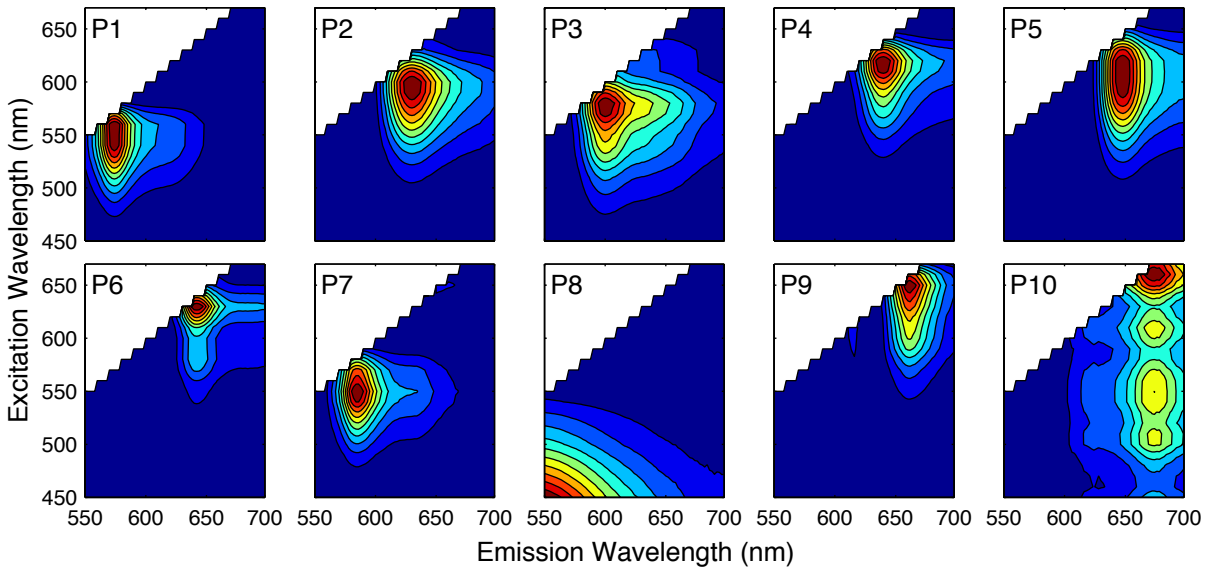

Figure 6.2 Components from the IOM Pigment PARAFAC model. The component number is indicated in the corner of each subplot.

PARAFAC models of humic substances have been published that range between 4 and 13 components (Cory and McKnight, 2005; Xu and Jiang, 2013). Due to the heterogeneous nature of DOM and knowledge gaps in fully understanding DOM fluorescence mechanisms, the number and location of DOM model components depend on the range of statistical variability in the dataset. This application provides a unique opportunity, because the model is restricted to cyanobacteria organic matter that has a limited number of fluorescing phycobiliproteins that have been well characterized. The model components were compared to literature data, not to provide conclusive identification, but to determine if the statistical components identified by PARAFAC fall within the range of known fluorescing phycobiliproteins and make physical sense. Comparisons with literature data relied on component maxima because full spectra were often not available.

Six of the ten Pigment Model components were found to be dominant in the isolated IOM in phosphate buffer for at least one cyanobacteria species. Preserving the samples did not have any systematic effect on the component loadings, and the standard deviations between replicates are less than 3% (Table 6.3). Three of the PARAFAC components (P2, P4, P5) are likely associated with the pigment phycocyanin (Table 6.2). These three components combined accounted for 82% and 93% of the fluorescence in MA and LYG (Table 6.3), respectively. Since OSC is phycoerythrin dominated, phycocyanin components only accounted for 22% of the fluorescence. The absorption and emission maximum for P2 is characteristic of the β155 fluorophore in phycocyanin (Debreczeny et al., 1993; Demidov and Mimuro, 1995). P4 and P5 components match closely to the monomer and trimer forms of phycocyanin, respectively (Alberts and Takács, 2004; Bryant, 1994; Debreczeny et al., 1993). A description of the different aggregation states is provided in Appendix B.1 and references therein. P4 accounted for a

significant portion of the fluorescence in all three cyanobacteria, whereas P5 was limited mostly to MA and LYG. Not only are the subtle differences in component peaks supported by literature, they highlight compositional differences between species that are not apparent using simpler techniques such as peak picking.

Components P1 and P7 are likely associated with phycoerythrin, and these components were found only in the OSC IOM, a benthic cyanobacteria, whereas MA and LYG are both planktonic species. Phycoerythrin is beneficial to benthic cyanobacteria, because the longer wavelengths of sunlight are attenuated with increasing depth resulting in predominately blue-green light exposure (MacColl, 1998). Phycoerythrin increases the ability of benthic cyanobacteria to utilize these wavelengths. Not all species produce phycoerythrin but some strains of both OSC and LYG are known producers (Bryant, 1982; Suda et al., 2002). P1 and P7 accounted for 68% of the OSC pigment fluorescence. The apparent dominance of phycoerythrin in OSC is likely a combination of two effects: (1) Cyanobacteria modify the proportions of phycoerythrin and phycocyanin produced based on chromatic adaptation (MacColl, 1998), and (2) Even if there were equal amounts of both, phycoerythrin also has a higher fluorescence quantum yield compared to other phycobiliproteins and could result in a greater apparent fluorescence intensity (Grabowski and Gantt, 1978).

Table 6.2 IOM Pigment PARAFAC Model components, suggested pigment material and occurrence in isolated IOM in LGW.

Comp	Ex (nm)	Em (nm)	Suggested Pigment	Ref.	Specie
P1	560	574	C-Phycoerythrin	1	OSC
P2	600	630	C-Phycocyanin (β155)	2, 3	MA, LYG
P3	530 (s), **580,** 610-620 (s)	600, 620(s)	Phycocyanin + DOM		
P4	620	640	C-Phycocyanin (trimer)	5	MA, OSC, LYG
P5	600-620	648	C-Phycocyanin (monomer)	2	MA, LYG
P6	580-600 (s), **630**	642	Phycocyanin + DOM		MA
P7	550	586	Phycoerythrin	6, 7	OSC
P8	< 450	< 550	DOM fluorescence		CRW
P9	650	662	Allophycocyanin (trimer)	5	MA, OSC
P10	(<450, 510, 550, 610, **660**)	674	Allophycocyanin (B), phycobilisome	5, 6, 8	MA

(s) indicates shoulder. Bold values indicate maximum absorbance.

References. [1](Bryant, 1982) [2](Debreczeny et al., 1993) [3](Demidov and Mimuro, 1995) [4](MacColl et al., 1981) [5](Bryant, 1994) [6](Rigbi et al., 1980) [7](MacColl, 1998) [8](Ley et al., 1977)

Table 6.3 Distribution of Pigment Model PARAFAC components between cyanobacteria IOM and CRW. Values presented as the percent contribution plus or minus the standard deviation between replicates (n=4 for cyanobacteria and n=3 for CRW). Dominant components for each sample are in bold.

	Pigment Model Component Percentage									
Sample	**P1**	**P2**	**P3**	**P4**	**P5**	**P6**	**P7**	**P8**	**P9**	**P10**
MA IOM	0 ± 0	**28 ± 0.1**	0 ± 0	**17 ± 2**	**37 ± 2**	**7 ± 1**	0 ± 0	0 ± 0	**9 ± 1**	1 ± 0.3
OSC IOM	**41 ± 3**	6 ± 0.4	0.4 ± 1	**11 ± 1**	5 ± 1	0 ± 0	**27 ± 3**	0 ± 0	**11 ± 2**	0 ± 0
LYG IOM	0 ± 0	**46 ± 1**	3 ± 2	**36 ± 2**	**11 ± 1**	1 ± 1	2 ± 1	0 ± 0	0 ± 0	0 ± 0
CRW	5 ± 0.1	0 ± 0	8 ± 0.1	0 ± 0	0 ± 0	0 ± 0	2 ± 0.4	**77 ± 1**	0 ± 0	8 ± 0.5

Component P6 accounted for about 7% of the MA IOM fluorescence, but was not found in the IOM from OSC and LYG. The peak emission for this component is similar to that of phycocyanin but its absorption maximum is shifted to longer wavelengths. This behavior is similar to phycocyanin monomer that is associated with a polypeptide linker. It has been shown that the association of a polypeptide linker leads to an absorbance red-shift, which increases spectral overlap for better energy transfer to allophycocyanin (Glauser et al., 1993). While this component only accounted for a small percentage of the MA IOM fluorescence, it was found to be important for characterizing IOM interactions with DOM and is discussed in Section 6.4.2.

Component P9 has the typical signature for allophycocyanin trimer (Bryant, 1994). Interestingly, this component was only identified in MA and OSC. Allophycocyanin makes up the core of all cyanobacteria phycobilisomes yet none was found in the LYG IOM. Even in MA and OSC, this component only accounted for about 10% of the IOM pigment fluorescence.

Component P10, only found in MA IOM, was difficult to compare to literature and only contributed to about 1% of the MA fluorescence. The red-shifted emission at 674 nm is characteristic of allophycocyanin B (AP-B), a phycobiliprotein that is found between allophycocyanin and chlorophyll *a* to facilitate more efficient energy transfer (Glazer and Bryant, 1975). P10 has an absorption maximum at 660 nm, which matches AP-B, but P10 has several other local maxima at lower wavelengths. Absorption maxima for purified AP-B have been reported at 619 and 669 nm, which do not match the model component (Glazer and Bryant, 1975; Ley et al., 1977). The multiple absorption peaks may also be indicative of intact phycobilisomes, where multiple phycobiliproteins are absorbing light and energy is transferred to the terminal AP-B before emission, but the P10 absorbance peaks do not match published literature and intact phycobilisomes are not likely these ionic strengths (Gray et al., 1973; Rigbi

et al., 1980; Wildman and Bowen, 1974). The residuals analysis statistically justifies the inclusion of this component but shows that this component does not fit all absorption maxima particularly well simultaneously (Appendix B.3.4, Figure B.6 and Figure B.7a). Both components P9 and P10 account for such little fluorescence compared to the other pigments that they are not practical for monitoring IOM and will not be further discussed.

Component P8 is associated with DOM in the CRW samples. The component spectrum has an exponential decay for both the absorption and emission. The signal in this region is low with maxima at excitation 450 nm and emission 550 nm of 0.015 RU for CRW. Past research has also confirmed DOM fluorescence into the visible region (Boyle et al., 2009). P8 accounted for 77% of the fluorescence in CRW samples. While Table 6.3 does include a low occurrence of some pigments in CRW, the percent contributions are amplified by the low signal in the original EEM. These values are not considered to be physically significant and are likely an artifact of the spectroscopic noise in the visible region.

PARAFAC is a purely statistical modeling process that does not have any preconception about the fluorescence phenomena. The six components contributing to isolated IOM fluorescence have fluorescence peaks that fall into the range of pigments known to occur in cyanobacteria. In other words, no components appear to be purely statistical artifacts but are known to exist within the range of phycobiliprotein fluorescence.

6.4.2 IOM Fluorescence Interactions with DOM

Characterizing IOM fluorescence in buffered LGW may not be representative of the fluorescence behavior in a heterogeneous background matrix. An ideal fluorescence surrogate for IOM would exhibit minimal interactions with background DOM. This section evaluates if IOM-specific fluorescence behaves independently of DOM or interacts to either enhance or quench

fluorescence. Isolated IOM was spiked into CRW at increasing concentrations to determine the effect of a background matrix on the IOM fluorescence signature.

6.4.2.1 Humic Region

The fluorescence index was found to be sensitive to changes in IOM concentration. Figure 6.3a shows that FI increases with increasing IOM concentration but the trend is not linear. An initial addition of IOM leads to the greatest increase in FI with subsequent additions leading to incrementally smaller FI increases. Past work has demonstrated that FI does not follow property balance principles, because there are competing effects of peak emission wavelength and spectrum curvature (Korak et al., 2014a). In this study, the peak emission wavelength for OSC and LYG was blue-shift compared to CRW but MA was not. As OSC and LYG IOM are spiked into CRW, the observed decrease in FI was due to primarily a shift in peak emission wavelength. For MA, there was no systematic shift in peak emission and the observed increase was due to a change in local curvature. For monitoring applications, an increase in FI may be an indicator for released cyanobacteria organic matter, but the magnitude of the increase is not directly proportional to the mass added.

Figure 6.3b depicts the Peak P fluorescence response to increasing IOM concentrations in CRW. By comparing the observed increases for IOM spiked into CRW to the specific peak intensities of the isolated IOM, an assessment of the interactions can be made. If there are no interactions, then the measured intensities should increase proportional to the specific fluorescence intensities in Table 6.1. Figure 6.3b shows that peak intensity increases proportionally to the IOM spike concentration. OSC and LYG both had similar Peak P specific peak intensities and showed similar Peak P increases when spiked in CRW. MA IOM had a higher Peak P specific fluorescence, and as a result it shows a larger increase in Peak P

fluorescence per unit increase in IOM DOC. The increase, however, was 20-30% less than predicted by the specific intensity of the isolated IOM, and MA showed signs of non-linearity at the highest spike concentration. These observations indicate that there are some interactions between the Peak P fluorescing species and background DOM that quenches the IOM Peak P fluorescence.

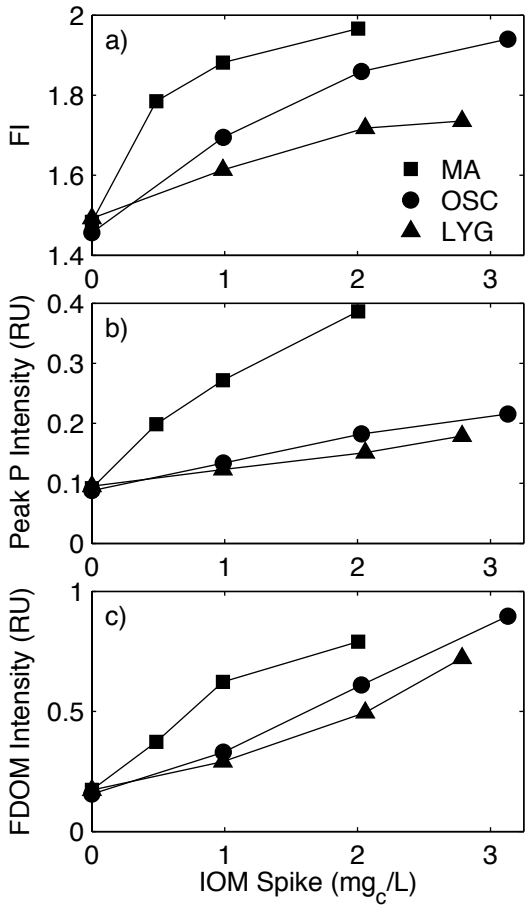

Figure 6.3 Humic Region fluorescence indicators responsive to IOM spiked into CRW plotted as a) Fluorescence index, b) Maximum protein-like fluorescence and c) FDOM fluorescence intensity (Ex 370 nm, Em 460 nm)

Lastly, the FDOM fluorescence intensity also increases with increasing IOM concentration (Figure 6.3c). The increase for OSC appears to be directly proportional to the increase in IOM concentration. The amount by which it increases is about 20% less than the

amount predicted by the specific peak intensities of the isolated IOM comparing the samples without preservatives (Table 6.1). These results suggest that the interactions between the IOM and DOM lead to a quenching of intensity in this region. For LYG, the observed fluorescence increase when spiked into CRW was about 40% greater than predicted suggesting a fluorescence enhancement. The concave-up curvature also suggests that the interactions are not uniform across the IOM concentration range. Intensity increases were greatest for MA IOM, which had the greatest specific fluorescence intensity in this region. Compared to the isolated IOM, however, the increase is about 80% greater than predicted.

These results highlight the importance of selecting appropriate metrics for monitoring dynamic systems or compositional changes in DOM. FI has potential to be an easily monitored fluorescence indicator because it is operationally easy to measure and does not require inner filter corrections for most applications (Korak et al., 2014a; McKnight et al., 2001). Since it is largely concentration-independent, it is robust towards fluctuations in background DOM quantity or quality and would be less dependent on baseline measurement before IOM release. The downside is that an FI increase is not directly proportional to the quantity of IOM introduced. Single point fluorescence intensities can provide better direct correlations between fluorescence response and changes in IOM mass. Disadvantages are that any quantitative calibrations must include interaction effects and cannot be based solely on isolated standards. Additionally, single point intensity methods are not robust against changes in background DOM composition and/or concentration unless they can be characterized in tandem.

6.4.2.2 Pigment Region

Analysis of the pigment region indicates that the fluorescence in this region is strongly affected by interactions between DOM and IOM in both intensity and spectra. The interactions

were assessed by spiking both IOM and pigment standards into CRW. Adding either phycocyanin or phycoerythrin standards to CRW found no indication of interaction effects. There was no change in the peak location and the fluorescence intensity increase was representative of the standard fluorescence in phosphate buffer (Figure 6.4, Figure B.17, and Figure B.18). When IOM is spiked into CRW, however, the pigment fluorescence intensity decreased by more than an order of magnitude across the entire region (Figure 6.4c). In addition to decreased intensity, new fluorescence behavior was observed from the interacting species (Figure 6.4, Figure B.11, Figure B.14, and Figure B.16). The 650 nm emission starts to show two distinct excitation maxima around 580 nm and 640 nm. There is also fluorescence that appears at a 580 nm excitation and 600 nm emission that was not present in the isolated IOM. Since this behavior was observed in all three cyanobacteria, this behavior is likely due to the interactions of phycocyanin rather than the other phycobiliproteins.

The PARAFAC model captured the complexity of the interactions. Two components, P3 and P6, were not found in the isolated IOM in any significant amount. When IOM was spiked into CRW, the phycocyanin components that accounted for much of the fluorescence in the isolated IOM (P2, P4 and P5) showed little increase with increasing IOM concentration and loadings were an order of magnitude less than the isolated IOM (Figure B.10, Figure B.13 and Figure B.15). Components P3 and P6, however, do increase with IOM concentration accounting for most of the fluorescence. P3 accounts for the new fluorescence observed at a 580 nm excitation and 600 nm emission. Component P6 has a red-shifted excitation maxima that occurs at 630 nm rather than the 600-620 nm excitation of phycocyanin.

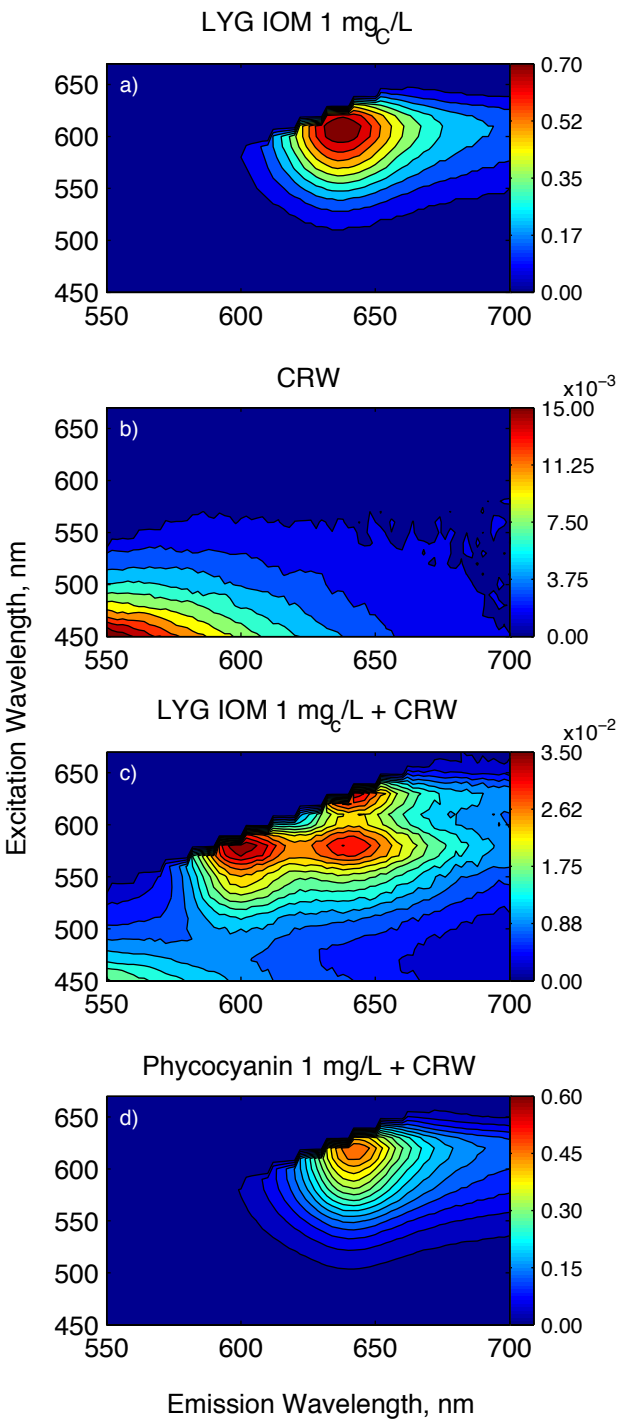

Figure 6.4 EEMs for a) Lyngbya IOM at 1 mg/L in LGW, b) Colorado River Water, and c) Lyngbya IOM at 1 mg/L spiked into CRW and d) Phycocyanin standard spiked into CRW

One study examined the interactions between phycobiliproteins and both glutardialdyhyde and benzoquinone and found that two different mechanisms can lead to a decrease in fluorescence intensity (Köst et al., 1981). Phycobiliproteins fluoresce because the tertiary polypeptide backbone provides molecular rigidity and prevents non-radiative decay (Köst et al., 1981). For glutardialdehyde, it was suspected that the intramolecular interactions of the tertiary structure are interrupted which increases molecular flexibility and decreases fluorescence. Benzoquinone, on the other hand, is thought to quench fluorescence through energy transfer interactions (Köst et al., 1981). Both quenching mechanisms have kinetic half lives ranging from less than 10 minutes to several hours (Köst et al., 1981). The specific mechanism causing the fluorescence quenching and wavelength shifts observed in the IOM are unknown. Samples from both the IOM and phycobiliproteins standard experiments were subjected to the similar experimental conditions, storage and holding times, which suggests that there is something compositionally different about the IOM samples affecting pigment fluorescence. The purified phycobiliproteins appear to behave differently and may be due to the absence of other components such as polypeptide linkers.

In any case, the interactions between the phycobiliproteins and DOM have some practical implications for using phycobiliproteins as an IOM fluorescence surrogate. Calibration to a standard solution would greatly underestimate the presence of IOM in a DOM matrix if interaction effects were not taken into account. Since the emission maxima shifts and the intensity is greatly reduced, the set wavelengths of existing probes may be of limited utility to detect IOM releases. There may also be kinetic aspects of the quenching interactions to be considered. This study showed that sample hold times as short as 3 days exhibit severe quenching interactions. Since the kinetics of these interactions are unknown, phycocyanin probes

with the ability in to measure fluorescence in real-time may still be applicable for detecting IOM released during preoxidation but require further characterization.

6.4.3 IOM Oxidation Studies

The three IOM isolates in phosphate buffer were exposed to ozone, free chlorine, chloramine and chlorine dioxide to determine how their fluorescence signatures change during oxidation. An ideal fluorescence surrogate would exhibit no change in its fluorescence signature to act as a conservative indicator for the release of other metabolites of interest. Oxidant dose is presented as the ratio of oxidant concentration to DOC concentration to normalize for differences in IOM concentration.

6.4.3.1 Humic Fluorescence Region

The oxidation behavior of the Humic Region fluorescence was characterized by following the change in FI and FDOM intensity. Analyzing both in tandem reveals how both IOM quantity and composition change during oxidation within the same EEM region. Figure 6.5 shows that ozone oxidation led to the greatest loss of FDOM intensity and a simultaneous change in composition as indicated by a decrease in FI. Chlorine dioxide and free chlorine oxidation both decreased the FDOM intensity, but not to the extent of ozone. The maximum decrease for chlorine dioxide was about 40% for OSC whereas the decrease for MA and LYG was closer to 10%. All three species had a decrease in FI at the lowest chlorine dioxide and free chlorine doses applied with little change at higher doses, indicating a compositional change. Chloramine oxidation had little effect on FDOM intensity for OSC and LYG but caused an enhancement for MA. This trend suggests that there are compositional differences between the species that lead to different oxidation responses despite similarities in their fluorescence signatures. There was little change in FI due to chloramine oxidation indicating that this oxidant is too weak to cause

significant compositional changes to the IOM. Peak P showed similar trends between oxidants and species are presented in Figure B.19.

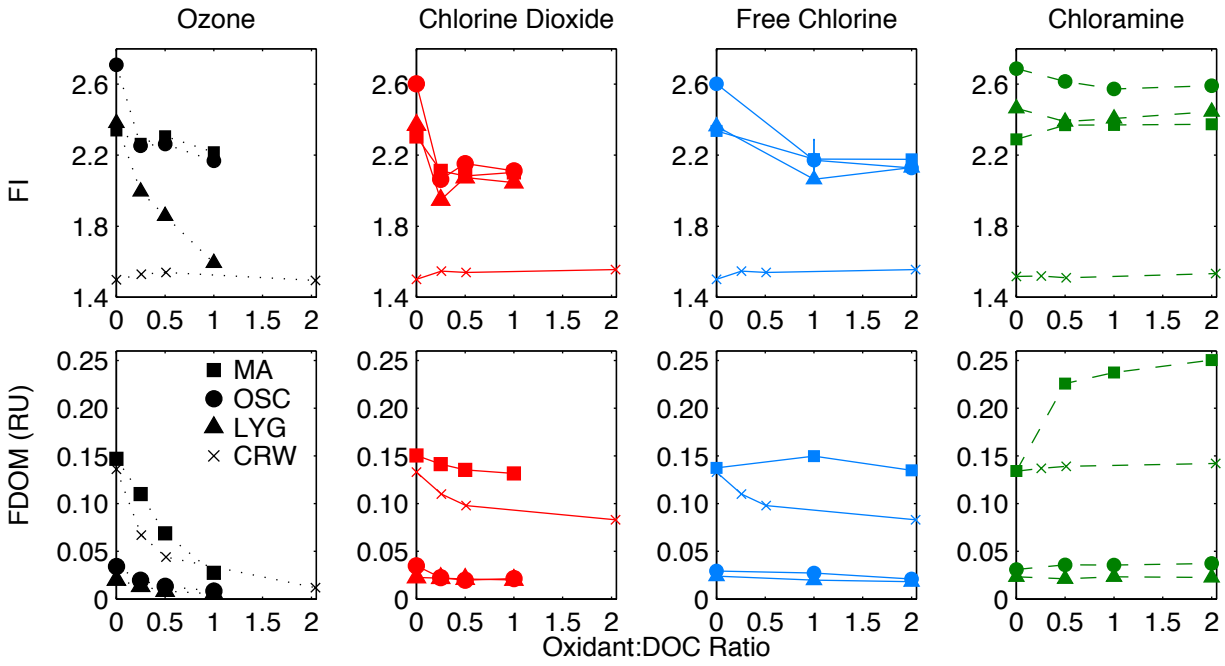

Figure 6.5 Response of humic region indicators to oxidation for IOM and CRW. The top row presents the FI data and the bottom row the FDOM intensity. One free chlorine dose ratio (1) was run as experimental duplicates and the error bars represent the standard deviation, but most error bars are smaller than the marker size.

Comparing the fluorescence responses to the different oxidants demonstrates that the utility of each fluorescence metric is oxidant-specific. IOM released during ozonation may react with continued exposure, lose its fluorescence signature, and become difficult detect by intensity changes alone. FI may be more effective than measuring regional intensity because the lowest FI values observed are still higher than that of bulk CRW and most other surface waters. Detection of IOM released during oxidation by free chlorine, chlorine dioxide and chloramines may be detectable by measuring FDOM intensity changes because the fluorescent IOM is less reactive. A disadvantage of measuring FDOM intensity is that it requires a baseline measurement and there may be sensitivity issues for some species with low specific intensities (i.e. OSC and LYG).

The large differences in FI between all three IOM and CRW suggest that FI would be a better method than FDOM intensities for detecting IOM release by tracking compositional changes.

6.4.3.2 Pigment Fluorescence Region

IOM fluorescence in the pigment region was also analyzed to determine how reactive the phycobiliproteins are towards oxidants. Figure 6.6 illustrates the behavior observed for the dominant IOM components in the Pigment Region. Component P1, related to the phycoerythrin in OSC, was very reactive and lost almost all fluorescence characteristics at the lowest ozone, free chlorine and chlorine dioxide dose ratios applied. P1 retained most of its fluorescence character during chloramination but is still more reactive than the fluorescing species in the Humic Region. Figure 6.6b and Figure 6.6c shows that the phycocyanin-like components (P2 and P5) are very reactive towards all four oxidants, even chloramines. The oxidation behaviors of the PARAFAC components agree well with the oxidation of phycocyanin and phycoerythrin standards (Figure B.20 and Table S-2). All PARAFAC components in this region showed similar reactivities; the complete data set is provided in Figure B.21 to Figure B.29.

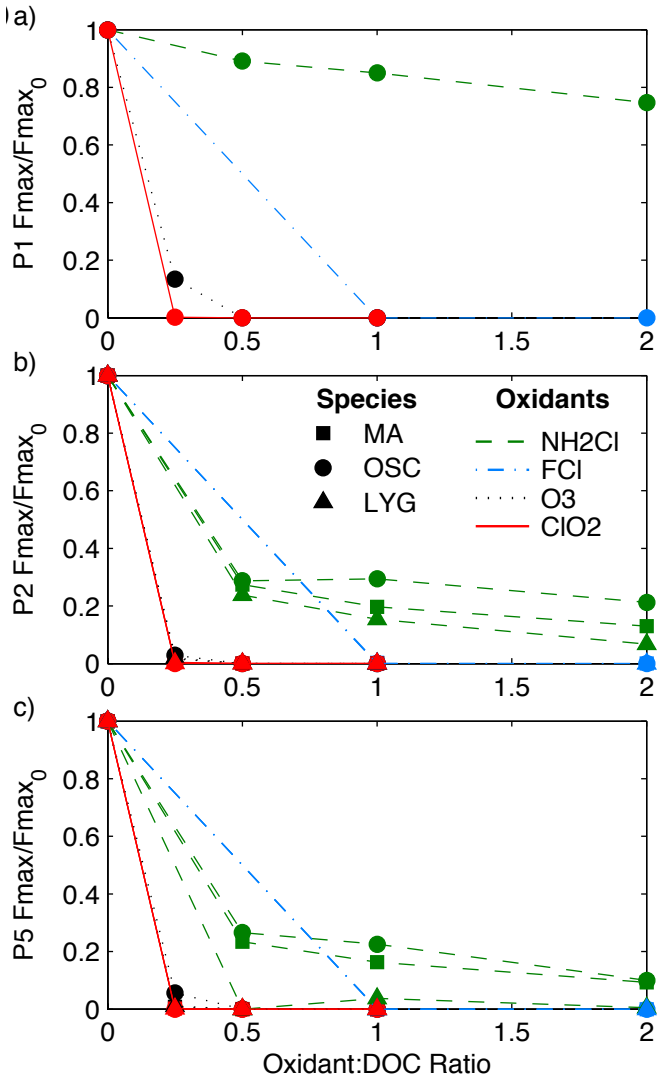

Figure 6.6 Response of Pigment PARAFAC components plotted on a relative basis during oxidation for a) P1 for OSC, b) P2 for MA, OSC and LYG, and c) P5 for MA, OSC and LYG.

Loss of fluorescence could be due to a couple different mechanisms. Electrophilic oxidants could be reacting directly with the tetrapyrrole chromophores that are electron rich systems with 6 to 8 conjugated double bonds (MacColl, 1998). As mentioned with regards to the quenching interactions, phycobiliprotein fluorescence relies on the molecular rigidity of the tertiary polypeptide structure (Köst et al., 1981). Loss of fluorescence during oxidation could also be due to a loss in the rigidity of the molecule.

The rapid loss of pigment fluorescence during oxidation may prevent phycobiliproteins from being a useful indicator of IOM release. While they are highly fluorescent and do not overlap with DOM fluorescence, they will likely react quickly once in the bulk solution and lose their fluorescence character in addition to quenching interactions with DOM. Chloramination is the only case where there may be a possibility of detecting these pigments in the bulk solution in the absence of quenching interactions. This study used preformed chloramines, but in applications where chloramines are formed by sequential addition free chlorine and ammonia, observed pigment loss may be closer to that of free chlorine.

6.5 Conclusions

- MA, OSC and LYG all show similarities in their fluorescence characteristics with strong protein-like fluorescence, a common emission at 460 nm and high FI values.
- MA and LYG were dominated by phycocyanin fluorescence whereas OSC had strong phycoerythrin fluorescence. PARAFAC decomposed the IOM phycobiliprotein fluorescence into components that fall within the range of fluorescence known to occur in cyanobacteria.
- FI appears to be the most promising fluorescence surrogate for IOM release by measuring compositional changes rather than intensity changes. It does not require robust baseline measurements for stable source waters, is sensitive even for cyanobacteria species with low specific fluorescence intensities and exhibits predictable interactions with background DOM. Under oxidizing conditions, FI values remain high compared to background DOM and offer a unique signature even though FDOM intensity decreases.

- The phycobiliproteins in IOM are not promising as a surrogate for IOM release, because their fluorescence intensity is severely quenched by interactions with DOM and their fluorescence intensity decreases during oxidation.

Chapter 7 Fluorescence indicators as a surrogate for intracellular organic matter and metabolites released from cyanobacteria cells upon oxidation

7.1 Abstract

Algal blooms can have severe impacts to drinking water systems, including decreased filter run times and increased concentrations of taste and odor compounds. During cyanobacteria blooms, for example, water treatment plants that apply preoxidation steps before physical cell removal have the potential to compromise cell integrity and release intracellular metabolites. Of particular interest to drinking water utilities is the development of optical methods to monitor cell concentrations and potential organic matter releases into the water. This study evaluated the use of fluorescence spectroscopy as a suitable indicator for the release of intracellular organic matter (IOM) and cell bound metabolites (i.e. microcystin-LR, MIB and geosmin) for three cyanobacteria species (*Microcystis aeruginosa, Oscillatoria sp. and Lyngbya sp.*). After evaluating several different methods for analyzing fluorescence data, the fluorescence index (FI) and FDOM intensity (Ex 370 nm, Em 460 nm) proved to be the most valuable surrogates. Phycobiliproteins, such as phycocyanin and phycoerythrin, were shown to be poor indicators. FI and FDOM intensity exhibited the greatest fluorescence response for *Microcystis* compared to *Oscillatoria* and *Lyngbya*. Fluorescence was also a better indicator for systems using weaker oxidants (free chlorine and chloramine) compared to strong oxidants (ozone and chlorine dioxide). FI and FDOM responses both correlated with the release of different metabolites (Microcystin-LR, 2-methylisoborneol (MIB) and geosmin). Comparing the two indicators, measuring compositional changes by FI in the dissolved phase acted as a better conservative surrogate for metabolite release.

7.2 Introduction

Cyanobacteria blooms are an emerging area of concern for water quality management and are expected to become more prevalent and persistent with climate change (Carey et al., 2012; Paerl and Paul, 2012). Some cyanobacteria contain cyanotoxins (e.g. Microcystin-LR) that pose a risk to human health when excreted (Hitzfeld et al., 2000; Pearson et al., 2010; Sinclair and S. Hall, 2008). For example, the World Health Organization has set a maximum concentration guideline of 1 μg/L (WHO, 2003). Other species produce metabolites that are taste and odor compounds (i.e. 2-methylisoborneol (MIB) and geosmin) that are aesthetically unpleasing and impact consumer confidence (Juttner and Watson, 2007; Smith et al., 2008; Watson, 2004; 2003). The occurrence of cyanobacteria blooms depends on a number of factors but is more common in nutrient-rich (i.e. phosphorous and nitrogen) environments.

Cyanobacteria blooms in source waters are of special concern to drinking water facilities. These blooms can cause operational problems when the cells enter a treatment plant. High cell concentrations cause operational problems by clogging filters. They can develop local cultures within the plant inhabiting multiple unit operations (Zamyadi et al., 2012b). In addition to affecting plant operation, cyanobacteria blooms change the source water quality. Cyanobacteria cells have the potential to release harmful metabolites into the dissolved phase. While coagulation and filtration can remove cyanobacteria cells intact (Henderson et al., 2008; Zamyadi et al., 2013; 2012b), some treatment plants apply oxidants upstream of these unit operations to achieve other treatment objections, such as controlling for invasive species, metal speciation or disinfection byproduct (DBP) precursors. Oxidation has the potential to compromise cell integrity and release intracellular organic matter (IOM), which also contains cyanotoxins, taste and odor compounds and DBP precursors (Ding et al., 2009; Latifi et al.,

2008; Wert et al., 2014; 2013; Wert and Rosario-Ortiz, 2013; Zamyadi et al., 2012a). Detecting IOM release with dissolved organic carbon (DOC) is difficult, because the concentration increase is small compared to instrument sensitivity (Wert et al., 2014). A rapid, online monitoring tool that can detect IOM and metabolite releases could be beneficial to utilities that are concerned about operating preoxidation processes during cyanobacteria blooms.

Fluorescence spectroscopy has been used to characterized cyanobacteria. Phycobiliproteins, light harvesting complexes attached to the thylakoid membrane, are strongly fluorescent, and they were originally identified based on their fluorescent signatures (Bryant, 1994; 1982; Ley et al., 1977; MacColl, 1998; Rigbi et al., 1980). Online probes have been used to measure the *in vivo* fluorescence of the phycobiliproteins phycocyanin and phycoerythrin (Brient et al., 2008; Izydorczyk et al., 2009; 2005; McQuaid et al., 2011; Zamyadi et al., 2012c), because the *in vivo* fluorescence intensities correlate well to cell or biomass concentration (Bastien et al., 2011; Brient et al., 2008; D. Stewart and Farmer, 1984; Watras and Baker, 1988; Zamyadi et al., 2012c). Use of these probes to detect phycobiliproteins released with IOM during oxidation processes has never been investigated. In addition to phycobiliproteins, recent work has characterized the fluorescence characteristics of IOM from three cyanobacteria species and found that IOM has unique fluorescence signatures in the Humic Region (Figure 7.1) that could also serve as viable tools for monitoring IOM release during oxidative processes (Korak et al., 2014c). All three cyanobacteria species exhibited strong fluorescence in the protein-like region, consistent fluorescence emission where commercial fluorescent dissolved organic matter (FDOM) sensors measure (Ex 370 nm, Em 460 nm) and high fluorescence index (FI) values greater than 2. Spiking IOM into a heterogeneous dissolved organic matter (DOM) matrix did reveal some non-ideal fluorescence behaviors, where the signals were not following linear

superposition principles (Korak et al., 2014c). Finally, each IOM fluorescence indicator behaved differently with exposure to different oxidants.

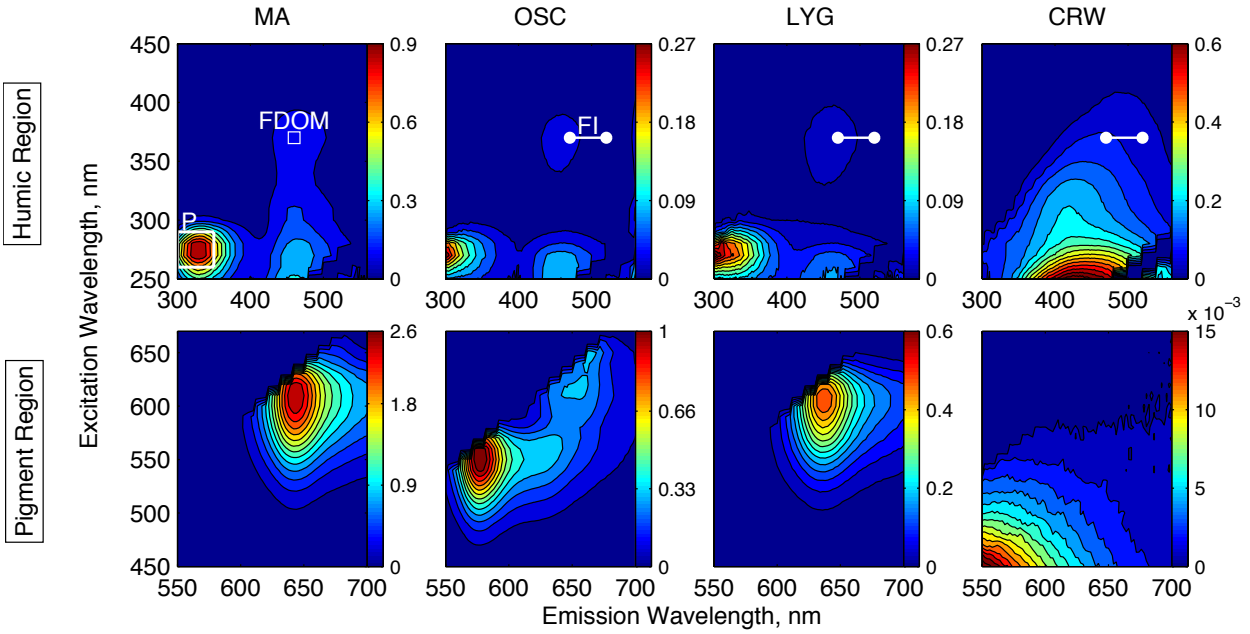

Figure 7.1 EEMs of isolated IOM from three cyanobacteria species (MA, OSC and LYG) and CRW (columns). Each row represents a different region of the EEM. The locations of Peak P, FDOM and FI are outlined in the top row.

This study investigates the utility of using fluorescence spectroscopy as an optical surrogate to detect IOM and metabolite release from cyanobacteria cells by monitoring changes in the dissolved phase fluorescence characteristics. Different fluorescence metrics are compared to determine the advantages and disadvantages of monitoring different fluorescence wavelengths. Finally, relationships between fluorescence response, metabolite release and viable cell counts are explored to determine if fluorescence can act as a conservative tracer for other processes of interest, such as cyanotoxin release.

7.3 Methods and Materials

7.3.1 Cyanobacteria Culturing

Three different cyanobacteria species were cultured in the lab in controlled environments. *Microcystis aeruginosa* (MA) (LB 2385, Culture Collection of Algae at the University of Texas, Austin, TX, USA) is a unicellular cyanobacteria and a confirmed producer of Microcystin-LR, a cyanotoxin. *Oscillatoria sp.* (OSC) (LM 603d, Metropolitan Water District of Southern California (MWDSC), La Verne, CA, USA) is a filamentous cyanobacteria with no mucilaginous sheath and a confirmed producer of MIB. *Lyngbya sp.* (LYG) (SDC 202d, MWDSC, La Verne, CA, USA) is a filamentous cyanobacteria with a mucilaginous sheath and a confirmed geosmin producer.

Full details of the growth media, experimental conditions and growth curves are published elsewhere (Wert et al., 2013). Briefly, the cells were cultured in batch mode inside a chamber that controlled temperature and light exposure (Geneva Scientific, Fontana, WI, USA). The cultures were exposed to 12 hours of light followed by 12 hours of darkness at 22°C. The cultures were grown in multiple 500 mL capacity Erlenmeyer flasks. The growth media was BG-11 for OSC and LYG and Bold 3N for MA. The cells were harvested on the 28^{th} day as the cultures approached the late exponential phase.

7.3.2 Cell Suspension Preparation

The cells were separated from the growth media and extracellular organic matter (EOM) by centrifuging the cells and decanting the supernatant. The cells were suspended in 10mM phosphate buffer (pH=7.5) and centrifuged again with the supernatant discarded.

The cell concentrations were determined using flow cytometry (FlowCAM, Fluid Imaging Technologies, Yarmouth, ME, USA). For the filamentous species (LYG and OSC), the total number cells were determined based on the average length of each filament and the average width of each cell within the filament. These cell counts are the nominal cell counts and were used to spike the aliquots of cells into Colorado River Water (CRW). These values are also reported in the figure legends even though the actual cell counts for each oxidation test varied. Viable cell concentrations were determined using the Trigger Mode feature that detected the number of fluorescent cells. The full details regarding this process are published in Wert et al (2013).

MA was spiked into CRW at nominal cell concentrations of 200,000 cells/mL and 50,000 cells/mL (for ozone only). OSC suspensions were tested at 2,800 cells/mL and 1,400 cells/mL. Finally, LYG cells were tested at nominal cell concentrations of 1,600 cells/mL and 800 cells/mL. The water quality characteristics of CRW were as follows: DOC of 2.65 mg/L, pH of 8.0, alkalinity of 138 mg/L and absorbance at 254 nm (UV_{254}) of 0.052 cm^{-1}.

7.3.3 Oxidation

The cells suspended in CRW were subjected to four different oxidants (ozone, free chlorine, chlorine dioxide and chloramine) at oxidant to DOC ratios of 0, 0.25, 0.5, 0.75, 1 and 2 based on an estimated DOC of 2.5 mg/L. The reaction period was 24 hours, during which time the samples were in 1L amber bottles and loosely capped. Residual ozone decayed after 30 minutes and no preservative was used. Free chlorine, chlorine dioxide and chloramine samples were quenched with 80 mg/L sodium thiosulfate. Samples were filtered through 0.7 µm GF/F filters prior to dissolved phase analysis. Oxidant exposure (CT values) were published in Wert et al (2013) along with the complete oxidation methods.

Ozone oxidation studies used a concentrated ozone stock solution in deionized water that had a concentration around 80 mg/L as determined by the indigo method (Standard Method 4500-O_3) (APHA et al., 1998). Free chlorine experiments were performed using a 1200 mg/L stock solutions prepared from 5.6% sodium hypochlorite solution (NaOCl, Fisher Scientific, USA). Free chlorine residuals were determined using the DPD method. Chlorine dioxide experiments were performed using a 3000 mg/L solution (CDG Environmental, Bethlehem, PA, USA). Residuals were measured using the DPD method with added glycine to eliminate free chlorine interferences. Chloramine tests were conducted using a preformed solution prepared by adding ammonia followed by sodium hypochlorite in a chlorine:ammonia ratio of 3:1. The pH was maintained above 10 to promote monochloramine formation.

7.3.4 Analytical Methods

7.3.4.1 Fluorescence Methods

Fluorescence excitation-emission matrices (EEMs) were measured for each filtered sample. Excitation wavelengths varied from 240 nm to 700 nm in 10 nm increments with a 5 nm bandpass. Emission wavelengths incremented from 300 nm to 800 nm in 2 nm increments with a 5 nm bandpass. All data was collected in ratio mode (signal divided by reference), and the integration time was set to 0.25 s. The data was corrected for primary and secondary inner filter effects using an absorption spectrum collected from 200 to 800 nm (Cary 100 Bio, Agilent, CA). All samples were blank subtracted and normalized to the area under the Raman spectrum of lab-grade water collected at an excitation wavelength of 350 nm.

The corrected data were analyzed using a couple of different metrics. FDOM intensity is defined at the fluorescence intensity at 370 nm excitation and 460 nm emission (Downing et al., 2012). FI is defined as the ratio of emission intensities (470 nm divided by 520 nm) at an

excitation wavelength of 370 nm (Cory et al., 2010; McKnight et al., 2001). Peak P intensity is defined as the maximum intensity within the region outlined between 260 nm and 290 nm excitation wavelengths and 300 nm and 350 nm emission wavelengths. The pigment region is defined as fluorescence occurring within the visible wavelength range depicted in the bottom row of Figure 7.1.

7.3.4.2 Metabolite Analysis

Full details regarding the analytical methods for Microcystin-LR, MIB and geosmin are published in Wert et al (2013) and the supplemental information therein. In summary, MIB and geosmin analysis samples were collected in head space free vials, concentrated using solid-phase micro extracted, and analyzed on a gas chromatography-tandem mass spectrometer (GC-MS/MS) in positive electron ionization (EI). The method reporting limit (MRL) was determined to be 5 ng/L for both compounds. Microcystin-LR was analyzed using liquid chromatography-mass spectrometer in negative electrospray ionization (ESI) mode using direct injection analysis. The MRL was determined to be 500 ng/L for Microcystin-LR.

7.4 Results and Discussion

7.4.1 Fluorescence Response due to Cell Oxidation

Fluorescence EEMs generate thousands of data points for a given sample and leave many possibilities for analyzing the data. Figure 7.1 depicts four different metrics that were found to be useful identifiers for IOM and common between all three species (Korak et al., 2014c). This section follows each metrics to determine which indicators generate a fluorescence response that is substantially different from CRW. In other words, this section evaluates each fluorescence metric to determine if it has a signal response during cell oxidation studies that could be useful for monitoring IOM and metabolite release.

7.4.1.1 FDOM (Ex 370 nm/Em 460 nm) intensity

FDOM intensity was evaluated to determine if it has a signal response indicative of IOM release due to cell oxidation. Figure 7.2 reports the relative change in FDOM intensity as function of oxidant to dose ratio. While the results are presented on a relative basis, the FDOM intensities of CRW with suspended cells prior to filtration were within 3% of samples without spiked cells, demonstrating that the suspended cells in the absence of oxidation do not affect the dissolved phase fluorescence.

Figure 7.2 shows that the FDOM fluorescence response depends on both the cyanobacteria species and oxidant used. MA exhibited the strongest fluorescence response to cell oxidation. For free chlorine, chlorine dioxide and chloramine, FDOM intensity increased 80-100% at the lowest oxidant to dose ratio (0.25). With increasing oxidant dose, FDOM intensity for chlorine dioxide and free chlorine decreased, but still remained greater than the initial value. The decrease observed suggests that the rate of fluorescence loss due to oxidation exceeds the rate of IOM released into the bulk solution. Increasing chloramine doses led to an increase in FDOM intensity. Past work oxidizing IOM isolates demonstrated that MA IOM FDOM intensity increases with increasing chloramine exposure (Korak et al., 2014c). Therefore, it is difficult to conclude if the continued increase at higher doses is due to an increase in IOM concentration or an increase in IOM fluorescence already released, simply due to oxidant exposure. For all three of these oxidants, FDOM intensity was greater than the CRW control samples, indicating a release of fluorescent IOM into the bulk water and demonstrates that fluorescence could be a valuable monitoring tool for MA cells in the presence of the chlorine-based oxidants.

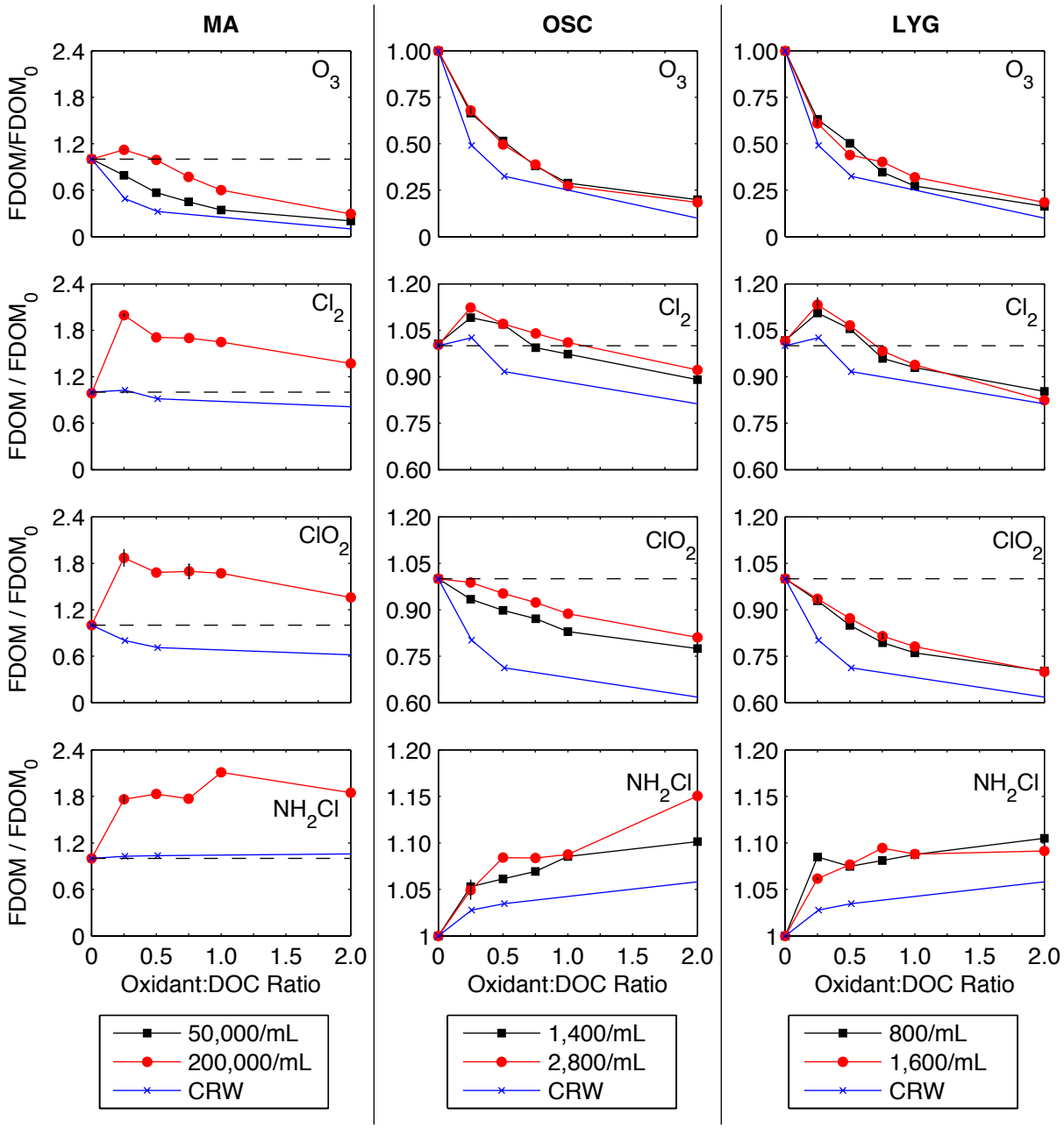

Figure 7.2 FDOM response as a function of oxidant:DOC ratio for cells from three cyanobacteria species (MA, OSC, and LYG) suspended in CRW and four oxidants (ozone, free chlorine, chlorine dioxide and chloramine).

FDOM intensity did not increase significantly for ozone oxidation of MA cells. Figure 7.2 shows that FDOM intensity for systems with and without MA cells decreased in a dose response manner. At the lowest dose ratio (0.25), there is a 12% increase in FDOM intensity for

a system with 200,000 cells/mL before decreasing at higher ozone doses. This dose ratio was conducted in duplicate with true experimental replicates. The relative standard deviation between samples was less than 1%, indicating that the 12% increase is significant. Once released, IOM FDOM intensity will decrease with increasing ozone exposure, because ozone is a strong electrophile that will likely attack chromophoric moieties (Korak et al., 2014c). At both cell concentrations, the decrease in FDOM intensity was less than the decrease observed in the CRW oxidation control study, and there was also a differentiation between the different cell concentrations. The decrease in intensity was less for the higher initial cell concentration (200,000 cells/mL) compared to the lower starting concentration (50,000 cells/mL). These results suggest one of two possible mechanisms. The first is that the greater FDOM intensity in the MA cell oxidation studies compared to the control is indicative of a release of fluorescent organic matter that, when counterbalanced with the loss of fluorescence due to oxidation, yields a slower apparent loss in fluorescence. The other possibility is that reactions between ozone and cellular material decrease the effective ozone dose and its ability to oxidize CRW yielding a smaller apparent loss in FDOM intensity. Since DOC and microcystin-LR measurements corroborated a release of organic matter upon ozone oxidation (Wert et al., 2014), it is likely that the smaller decrease in FDOM intensity observed during MA cell oxidation is due to the counter balancing effects of IOM release and subsequent oxidation. This type of analysis relies on inferring differences in the decay rate, which is not an ideal method for developing a rapid fluorescence monitoring probes. Therefore, species-oxidant combinations that the do not generate a significant increase in FDOM intensity will not be considered in Section 7.4.2 for the development of relationships with metabolite release.

OSC and LYG cell oxidation exhibited almost identical behaviors to each other in terms of the magnitude of the fluorescence response and the general behavior. FDOM intensity decreased with exposure to ozone and chlorine dioxide. In both cases, the observed decrease during cell oxidation was less than the decrease observed for CRW without suspended cells. There was a difference in cell concentrations for OSC with chlorine dioxide but not for the other combinations. Data from previous work (Wert et al., 2014) supports the release of IOM for both species with chlorine dioxide and for OSC with ozone. Like MA oxidation with ozone, FDOM intensities can only detect IOM release if the relative differences in decay rates are inferred as such. This approach is not ideal and demonstrates that FDOM may not be the most powerful monitoring tool for ozone in general and chlorine dioxide for these species.

Free chlorine and chloramine oxidation both caused FDOM intensity responses indicative of IOM release from OSC and LYG. Oxidation by free chlorine exhibited a small increase in FDOM intensity followed by a decrease with increasing oxidant dose. The increase suggests a scenario where the rate of release for IOM fluorescent material exceeds the rate of fluorescence loss by oxidation. Upon oxidation with chloramine, FDOM intensity increased at the lowest doses and then exhibited little change at the higher doses. While the FDOM intensity of CRW also increased with chloramine exposure, the intensity increase was greater with suspended cells and suggests increased fluorescent material in the dissolved phase due to IOM release. Data from Wert et al (2014) provides secondary lines of evidence that the increases in fluorescence intensity are associated with the release of IOM.

The smaller magnitude of the fluorescence response for OSC and LYG compared to MA may be due to several different factors. The differences in cell concentrations are likely not the reason for the lower response. Trigger mode data quantifying the number of viable cells showed

that LYG and OSC are much more resistant to oxidation (Wert et al., 2013). Since the cell concentrations were at least an order of magnitude smaller compared to MA, there was effectively a higher oxidant concentration per cell in the system. Even with proportionally more oxidant molecules, the cell destruction rate was slower. This suggests that there is something inherently different about OSC and LYG (perhaps morphology) that makes it more resistant to IOM release. Even though there was a large difference in the cell concentrations, the amount of DOC released was comparable between all three species. Measured DOC concentrations showed that all oxidation studies led to less than 0.3 mg_C/L increase in DOC (Wert et al., 2014). MA oxidation did not lead to any greater increase in DOC compared to LYG even though the cell concentrations differed by two orders of magnitude. MA IOM has a greater specific FDOM intensity compared to LYG and OSC (Korak et al., 2014c). If the same mass of IOM is released, MA IOM will have a greater fluorescence intensity simply due to the compositional differences in the IOM, which best explains the lower fluorescence response for LYG and OSC.

7.4.1.2 Fluorescence Index

FI was measured to detect differences in the dissolved phase organic matter composition and determine if monitoring compositional changes is a viable surrogate for IOM release. An 0.05 increase in FI was considered a significant increase based on the reproducibility of the FI measurement (Korak et al., 2014a) and the maximum increase observed in the CRW control samples. The FI of CRW during the OSC studies was statistically lower than the FI during the MA, LYG and control studies ($p<0.001$). There was no statistical difference in FI between the MA, LYG and control studies. Therefore, the FI for CRW in the OSC studies was estimated based on the differential change and the starting FI value from that batch in order to provide a baseline.

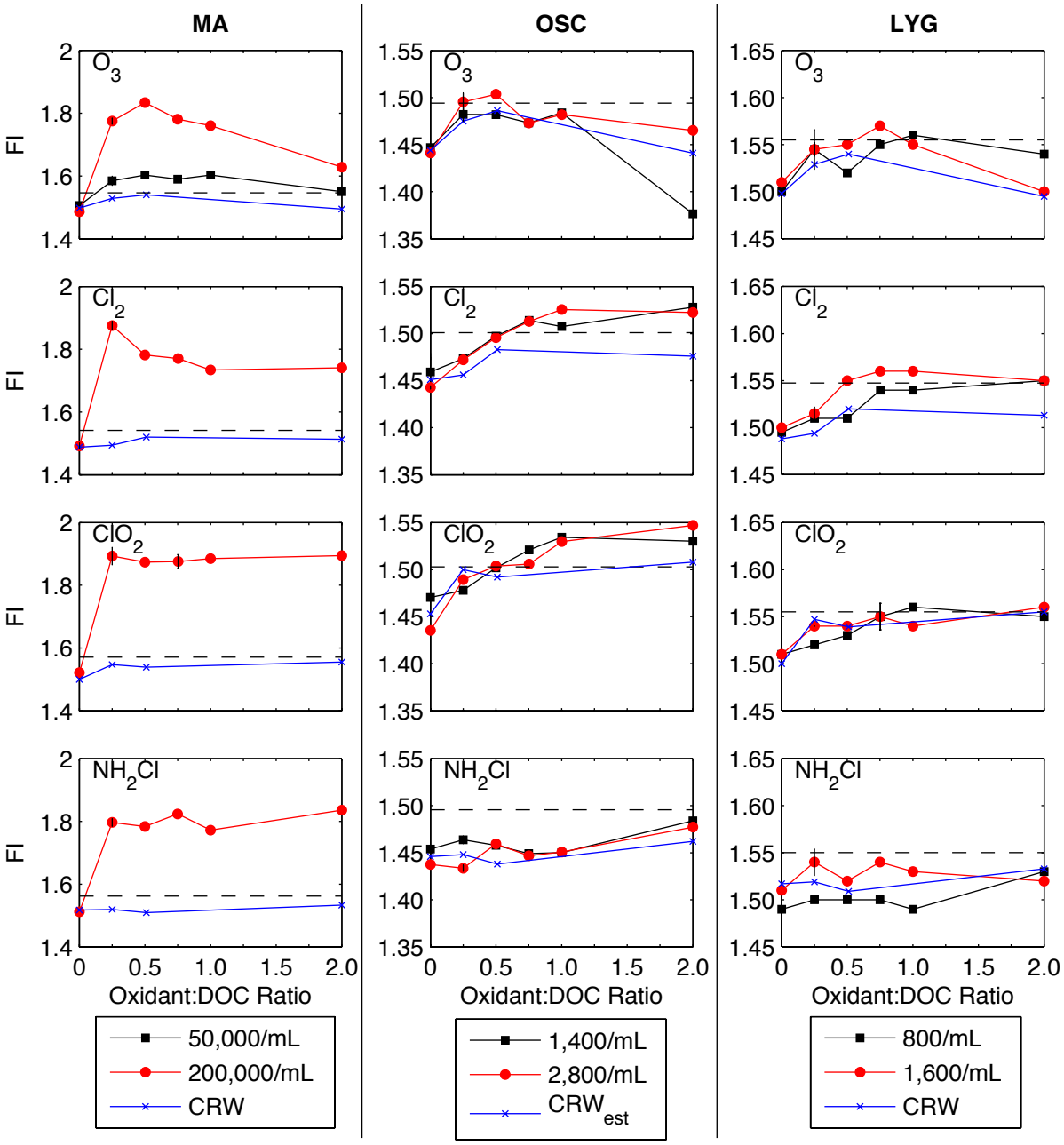

Figure 7.3 FI response as a function of oxidant:dose ratio for the oxidation of cyanobacteria cells suspended in CRW for three different species (MA, OSC, LYG) and four oxidants (ozone, free chlorine, chlorine dioxide and chloramine). Dashed line represents threshold defining a significant increase.

For MA, FI shows a similar trend compared to FDOM for oxidation by free chlorine, chlorine dioxide and chloramines. FI increased at the lowest oxidant dose (Figure 7.3). For

chlorine dioxide and chloramine, there was little change in FI at higher doses. FI decreased with increasing free chlorine dose as the fluorescence characteristic of released IOM change. Figure 7.3 shows that the free chlorine and chloramine FI trends at higher oxidant doses agree well with the trends observed in the IOM oxidation studies (Korak et al., 2014c). These results demonstrate that FI is a suitable surrogate to investigate further as an indicator for MA metabolite release due to the three chlorine-based oxidants.

For detecting IOM release from MA during ozone oxidation, FI performed better than FDOM intensities. Even though FDOM intensity decreased, FI increased at the lowest oxidant doses following the same trend as the other three oxidants. The improved sensitivity of FI is expected. Based on mixing studies in Korak et al (2014a and 2014b), FI has the greatest increase for the first increment of high FI material added and incrementally smaller increases with further additions. At higher doses, FI decreases, which is expected based on the large decrease observed in the IOM oxidation studies (Korak et al., 2014c). Even though the fluorescence intensity decreases due to ozone oxidation, there is a shift in DOM composition that is captured by FI indicating the increased contribution of high FI material. Using FDOM intensities, IOM release is inferred from differences in the relative decrease in intensity, but the FI response provides a direct measurement that directly corresponds to the DOC response (Wert et al., 2014).

Similar to FDOM intensity, OSC and LYG had similar FI responses to each other. FI is not a practical monitoring tool for detecting IOM release during ozone oxidation at the cell concentrations tested. A couple of doses produced an FI that was 0.05 greater than the initial value, but it decreases at higher doses due to continued oxidant exposure following the trends in the IOM oxidation studies. For OSC (chlorine and chlorine dioxide) and LYG (chlorine), FI increased but exhibited a plateau at higher oxidant doses. The increase observed during the cell

oxidation studies was greater than the CRW studies indicating that FI is detecting increased IOM contribution in the bulk solution and are a potential surrogate for metabolite release. These results demonstrate that FI is sensitive to subtle changes in composition for rather low cell concentrations (800 cells/mL). There was no significant increase in FI during chloramine oxidation, demonstrating that FDOM provides a better indicator of IOM release than FI in this case. One advantage of FI over FDOM is that FI increases throughout the dose range whereas FDOM intensity decreases at higher doses. Therefore, IOM release does not have to be inferred from relative rates of decrease, and this approach may be easier to interpret from a monitoring perspective.

7.4.1.3 Protein Peak

Even though all three cyanobacteria IOM isolates exhibited strong fluorescence in the Peak P region, this region of the EEM was determined to be a poor indicator of IOM release. In general, this metric had worse accuracy with greater relative standard deviations as indicated by the error bars in Figure C.1. There was also evidence of non-ideal quenching interactions between the IOM and DOM, which was predicted based on the IOM isolate study (Korak et al., 2014c). Full details regarding Peak P results are provided in Appendix C.1.

7.4.1.4 Pigments

Phycobiliproteins also proved to be poor surrogates for IOM release, even though fluorescence in this region is unique to cyanobacteria. No fluorescence from the phycobiliproteins was observed at any of the low initial cell concentrations. At the high initial cell concentration, phycobiliproteins fluorescence was observed in only two cases. A low intensity signal was observed for MA (200,000 cells/mL) with ozone (Figure 7.4) and MA with

chloramines (Figure 7.5). No OSC or LYG EEMs exhibited well-defined contours indicative of phycobiliproteins as shown in Figure C.2 to Figure C.12.

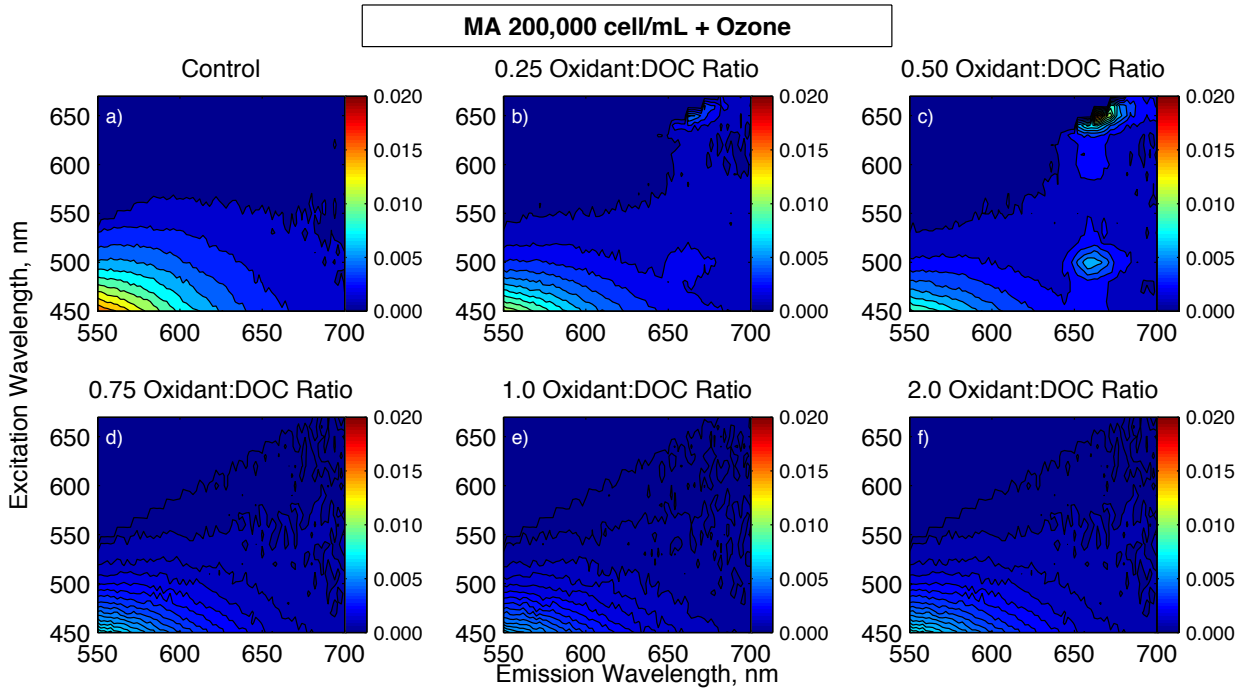

Figure 7.4 Fluorescence EEMs in the Pigment Region for MA cells (200,000 cells/mL) suspended in CRW and exposed to increasing doses of ozone.

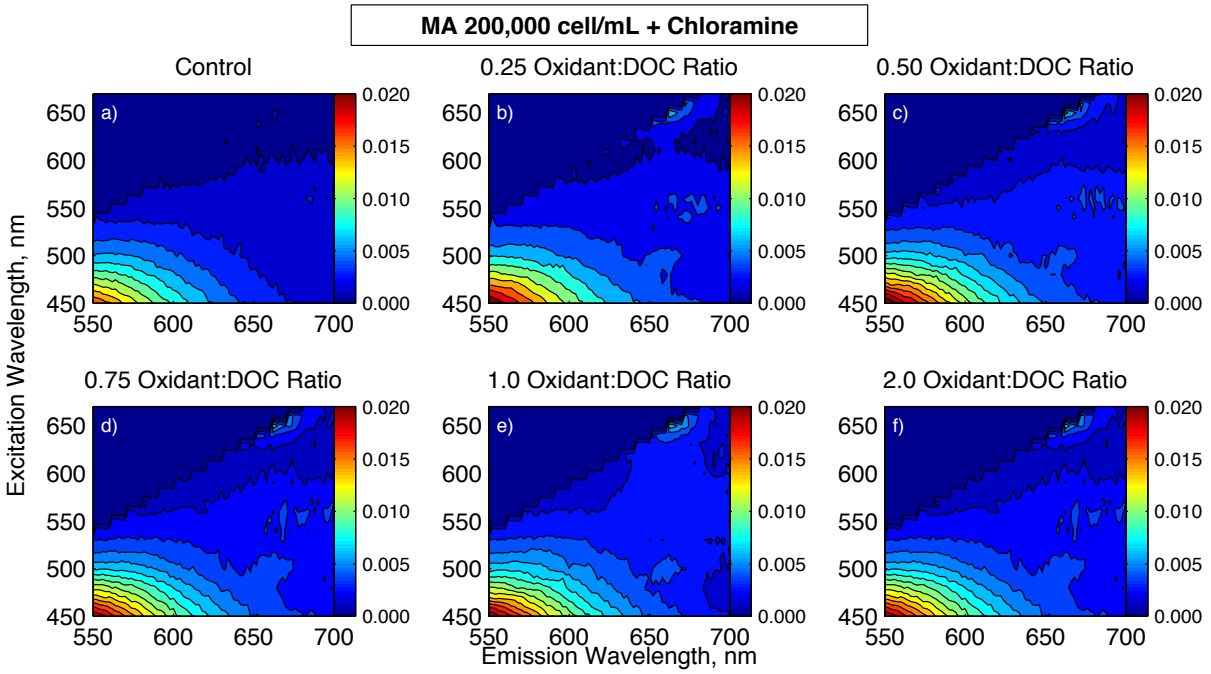

Figure 7.5 Fluorescence EEMs in the Pigment Region for MA cells (200,000 cells/mL) suspended in CRW and exposed to increasing doses of chloramine.

For both cases, the fluorescence peaks occur in the same locations, neither of which corresponded to the more commonly measured phycobiliproteins phycocyanin and phycoerythrin. The higher excitation wavelength signal (650 nm, 664 nm) suggests the compound is related to allophycocyanin (Bryant, 1994) and is similar to component P9 found in a PARAFAC model from the three IOM isolates (Korak et al., 2014c). The signal occurring at the lower excitation wavelength (500 nm, 658 nm) does not correspond with a PARAFAC component but was identified during the PARAFAC model residuals analysis. Fluorescence at this location was measured when MA was spiked into CRW, but this residual was not abundant enough to be captured as an individual PARAFAC component (Appendix B.3.4).

A lack of fluorescence intensity in this region is expected based on the experiments with isolated IOM (Korak et al., 2014c). Oxidation studies found that the phycobiliproteins readily react with all four oxidants and lose most of their fluorescence signal at low oxidant doses.

Additionally, the phycobiliproteins strongly interact with the CRW DOM and quench the fluorescence intensity. The signal that does appear in a few cases does not occur in the same regions as phycocyanin or phycoerythrin. Therefore, probes that are designed to monitor wavelengths corresponding with those phycobiliproteins would effectively not capture any signal from released IOM.

7.4.1.5 Comparison of Fluorescence Metrics

The results presented in the preceding sections demonstrate that the fluorescence response depends on the metric, the cyanobacteria species, and oxidant used. Monitoring for phycobiliproteins performed poorly for all species and oxidants fluorescence in this range is specific to cyanobacteria. FDOM and FI both performed well and had good reproducibility between experimental replicates. Although IOM has a high Peak P intensity per unit carbon compared to CRW, this metric also responded poorly. It exhibited poor reproducibility and is likely affected by non-ideal quenching interactions.

For any given fluorescence metric and oxidant, MA yielded a greater response compared to OSC and LYG. This trend is likely due to compositional differences in the IOM, because MA IOM has a greater fluorescence intensity in both FDOM and Peak P regions per unit carbon compared to OSC and LYG. Cell concentrations do not appear to be as important of a factor, because all three species released similar amounts of DOC.

Comparing different oxidants, fluorescence measurements had greater responses for weaker oxidants. The response for cell oxidation by ozone was generally less than the response by the other three oxidants. After an initial response, the difference between cell oxidation samples and CRW samples is sustained with weaker oxidants compared to the stronger oxidants, where the fluorescence response trends towards that of the CRW control samples at higher doses.

7.4.2 Optical Properties as a Surrogate for Metabolite Release

The following section analyzing how the fluorescence response compares to metabolite release and the loss of viable cells. Based on the previous section, the fluorescence analysis is limited to following FDOM intensities and FI for only the oxidant/cyanobacteria combinations that yielded a significant fluorescence increase in Figure 7.2 and Figure 7.3. Cases where IOM release may be inferred from the differential decrease are not considered, because this scenario is not practical for monitoring applications.

7.4.2.1 Release of Microcystin-LR

FDOM intensity and FI are plotted against the measured Microcystin-LR (MC-LR) concentration to determine if there is a correlation between the metabolite release and fluorescence response. Figure 7.6a shows that the initial condition (cells with no oxidant) had MC-LR concentrations at or just above the detection limit of 0.5 μg/L. At the lowest oxidant:dose ratio (0.25), FI increases from 1.5 to about 1.8 for all four oxidants with a simultaneous increase in MC-LR (as indicated by the black arrows). The increase in both FI and MC-LR were similar for free chlorine, chlorine dioxide and chloramine. Ozone oxidation exhibited a similar increase in FI but a much smaller increase in MC-LR. These differences are likely attributed to differences in oxidation rates. The reported MC-LR reaction rate constants for ozone and hydroxyl radical (k_{app}=4.1 × 10^5 M^{-1} s^{-1} and k_{app}=1.1 × 10^{10} M^{-1} s^{-1}, respectively) are much greater compared to free chlorine (k_{app}=33 M^{-1} s^{-1}), chlorine dioxide (k_{app}=1 M^{-1} s^{-1}) and chloramine (k_{app}<1 M^{-1} s^{-1}) (Rodriguez et al., 2007). Therefore, MC-LR released to the bulk solution will readily degrade in the presence of ozone.

As the oxidant dose increases, there was no change in MC-LR for chloramine oxidation, which is expected due to the low reaction rate constant. With all other oxidants, the MC-LR

concentration decreases towards the detection level, but there is little change in FI. FI decreases slightly with increasing exposure but is still greater than the initial condition. Only the first three data points for ozone oxidation are shown on Figure 7.6 for clarity. With increasing ozone dose, FI decreased and MC-LR was below the detection limit for all samples. The decreases in FI with increasing dose agree with the IOM oxidation study results, which showed that IOM exposed to ozone, free chlorine, and chlorine dioxide would exhibit decreases in FI to different degrees (Korak et al., 2014c).

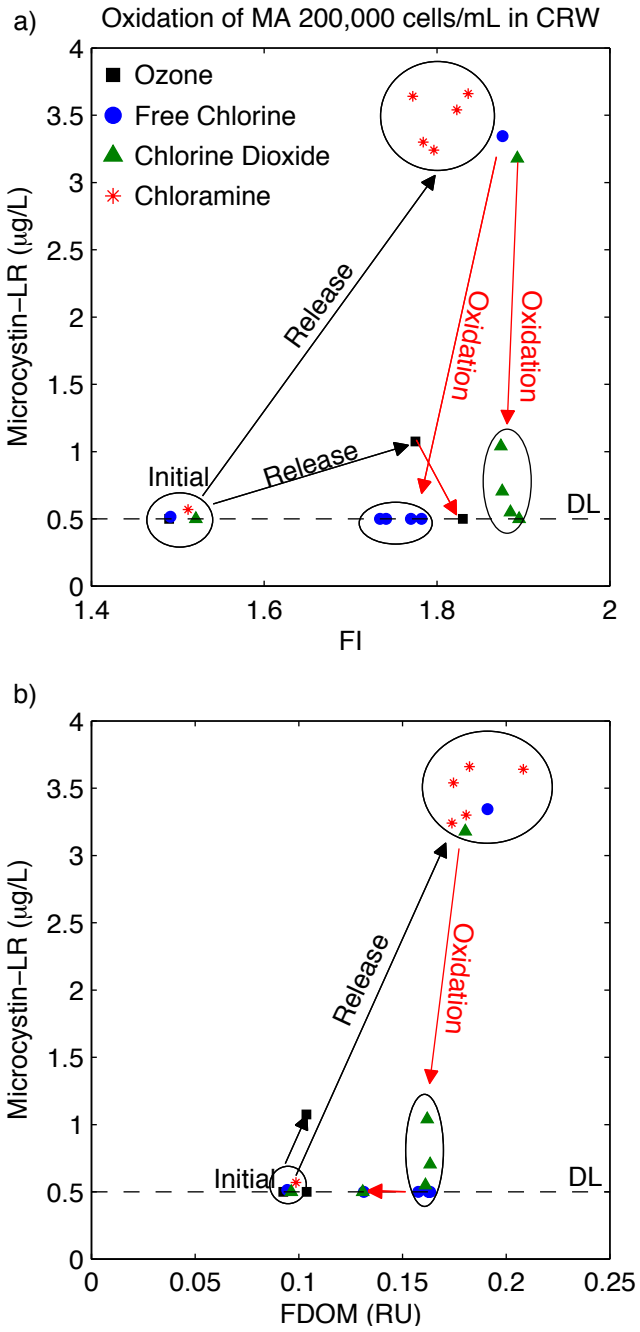

Figure 7.6 Relationship between Microcystin-LR and fluorescent surrogates a) FI and b) FDOM intensity for MA cell oxidation studies. Samples below the detection limit (DL) are shown at the detection limit line.

Similar relationships were found following FDOM intensity as a surrogate. At the lowest oxidant dose ratio (0.25), there was a simultaneous increase in both fluorescence intensity and

MC-LR concentration. Unlike FI, the increase in FDOM intensity was much smaller for ozone compared to the other oxidants and was more representative of the smaller MC-LR increase. At increasing oxidant doses when MC-LR degraded, FDOM intensity decreased for ozone, free chlorine and chlorine dioxide, but still remained above the initial value. There was no change in either FDOM or MC-LR concentration with increasing chloramine dose.

The results in Figure 7.6 demonstrate that FI and FDOM can be an effective conservative surrogates for MC-LR. FI and FDOM both act as conservative surrogates for oxidation by free chlorine, chlorine dioxide and chloramines. If an increase was measured during the oxidation of MA cells, then there was likely a release of MC-LR into the bulk phase. If chloramine was used, then MC-LR is likely still present. For free chlorine and chlorine dioxide, the MC-LR may still be present if low doses of oxidant were used or it may have degraded. In either case, an increase would trigger additional testing. For ozone, an increase would also indicate a likely MC-LR spike, but the increase in both fluorescence and MC-LR could be easily missed depending on the oxidant dose used. Although MC-LR rapidly degrades, the same may not be true of DBP precursors within the IOM as only 19% of the MA IOM DOC was measured to be assimilable organic carbon (Wert and Rosario-Ortiz, 2013).

7.4.2.2 Release of MIB

A similar analysis was performed comparing the change in MIB to FI and FDOM fluorescence for both cell concentrations tested. The relationship between MIB and FI was investigated for only free chlorine and chlorine dioxide, because these two oxidants exhibited significant increases in Figure 7.3. Figure 7.7a shows that at the lowest dose ratio (0.25), there is a simultaneous increase in both FI and MIB concentration as indicated by the “release” arrows. There were slightly different starting values for the initial conditions at the two cell

concentrations. Although the final FI for both cell concentrations is similar, the change in FI for the high cell concentration was greater, which also corresponded to a greater increase in MIB.

As the oxidant dose increased, FI increased but there was no change in MIB. These results indicate that most of the MIB is released at the lowest dose ratio, and there is no degradation with continued exposure. Previous studies have shown that free chlorine, chlorine dioxide and chloramines are ineffective at degrading MIB at typical oxidant doses used in full-scale operations (Glaze et al., 1990; Lalezary et al., 1986). When the gradual increase in FI in Figure 7.3 is compared to the results here, it suggests that the kinetics of MIB release and high FI IOM is different. MIB is released almost instantaneously. Therefore, the increase in FI is not representative of the amount of MIB released but would act as an indicator that MIB has been released.

The relationship between MIB and FDOM intensity was investigated for free chlorine and chloramine, because these exhibited a positive response in Figure 7.2. At the lowest free chlorine and chloramine doses (0.25), FDOM intensity and MIB concentrations both increased. At higher chloramine doses, there was no change in either MIB or FDOM intensity. Chloramine does not effectively degrade MIB, and the OSC IOM was shown to be insensitive to chloramine exposure (Korak et al., 2014c). At higher free chlorine doses, FDOM intensity decreased, which is expected based on IOM oxidation studies.

Comparing FI and FDOM fluorescence surrogates, FI is a more conservative surrogate for detecting MIB release. Both fluorescence surrogates perform equally for chloramine oxidation, because the fluorescence characteristics of the IOM are insensitive to chloramine exposure. The same is not true for free chlorine oxidation, because FDOM intensity decreases with prolonged exposure in the bulk phase. For any free chlorine dose applied, an observed

increase in FI corresponded to an increase in MIB. Using FDOM intensities, an increase in intensity was only observed at the lowest oxidant doses applied. At higher doses, FDOM intensity can decrease even though there has been a release of MIB. Therefore, FDOM can only be an effective surrogate at low doses, whereas FI is effective across a range of oxidant doses.

The biological stability of the FI and FDOM indicators are unknown at timescales longer than the experimental conditions. OSC IOM was found to be almost all assimilable organic carbon (>99%) (Wert and Rosario-Ortiz, 2013). Samples were filtered after the 24 hour reaction period and refrigerated to minimize microbial degradation. These results may not be valid for applications with residence times longer than 24 hours as the timescale for microbial degradation of IOM is unknown.

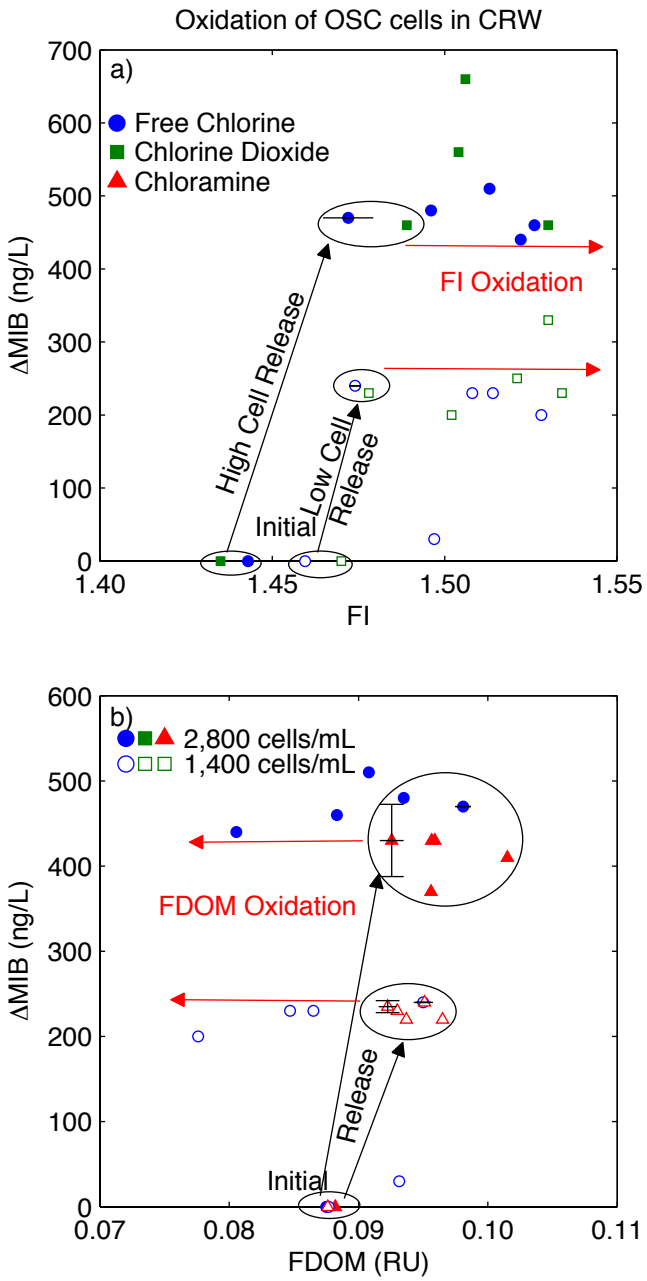

Figure 7.7 Relationship between change in MIB and fluorescent surrogates a) FI and b) FDOM intensity for OSC cell oxidation studies. Error bars on experimental duplicates represent the standard deviations for both measurements.

7.4.2.3 Release of Geosmin

Finally, similar trends were observed for geosmin released from LYG cells as for MIB released from OSC cells. Oxidation by free chlorine led to an increase in both FI and geosmin concentration as shown in Figure 7.8a. Most of the geosmin was released at the lowest oxidant dose ratio (0.25) at which point the increase in FI was quite small. As the oxidant dose increased, FI continued to increase along with the geosmin concentration. This trend is expected, because free chlorine is ineffective at degrading geosmin (Glaze et al., 1990; Lalezary et al., 1986).

The trend observed for FDOM intensity and geosmin release is almost identical to the MIB trend in Figure 7.8b. At the lowest oxidant dose, FDOM intensity increases simultaneously with geosmin concentration as shown in Figure 7.8b. There is no change in the responses at higher chloramine concentrations, because both geosmin and FDOM fluorescence in IOM are insensitive. FDOM intensity decreased at higher free chlorine doses as the IOM and CRW fluorescence characteristics change. Therefore, FDOM would not be a practical surrogate for geosmin released due to free chlorine oxidation, because a decrease may be observed even though geosmin has been released. Similar to OSC, LYG IOM is almost all assimilable organic carbon (>99%) (Wert and Rosario-Ortiz, 2013). The persistence of these fluorescence indicators is unknown past the 24 hour reaction time used in this study.

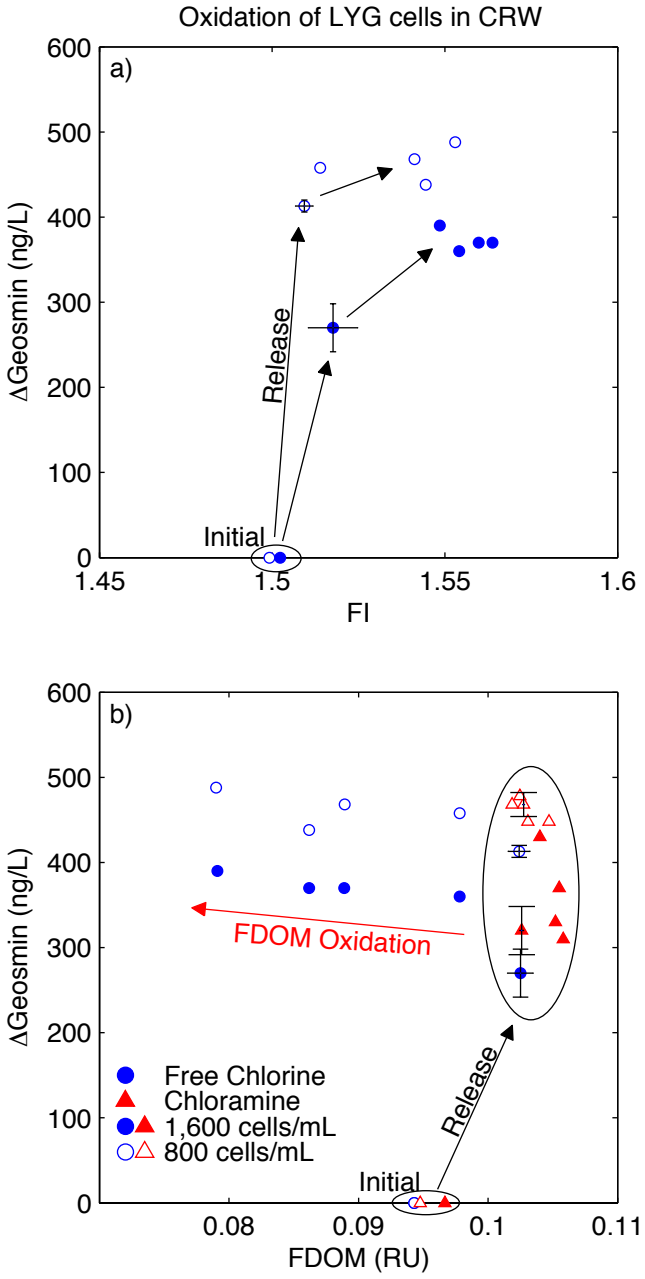

Figure 7.8 Relationship between change in geosmin and fluorescent surrogates a) FI and b) FDOM intensity for LYG cell oxidation studies. Error bars on experimental duplicates represent the standard deviations for both measurements.

7.4.2.4 Loss of Cell Viability

Section 7.4.1 showed that there is a fluorescence response that changes as a function of oxidant dose. Figure 7.9 shows how the fluorescence response is related to the loss of viable cells determined by the trigger mode cell counts. Nearly all viable MA cells are lost at the lowest oxidant:dose ratio of 0.25 for all four oxidants tested, which corresponded with the release of most metabolites. The initial increase in both FDOM intensity and FI coincides with the large loss in viable cells at the same dose. Past work found that there was no decrease in the total cell concentration, only viable fluorescent cells (Wert et al., 2013). These data suggest that the change in the dissolved phase fluorescence characteristics corresponds to a release of IOM across the membrane without fragmenting the cell.

Figure 7.9 also shows that the fluorescence response is more representative of the loss in viable cells compared to UV_{254}. At the same dose ratio (0.25), UV_{254} decreased during ozone, free chlorine and chloramine oxidation studies. Even though UV_{254} continued to decrease with increasing ozone dose, it increased with exposure to the other four oxidants ultimately reaching 3 to 4 times its initial value. Unlike fluorescence, UV_{254} did not reach its maximum value until a dose ratio of 0.75. The observed rate of UV_{254} increase suggests that there is a more gradual rate of cell loss (and IOM release) that does not reach a steady state value until a higher dose. These results, if interpreted in isolation, could lead to the incorrect conclusion that the majority of cell destruction and IOM release does not occur until the 0.25 to 0.75 dose ratio range. The closer trend between the spike in fluorescence and the decrease in viable cell count demonstrates that fluorescence is a more sensitive monitoring tool that responds better to the nearly complete loss of viable cells at the lowest dose tested.

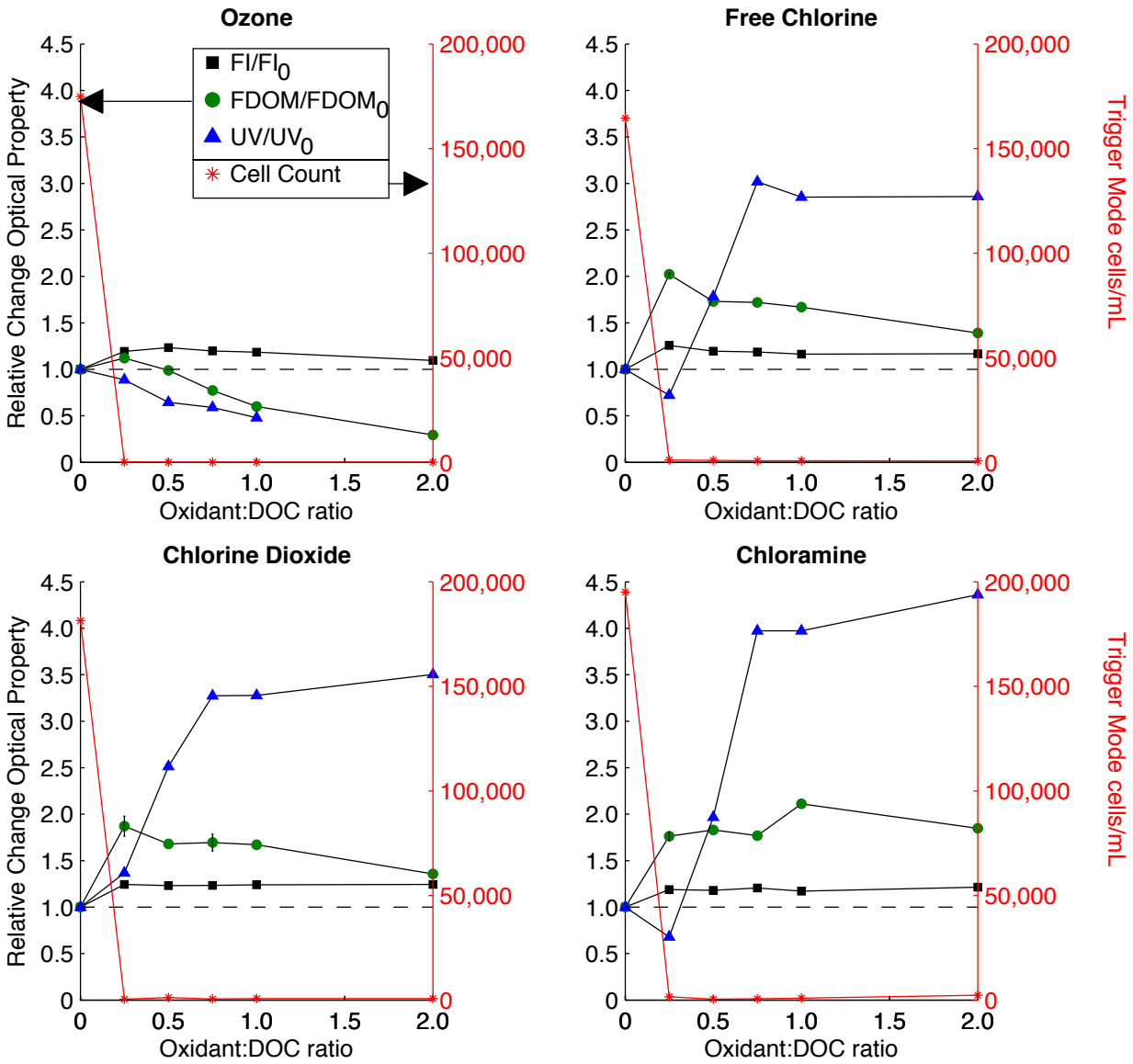

Figure 7.9 Comparison of fluorescence and UV indicators as a surrogate for loss of cell viability (Trigger Mode cell concentration) for MA at the nominal starting concentration of 200,000 cells/mL.

Finally, the different responses between fluorescence and UV_{254} also demonstrates that the fluorescing and UV-absorbing components in the IOM are not the same. Since the dissolved phase optical characteristics change at different rates, there is likely different source materials contributing to each measurement. This material may be released from the cell at different rates and oxidized in the dissolved solution at different rates.

7.5 Conclusions

Different fluorescence metrics were evaluated to determine their feasibility to detect IOM and metabolite release from cyanobacteria cells. Initially, each fluorescence metric was screened to determine if there was a response that exceeded that of the background DOM and instrument analytical error. Based on those analysis, FI and FDOM intensity were determined to be the most promising metrics. Phycobiliproteins (phycocyanin and phycoerythrin) were not measured in any appreciable amount, likely due to their fast oxidation and quenching interactions with DOM. The magnitude of the FI and FDOM response varied between cyanobacteria species. The response from MA was greater in magnitude than OSC and LYG. These differences are likely due to differing IOM composition, because MA IOM had a greater fluorescence intensity per unit carbon.

The FI and FDOM responses were compared to the release of metabolites (Microcystin-LR, MIB and geosmin) and found that FI was a better conservative indicator. For chloramine oxidation, both FDOM and FI performed equally as optical surrogates, because neither measurement changed with additional oxidant exposure. For stronger oxidants, such as free chlorine and chlorine dioxide, FDOM intensity decreased relative to the initial value at higher doses even though there was a release of metabolites.

Comparing fluorescence and UV_{254} as optical surrogates, fluorescence indicators performed better than UV. Fluorescence indicators responded at the lowest dose ratios simultaneously with the loss of viable cells and metabolite release. UV_{254} did not exhibit a response indicative of IOM release until higher oxidant doses and did not adequately capture the changes in cell concentration and metabolite concentrations at lower doses.

These results demonstrated that FI could be a valuable monitoring tool for utilities concerned about the release of cell-bound metabolites due to oxidation. Development of an effective monitoring system will depend on the species present and oxidant used.

Chapter 8 Conclusions, Future Work and Reflections

8.1 Future Work

This thesis as a whole demonstrates that fluorescence has a large potential to enhance our understanding of DOM in both environmental and engineered systems. From a practical standpoint, this work demonstrated that fluorescence has the potential to become a powerful monitoring tool for utilities. It has the ability to predict DOM removal by coagulation across many waters and to act as a surrogate for cyanobacteria metabolite release in water treatment plants. The work presented here represents the foundations, and more work is necessary to extend the bench-scale fluorescence experiments to full-scale applications.

The coagulation work found that fluorescence, in the way in which it was characterized, does not offer any appreciable benefits over absorbance measurements. These results do not suggest, however, that the use of fluorescence for coagulation should be abandoned. It only suggests that the methods by which fluorescence data is measured and analyzed need to be become more innovative. The kinetics of the process (DOM removal as a function of time) have not been considered. Fluorescence measurements collected as function of time during the jar tests may reveal new insights into DOM behavior. Steady state fluorescence is also only one method; future work could include transient fluorescence properties, anisotropy and low temperature phosphorescence to gain further insight into the process. Hopefully, approaching the problem from a new perspective will reveal new ways in which fluorescence enhances our understanding of DOM removal and provides predictive power for engineers to design and optimize processes.

The application of fluorescence to monitor cyanobacteria blooms provides an example where fluorescence has the potential to be a more valuable monitoring tool compared to UV

absorbance. Before these methods can be applied in a full-scale operation, there are still questions that need to be answered. The first step is to determine the kinetics of metabolite release with respect to the fluorescence response. The work herein measured the response after 24 hours. Ideally, a probe would be located downstream of the point of oxidation but upstream of coagulant addition. The residence time between these two locations is much shorter than 24 hours, and it is unknown if the same fluorescence responses measured here would occur within that time period.

Before any large-scale deployment of fluorescent probes is feasible, there are still knowledge gaps that need to be filled. In general, the large bandpasses found in commercial sensors limits the ability to transfer methods developed on bench-top instruments to field-deployable instruments. The ability to correct for sample absorbance simultaneously with fluorescence data acquisition needs to be developed as well. The effects of temperature, DOM concentration, and inorganic species are not well understood or quantified. Tools would need to be developed to allow for these effects to be determined and accounted for, ideally *a priori*. Systematically investigating these effects may reveal new insights into DOM in general.

8.2 General Reflections

Compared to other characterization methods, fluorescence is attractive because of its small sample requirement and non-intensive procedure. The development of new instrument components, such as CCD detectors, will further decrease analysis time and make it easier to amass large data sets. However, this thesis has also demonstrated that despite its analytical simplicity, fluorescence is not without its own complications and disadvantages.

Since fluorescence measures a photophysical process, its response depends on not only the DOM concentration and composition, but also its environment. Chapter 2 demonstrated that

fluorescence metrics traditionally interpreted as compositional properties can exhibit concentration dependencies. Chapter 3 demonstrated how the presence of metal species could lead to false conclusions, if the fluorescence data is interpreted without regard to other characterization methods. Chapter 5 provided another example of how highly fluorescent organic compounds (phycocyanin and phycoerythrin) almost completely lose their fluorescence signature in the presence of DOM. Before fluorescence can reach its full potential as a practical engineering tool, the environmental effects need to be better understood and taken into account more consistently. In particular, the effects of DOM concentration, DOM interactions with different constituents and experimental conditions (e.g., temperature, pH, particles) need to have standardized methods throughout the applied field.

Chapter 2 demonstrated the need for better experimental design and data analysis in the future. While fluorescence on its own is a precise measurement compared to others, when other measurements (e.g. DOC) are used, the analytical accuracy decreases. Other instrumental settings, such as bandpass, affect the discriminatory power of fluorescence to detect differences in DOM composition. Statistics need to play a larger role in fluorescence data analysis to evaluate data more objectively. Finally, the use of different fluorescence metrics ought to be chosen more strategically based on specific applications. It is important to consider whether or not a specific fluorescence metric follows conservative property principles and how such differences affect interpretations and conclusions.

Chapters 3 and 4 both demonstrate the need to evaluate proposed interpretations critically rather than accept them blindly at face value. Relating regional fluorescence to humic- and fulvic-acids has been a popular interpretation method for the past decade, especially in engineering applications. The coagulation results, coupled with data regarding humic-acid

abundance and quantum yields, refute this compositional assignment. New methods of interpreting fluorescence data will continue to be developed as research continues. Moving forward, my hope is that there will continue to be an open dialogue about each method's merits, limits and intended applications.

Finally, this work also demonstrates that sometimes less is more. When I started this work, I had the impression that fluorescence is superior to absorbance (an arguably simpler tool) in every respect, because it is a multivariable measurement. Chapter 4 is a prime example of how absorbance provides more utility than fluorescence in applications like coagulation and DBP reactivity. Chapter 6 illustrates a case where the opposite is true; fluorescence is a better monitoring tool than absorbance as a surrogate for cyanobacteria metabolite release. As an engineer trying to find elegant solutions for complex problems, it is important to recognize when a simpler solution suffices.

Chapter 9 References

Afcharian, A., Levi, Y., Kiene, L., Scribe, P., 1997. Fractionation of dissolved organic matter from surface waters using macroporous resins. Water Research 31, 2989–2996.

Alberts, J.J., Takacs, M., Egeberg, P.K., 2002. Total luminescence spectral characteristics of natural organic matter (NOM) size fractions as defined by ultrafiltration and high performance size exclusion chromatography (HPSEC). Org Geochem 33, 817–828.

Alberts, J.J., Takács, M., 2004. Total luminescence spectra of IHSS standard and reference fulvic acids, humic acids and natural organic matter: comparison of aquatic and terrestrial source terms. Org Geochem 35, 243–256.

Alberts, J.J., Takács, M., Schalles, J., 2004. Ultraviolet-visible and fluorescence spectral evidence of natural organic matter (NOM) changes along an estuarine salinity gradient. Estuaries 27, 296–310.

Allpike, B., Heitz, A., Joll, C., Kagi, R., Abbt-Braun, G., Frimmel, F., Brinkmann, T., Her, N., Amy, G.L., 2005. Size exclusion chromatography to characterize DOC removal in drinking water treatment. Environ Sci Technol 39, 2334–2342.

APHA, AWWA, WEF, 1998. Standard Methods for Examination of Water & Wastewater, 20 ed. APHA, Washington DC.

Ates, N., Kitis, M., Yetis, U., 2007. Formation of chlorination by-products in waters with low SUVA—correlations with SUVA and differential UV spectroscopy. Water Research 41, 4139–4148.

AWWA Research Committee on Coagulation, 1979. Organics Removal by Coagulation: A Review and Research Needs. Journal AWWA 71, 588–603.

Ayache, C., Pidou, M., Croue, J.-P., Labanowski, J., Poussade, Y., Tazi-Pain, A., Keller, J., Gernjak, W., 2013. Impact of effluent organic matter on low-pressure membrane fouling in tertiary treatment. Water Research 47, 2633–2642.

Babcock, D.B., Singer, P.C., 1979. Chlorination and Coagulation of Humic and Fulvic Acids. Journal AWWA 71, 149–152.

Baddi, G.A., Antizar-Ladislao, B., Alcuta, A., Mazeas, L., Li, T., Duquennoi, C., Redon, E., Bouchez, T., 2013. Municipal Solid Waste Stabilization Efficiency Using Fluorescence Excitation–Emission Spectroscopy. Environ Eng Sci 30, 232–240.

Baghoth, S.A., Sharma, S.K., Amy, G.L., 2011a. Tracking natural organic matter (NOM) in a drinking water treatment plant using fluorescence excitation–emission matrices and PARAFAC. Water Research 45, 797–809.

Baghoth, S.A., Sharma, S.K., Guitard, M., Heim, V., Croue, J.-P., Amy, G.L., 2011b. Removal of NOM-constituents as characterized by LC-OCD and F-EEM during drinking water treatment. J Water Supply Res T 60, 412–424.

Baker, A., 2001. Fluorescence Excitation−Emission Matrix Characterization of Some Sewage-Impacted Rivers. Environ Sci Technol 35, 948–953.

Baker, A., Tipping, E., Thacker, S.A., Gondar, D., 2008. Relating dissolved organic matter fluorescence and functional properties. Chemosphere 73, 1765–1772.

Bastien, C., Cardin, R., Veilleux, É., Deblois, C., Warren, A., Laurion, I., 2011. Performance evaluation of phycocyanin probes for the monitoring of cyanobacteria. J. Environ. Monit. 13, 110–118.

Beggs, K.M.H., Billica, J.A., Korak, J.A., Rosario-Ortiz, F.L., McKnight, D.M., Summers, R.S., 2013. Spectral evaluation of watershed DOM and DBP precursors. Journal AWWA 105, E173–E188.

Beggs, K.M.H., Summers, R.S., 2011. Character and Chlorine Reactivity of Dissolved Organic Matter from a Mountain Pine Beetle Impacted Watershed. Environ Sci Technol 45, 5717–5724.

Beggs, K.M.H., Summers, R.S., McKnight, D.M., 2009. Characterizing chlorine oxidation of dissolved organic matter and disinfection by-product formation with fluorescence spectroscopy and parallel factor analysis. J Geophys Res 114, G04001.

Belzile, C., Guo, L., 2006. Optical properties of low molecular weight and colloidal organic matter: Application of the ultrafiltration permeation model to DOM absorption and fluorescence. Mar Chem 98, 183–196.

Bergamaschi, B.A., Krabbenhoft, D.P., Aiken, G.R., Patino, E., Rumbold, D.G., Orem, W.H., 2012. Tidally Driven Export of Dissolved Organic Carbon, Total Mercury, and Methylmercury from a Mangrove-Dominated Estuary. Environ Sci Technol 46, 1371–1378.

Bieroza, M., Baker, A., Bridgeman, J., 2009. Relating freshwater organic matter fluorescence to organic carbon removal efficiency in drinking water treatment. Sci Total Environ 407, 1765–1774.

Bieroza, M., Baker, A., Bridgeman, J., 2011. Assessment of Low pH Coagulation Performance Using Fluorescence Spectroscopy. J Environ Eng 137, 596–601.

Birks, J.B., 1970. Photophysics of Aromatic Molecules. Wiley Interscience.

Boyle, E.S., Guerriero, N., Thiallet, A., Vecchio, R.D., Blough, N.V., 2009. Optical Properties of Humic Substances and CDOM: Relation to Structure. Environ Sci Technol 43, 2262–2268.

Brient, L., Lengronne, M., Bertrand, E., Rolland, D., Sipel, A., Steinmann, D., Baudin, I., Legeas, M., Le Rouzic, B., Bormans, M., 2008. A phycocyanin probe as a tool for monitoring cyanobacteria in freshwater bodies. J. Environ. Monit. 10, 248–255.

Bruccoleri, A.G., Pant, B.C., Sharma, D.K., Langford, C.H., 1993. Evaluation of primary photoproduct quantum yields in fulvic acid. Environ Sci Technol 27, 889–894.

Bryant, D.A., 1982. Phycoerythrocyanin and phycoerythrin: properties and occurrence in cyanobacteria. Journal of General Microbiology 128, 835–844.

Bryant, D.A., 1994. Molecular Biology of Cyanobacteria. Kluwer Academic Publishers.

Bu, L., Wang, K., Zhao, Q.-L., Wei, L.-L., Zhang, J., Yang, J.-C., 2010. Characterization of dissolved organic matter during landfill leachate treatment by sequencing batch reactor, aeration corrosive cell-Fenton, and granular activated carbon in series. J Hazard Mater 179, 1096–1105.

Cabaniss, S.E., 1992. Synchronous Fluorescence-Spectra of Metal-Fulvic Acid Complexes. Environ Sci Technol 26, 1133–1139.

Carey, C.C., Ibelings, B.W., Hoffmann, E.P., Hamilton, D.P., Brookes, J.D., 2012. Eco-physiological adaptations that favour freshwater cyanobacteria in a changing climate. Water Research 46, 1394–1407.

Carpenter, K.D., Kraus, T.E.C., Goldman, J.H., Saraceno, J.F., Downing, B.D., Bergamaschi, B.A., McGhee, G., 2012. Sources and Characteristics of Organic Carbon in the Clackamas River, Oregon, Related to the Formation of Disinfection By-Products in Treated Drinking Water. U.S. Geological Survey.

Cavani, L., Halladja, S., Halle, A., Guyot, G., Corrado, G., Ciavatta, C., Boulkamh, A., Richard, C., 2009. Relationship between Photosensitizing and Emission Properties of Peat Humic Acid Fractions Obtained by Tangential Ultrafiltration. Environ Sci Technol 43, 4348–4354.

Chen, W., Westerhoff, P., Leenheer, J.A., Booksh, K., 2003. Fluorescence excitation - Emission matrix regional integration to quantify spectra for dissolved organic matter. Environ Sci Technol 37, 5701–5710.

Cheng, W., Chi, F., Yu, R., 2004. Evaluating the efficiency of coagulation in the removal of dissolved organic carbon from reservoir water using fluorescence and ultraviolet photometry. Environ Monit Assess 98, 421–431.

Chin, Y.-P., Aiken, G.R., O'Loughlin, E., 1994. Molecular weight, polydispersity, and spectroscopic properties of aquatic humic substances. Environ Sci Technol 28, 1853–1858.

Chiou, C.T., Malcolm, R.L., Brinton, T.I., Kile, D.E., 1986. Water Solubility Enhancement of Some Organic Pollutants and Pesticides by Dissolved Humic and Fulvic-Acids. Environ Sci Technol 20, 502–508.

Christmann, D.R., Crouch, S.R., Timnick, A., 1981. Precision and accuracy of absorption-corrected molecular fluorescence measurements by the cell shift method. Anal Chem 53, 2040–2044.

Coble, P., 1996. Characterization of marine and terrestrial DOM in seawater using excitation emission matrix spectroscopy. Mar Chem 51, 325–346.

Coble, P., Green, S.A., Blough, N.V., Gagosian, R.B., 1990. Characterization of Dissolved Organic-Matter in the Black-Sea by Fluorescence Spectroscopy. Nature 348, 432–435.

Cory, R.M., McKnight, D.M., 2005. Fluorescence spectroscopy reveals ubiquitous presence of oxidized and reduced quinones in dissolved organic matter. Environ Sci Technol 39, 8142–8149.

Cory, R.M., Miller, M.P., McKnight, D.M., Guerard, J.J., Miller, P.L., 2010. Effect of instrument-specific response on the analysis of fulvic acid fluorescence spectra. Limnol Oceanogr-Methods 8, 67–78.

Cottrell, B.A., Timko, S.A., Devera, L., Robinson, A.K., Gonsior, M., Vizenor, A.E., Simpson, A.J., Cooper, W.J., 2013. Photochemistry of excited-state species in natural waters: A role for particulate organic matter. Water Research 47, 5189–5199.

Cumberland, S.A., Baker, A., 2007. The freshwater dissolved organic matter fluorescence-total organic carbon relationship. Hydrol Process 21, 2093–2099.

Debreczeny, M.P., Sauer, K., Zhou, J., Bryant, D.A., 1993. Monomeric C-phycocyanin at room

temperature and 77 K: resolution of the absorption and fluorescence spectra of the individual chromophores and the energy-transfer rate constants. Journal of Physical Chemistry 97, 9852–9862.

Del Vecchio, R., Blough, N.V., 2004. On the origin of the optical properties of humic substances. Environ Sci Technol 38, 3885–3891.

Demidov, A.A., Mimuro, M., 1995. Deconvolution of C-phycocyanin beta-84 and beta-155 chromophore absorption and fluorescence spectra of cyanobacterium Mastigocladus laminosus. Biophyscial Journal 68, 1500–1506.

Dempsey, B.A., Ganho, R.M., O'Melia, C.R., 1984. The Coagulation of Humic Substances by Means of Aluminum Salts. Journal AWWA 76, 141–150.

Ding, J., Shi, H., Timmons, T., Adams, C., 2009. Release and removal of microcystins from microcystis during oxidative-, physical-, and UV-based disinfection. J Environ Eng 136, 2–11.

Downing, B.D., Pellerin, B.A., Bergamaschi, B.A., Saraceno, J.F., Kraus, T.E.C., 2012. Seeing the light: The effects of particles, dissolved materials, and temperature on in situ measurements of DOM fluorescence in rivers and streams. Limnol Oceanogr-Methods 10, 767–775.

Dunnivant, F.M., Schwarzenbach, R.P., 1992. Reduction of substituted nitrobenzenes in aqueous solutions containing natural organic matter. Environ Sci Technol 26, 2133-2141.

Dwyer, J., Griffiths, P., Lant, P., 2009. Simultaneous colour and DON removal from sewage treatment plant effluent: Alum coagulation of melanoidin. Water Research 43, 553–561.

Edwards, M., 1997. Predicting DOC removal during enhanced coagulation. Journal AWWA.

Edzwald, J.K., 1978. Coagulation of Humic Substances. Water-1978 (AICHE Symposium Series) 75, 54–62.

Edzwald, J.K., 1993. Coagulation in drinking water treatment: particles, organics and coagulants. Water Sci Technol 27, 21–35.

Edzwald, J.K., Becker, W.C., Wattier, K.L., 1985. Surrogate parameters for monitoring organic matter and THM precursors. Journal AWWA 77, 122–132.

Elkins, K.M., Nelson, D.J., 2002. Spectroscopic approaches to the study of the interaction of aluminum with humic substances. Coordin Chem Rev 228, 205–225.

Esparza-Soto, M., Núñez-Hernández, S., Fall, C., 2011. Spectrometric characterization of effluent organic matter of a sequencing batch reactor operated at three sludge retention times. Water Research 45, 6555–6563.

Fang, J., Yang, X., Ma, J., Shang, C., Zhao, Q., 2010. Characterization of algal organic matter and formation of DBPs from chlor(am)ination. Water Research 44, 5897–5906.

Fellman, J.B., Hood, E., Spencer, R.G.M., 2010. Fluorescence spectroscopy opens new windows into dissolved organic matter dynamics in freshwater ecosystems: A review. Limnol Oceanogr 55, 2452–2462.

Fleck, J.A., Gill, G., Bergamaschi, B.A., Kraus, T.E.C., Downing, B.D., Alpers, C.N., 2014. Concurrent photolytic degradation of aqueous methylmercury and dissolved organic matter.

Sci Total Environ 484, 263-275.

Glauser, M., Sidler, W., Zuber, H., 1993. Isolation, Characterization and Reconstitution of Phycobiliprotein Rod-Core Linker Polypeptide Complexes from the Phycobilisome of Mastigocladus Laminosus. Photochemistry and Photobiology 57, 344–351.

Glaze, W.H., Schep, R., Chauncey, W., Ruth, E.C., Zarnoch, J.J., Aieta, E., Tate, C.H., McGuire, M.J., 1990. Evaluating oxidants for the removal of model taste and odor compounds from a municipal water supply. Journal AWWA 82, 79–84.

Glazer, A.N., 1977. Structure and molecular organization of the photosynthetic accessory pigments of cyanobacteria and red algae. Molecular and cellular biochemistry 18, 125–140.

Glazer, A.N., Bryant, D.A., 1975. Allophycocyanin B (λmax 671, 618 nm). Archives of microbiology 104, 15–22.

Glazer, A.N., Fang, S., 1973. Chromophore content of blue-green algal phycobiliproteins. Journal of Biological Chemistry 248, 659–662.

Glover, C., Sharma, S., Wood, C., 2005. Heterogeneity in physicochemical properties explains differences in silver toxicity amelioration by natural organic matter to Daphnia magna. Environmental Toxicology and Chemistry 24, 2941–2947.

Goldman, J.H., Rounds, S.A., Needoba, J.A., 2012. Applications of Fluorescence Spectroscopy for Predicting Percent Wastewater in an Urban Stream. Environ Sci Technol 46, 4374–4381.

Gone, D.L., Seidel, J.-L., Batiot, C., Bamory, K., Ligban, R., Biemi, J., 2009. Using fluorescence spectroscopy EEM to evaluate the efficiency of organic matter removal during coagulation-flocculation of a tropical surface water (Agbo reservoir). J Hazard Mater 172, 693–699.

González-Pérez, J.A., González-Vila, F.J., Almendros, G., Knicker, H., 2004. The effect of fire on soil organic matter—a review. Environment International 30, 855–870.

Grabowski, J., Gantt, E., 1978. Photophysical properties of phycobiliproteins from phycobilisomes: fluorescence lifetimes, quantum yields, and polarization spectra. Photochemistry and Photobiology 28, 39–45.

Gray, B.H., Lipschultz, C.A., Gantt, E., 1973. Phycobilisomes from a blue-green alga Nostoc species. Journal of Bacteriology 116, 471–478.

Green, S.A., Blough, N.V., 1994. Optical-Absorption and Fluorescence Properties of Chromophoric Dissolved Organic-Matter in Natural-Waters. Limnol Oceanogr 39, 1903–1916.

Gregor, J., Maršálek, B., Šípková, H., 2007. Detection and estimation of potentially toxic cyanobacteria in raw water at the drinking water treatment plant by in vivo fluorescence method. Water Research 41, 228–234.

Gu, Q., Kenny, J.E., 2009. Improvement of Inner Filter Effect Correction Based on Determination of Effective Geometric Parameters Using a Conventional Fluorimeter. Anal Chem 81, 420–426.

Guéguen, C., Cuss, C.W., 2011. Characterization of aquatic dissolved organic matter by asymmetrical flow field-flow fractionation coupled to UV–Visible diode array and excitation emission matrix fluorescence. J Chromatogr A 1218, 4188–4198.

Hall, E.S., Packham, R.F., 1965. Coagulation of Organic Color With Hydrolyzing Coagulants. Journal AWWA 57, 1149–1166.

Heaney, S.I., 1976. Some Observations on Use of Invivo Fluorescence Technique to Determine Chlorophyll-a in Natural Populations and Cultures of Freshwater Phycoplankton. Freshwater Biology 8, 115–126.

Henderson, R., Parsons, S.A., Jefferson, B., 2008. The impact of algal properties and pre-oxidation on solid-liquid separation of algae. Water Research 42, 1827–1845.

Hernes, P.J., Bergamaschi, B.A., Eckard, R.S., Spencer, R.G.M., 2009. Fluorescence-based proxies for lignin in freshwater dissolved organic matter. J Geophys Res-Biogeo 114.

Hitzfeld, B.C., Höger, S.J., Dietrich, D.R., 2000. Cyanobacterial toxins: removal during drinking water treatment, and human risk assessment. Environ Health Persp 108, 113.

Holbrook, R.D., DeRose, P.C., Leigh, S.D., Rukhin, A.L., Heckert, N.A., 2006. Excitation-emission matrix fluorescence spectroscopy for natural organic matter characterization: A quantitative evaluation of calibration and spectral correction procedures. Appl Spectrosc 60, 791–799.

Holland, J.F., Teets, R.E., Kelly, P.M., Timnick, A., 1977. Correction of right-angle fluorescence measurements for the absorption of excitation radiation. Anal Chem 49, 706–710.

Horiba Scientific, 2009. FluoroMax-4 & FluoroMax-4P with USB Operation Manual. Horiba Scientific.

Hua, G., Reckhow, D.A., 2007. Characterization of Disinfection Byproduct Precursors Based on Hydrophobicity and Molecular Size. Environ Sci Technol 41, 3309–3315.

Hudson, N., Baker, A., Reynolds, D., 2007. Fluorescence analysis of dissolved organic matter in natural, waste and polluted waters—a review. River Res. Applic. 23, 631–649.

Huguet, A., Vacher, L., Relexans, S., Saubusse, S., Froidefond, J.M., Parlanti, E., 2009. Properties of fluorescent dissolved organic matter in the Gironde Estuary. Org Geochem 40, 706–719.

Ishii, S.K., Boyer, T.H., 2012. Behavior of reoccurring PARAFAC components in fluorescent dissolved organic matter in natural and engineered systems: A critical review. Environ Sci Technol 46, 2006–2017.

Izydorczyk, K., Carpentier, C., Mrowczynski, J., Wagenvoort, A., Jurczak, T., Tarczynska, M., 2009. Establishment of an Alert Level Framework for cyanobacteria in drinking water resources by using the Algae Online Analyser for monitoring cyanobacterial chlorophyll a. Water Research 43, 989–996.

Izydorczyk, K., Tarczynska, M., Jurczak, T., Mrowczynski, J., Zalewski, M., 2005. Measurement of phycocyanin fluorescence as an online early warning system for cyanobacteria in reservoir intake water. Environ. Toxicol. 20, 425–430.

Jaffe, R., Boyer, J., Lu, X., Maie, N., Yang, C., Scully, N.M., Mock, S., 2004. Source characterization of dissolved organic matter in a subtropical mangrove-dominated estuary by fluorescence analysis. Mar Chem 84, 195–210.

Jiang, W., Xia, S., Liang, J., Zhang, Z., Hermanowicz, S.W., 2013. Effect of quorum quenching

on the reactor performance, biofouling and biomass characteristics in membrane bioreactors. Water Research 47, 187–196.

Johnstone, D.W., Sanchez, N.P., Miller, C.M., 2009. Parallel Factor Analysis of Excitation-Emission Matrices to Assess Drinking Water Disinfection Byproduct Formation During a Peak Formation Period. Environ Eng Sci 26, 1551–1559.

Juttner, F., Watson, S.B., 2007. Biochemical and Ecological Control of Geosmin and 2-Methylisoborneol in Source Waters. Applied and Environmental Microbiology 73, 4395–4406.

Kalbitz, K., Geyer, W., Geyer, S., 1999. Spectroscopic properties of dissolved humic substances - a reflection of land use history in a fen area. Biogeochemistry 47, 219–238.

Kasha, M., 1950. Characterization of electronic transitions in complex molecules. Discuss. Faraday Soc. 9, 14–19.

Korak, J.A., Dotson, A.D., Summers, R.S., Rosario-Ortiz, F.L., 2014a. Critical Analysis of Commonly Used Fluorescence Metrics to Characterize Dissolved Organic Matter. Water Research 49, 327–338.

Korak, J.A., Rosario-Ortiz, F.L., Summers, R.S., 2014b. Fluorescence characterization of humic substance coagulation: Application of new tools to an old process, in: Rosario-Ortiz, F.L. (Ed.), Advances in the Physiochemical Characterization of Organic Matter. American Chemical Society Symposium Series 1160, Washington DC.

Korak, J.A., Wert, E.C., Rosario-Ortiz, F.L., 2014c. Evaluating fluorescence spectroscopy as a tool to characterize cyanobacteria intracellular organic matter upon simulated release and oxidation in natural water. Submitted to Water Research.

Kothawala, D.N., Murphy, K.R., Stedmon, C.A., Weyhenmeyer, G.A., Tranvik, L.J., 2013. Inner filter correction of dissolved organic matter fluorescence. Limnol Oceanogr-Methods 11, 616–630.

Köst, H.P., Rath, K., Wanner, G., Scheer, H., 1981. Phycobilisomes and isolated phycobiliproteins. Effect of glutardialdehyde and benzoquinone on fluorescence. Photochemistry and Photobiology 34, 139–143.

Kraus, T.E.C., Anderson, C.A., Morgenstern, K., Downing, B.D., Pellerin, B.A., Bergamaschi, B.A., 2010. Determining Sources of Dissolved Organic Carbon and Disinfection Byproduct Precursors to the McKenzie River, Oregon. J Environ Qual 39, 2100–2112.

Kubista, M., Sj back, R., Eriksson, S., Albinsson, B., 1994. Experimental correction for the inner-filter effect in fluorescence spectra. Analyst 119, 417–419.

Lakowicz, J.R., 2006. Principles of fluorescence spectroscopy. Springer Verlag.

Lalezary, S., Pirbazari, M., McGuire, M.J., 1986. Oxidation of Five Earthy-Musty Taste and Odor Compounds. Journal AWWA 78, 62–69.

Latifi, A., Ruiz, M., Zhang, C.-C., 2008. Oxidative stress in cyanobacteria. FEMS Microbiology Reviews 33, 258–278.

Lawaetz, A.J., Stedmon, C.A., 2009. Fluorescence Intensity Calibration Using the Raman Scatter Peak of Water. Appl Spectrosc 63, 936–940.

Leenheer, J.A., 2009. Systematic Approaches to Comprehensive Analyses of Natural Organic Matter. Annals of Environmental Science 3, 1–130.

Letterman, R.D., Yiacoumi, S., 2011. Coagulation and Flocculation, in: Edzwald, J.K. (Ed.), Water Quality & Treatment, Water Quality and Treatment. McGraw Hill, Denver.

Ley, A.C., Butler, W.L., Bryant, D.A., Glazer, A.N., 1977. Isolation and function of allophycocyanin B of Porphyridium cruentum. Plant Physiology 59, 974–980.

Li, W.T., Xu, Z.X., Li, A.M., Zhou, Q., Wang, J.N., 2013. HPLC/HPSEC-FLD with Multi-Excitation/Emission Scan for EEM Interpretation and DOM Analysis. Water Research 47, 1246–1256.

Liang, L., Singer, P.C., 2003. Factors Influencing the Formation and Relative Distribution of Haloacetic Acids and Trihalomethanes in Drinking Water. Environ Sci Technol 37, 2920–2928.

Luciani, X., Mounier, S., Redon, R., Bois, A., 2009. A simple correction method of inner filter effects affecting FEEM and its application to the PARAFAC decomposition. Chemometrics and Intelligent Laboratory Systems 96, 227–238.

Luster, J., Lloyd, T., Sposito, G., Fry, I.V., 1996. Multi-Wavelength Molecular Fluorescence Spectrometry for Quantitative Characterization of Copper(II) and Aluminum(III) Complexation by Dissolved Organic Matter. Environ Sci Technol 30, 1565–1574.

Lønborg, C., Álvarez-Salgado, X.A., Davidson, K., Martínez-García, S., Teira, E., 2010. Assessing the microbial bioavailability and degradation rate constants of dissolved organic matter by fluorescence spectroscopy in the coastal upwelling system of the Ría de Vigo. Mar Chem 119, 121–129.

MacColl, R., 1998. Cyanobacterial phycobilisomes. J Struct Biol 124, 311–334.

MacColl, R., O'Connor, G., Crofton, G., Csatorday, K., 1981. Phycoerythrocyanin: its spectroscopic behavior and properties. Photochemistry and Photobiology 34, 719–723.

MacDonald, B.C., Lvin, S.J., Patterson, H., 1997. Correction of fluorescence inner filter effects and the partitioning of pyrene to dissolved organic carbon. Anal Chim Acta 338, 155–162.

Maie, N., Scully, N.M., Pisani, O., Jaffe, R., 2007. Composition of a protein-like fluorophore of dissolved organic matter in coastal wetland and estuarine ecosystems. Water Research 41, 563–570.

McKnight, D.M., Boyer, E.W., Westerhoff, P., Doran, P., Kulbe, T., Andersen, D., 2001. Spectrofluorometric characterization of dissolved organic matter for indication of precursor organic material and aromaticity. Limnol Oceanogr 46, 38–48.

McQuaid, N., Zamyadi, A., Prévost, M., Bird, D.F., Dorner, S., 2011. Use of in vivo phycocyanin fluorescence to monitor potential microcystin-producing cyanobacterial biovolume in a drinking water source. J. Environ. Monit. 13, 455.

Miano, T.M., Martin, J.P., Sposito, G., 1988. Fluorescence Spectroscopy of Humic Substances. Soil Science Society of America Journal 52, 1016–1019.

Miano, T.M., Senesi, N., 1992. Synchronous excitation fluorescence spectroscopy applied to soil humic substances chemistry. Sci Total Environ 117, 41–51.

Miller, M.P., Simone, B.E., McKnight, D.M., Cory, R.M., Williams, M.W., Boyer, E.W., 2010. New light on a dark subject: comment. Aquat Sci 72, 269–275.

Mostafa, S., Korak, J.A., Shimabuku, K., Glover, C.M., Rosario-Ortiz, F.L., 2014. Relation between optical properties and formation of reactive intermediates from different size fractions of organic matter, in: Rosario-Ortiz, F.L. (Ed.), Advances in the Physiochemical Characterization of Organic Matter. American Chemical Society Symposium Series 1160, Washington DC.

Murphy, K.R., 2011. A Note on Determining the Extent of the Water Raman Peak in Fluorescence Spectroscopy. Appl Spectrosc 65, 233–236.

Murphy, K.R., Butler, K.D., Spencer, R.G.M., Stedmon, C.A., Boehme, J.R., Aiken, G.R., 2010. Measurement of Dissolved Organic Matter Fluorescence in Aquatic Environments: An Interlaboratory Comparison. Environ Sci Technol 44, 9405–9412.

Murphy, K.R., Stedmon, C.A., Graeber, D., Bro, R., 2013. Fluorescence spectroscopy and multi-way techniques. PARAFAC. Analytical Methods 5, 6557–6566.

Narkis, N., Rebhun, M., 1977. Stoichiometric Relationship between Humic and Fulvic Acids and Flocculants. Journal AWWA 69, 325–328.

Nguyen, M., Westerhoff, P., Baker, L., Hu, Q., Esparza-Soto, M., Sommerfeld, M., 2005. Characteristics and reactivity of algae-produced dissolved organic carbon. J Environ Eng 131, 1574–1582.

Ohno, T., 2002. Fluorescence inner-filtering correction for determining the humification index of dissolved organic matter. Environ Sci Technol 36, 742–746.

Ohno, T., Amirbahman, A., Bro, R., 2008. Parallel factor analysis of excitation-emission matrix fluorescence spectra of water soluble soil organic matter as basis for the determination of conditional metal binding parameters. Environ Sci Technol 42, 186–192.

Ong, L.J., Glazer, A.N., 1991. Phycoerythrins of marine unicellular cyanobacteria. I. Bilin types and locations and energy transfer pathways in Synechococcus spp. phycoerythrins. Journal of Biological Chemistry 266, 9515–9527.

Paerl, H.W., Paul, V.J., 2012. Climate change: Links to global expansion of harmful cyanobacteria. Water Research 46, 1349–1363.

Parker, C.A., Barnes, W.J., 1957. Some experiments with spectrofluorimeters and filter fluorimeters. Analyst 82, 606.

Parker, C.A., Rees, W.T., 1962. Fluorescence spectrometry. A review. Analyst 87, 83–111.

Pearson, L., Mihali, T., Moffitt, M., Kellmann, R., Neilan, B., 2010. On the Chemistry, Toxicology and Genetics of the Cyanobacterial Toxins, Microcystin, Nodularin, Saxitoxin and Cylindrospermopsin. Marine Drugs 8, 1650–1680.

Perdue, E.M., 2009. Natural Organic Matter. Encyclopedia of Inland Waters 2, 806–819.

Perdue, E.M., Ritchie, J.D., 2009. Dissolved Organic Matter in Freshwaters, in: Holland, H.D., Turekian, K.K. (Eds.), Treatise on Geochemistry. Elsevier, pp. 1–46.

Perrette, Y., Delannoy, J., Desmet, M., Lignier, V., Destombes, J., 2005. Speleothem organic matter content imaging. The use of a Fluorescence Index to characterise the maximum

emission wavelength. Chemical Geology 214, 193–208.

Pifer, A.D., Fairey, J.L., 2012. Improving on SUVA(254) using fluorescence-PARAFAC analysis and asymmetric flow-field flow fractionation for assessing disinfection byproduct formation and control. Water Research 46, 2927–2936.

Pifer, A.D., Fairey, J.L., 2014. Suitability of Organic Matter Surrogates to Predict Trihalomethane Formation in Drinking Water Sources. Environ Eng Sci 31, 117–126.

Power, J.F., Langford, C.H., 1988. Optical absorbance of dissolved organic matter in natural water studies using the thermal lens effect. Anal Chem 60, 842–846.

Qu, F., Liang, H., Wang, Z., Wang, H., Yu, H., 2012. Ultrafiltration membrane fouling by extracellular organic matters (EOM) of Microcystis aeruginosa in stationary phase: Influences of interfacial characteristics of foulants and fouling mechanisms. Water Research 46, 1490–1500.

Randtke, S.J., 1988. Organic Contaminant Removal by Coagulation and Related Process Combinations. Journal AWWA 80, 40–56.

Randtke, S.J., Jepsen, C.P., 1981. Chemical pretreatment for activated-carbon adsorption. Journal AWWA 73, 411–419.

Rendell, D., 1987. Fluorescence and Phosphorescence. John Wiley & Sons, London.

Reuter, J.H., Perdue, E.M., 1977. Importance of Heavy Metal-Organic Matter Interactions in Natural-Waters. Geochim Cosmochim Ac 41, 325–334.

Reynolds, D.M., 2003. Rapid and direct determination of tryptophan in water using synchronous fluorescence spectroscopy. Water Research 37, 3055–3060.

Richard, C., Trubetskaya, O., Trubetskoj, O., Reznikova, O., Afanas'eva, G., Aguer, J.P., Guyot, G., 2004. Key Role of the Low Molecular Size Fraction of Soil Humic Acids for Fluorescence and Photoinductive Activity. Environ Sci Technol 38, 2052–2057.

Richardson, S.D., 2012. Environmental Mass Spectrometry: Emerging Contaminants and Current Issues. Anal Chem 84, 747–778.

Rigbi, M., Rosinski, J., Siegelman, H.W., Sutherland, J.C., 1980. Cyanobacterial phycobilisomes: Selective dissociation monitored by fluorescence and circular dichroism 77, 1961–1965.

Roccaro, P., Vagliasindi, F.G.A., 2009. Differential vs. absolute UV absorbance approaches in studying NOM reactivity in DBPs formation: Comparison and applicability. Water Research 43, 744–750.

Rodriguez, E., Onstad, G.D., Kull, T.P.J., Metcalf, J.S., Acero, J.L., Gunten, Von, U., 2007. Oxidative elimination of cyanotoxins: Comparison of ozone, chlorine, chlorine dioxide and permanganate. Water Research 41, 3381–3393.

Romera-Castillo, C., Sarmento, H., Álvarez-Salgado, X.A., Gasol, J.M., Marrase, C., 2011. Net Production and Consumption of Fluorescent Colored Dissolved Organic Matter by Natural Bacterial Assemblages Growing on Marine Phytoplankton Exudates. Applied and Environmental Microbiology 77, 7490–7498.

Rook, J., 1977. Chlorination Reactions of Fulvic Acids in Natural-Waters. Environ Sci Technol

11, 478–482.

Rook, J.J., 1976. Haloforms in drinking water. Journal AWWA 68, 168–172.

Sanchez, N.P., Skeriotis, A.T., Miller, C.M., 2013. Assessment of dissolved organic matter fluorescence PARAFAC components before and after coagulation–filtration in a full scale water treatment plant. Water Research 47, 1679–1690.

Saraceno, J.F., Pellerin, B.A., Downing, B.D., Boss, E., Bachand, P.M., Bergamaschi, B.A., 2009. High-frequency in situ optical measurements during a storm event: Assessing relationships between dissolved organic matter, sediment concentrations, and hydrologic processes. J Geophys Res-Biogeo 114, G00F09.

Senesi, N., Miano, T.M., Provenzano, M.R., Brunetti, G., 1989. Spectroscopic and Compositional Comparative Characterization of I.H.S.S. Reference and Standard Fulvic and Humic Acids of Various Origin. Sci Total Environ 81, 143–156.

Senesi, N., Miano, T.M., Provenzano, M.R., Brunetti, G., 1991. Characterization, differentiation, and classification of humic substances by fluorescence spectroscopy. Soil Sci 152, 259–271.

Shapiro, J., 1957. Chemical and biological studies on the yellow organic acids of lake water. Limnol Oceanogr 161–179.

Sharpless, C., McGown, L., 1999. Effects of aluminum-induced aggregation on the fluorescence of humic substances. Environ Sci Technol 33, 3264–3270.

Sharpless, C.M., 2012. Lifetimes of Triplet Dissolved Natural Organic Matter (DOM) and the Effect of NaBH4 Reduction on Singlet Oxygen Quantum Yields: Implications for DOM Photophysics. Environ Sci Technol 46, 4466–4473.

Shutova, Y., Baker, A., Bridgeman, J., Henderson, R., 2014. Spectroscopic characterisation of dissolved organic matter changes in drinking water treatment: From PARAFAC analysis to online monitoring wavelengths. Water Research 54, 159–169.

Sinclair, J.L., Hall, S., 2008. Chapter 3: Occurrence of Cyanobacterial Harmful Algal Blooms Workgroup Report, in: Hudnell, H.K. (Ed.), Cyanobacterial Harmful Algal Blooms: State of the Science and Research Needs. Springer New York, New York, pp. 45–103.

Skoog, D.A., Holler, F.J., Crouch, S.R., 2006. Principles of Instrument Analysis, 6 ed. Cengage Learning.

Smith, J.L., Boyer, G.L., Zimba, P.V., 2008. A review of cyanobacterial odorous and bioactive metabolites: Impacts and management alternatives in aquaculture. Aquaculture 280, 5–20.

Stadnichuk, I.N., Romanova, N.I., Selyakh, I.O., 1985. A phycourobilin-containing phycoerythrin from the cyanobacterium Oscillatoria sp. Archives of microbiology 143, 20–25.

Stedmon, C., Markager, S., Bro, R., 2003. Tracing dissolved organic matter in aquatic environments using a new approach to fluorescence spectroscopy. Mar Chem 82, 239–254. Stedmon, C.A., Bro, R., 2008. Characterizing dissolved organic matter fluorescence with parallel factor analysis: a tutorial. Limnol Oceanogr-Methods 6, 572–579.

Steinberg, C.E.W., 2003. Ecology of Humic Substances in Freshwater. Springer, Berlin.

Stewart, A.J., Wetzel, R.G., 1981. Asymmetrical Relationships between Absorbance,

fluorescence and dissolved organic carbon. Limnol Oceanogr 26, 590–597.

Stewart, D., Farmer, F., 1984. Extraction, identification, and quantitation of phycobiliprotein pigments from phototrophic plankton. Limonology and Oceanography 29, 392–397.

Suda, S., Watanabe, M.M., Otsuka, S., Mahakahant, A., Yongmanitchai, W., Nopartnaraporn, N., Liu, Y.D., Day, J.G., 2002. Taxonomic revision of water-bloom-forming species of oscillatorioid cyanobacteria. International Journal of Systematic and Evolutionary Microbiology 52, 1577–1595.

Summers, R.S., Cornel, P.K., Roberts, P.V., 1987. Molecular size distribution and spectroscopic characterization of humic substances. Sci Total Environ 62, 27–37.

Summers, R.S., Hooper, S., Shukairy, H., 1996. Assessing DBP yield: uniform formation conditions. Journal AWWA.

Swietlik, J., Sikorska, E., 2004. Application of fluorescence spectroscopy in the studies of natural organic matter fractions reactivity with chlorine dioxide and ozone. Water Research 38, 3791–3799.

Taylor, J.R., 1997. An Introduction to Error Analysis, 2nd ed. University Science Books.

Thorn, K.A., Folan, D.W., MacCarthy, P., 1989. Characterization of the International Humic Substances Society Standard and Reference Fulvic and Humic Acids by Solution State Carbon-13 (13C) and Hydrogen-1 (1H) Nuclear Magnetic Resonance Spectrometry (No. 89-4196). U.S. Geological Survey, Denver, CO.

Traina, S.J., Novak, J., Smeck, N.E., 1990. An ultraviolet absorbance method of estimating the percent aromatic carbon content of humic acids. Journal of Environment Quality 19, 151–153.

Tucker, S.A., Amszi, V.L., Acree, W.E., 1992. Primary and secondary inner filtering. Effect of K2Cr2O7 on fluorescence emission intensities of quinine sulfate. Journal of Chemical Education 69, 8.

USEPA, 2006. National Primary Drinking Water Regulations: Stage 2 Disinfectants and Disinfection Byproducts Rule. 40 CFR Parts 9, 141, and 142.

Valeur, B., 2002. Molecular Fluorescence. Wiley-VCH, Weinheim, Germany.

Velapoldi, R.A., Mielenz, K.D., 1980. A fluorescence standard reference material: quinine sulfate dihydrate (No. 260-64). National Bureau of Standards.

Volk, C., Bell, K., Ibrahim, E., Verges, D., Amy, G.L., Lechevallier, M., 2000. Impact of enhanced and optimized coagulation on removal of organic matter and its biodegradable fraction in drinking water. Water Research 34, 3247–3257.

Wang, Z., Wu, Z., Tang, S., 2009. Characterization of dissolved organic matter in a submerged membrane bioreactor by using three-dimensional excitation and emission matrix fluorescence spectroscopy. Water Research 43, 1533–1540.

Wang, Z.-D., C Pant, B., H Langford, C., 1990. Spectroscopic and structural characterization of a Laurentian fulvic acid: notes on the origin of the color. Anal Chim Acta 232, 43–49.

Watras, C.J., Baker, A.L., 1988. Detection of planktonic cyanobacteria by tandem in vivo fluorometry. Hydrobiologia 169, 77–84.

Watson, S.B., 2003. Cyanobacterial and eukaryotic algal odour compounds: signals or by-products? A review of their biological activity. Phycologia 42, 332–350.

Watson, S.B., 2004. Aquatic Taste and Odor: a Primary Signal of Drinking-Water Integrity. Journal of Toxicology and Environmental Health, Part A: Current Issues 67, 1779–1795.

Weishaar, J.L., Aiken, G.R., Bergamaschi, B.A., Fram, M.S., Fujii, R., Mopper, K., 2003. Evaluation of Specific Ultraviolet Absorbance as an Indicator of the Chemical Composition and Reactivity of Dissolved Organic Carbon. Environ Sci Technol 37, 4702–4708.

Wert, E.C., Dong, M.M., Rosario-Ortiz, F.L., 2013. Using digital flow cytometry to assess the degradation of three cyanobacteria species after oxidation processes. Water Research 47, 3752–3761.

Wert, E.C., Korak, J.A., Trenholm, R.A., Rosario-Ortiz, F.L., 2014. Effect of oxidant exposure on the release of intracellular microcystin, MIB, and geosmin from three cyanobacteria species. Water Research 251–259.

Wert, E.C., Rosario-Ortiz, F.L., 2013. Intracellular Organic Matter from Cyanobacteria as a Precursor for Carbonaceous and Nitrogenous Disinfection Byproducts. Environ Sci Technol 6332–6340.

Wert, E.C., Rosario-Ortiz, F.L., Snyder, S.A., 2009. Effect of ozone exposure on the oxidation of trace organic contaminants in wastewater. Water Research 43, 1005–1014.

White, M., Thompson, J., Harrington, G., 1997. Evaluation criteria for enhanced coagulation compliance. Journal AWWA.

WHO, 2003. Cyanobacterial toxins: Microcystin-LR in drinking water. Background document for preparation of WHO guidelines for drinking-water quality (No. WHO/SDS/WSH/03.04/57). World Health Organization, Geneva.

Wildman, R.B., Bowen, C.C., 1974. Phycobilisomes in Blue-Green-Algae. Journal of Bacteriology 117, 866–881.

Win, Y., Kumke, M., Specht, C., Schindelin, A., Kolliopoulos, G., Ohlenbusch, G., Kleiser, G., Hesse, S., Frimmel, F., 2000. Influence of oxidation of dissolved organic matter (DOM) on subsequent water treatment processes. Water Research 34, 2098–2104.

Wolfbeis, O.S., 1985. Fluorescence of Organic Natural Products, in: Schulman, S.G. (Ed.), Molecular Luminescence Spectroscopy, Part 1. John Wiley & Sons, New York, pp. 167–370.

Wu, F.C., Kothawala, D.N., Evans, R.D., Dillon, P.J., Cai, Y.R., 2007. Relationships between DOC concentration, molecular size and fluorescence properties of DOM in a stream. Appl Geochem 22, 1659–1667.

Xu, H., Jiang, H., 2013. UV-induced photochemical heterogeneity of dissolved and attached organic matter associated with cyanobacterial blooms in a eutrophic freshwater lake. Water Research in press.

Yang, W., Li, X., Pan, B., Lv, L., Zhang, W., 2013. Effective removal of effluent organic matter (EfOM) from bio-treated coking wastewater by a recyclable aminated hyper-cross-linked polymer. Water Research 47, 4730–4738.

Yang, X., Shang, C., Lee, W., Westerhoff, P., Fan, C., 2008. Correlations between organic

matter properties and DBP formation during chloramination. Water Research 42, 2329–2339.

Yappert, M.C., Ingle, J.D., 1989. Correction of polychromatic luminescence signals for inner-filter effects. Appl Spectrosc 43, 759–767.

Zamyadi, A., Dorner, S., Sauvé, S., Ellis, D., Bolduc, A., Bastien, C., Prévost, M., 2013. Species-dependence of cyanobacteria removal efficiency by different drinking water treatment processes. Water Research 47, 2689–2700.

Zamyadi, A., Ho, L., Newcombe, G., Bustamante, H., Prévost, M., 2012a. Fate of toxic cyanobacterial cells and disinfection by-products formation after chlorination. Water Research 46, 1524–1535.

Zamyadi, A., MacLeod, S.L., Fan, Y., McQuaid, N., Dorner, S., Sauvé, S., Prévost, M., 2012b. Toxic cyanobacterial breakthrough and accumulation in a drinking water plant: a monitoring and treatment challenge. Water Research 46, 1511–1523.

Zamyadi, A., McQuaid, N., Prévost, M., Dorner, S., 2012c. Monitoring of potentially toxic cyanobacteria using an online multi-probe in drinking water sources. J. Environ. Monit. 14, 579–588.

Zepp, R., Sheldon, W., Moran, M., 2004. Dissolved organic fluorophores in southeastern US coastal waters: correction method for eliminating Rayleigh and Raman scattering peaks in excitation-emission matrices. Marine Chemistry, 89, 15–36.

Zhang, W., Li, Y., Wang, C., Wang, P., Wang, Q., 2013. Energy recovery during advanced wastewater treatment: Simultaneous estrogenic activity removal and hydrogen production through solar photocatalysis. Water Research 47, 1480–1490.

Zhou, J., Wang, J.-J., Baudon, A., Chow, A.T., 2013. Improved Fluorescence Excitation-Emission Matrix Regional Integration to Quantify Spectra for Fluorescent Dissolved Organic Matter. Journal of Environment Quality 42, 925–930.

Zsolnay, A., Baigar, E., Jimenez, M., Steinweg, B., Saccomandi, F., 1999. Differentiating with fluorescence spectroscopy the sources of dissolved organic matter in soils subjected to drying. Chemosphere 38, 45–50.

Appendix A Supplemental Data for Chapter 2

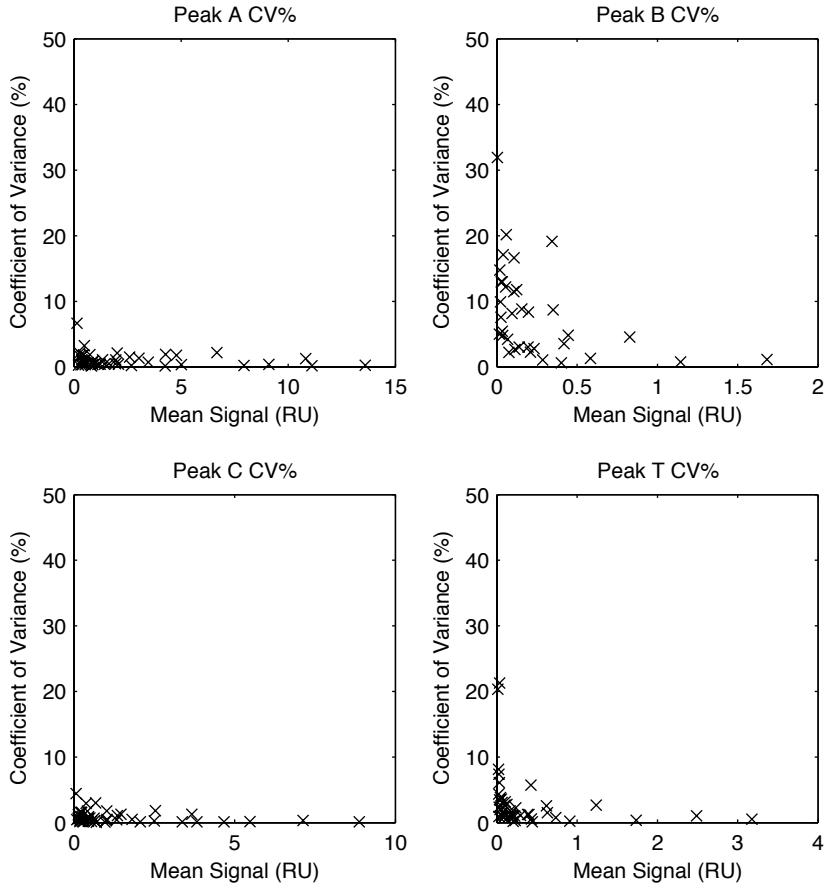

Figure A.1 Coefficient of variance between triplicate measurements as a function of mean signal intensity for each peak center with inner filter corrections applied.

Table A.1. Summary of compositional metrics for IHSS isolates and individual waters used for FI analysis. For the IHSS isolates and BEM, an average value across with linear range is reported with its standard deviation.

DOM Source	UV_{254} (cm^{-1})	DOC $mg_c\ L^{-1}$	SUVA $L\ mg_c^{-1}\ m^{-1}$	Sp. A $RU\ L\ mg_c^{-1}$	Sp. B $RU\ L\ mg_c^{-1}$	Sp. C $RU\ L\ mg_c^{-1}$	Sp. T $RU\ L\ mg_c^{-1}$	FI	Peak wavelength at Ex=370 nm	IHSS Aromatic Carbon %
PLFA	--	--	2.56 ± 0.03	0.30 ± 0.015	0.04 ± 0.002	0.12 ± 0.006	0.06 ± 0.003	1.46 ± 0.007	461 ± 1.4	12
SRNOM	--	--	3.74 ± 0.16	0.28 ± 0.014	--	0.10 ± 0.005	0.02 ± 0.0017	1.29 ± 0.007	474 ± 1.4	23
SRFA	--	--	3.97 ± 0.12	0.41 ± 0.02	--	0.14 ± 0.007	0.03 ± 0.002	1.31 ± 0.011	474 ± 0.6	24
SRHA	--	--	6.20 ± 0.27	0.27 ± 0.013	--	0.10 ± 0.005	0.02 ± 0.004	1.08 ± 0.008	484 ± 1.9	31
BEM	--	--	2.18 ± 0.05	0.25 ± 0.012	0.05 ± 0.005	0.08 ± 0.004	0.05 ± 0.003	1.46 ± 0.007	463 ± 2.4	--
Betasso WTP*	0.3	7.7	4	0.31	0.02	0.11	0.03	1.34	468	--
Boulder Reservoir	0.07	3.5	2	0.15	0.04	0.05	0.04	1.4	468	--
Barr Lake	0.11	6.2	1.8	0.32	0.09	0.1	0.09	1.83	462	--
Boulder WW	0.11	n/a	n/a	--	--	--	--	1.95	444	--

*diluted before analysis

Aromatic Carbon values from (Thorn et al., 1989)

A.1 Linear relationship between fluorescence and concentration

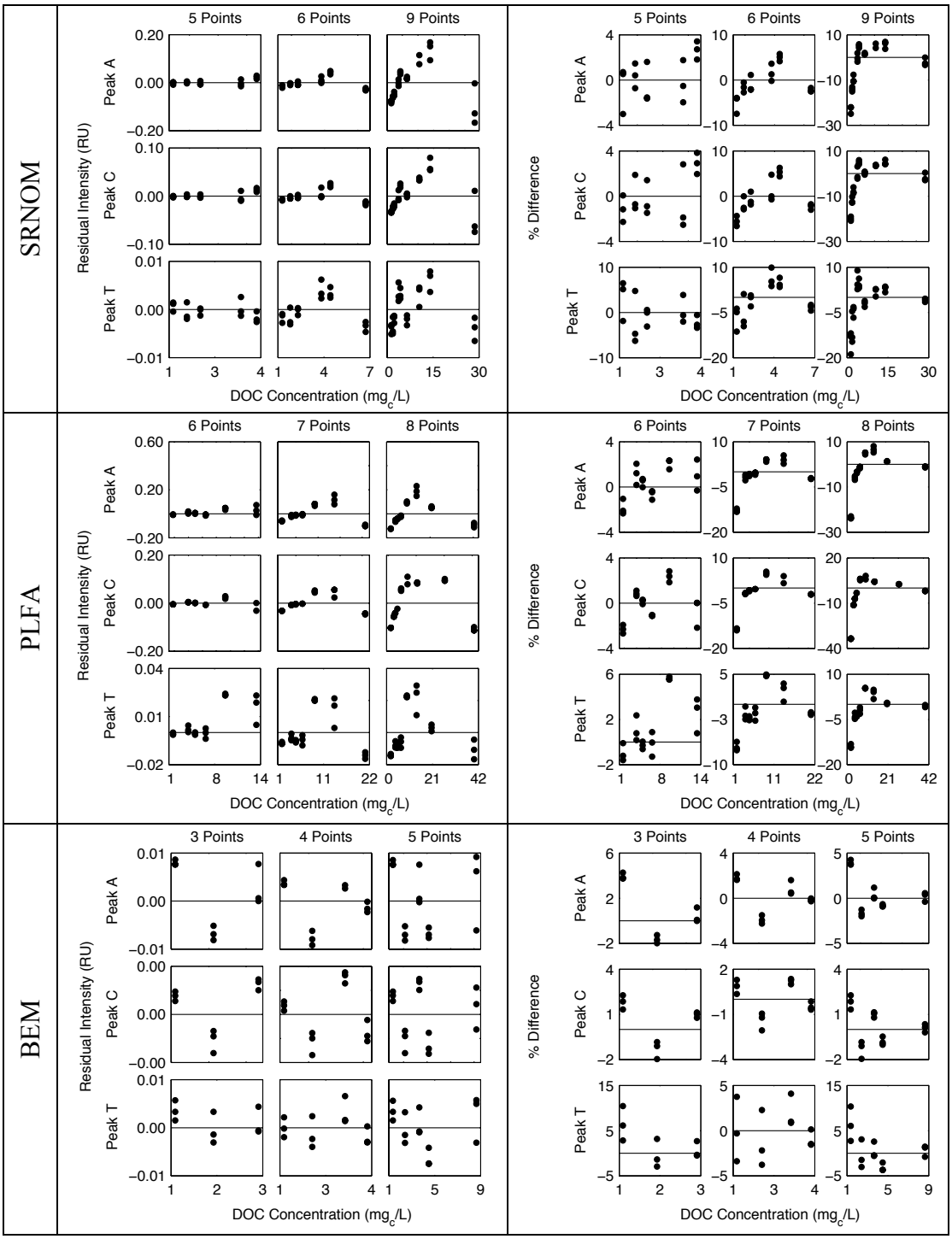

Figure A.2 Residual analysis for SRNOM, PLFA and BEM showing the upper and lower limits of the linearity threshold and full range of DOC concentrations. The left column presents the residuals in Raman units and the right column presents the residuals as a percentage of the measured intensity.

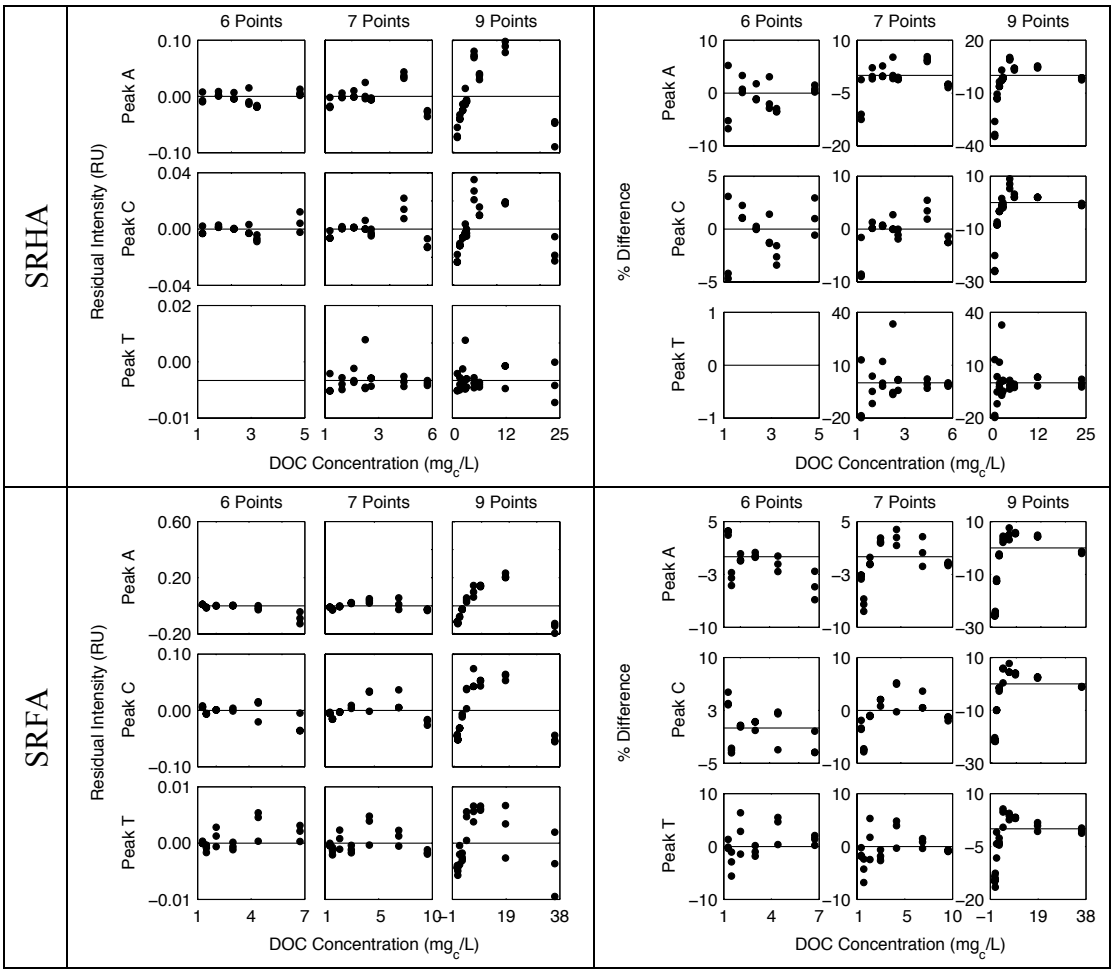

Figure A.3 Residual analysis for SRHA and SRFA showing the upper and lower limits of the linearity threshold and full range of DOC concentrations. The left column presents the residuals in Raman units and the right column presents the residuals as a percentage of the measured intensity.

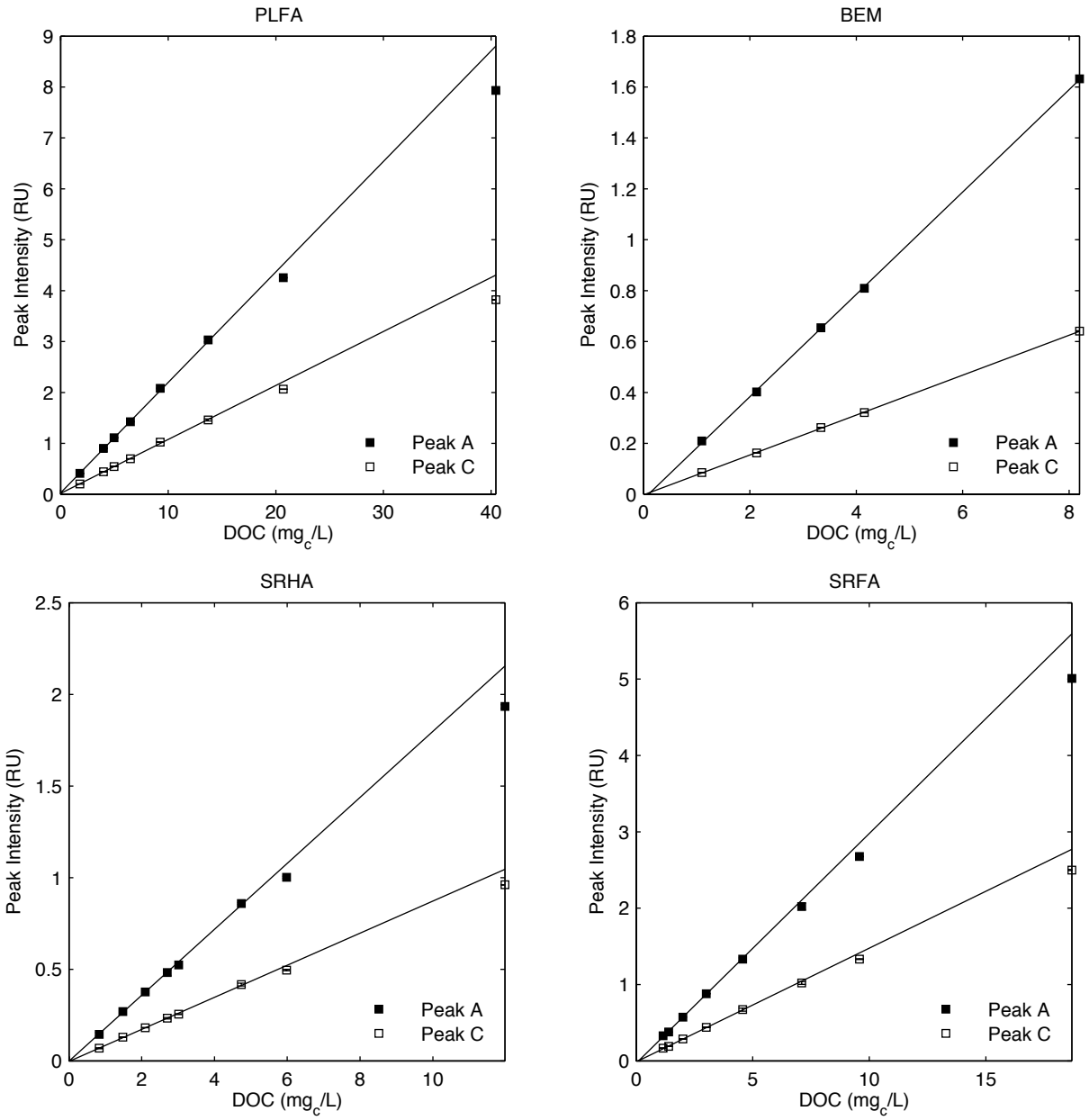

Figure A.4 Peak A and C intensity as a function of DOC concentration for PLFA, BEM, SRHA and SRFA. The lines represent a linear model fit to the lowest 5 DOC concentrations. Error bars representing the standard deviation between triplicate measurements may be smaller than the marker.

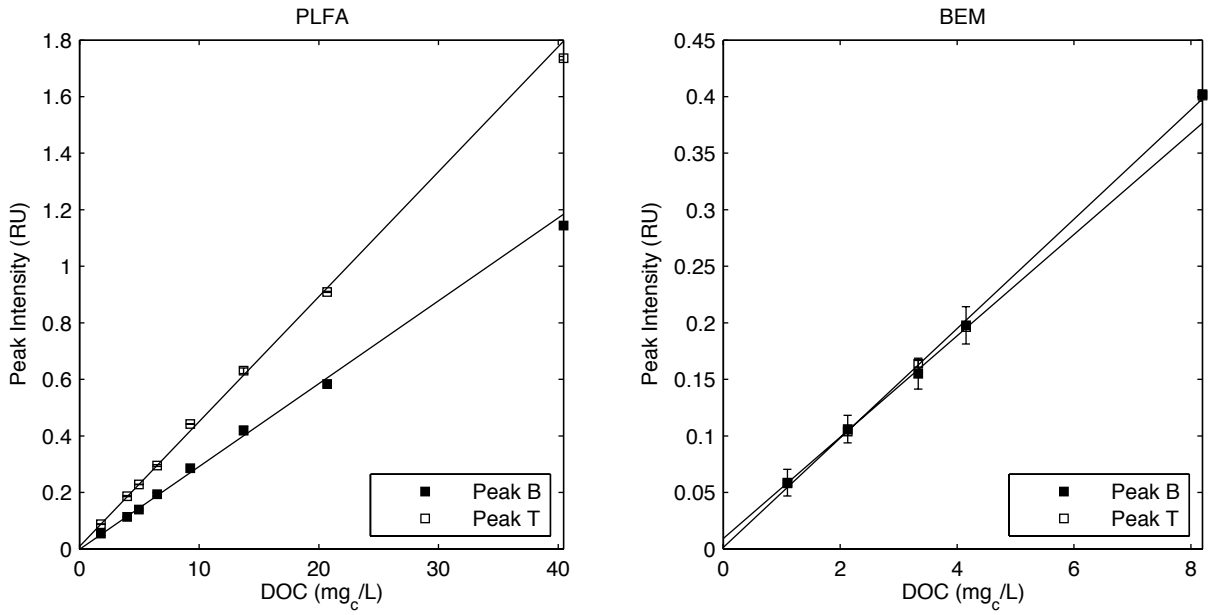

Figure A.5 Peak B and T intensity as a function of DOC concentration for PLFA and BEM. The lines represent a linear model fit to the lowest 5 DOC concentrations. Error bars representing the standard deviation between triplicate measurements may be smaller than the marker.

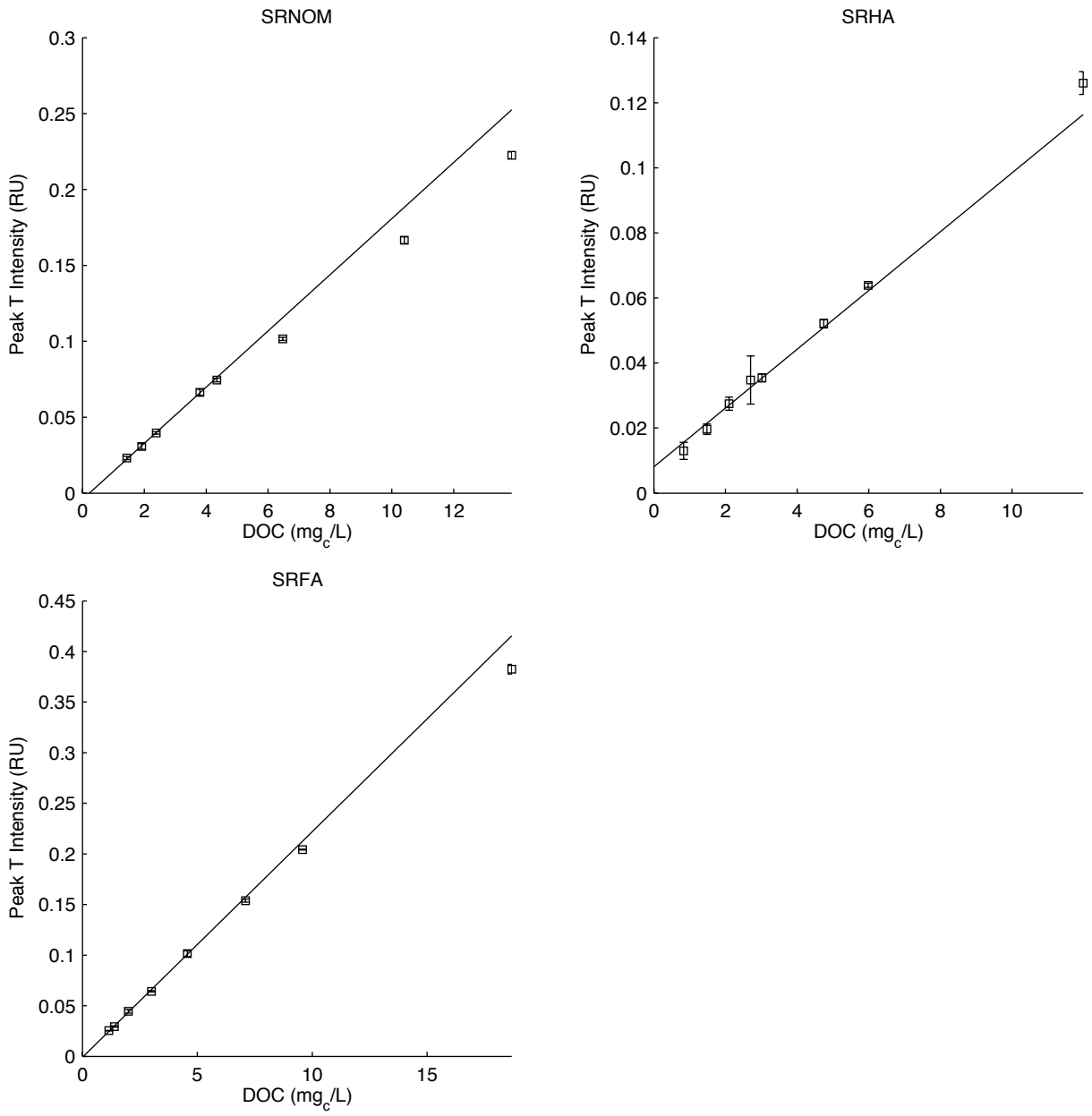

Figure A.6 Peak T intensity as a function of DOC concentration for SRNOM, SRHA and SRFA. The lines represent a linear model fit to the lowest 5 DOC concentrations. Error bars representing the standard deviation between triplicate measurements may be smaller than the marker.

Table A.2. Linear regression analyses for peak intensity (y) in RU as a function of DOC concentration (x) in $mg_c\ L^{-1}$ for $\alpha = 0.05$ for the lowest 5 concentrations (below the linearity threshold) and lowest 8 concentrations (crossing threshold). Slope p values and R^2 values are also provided. All regressions with 8 DOC concentrations failed to pass model adequacy criteria of random residuals, except peak T for SRHA.

DOM Source	# DOCs in Model	Max. DOC mg L^{-1}	Peak A			Peak B		
			Regression	Slope p	R^2	Regression	Slope p	R^2
SRNOM	5	4.3	y=0.209x-0.038	<0.01	0.998	BQL		
	8	13.9	y=0.186+0.021	<0.01	0.999			
PLFA	5	9.3	y=0.222x+0.008	<0.01	0.999	y=0.031x-0.008	<0.01	0.993
	8	40.4	y=0.194x+0.188	<0.01	0.998	y=0.028x+0.010	<0.01	0.998
BEM	5	8.2	y=0.201x-0.019	<0.01	0.999	y=0.049x+0.000	<0.01	0.991
SRHA	5	3.02	y=0.174x+0.005	<0.01	0.996	BQL		
	8	12.0	y=0.160x+0.04	<0.01	0.998			
SRFA	5	4.6	y=0.297x-0.02	<0.01	0.999	BQL		
	8	18.7	y=0.268x+0.060	<0.01	0.999			

DOM Source	# DOCs in Model	Max. DOC mg L^{-1}	Peak C			Peak T		
			Regression	Slope p	R^2	Regression	Slope p	R^2
SRNOM	5	4.3	y=0.107x-0.021	<0.01	0.997	y=0.018x-0.003	<0.01	0.995
	8	13.9	y=0.097x-0.005	<0.01	0.999	y=0.016x+0.002	<0.01	0.998
PLFA	5	9.3	y=0.107x-0.020	<0.01	0.999	y=0.047x-0.002	<0.01	0.997
	8	40.4	y=0.0978x-0.0005	<0.01	0.998	y=0.043x-0.025	<0.01	0.999
BEM	5	8.2	y=0.078x-0.002	<0.01	0.999	y=0.048x+0.001	<0.01	0.999
SRHA	5	3.02	y=0.085x+0.000	<0.01	0.998	y=0.011x+0.004	<0.01	0.880
	8	12.0	y=0.080x+0.015	<0.01	0.998	y=0.010x+0.005	<0.01	0.993
SRFA	5	4.6	y=0.150x-0.012	<0.01	0.998	y=0.022x-0.001	<0.01	0.997
	8	18.7	y=0.134x+0.033	<0.01	0.999	y=0.020x+0.004	<0.01	0.999

A.2 Inner Filter Corrections

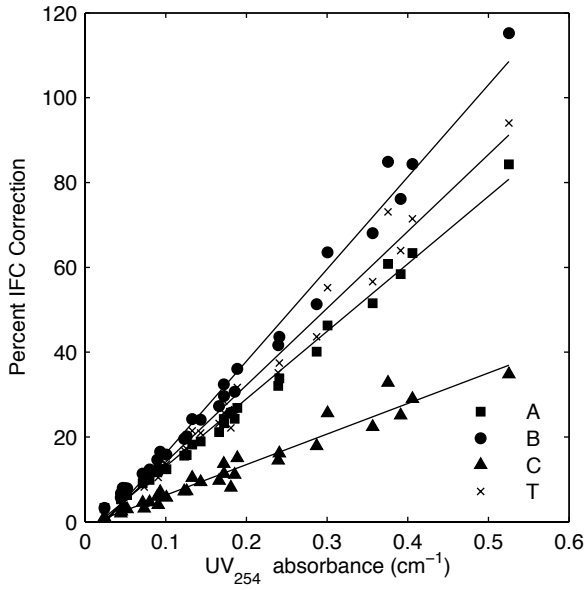

Figure A.7 Inner-filter correction as a function of UV254 absorbance. A point in the center of each peak region was chosen to compare regions. Lines indicate the general trend.

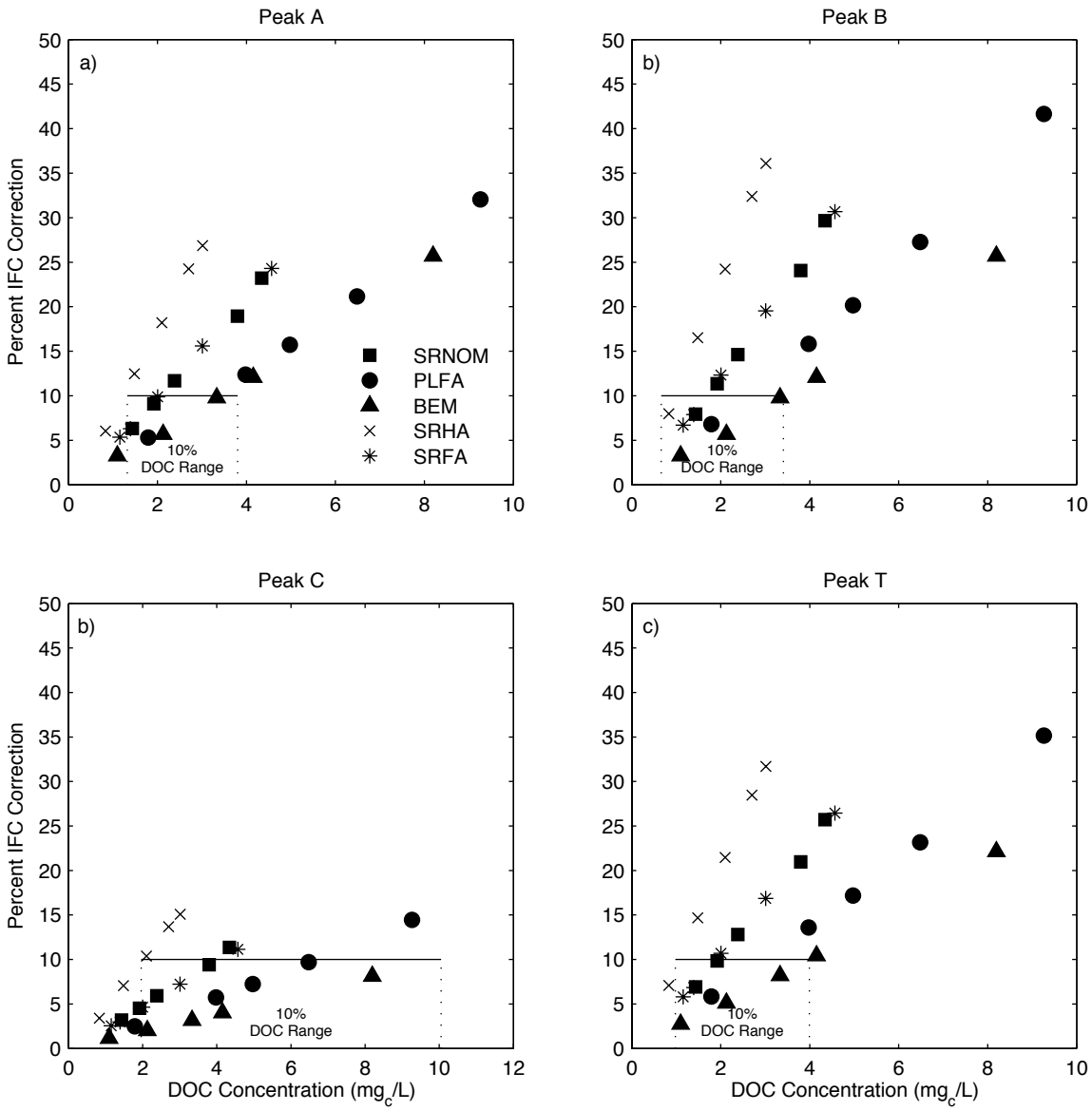

Figure A.8 Percent inner filter correction as a function of DOC concentrations for the center of a) Peak A b) Peak B c) Peak C and d) Peak T

A.3 Specific Peak Intensity

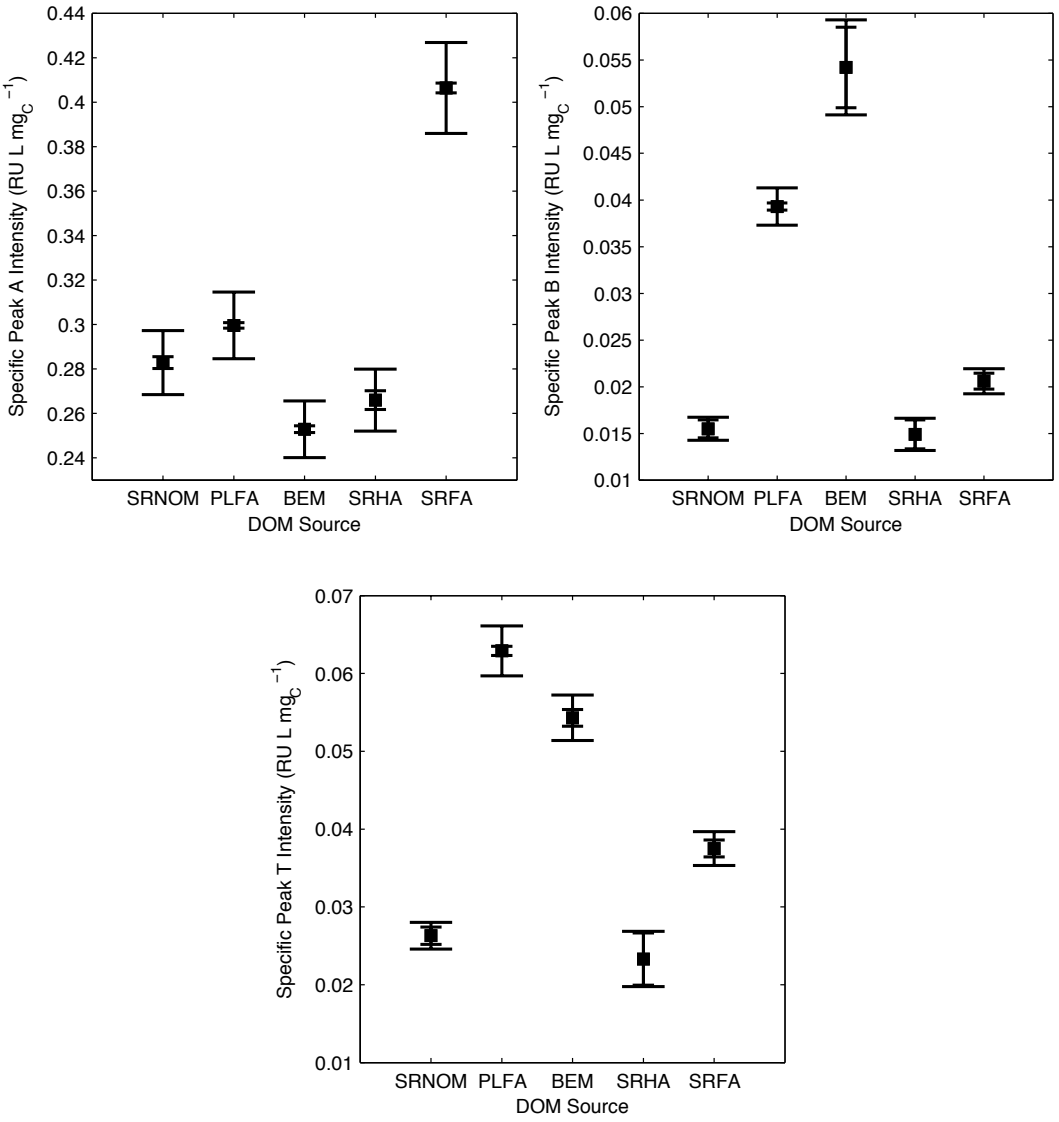

Figure A.9 Specific peak intensity for 5 DOM sources within linear concentration range with IFCs applied for peaks A, B and T. The inner (shorter) error bar represents the uncertainty associated with only fluorescence. The outer (wider) error bar is the uncertainty associated with both fluorescence and DOC measurements.

A.4 Peak Location Analysis

The concentration dependence of peak location was evaluated. No correlation was found between peak location and concentration for all DOC concentrations (including the non-linear regime) when samples have IFCs applied. If samples are not corrected, then there may be a correlation between concentration and peak emission wavelength for Peaks A and C (Peaks B and T are always confined to the boundary). Peak emission wavelength for SRFA and PLFA shifted to longer wavelengths with increasing concentration as also seen by others (Ohno, 2002). However, no correlation was seen at low concentrations, below about 10 mg L^{-1}, but only above this threshold. These observations suggest that peak location is an acceptable compositional metric to use across a variety of concentrations when samples have IFC but are only acceptable at low concentrations in the absence of absorbance corrections.

The impact of IFCs was also investigated to determine how different correction methods affect interpretations. Relationships between Peak C emission wavelength and other compositional properties, like aromaticity, hydrophobicity or DOM fraction, have been presented (Alberts et al., 2002; A. Baker et al., 2008; Lakowicz, 2006; Miano and Senesi, 1992; Senesi et al., 1991; Thorn et al., 1989). Different correction methods may bias results or prevent them from being universally applicable. A paired t-test analysis was used to determine if the application of inner filter corrections lead to a systematic change in Peak C emission wavelength. Peaks B and T were not considered because of the limitations already addressed. Without IFCs, SRNOM and SRFA Peak C emission wavelength shifted to longer wavelengths at an OD_{Total} for Peak C center of 0.04 and 0.09 cm^{-1}, respectively. PLFA was less sensitive and demonstrated systematic shifts at OD_{Total} above 0.17 cm^{-1}. The magnitude of the shift increased from 4nm up to 10nm with increasing concentration. A shift in emission wavelength was simultaneously accompanied by a shift to higher excitation wavelengths with increasing absorbance attenuation.

The effect of IFCs on Peak C emission wavelength become important at environmentally relevant concentrations and may bias results if neglected.

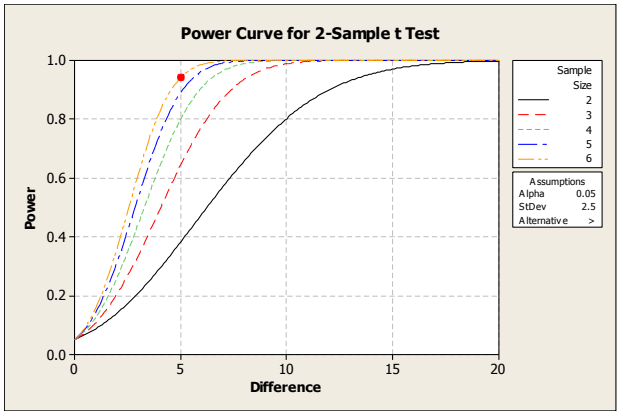

Figure A.10 Operating characteristic curve for Peak C emission wavelength detection assuming a standard deviation of 2.5 nm, α=0.05 and β=0.1. Additional curves represent the number of replicates.

A.5 Fluorescence Index

Table A.3 Linear regression analyses for fluorescence index (y, unitless) as a function of DOC concentration (x) in $mg_c\ L^{-1}$ for α=0.05 with and without inner filter corrections. Only statistically significant regressions are shown. Average values reported are unitless.

DOM	With IFCs – Linear Regime				Without IFCs – Linear Regime			
Source	Avg.	CV	Regression	slope p	Avg.	CV	Regression	slope p
SRNOM	1.29	0.6%	y=-0.0034x+1.303	0.051	1.29	0.7%	y=-0.0049x+1.304	0.017
PLFA	1.45	1.3%	y=-0.0052x+1.487	<0.001	1.45	1.5%	y=-0.0061x+1.487	<0.001
BEM	1.46	0.5%	--	0.34	1.45	0.6%	--	0.312
SRHA	1.08	0.8%	y=-0.0053x+1.087	0.0687	1.07	0.9%	y=-0.008x+1.088	0.010
SRFA	1.31	0.9%	y=-0.0041x+1.326	0.024	1.31	1.0%	y=-0.0052x+1.32	0.006

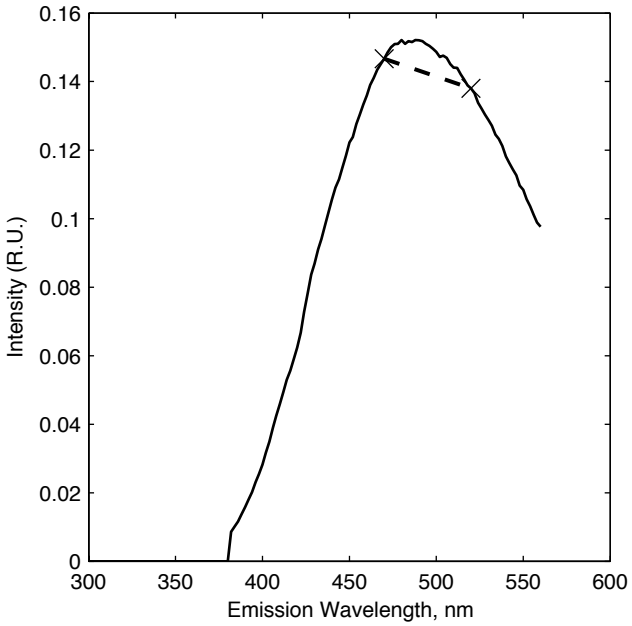

Figure A.11 Emission scan at excitation 370 nm. Intensities for SRHA using the I_{470}/I_{520} method are indicated by the markers.

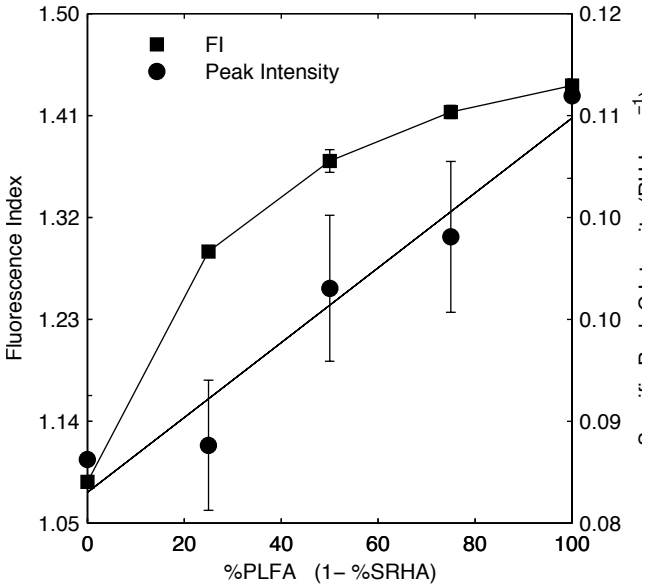

Figure A.12 Specific peak intensity and fluorescence index as a function of composition. Error bars for fluorescence index represent the standard deviation between triplicates. Error bars for specific peak intensity represent the error propagation for both fluorescence and DOC concentration measurements.

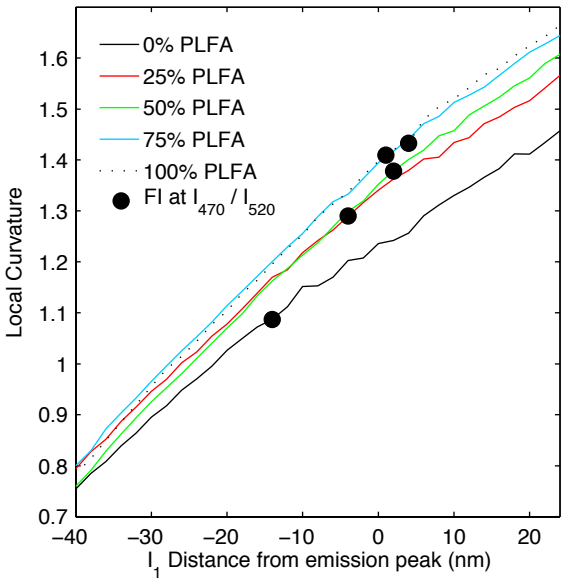

Figure A.13. Graphical representation for changes in both peak emission wavelength and local curvature for mixing experiments. Circles indicate the location of the FI measurement using the I_{470}/I_{520} convention.

Appendix B Supplemental Data for Chapter 5

B.1 Cyanobacteria Pigments (Phycobiliproteins) Background

Phycobilisomes are light harvesting complexes attached to the thylakoid membrane in cyanobacteria that expand the range of wavelengths the organism can utilize for photosynthesis. They absorb light in the visible range predominately from 550 to 650 nm, where chlorophyll *a* cannot absorb light (Bryant, 1994). Phycobilisomes in most cyanobacteria are hemidiscoidal with a tricylindrical core (MacColl, 1998). The tricylindrical core closest to the thylakoid membrane contains the phycobiliprotein allophycocyanin. Six rods extending from the core contain other phycobiliproteins such as phycocyanin, phycoerythrin or phycoerythrocyanin. Phycobiliproteins are arranged such that the ones that absorb at the lowest wavelength (ie phycoerythrin) are located at the ends of the rods whereas allophycocyanin, which absorbs at the highest wavelength, is located in the core next to the membrane. This arrangement allows for efficient energy transfer of absorbed light through the phycobilisome to allophycocyanin, which is then transferred to chlorophyll *a*. Energy transfer is a very efficient, nonradiative process that occurs mainly due to Förster resonance energy transfer and some exciton state coupling (MacColl, 1998).

Bilins are open-chain tetrapyrroles and are the active chromo- and fluorophores. There are four bilins (phycocyanobilin, phycoerythrobilin, phycocourobilin and phycoviolobilin) with varying degrees of conjugated double bonds that determine the range in which they absorb light. Phycourobilin has 5 conjugated double bonds and absorbs near 495 nm whereas phycocyanobilin has 8 conjugated double bonds and absorbs at wavelengths greater than 600 nm (MacColl, 1998). Bilins are covalently bonded to a polypeptide backbone between 15,000 and 20,000 Da at cysteine residues to form the phycobiliproteins (MacColl, 1998). Each phycobiliprotein monomer consists of two subunits (denoted α and β) and is defined by which bilins are attached

and the location at which they are attached. For example, phycocyanin has one phycocyanobilin attached to the α subunit at the 84th residue (α84) and two phycocyanobilins attached to the β subunit at residues 84 and 155 (denoted β84 and β155, respectively). Allophycocyanin only has one phycocyanobilin attached to each subunit (α84 and β84) and is a distinctly different phycobiliproteins (Debreczeny et al., 1993). The monomers have a distinct fluorescence signature and energy transfer between the bilins. Three monomers can aggregate to form a disc-shaped trimer, which can then stack together to form hexamers (Bryant, 1994). The formation of larger aggregates changes the fluorescence signature. In addition to the phycobiliproteins, polypeptide linkers that connect the substructure of the phycobilisome also alter the optical properties (MacColl, 1998).

B.2 IOM and CRW Excitation-Emission Matrices (EEMs)

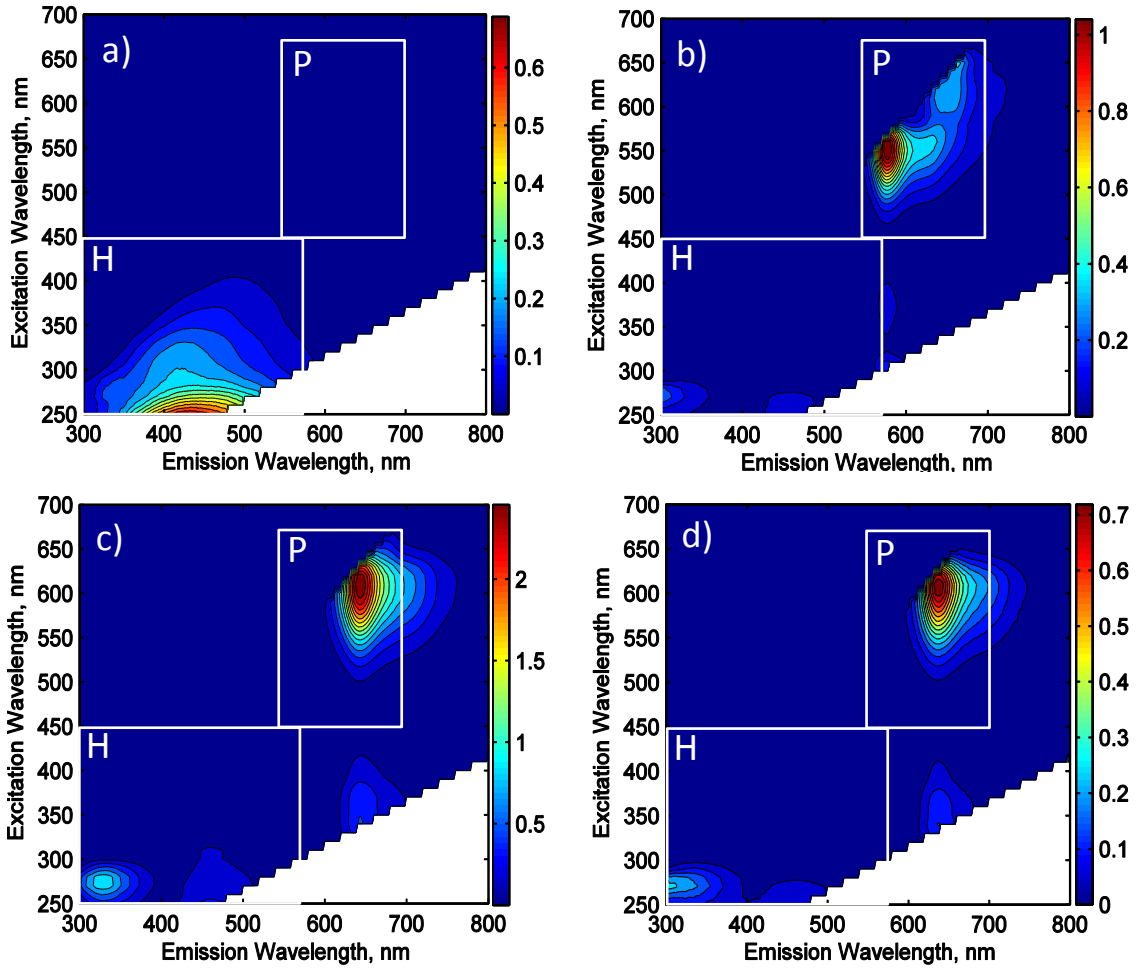

Figure B.1 Excitation-emission matrices of a) Colorado River Water, b) Oscillatoria sp., c) Microcystis aeruginosa and d) Lyngbya sp. The Humic (H) and Pigment (P) Regions are outlined in white boxes.

B.3 Pigment PARAFAC Model

B.3.1 Model Validation

PARAFAC models with up to 12 components were compared to determine the best-fit model. Ultimately, a model with 10 components was determined to be the best model based on published validation methods (Stedmon and Bro, 2008). More emphasis was placed on the residuals analysis to determine if there was systematic behavior present that is not captured in the model. The following sections present the results from the sum squared error analysis, split half analysis, random initialization and residuals analysis.

B.3.2 Sum Squared Error

The sum squared error as a function of excitation and emission wavelength was compared for models with successively higher numbers of components. Figure B.2 shows that 6 and 7 component models have systematic residuals at 570 and 590 nm emission wavelengths that are eliminated with the addition of the eighth component. The 9 component model shows some improvements over the 8 component model at emission wavelengths of 600 and 640 nm and an excitation wavelength of 610 nm. There was little difference in the error distribution between the 9 and 10 component models when plotted against the excitation wavelength. Ultimately, the residuals analysis dictated the use of the 10 component model over the 9 component model even though there was little difference in SSE.

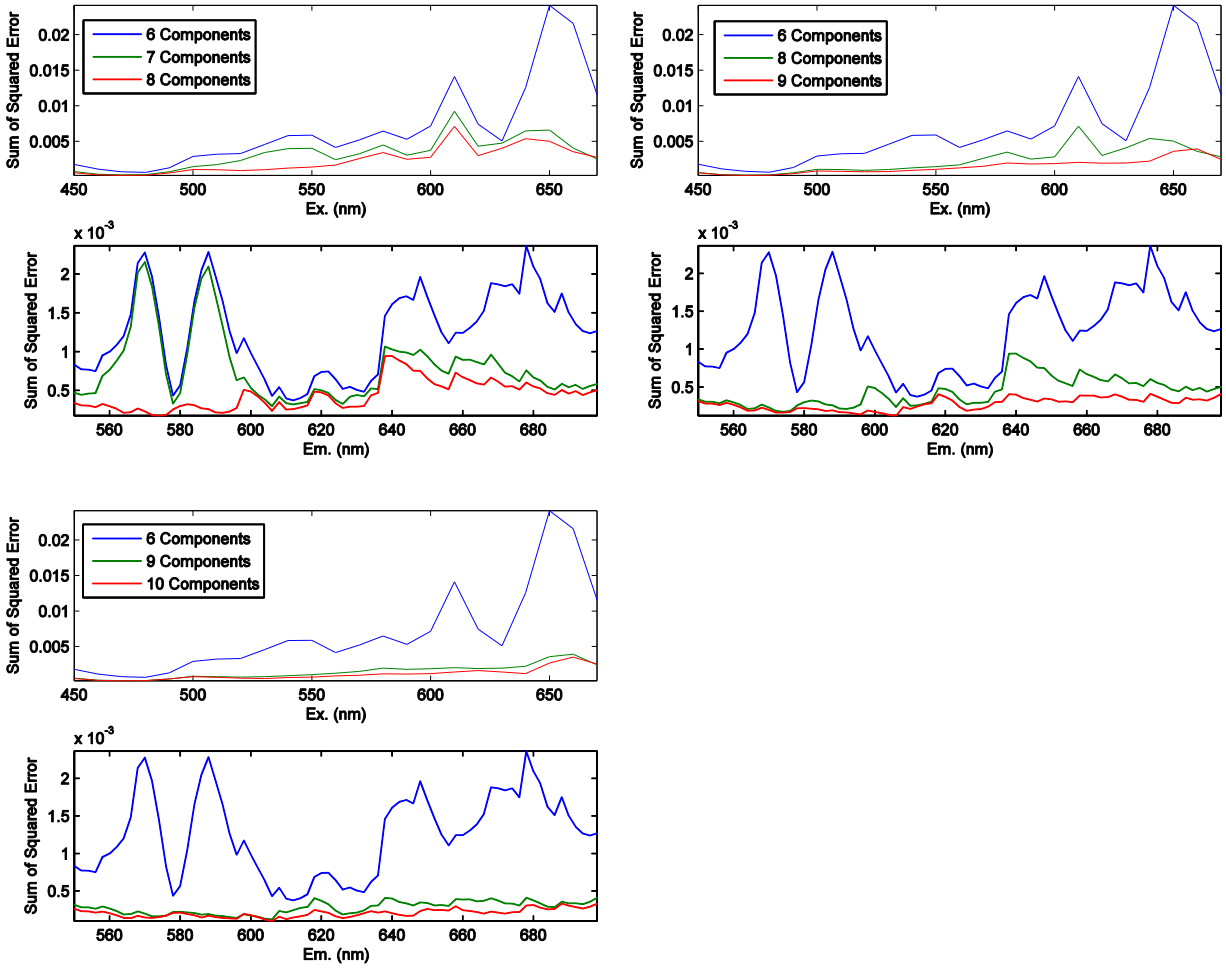

Figure B.2 Comparison of models with increasing numbers of components in terms of sum squared error as a function of excitation and emission wavelengths.

B.3.3 Random Initialization

The random initialization procedure in the DOMFluor toolbox generated the 10 component model 10 times by using random values for the initial estimates in order to ensure the fitted model represents a least squares fit and not a local minimum. Figure B.3 and Figure B.4 show good agreement between the model components and the minimum iteration identified by random initialization indicating that the model output is a true least squares fit and not a local minimum.

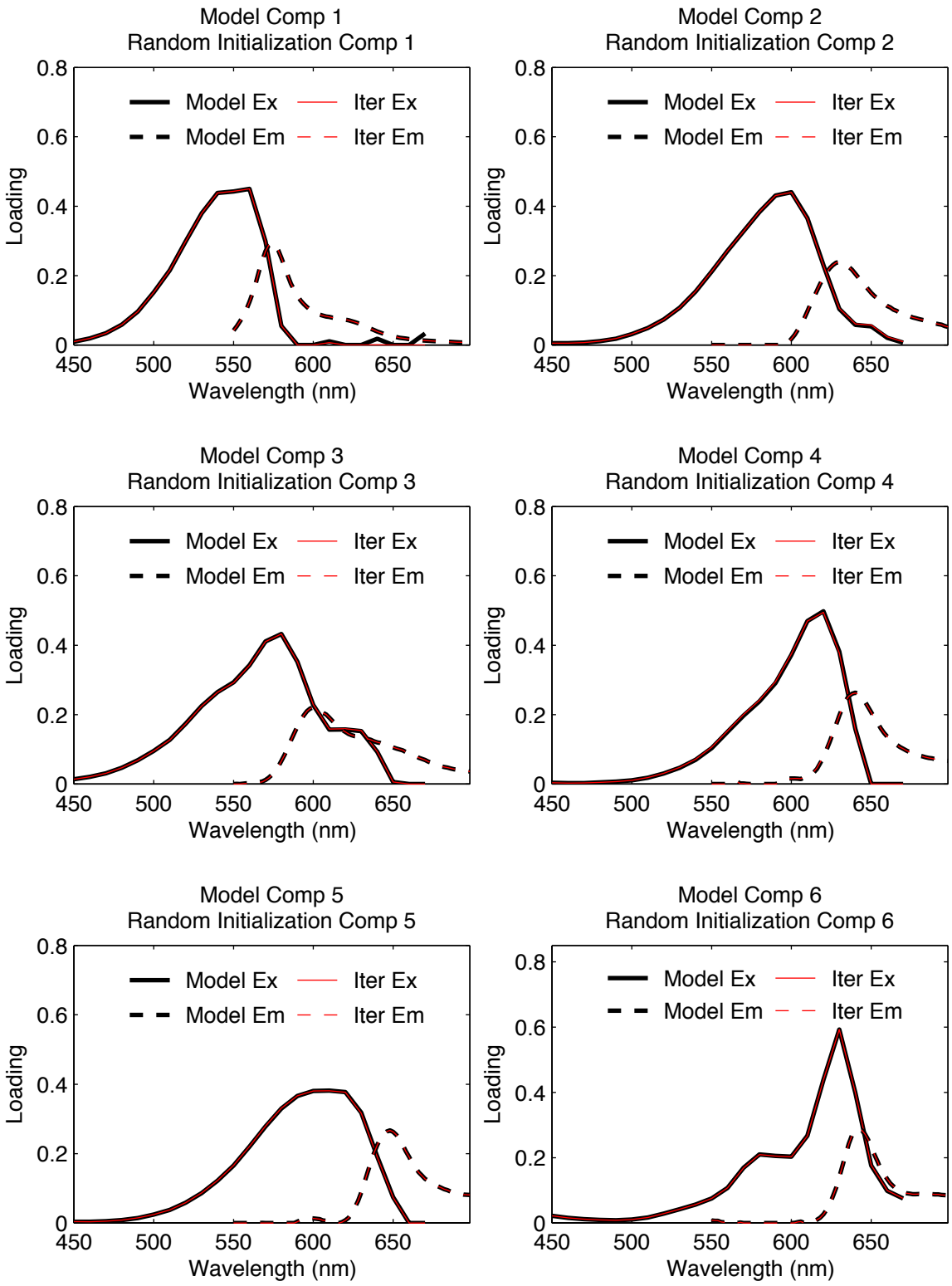

Figure B.3 Components P1 to P6 random initialization results. The excitation loadings are depicted as solid lines and the emission loadings as dashed lines for both the model (black) and minimum iteration (red).

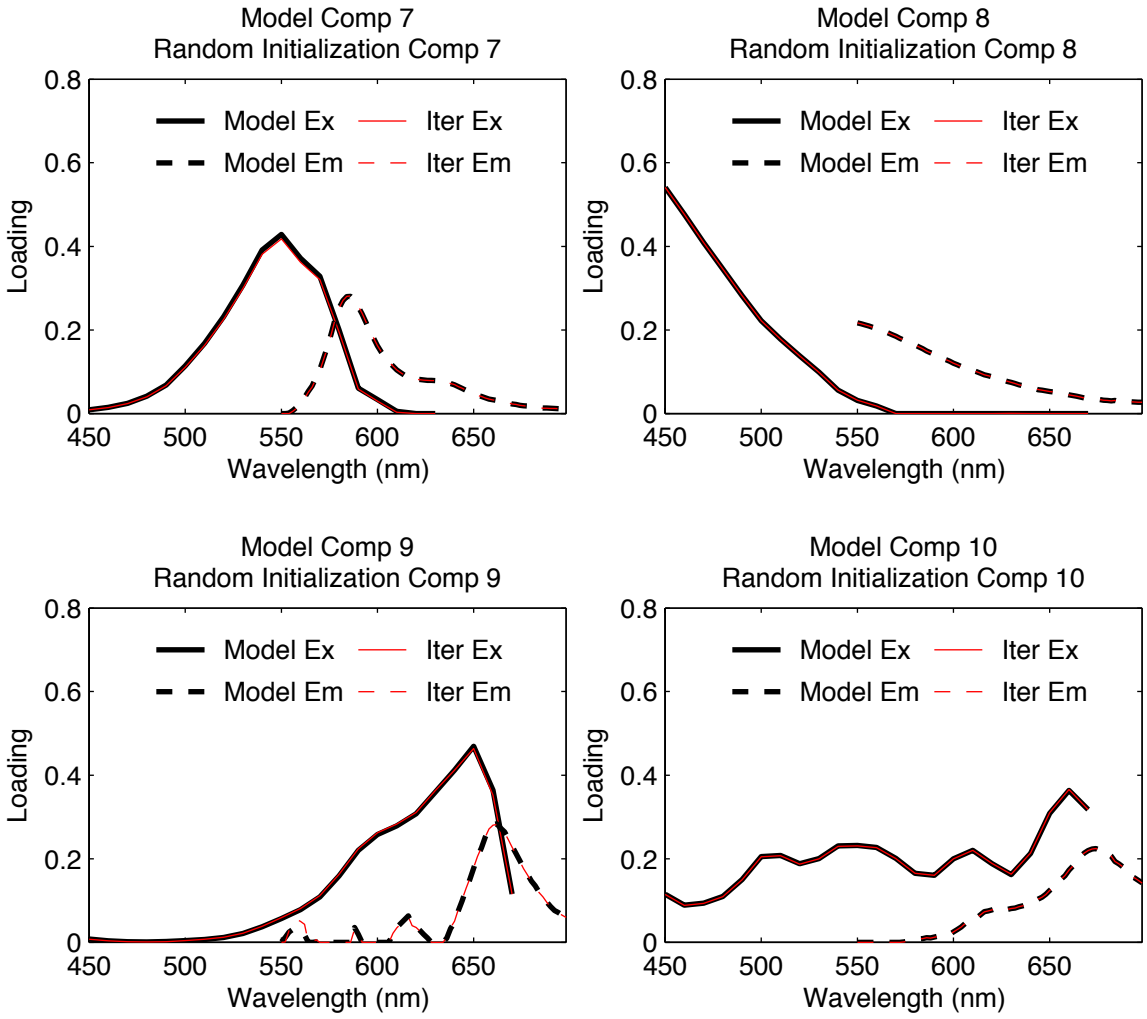

Figure B.4 Components 7 to 10 random initialization results. The excitation loading are depicted as solid lines and the emission loadings as dashed lines for both the model (black) and minimum iteration (red).

B.3.4 Residuals Analysis

Model adequacy was also evaluated by analyzing the model residuals to look for systematic trends. Figure B.5 shows that the 10 component PARAFAC pigment model adequately models the three IOM samples and CRW with residuals more than an order of magnitude smaller than the measured EEM. The residuals for LYG do show some systematic behavior but the magnitude is small compared to the measured intensity and deemed acceptable. Figure B.6 shows the effect of adding additional components to the systematic residuals at 670 nm emission. Adding the 10^{th} component reduces the magnitude of the residuals, although not entirely, and justifies the higher component model.

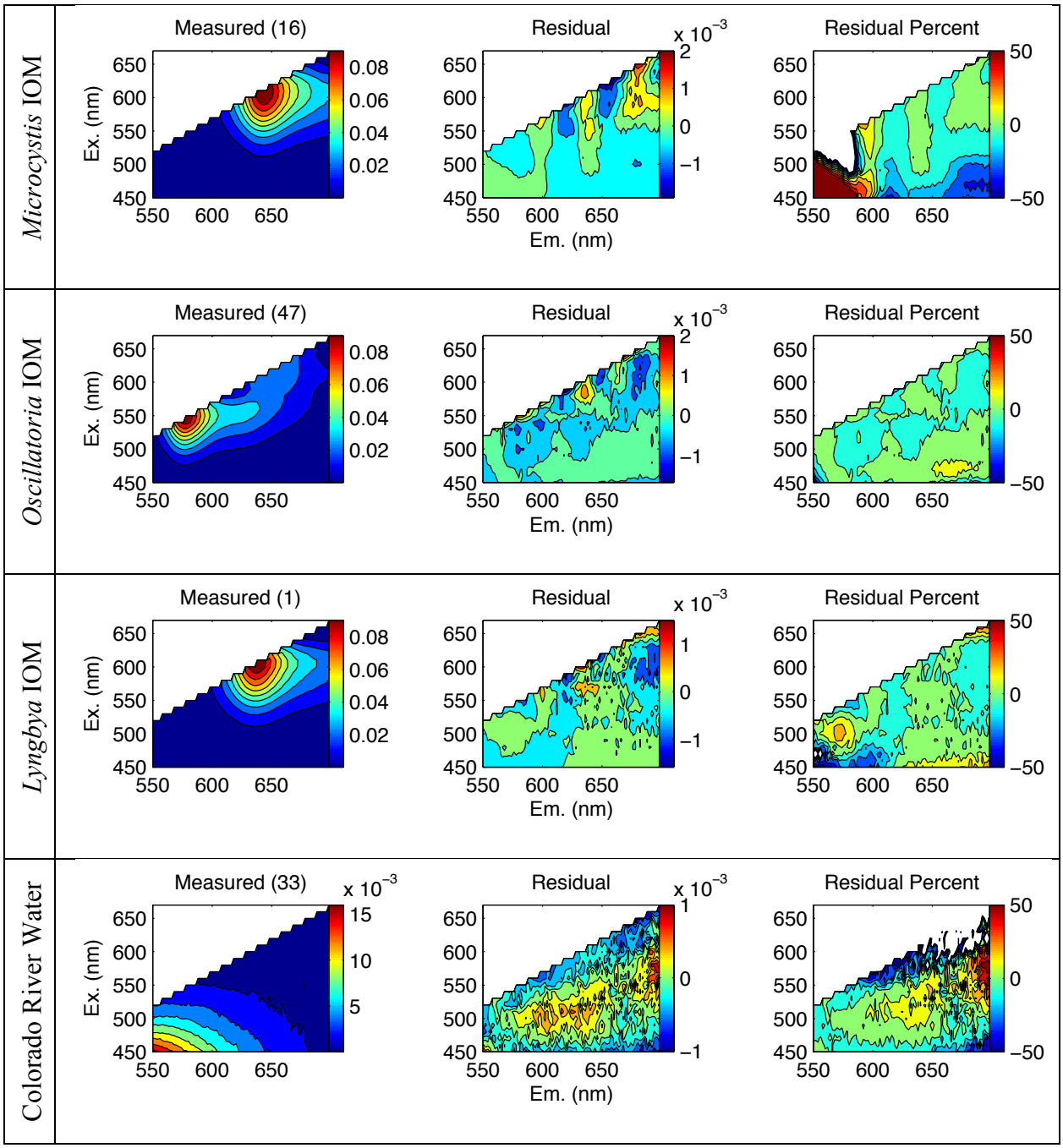

Figure B.5. Pigment model residuals for Microcystis IOM, Oscillatoria IOM, Lyngbya IOM and CRW. The frames show the measured EEM, the residual in RU and the residuals on a percent basis relative to the measured intensity.

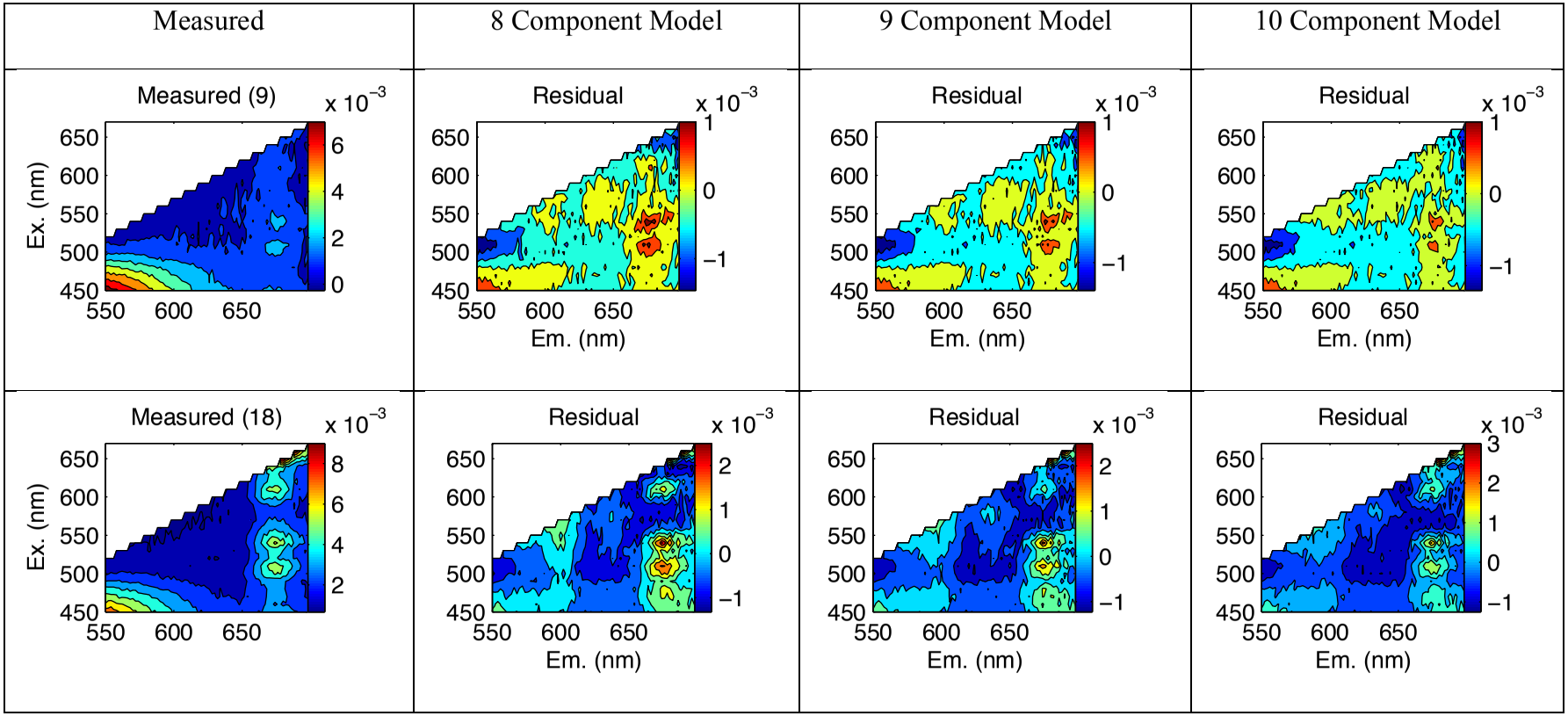

Figure B.6. Reduction of systematic residuals 670 nm emission with additional components for 8, 9 and 10 component models.

Figure B.7 shows example residuals where there is evidence of systemic behavior in the 10 component model. The magnitude of all except the first one are an order of magnitude less than the measured intensity and the overall model was determined to be acceptable. The occurrence of these residuals was analyzed to determine if there is a subset of samples that the model cannot consistently capture.

The residuals depicted in Figure B.7a show systematic residuals at an emission of 670 nm, which corresponds to component 10. Component 10 has multiple excitation wavelengths with the dominant absorbing chromophore at 660 nm, as indicated by a higher component loading. The residual plots indicate that the model is attempting to match the fluorescence at an absorbance of 660 nm but there is a positive residual at the other excitation local maxima. This trend indicates that the relative excitation loading maxima for this sample is different in this sample compared to the model output. This systematic behavior occurred in two samples: MA IOM from the 3/2012 batch and MA IOM exposed to 1 mg/L ClO_2 from the 3/2012 batch. The isolation of the behavior to the first MA batch suggests that there could have been slight differences in the phycobiliprotein composition.

The residual depicted in Figure B.7b occurs at an excitation of 500 nm and emission of 664 nm. These residuals only occurred in the three samples where MA IOM was spiked into CRW from the 04/2012 batch. It is unlikely that this fluorescence is due to pigments unaccounted for in the PARAFAC model. An absorbance maxima of 500 nm is characteristic of the bilin phycourobilin, but this chromophore is associated with phycoerythrin-containing cyanobacteria, which *Microcystis* is not (Bryant, 1982; Stadnichuk et al., 1985). An emission of 664 nm is characteristic of allophycocyanin. Even if *Microcystis* did have phycourobilin-containing phycoerythrin, it is highly unlikely that the entire phycobilisome would be intact after

isolation for direct energy transfer from phycoerythrin to allophycocyanin, because the ionic strength of the buffer is too low (Glazer, 1977). This residual is most likely indicative of an additional interaction between the DOM in CRW that was not abundant enough to warrant a new component.

The residuals depicted in Figure B.7c occurred at an excitation of 510 nm and an emission of 582 nm. The occurrence of this unaccounted for fluorescence is limited to the oxidation of Lyngbya IOM with chloramines. The intensity of this residual is constant around 0.002 RU across all chloramine doses. This systematic residual may be indicative of a fluorescent oxidation product.

Finally, there was a systematic residual at an excitation of 450 nm and emission of 682 nm on the edge of the EEM range shown in Figure B.7d. Based on the contours, the maximum likely occurs at an excitation less than 450 nm. This residual may be associated with small amounts of chlorophyll *a*. In vivo fluorescence typically measures the chlorophyll a signature at excitation 430 nm and emission 682 nm (Watras and Baker, 1988). This residual was only seen in the samples where *Microcysits* IOM (April 2012 batch) was spiked into CRW with the residual intensity increasing from 0.002 RU at 0.5 ppm IOM up to 0.007 RU at 2 ppm IOM. This suggests that there may be low concentrations of chlorophyll *a* in the isolated IOM. Chlorophyll is not expected to be a dominant pigment in the isolated IOM and resulting PARAFAC model because it is not soluble in water and is usually extracted in an organic solvent.

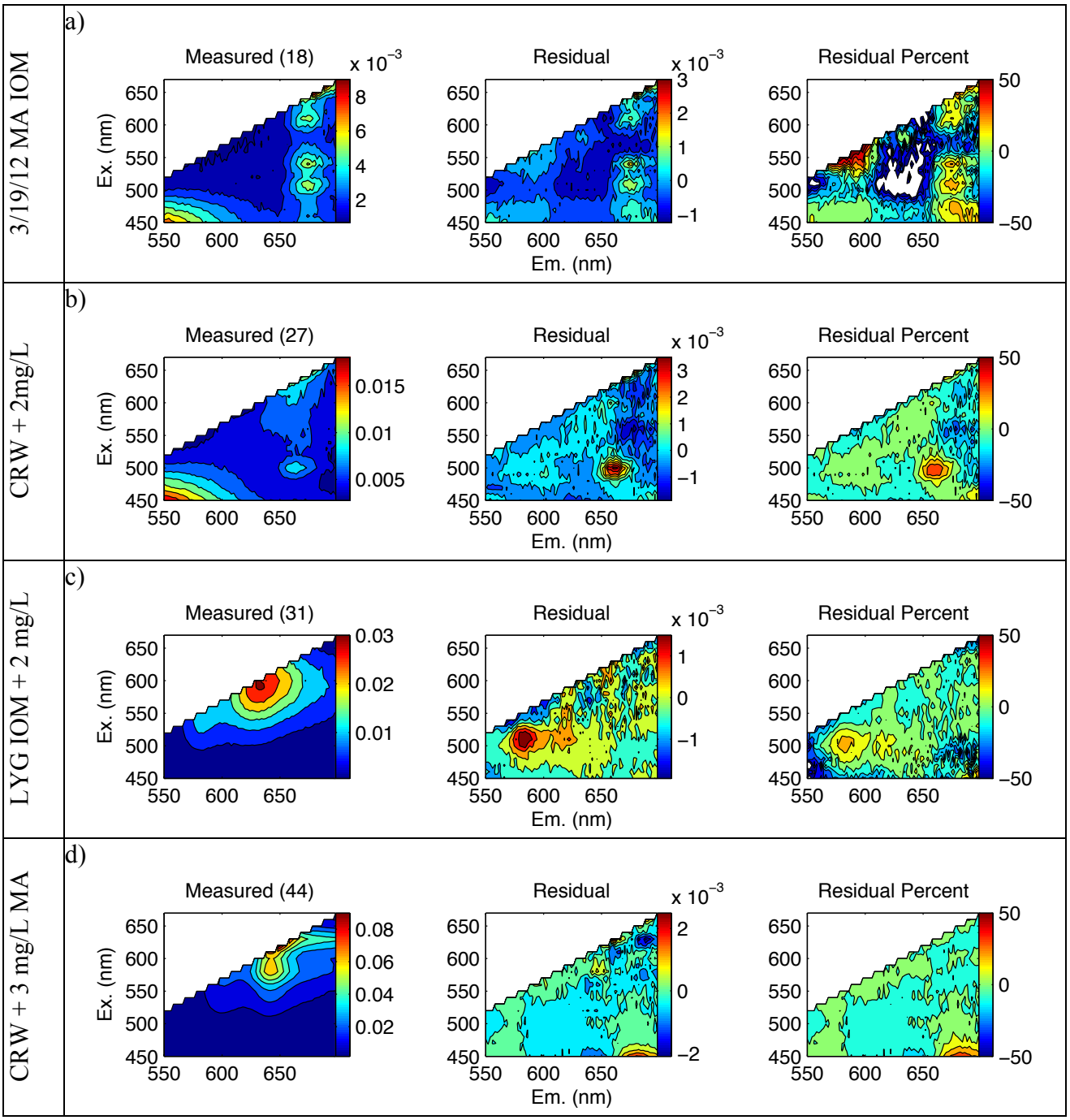

Figure B.7. Select pigment model residuals that show systematic behavior. The frames show the measured EEM, the residual in RU and the residuals on a percent basis relative to the measured intensity.

B.3.5 Split Half Analysis

No component model was able to be validated using split half analysis. Successful validation by this method requires there to be a well distributed dataset before it is split into the fractions and modeled. This data set is affected by both the distribution of EEMs and number. Only one of the cyanobacteria species, *Oscillatoria*, contains phycoerythrin, which is responsible for the lower wavelength signals. *Oscillatoria* only accounted for 20% of the total EEMs in the model. Of that 20%, a number of them were oxidized samples where the signal is readily destroyed, leaving the fraction of samples with this signal to be much smaller. These effects are illustrated in Figure B.8 as each split has a different distribution of fluorescence signals.

Validation by split half analysis can also be hindered if the data set is too small (Murphy et al., 2013). The total model has 78 EEMs, and a split model including half the EEMs only has 39 EEMs. Of those 39 EEMs, roughly half have low signals because ozone, free chlorine and chlorine dioxide react with the pigments to eliminate nearly all their fluorescent signal. When all this is taken into consideration, split half analysis has so few EEMs with strong signals and it is heavily swayed by the uneven distribution of phycoerythrin containing compounds. Even with so few EEMs, Figure B.9 shows that split half analysis generates models for each split that show similarities between components but the model with more phycoerythrin-containing EEMs identifies a component in this region whereas the other split does not. Therefore, validation relied more on analyzing residuals and random initialization, which rely on models built with all EEMs.

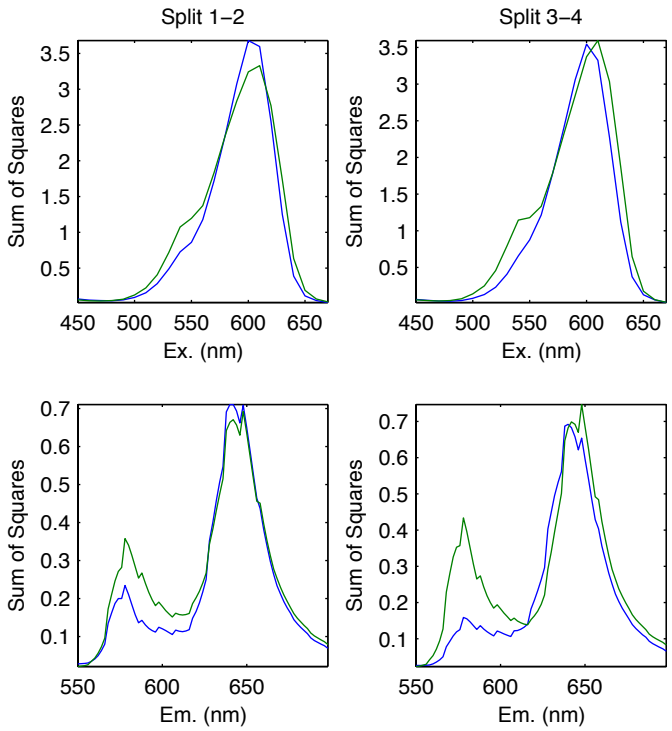

Figure B.8. Sum of squares for each split used in the split half analysis.

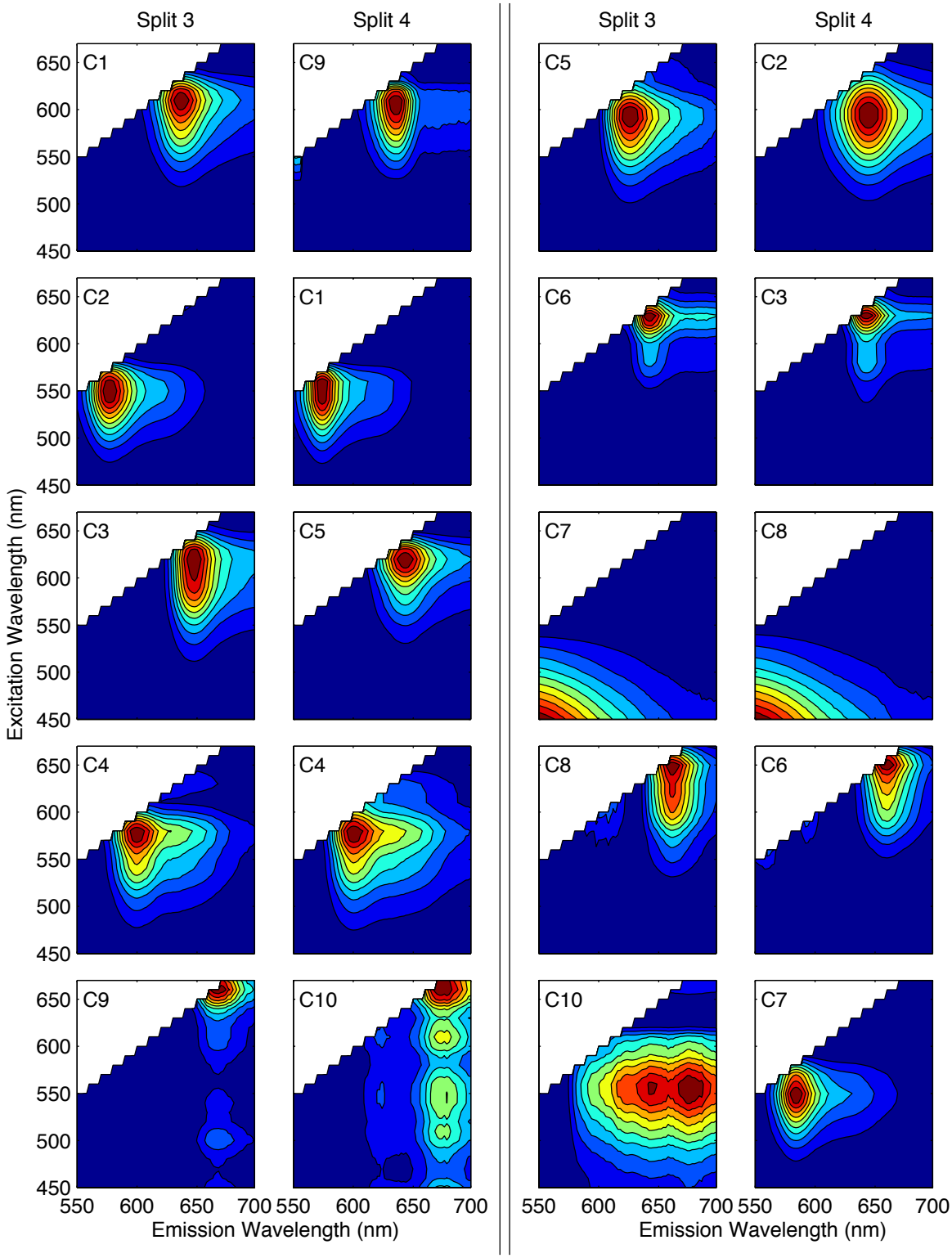

Figure B.9. Comparison of the model components from split half analysis validation methods. Components from each half that show good agreement with each other are shown side-by-side, except for Component 10 in Split 3 and Component 7 in Split 4.

B.4 Literature Data to Support Suggested Component Assignment

Suggested phycobiliproteins were assigned to each PARAFAC component based on values reported in literature. Table B.1 details the results found in other studies to support the assignment of possible proteins for the model.

Table B.1. Compilation of literature values to support the suggested pigment for each PARAFAC component.

Comp	Phycobiliprotein	(Ex, Em)	Reference	Notes
P1	Phycoerythrin	(560, 577)	Bryant, 1982	
P2	β-155 chromophore of phycocyanin	(596, 625)	Demidov and Mimuro, 1995	B-155 fluorophore by differential methods
		(600, 630)	Debreczeny et al., 1993	B-155 fluorophore by modeling approaches
P3	Phycocyanin + DOM			Abs spectra matches PEC but fluorescence. 20nm blue-shifted
P4	C-Phycocyanin (trimer)	(616, 642)	Bryant, 1994	$(\alpha^{PC}\beta^{PC})_3$
		(617.4, 644)	Bryant, 1994	$(\alpha^{PC}\beta^{PC})_3$
P5	C-Phycocyanin (monomer)	(616, 644)	Debreczeny 1993	Broad absorption maxima
P6	C-Phycocyanin + polypeptide linker	(632.4, 645)	Bryant, 1994	$(\alpha^{PC}\beta^{PC})L_{RC}^{29.5}$
P7	Phycoerythrin		MacColl, 1998	PE absorbs 545-565nm
		(545, 580)	Rigbi, 1980	
P8	DOM			
P9	Allophycocyanin (trimer)	(651, 660-662)	Bryant, 1994	$(\alpha^{APC}\beta^{APC})_3$ form
P10	Allophycocyanin (B)	(654nm, 679nm)	Bryant, 1994	545, 580nm absorb, 676nm emit
	Allophycocyanin (B)	(654, 670)	Bryant, 1994	for $\beta^{16.5}$ subunit
	Allophycocyanin (B)	Abs: 619, 669. Fluor: 673	Bryant, 1994	
	Intact phycobilisome	Abs: 545, 580 Fluor 676	Rigbi, 1980	

B.5 IOM Pigment Fluorescence Interactions with DOM

The following graphs present the full dataset related to pigment fluorescence in the presence of DOM. For each IOM, a series of EEMs is presented showing the change in fluorescence at increasing IOM concentrations compared to the samples before mixing in lab-grade water (LGW) (Figure B.11, B.14 and B.16). The changes in the PARAFAC components are also presented on a percent contribution basis (Figure B.10, Figure B.13 and Figure B.15) demonstrating that the components that account for the fluorescence in the isolated sample are not found at the same relative amount after mixing. Additionally, Figure B.12 shows how the PARAFAC component change for a series of MA IOM isolates in phosphate buffer at increasing concentrations to show that the interaction effects are not due to self-quenching. Lastly, Figures B.17 and B.18 show series of EEMs for the phycocyanin and phycoerythrin standards spiked into CRW and demonstrate that no shifts or quenching of fluorescence was observed with the purchased standards.

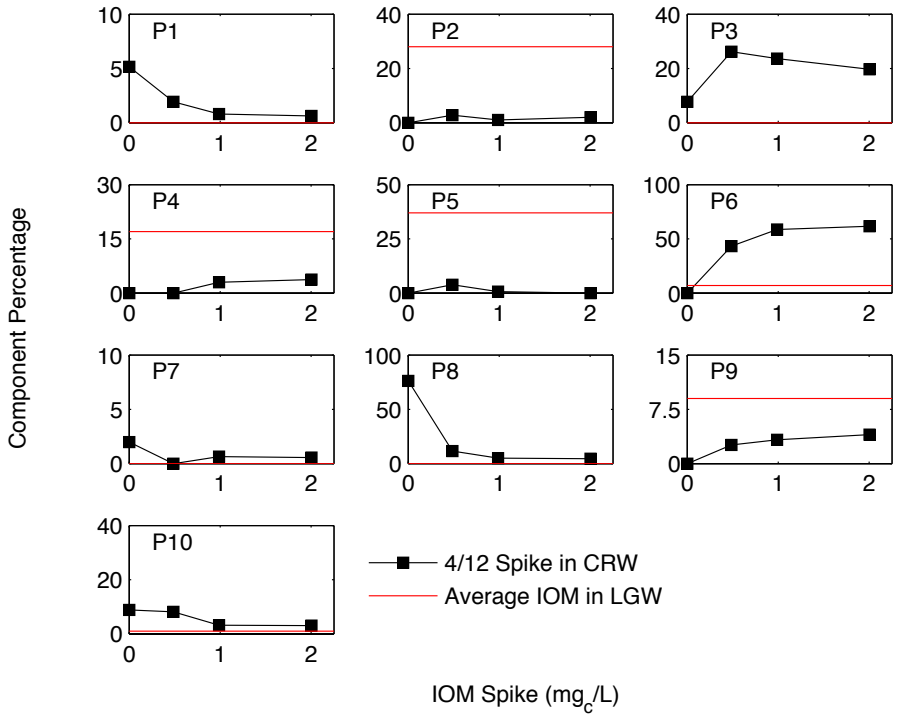

Figure B.10. Change in Pigment Region PARAFAC components when MA IOM is spiked into CRW. Data is presented on as a percent contribution of the overall fluorescence. The red line indicates the percent contribution measured in the isolated IOM.

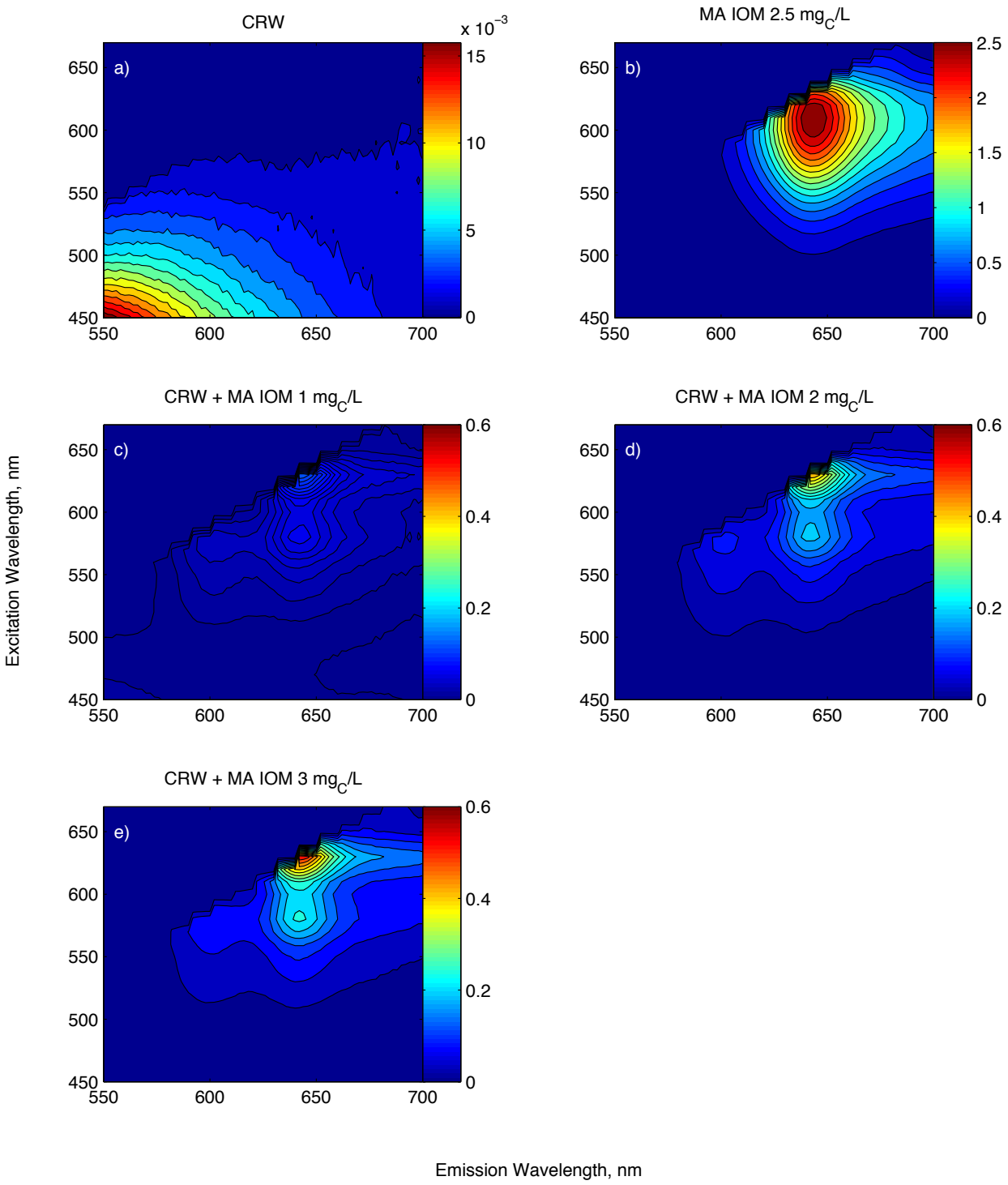

Figure B.11. EEMs for a) Microcystis IOM at 2.5 mg_c/L in LGW, b) Colorado River Water, and c-e) Microcystis IOM spiked into CRW at increasing concentrations.

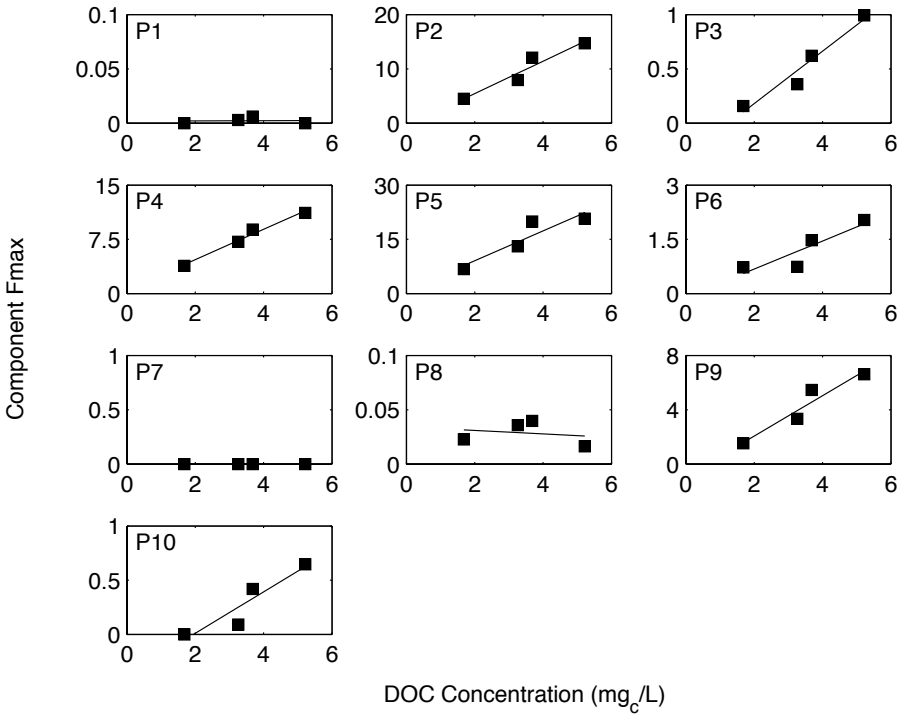

Figure B.12. Pigment Component Fmax values for MA IOM in increasing concentration diluted in 10 mM phosphate buffer.

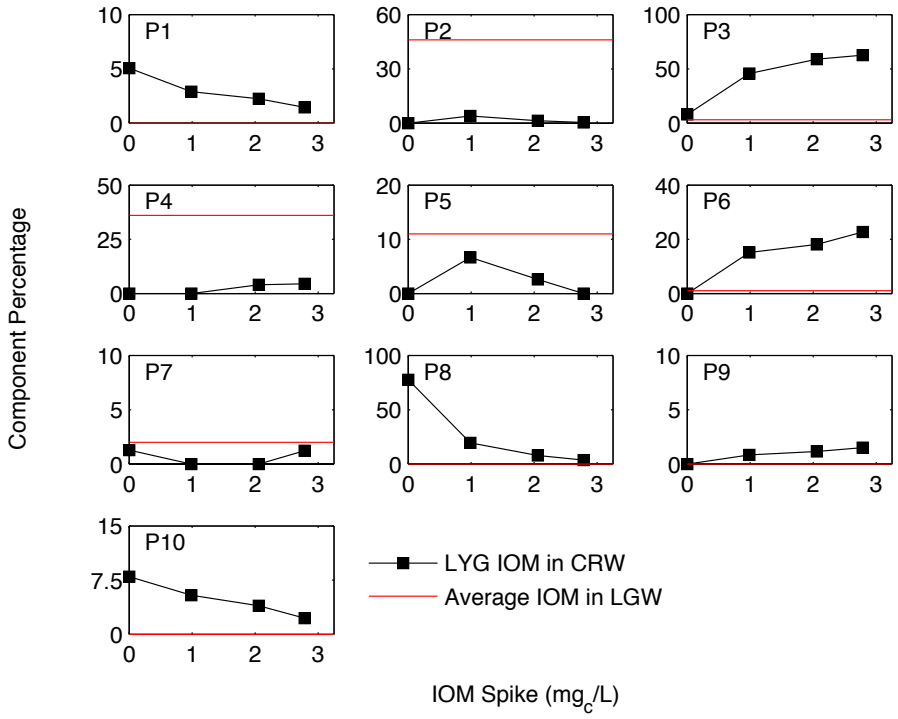

Figure B.13. Change in Pigment Region PARAFAC components when LYG IOM is spiked into CRW. Data is presented on as a percent contribution of the overall fluorescence. The red line indicates the percent contribution measured in the isolated IOM.

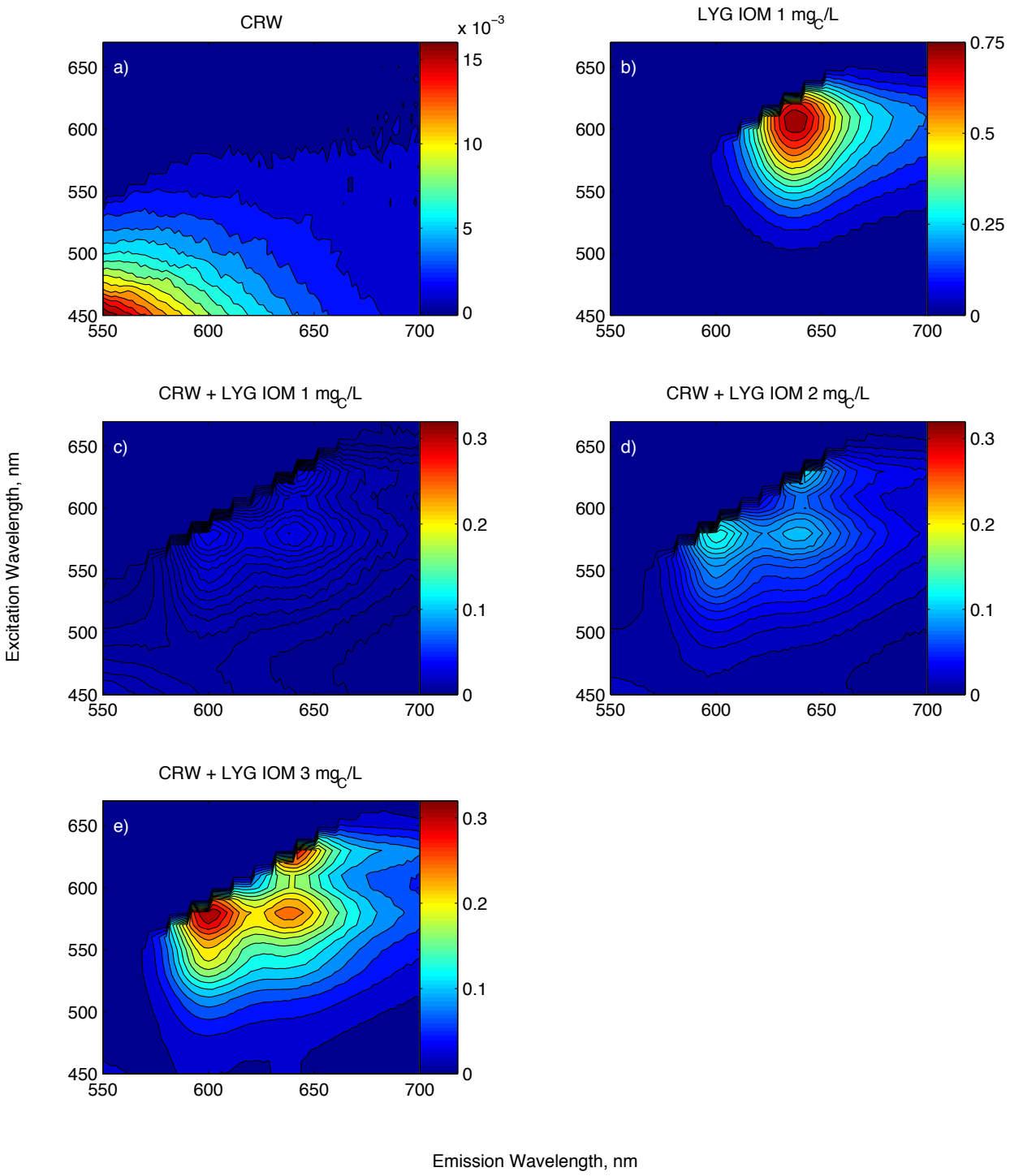

Figure B.14. EEMs for a) Lyngbya IOM at 1 mg_C/L in LGW, b) Colorado River Water, and c-e) Lyngbya IOM spiked into CRW at increasing concentrations.

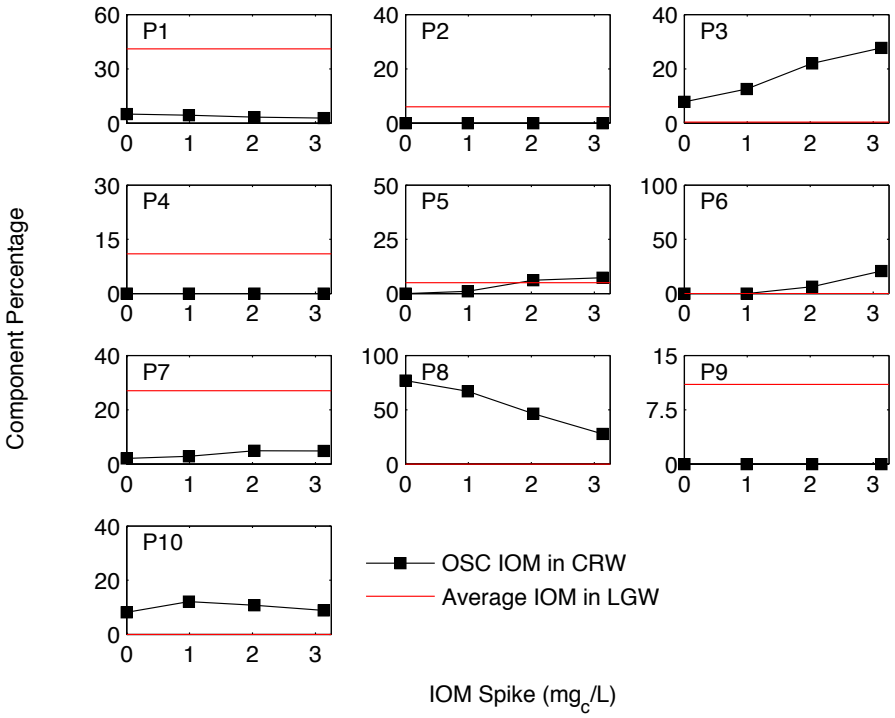

Figure B.15. Change in Pigment Region PARAFAC components when OSC IOM is spiked into CRW. Data is presented on as a percent contribution of the overall fluorescence. The red line indicates the percent contribution measured in the isolated IOM.

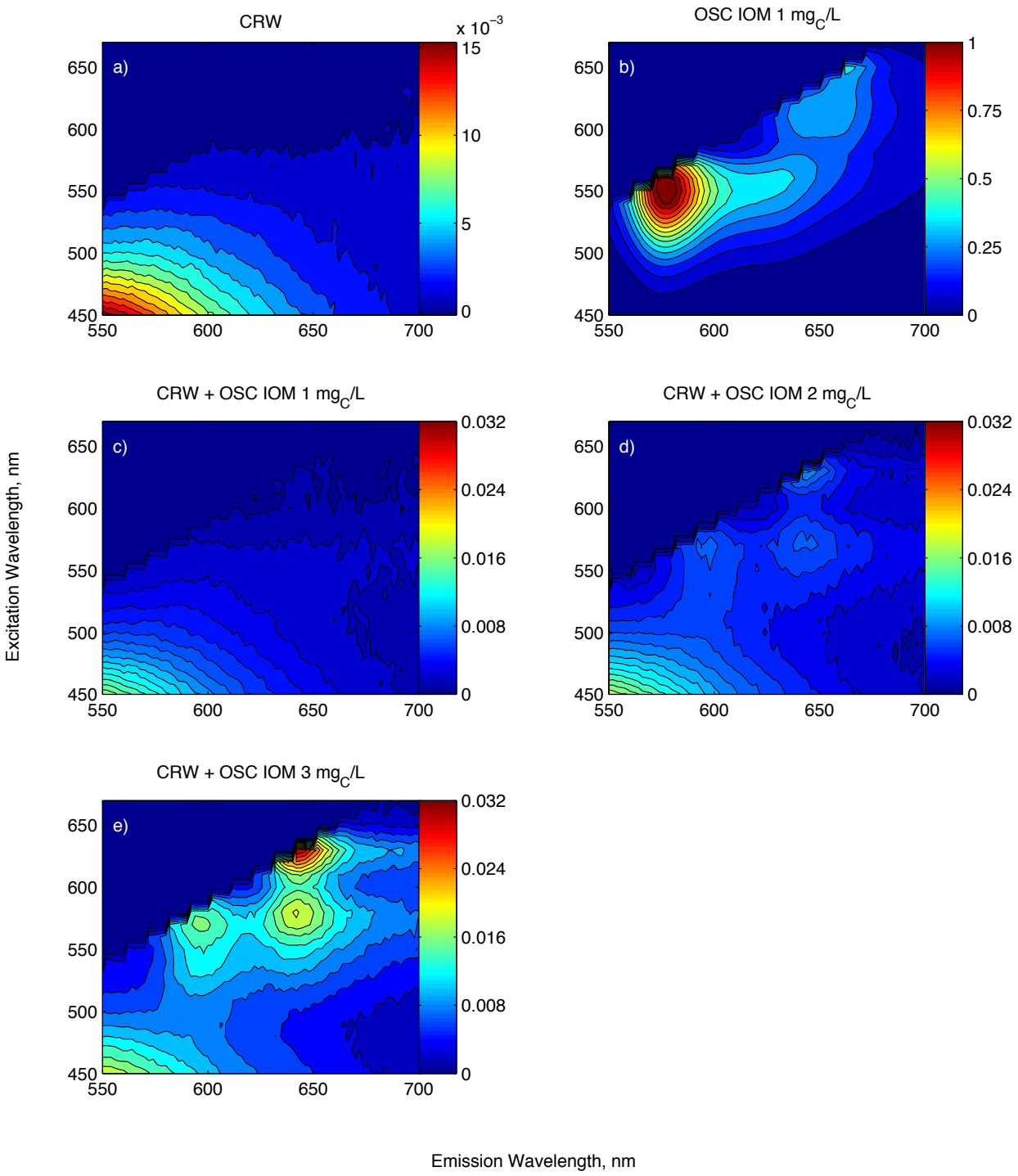

Figure B.16. EEMs for a) Oscillatoria IOM at 1 mg_C/L in LGW, b) Colorado River Water, and c-e) Oscillatoria IOM spiked into CRW at increasing concentrations.

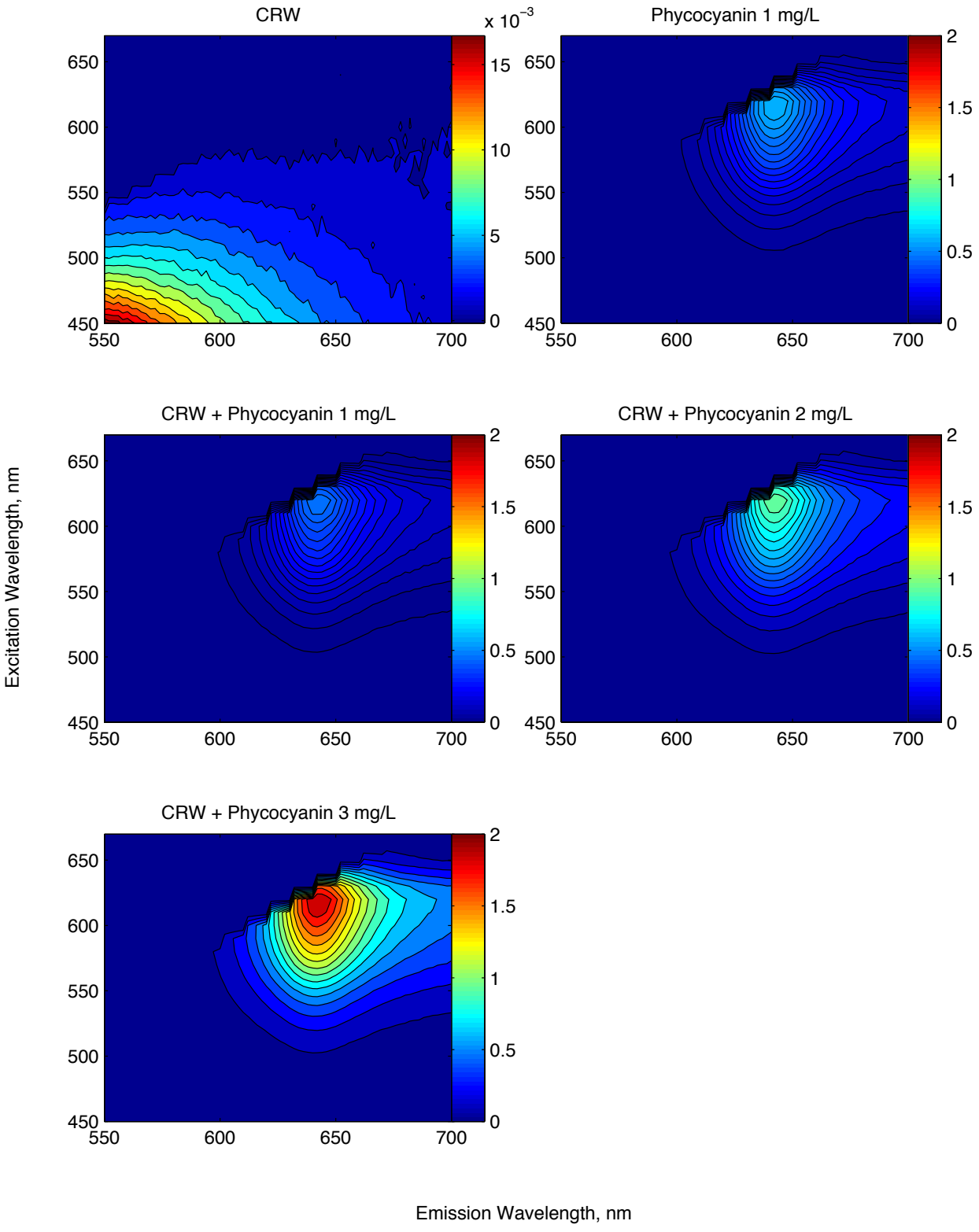

Figure B.17. EEMs of CRW, phycocyanin standards in phosphate buffer and phycocyanin spiked into CRW in increasing concentrations.

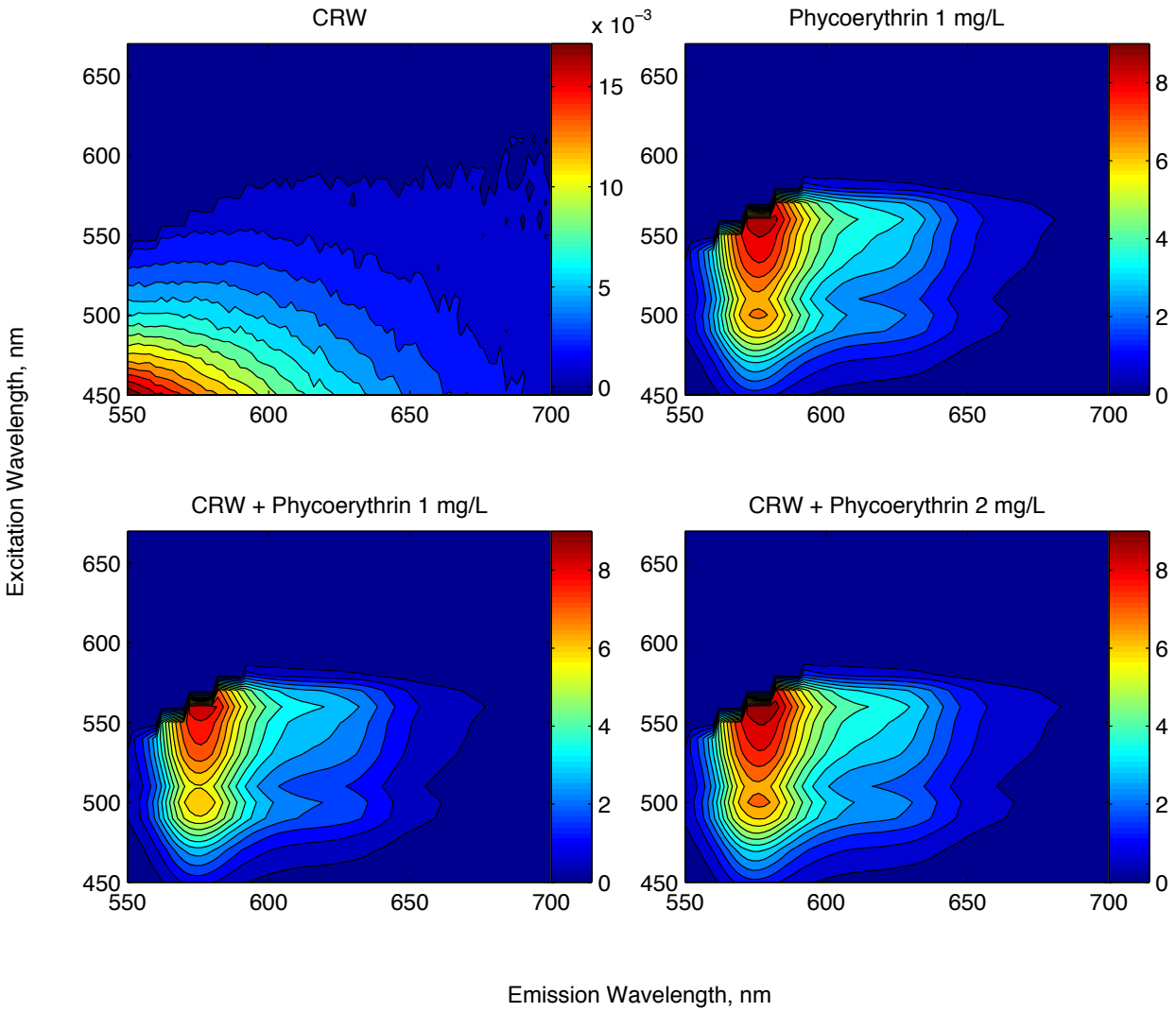

Figure B.18. EEMs of CRW, phycoerythrin standards in phosphate buffer and phycoerythrin spiked into CRW in increasing concentrations.

B.6 Oxidation Results

B.6.1 Humic Region

This section presents the supplementary data from the batch oxidation studies. Figure B.19 follows the Peak P intensity and shows that ozone, chlorine dioxide and free chlorine all lead to a decrease in intensity for MA, LYG and OSC. Chloramines led to a decrease in MA intensity but did not have much effect on LYG or OSC in intensity. These differences indicate that there are compositional differences between species that affect the relative reactivities to chloramines. Peak P would also be a poor fluorescence surrogate for preoxidation with ozone, chlorine dioxide and free chlorine, because the intensity will continue to decrease with continued exposure in the bulk phase.

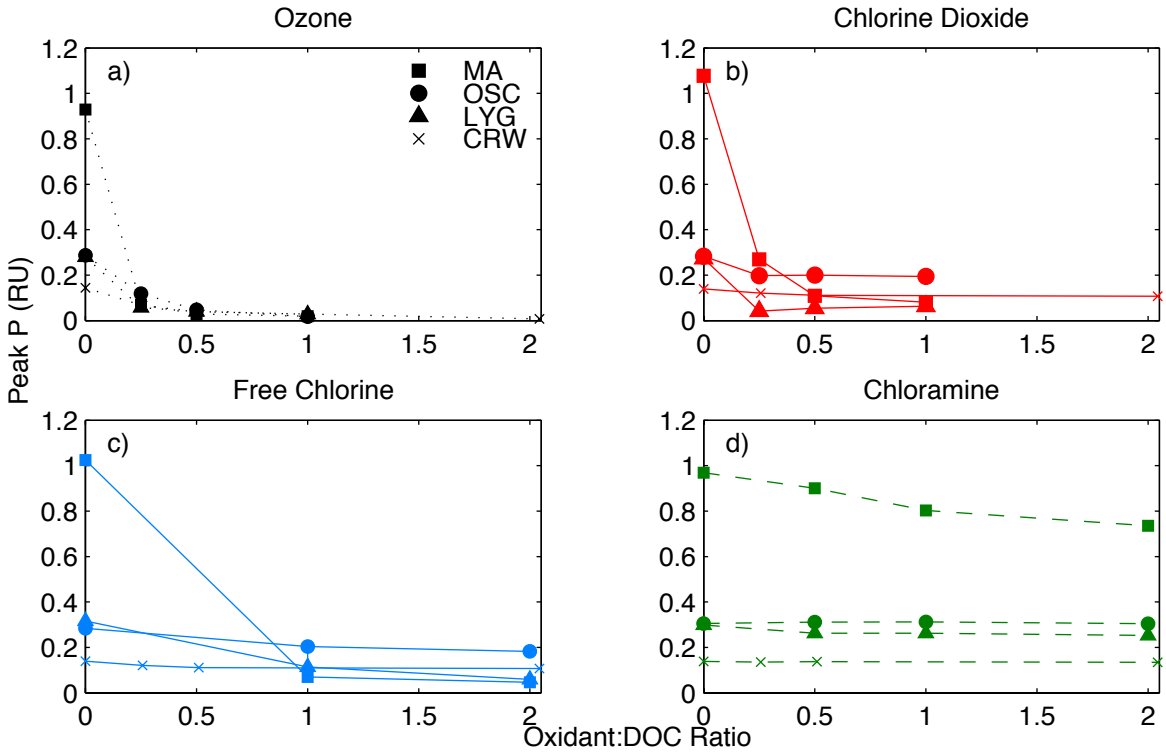

Figure B.19. Peak P oxidation as a function of oxidant:DOC ratio for a) Ozone, b) Chlorine Dioxide, c) Free Chlorine and d) Chloramine.

B.6.2 Pigment Region

Figure B.20 and Table B.2 summarize the oxidation responses of the phycocyanin standard and phycoerythrin standards in lab grade water. Ozone, chlorine dioxide and free chlorine oxidation caused a severe loss of fluorescence intensity. About 50% of the phycocyanin intensity was destroyed at the highest chloramine dose measured. Phycoerythrin fluorescence was only evaluated at an oxidant:dose ratio of 1. Ozone and chlorine dioxide oxidation led to almost a complete loss in fluorescence at this dose ratio. Free chlorine decreased the intensity by about 75% and chloramines had almost no effect on phycoerythrin fluorescence.

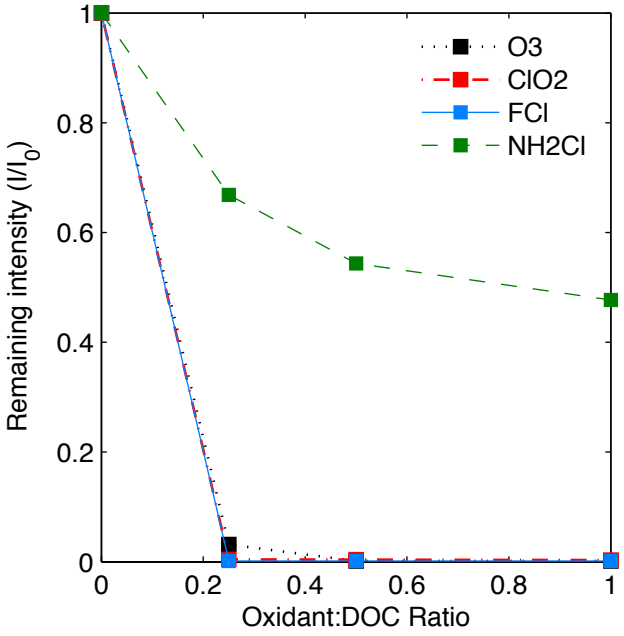

Figure B.20. Fraction of phycocyanin fluorescence intensity remaining as a function of oxidant to DOC ratio for ozone, chlorine dioxide, free chlorine and chloramine.

Table B.2. Phycoerythrin standard intensity after oxidation by ozone, free chlorine, chlorine dioxide and chloramine represented by the measured intensity and intensity relative to the control.

Oxidant	Oxidant:DOC Ratio	Max Intensity (RU)	Remaining Fluorescence (%)
Control	0	9.05	100%
Ozone	1	0.00	0.04%
Free Chlorine	1	2.14	24%
Chlorine Dioxide	1	0.22	2.4%
Chloramine	1	8.97	99%

Figure B.21 to B.28 present the complete Pigment Model PARAFAC results for the oxidation studies. PARAFAC results are presented as Fmax factors, relative change in Fmax from the isolated IOM and as a percentage of total fluorescence. Species in which the IOM did not contain a component are not included. For example, P1 and P7 only present the OSC results because phycoerythrin was not measured in the other two species. P3 is not included because this component was not found in any of the isolated IOM or oxidized samples.

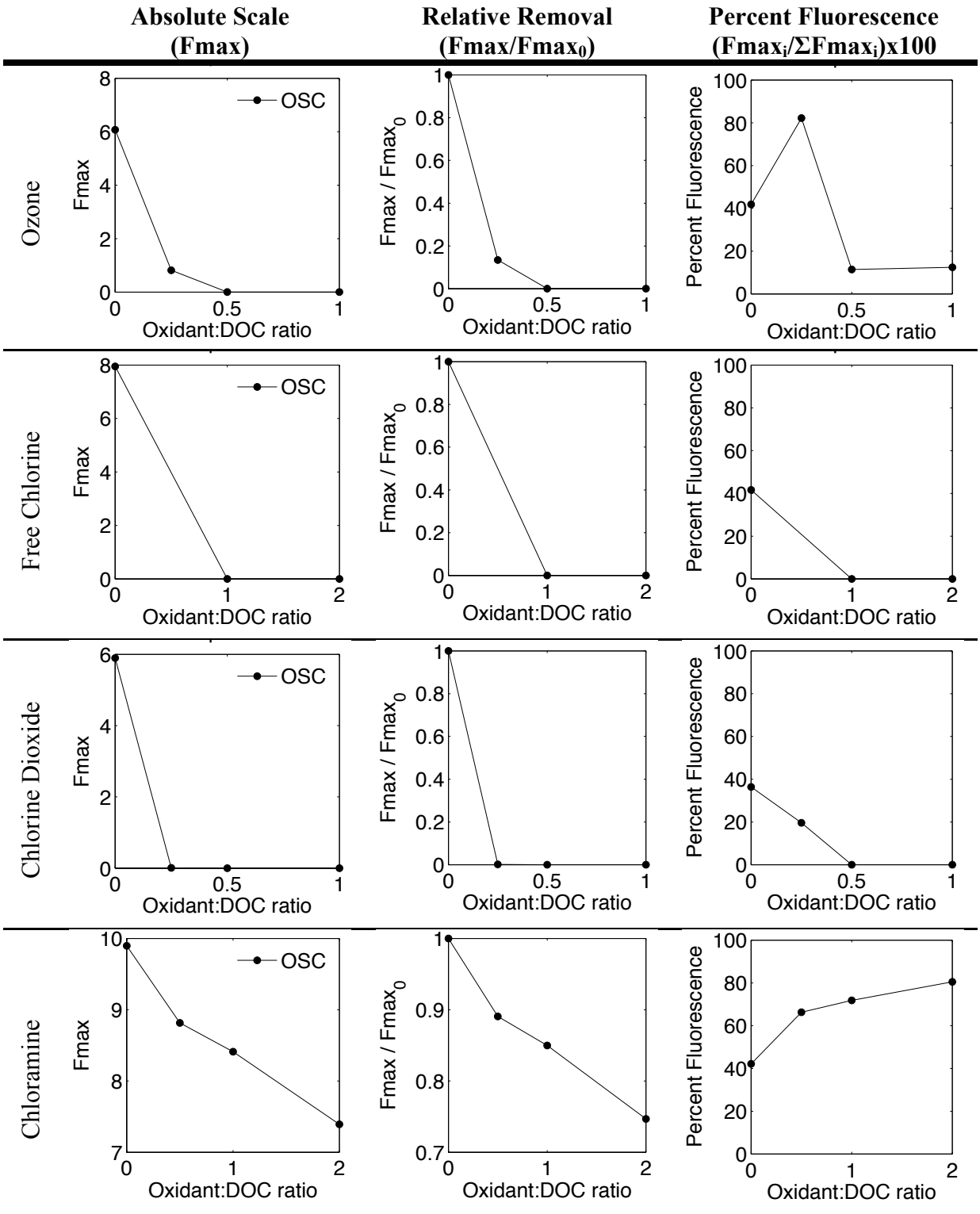

Figure B.21. Component P1 as a function of oxidant dose for all four oxidants evaluated. Data presented on an absolute scale, relative to the initial component Fmax and relative to the sum of all components.

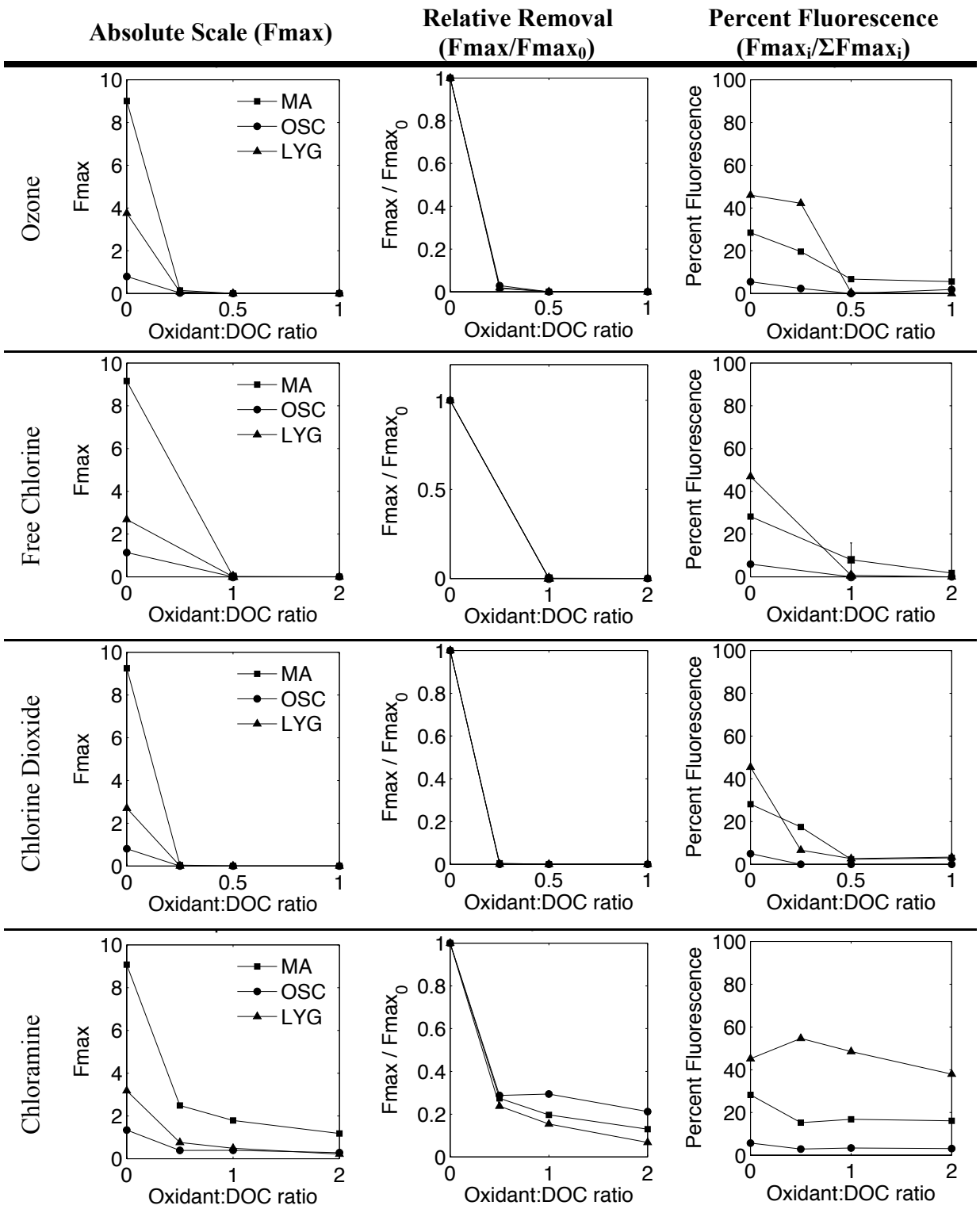

Figure B.22. Component P2 as a function of oxidant dose for all four oxidants evaluated. Data presented on an absolute scale, relative to the initial component Fmax and relative to the sum of all components.

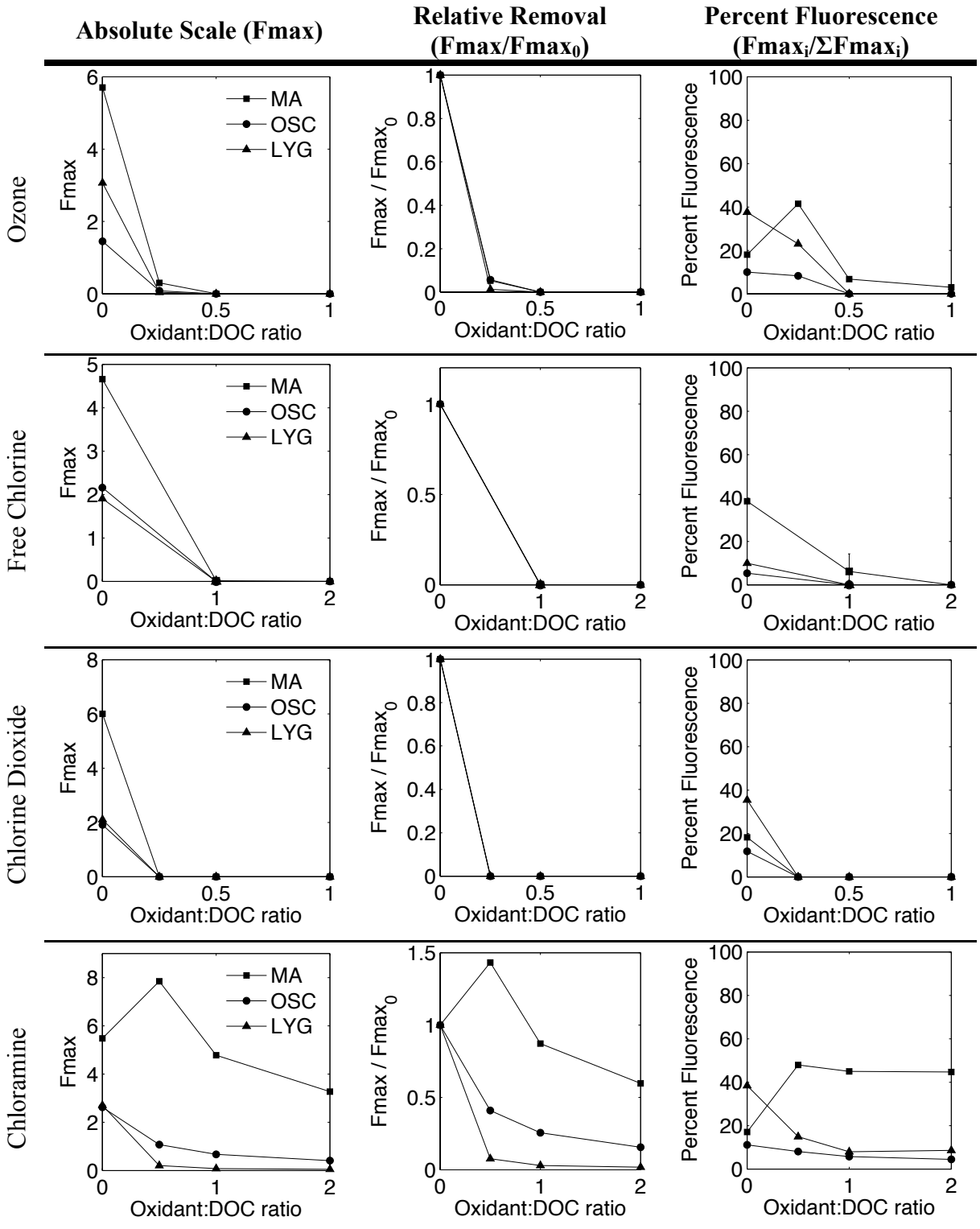

Figure B.23. Component P4 as a function of oxidant dose for all four oxidants evaluated. Data presented on an absolute scale, relative to the initial component Fmax and relative to the sum of all components.

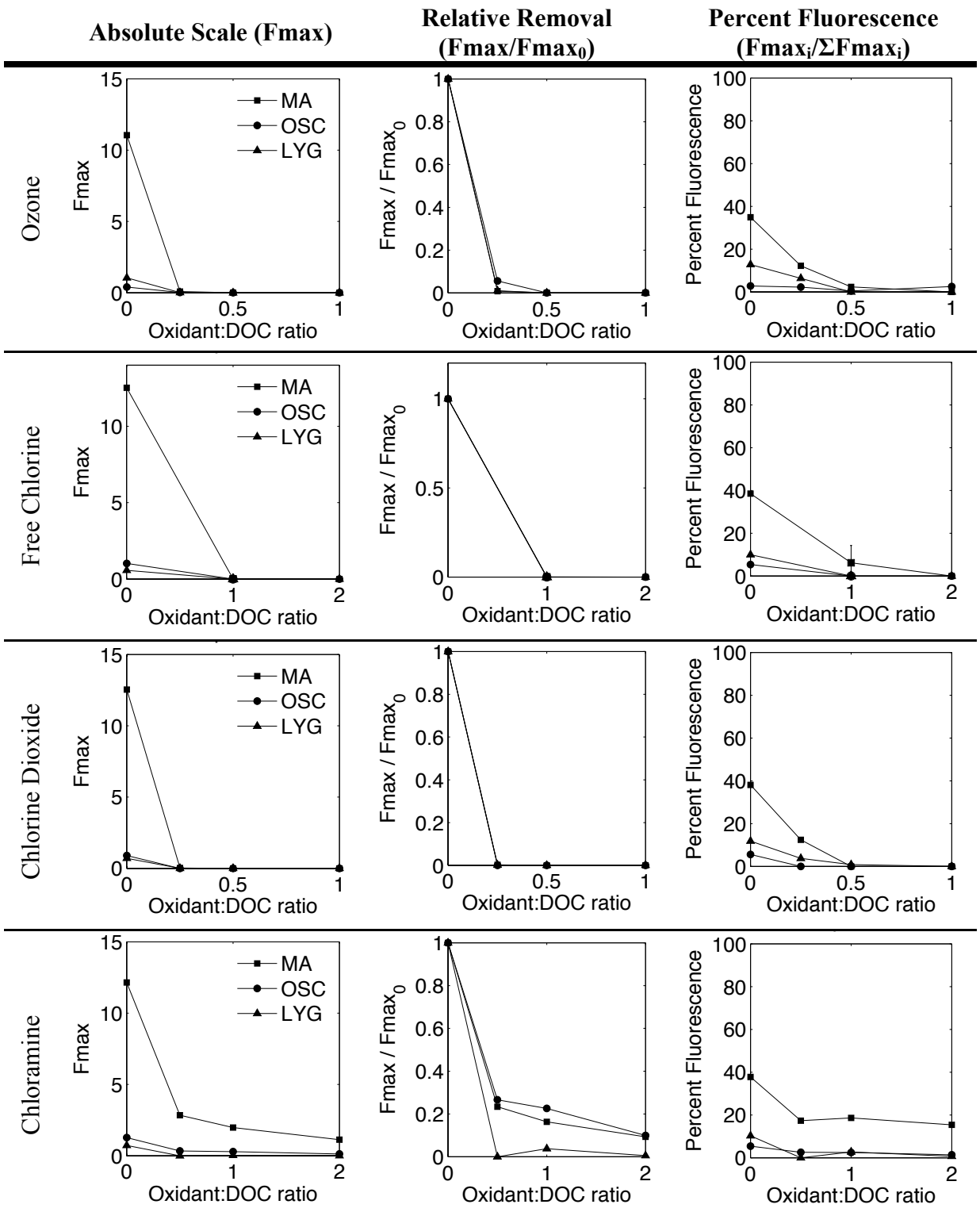

Figure B.24. Component P5 as a function of oxidant dose for all four oxidants evaluated. Data presented on an absolute scale, relative to the initial component Fmax and relative to the sum of all components.

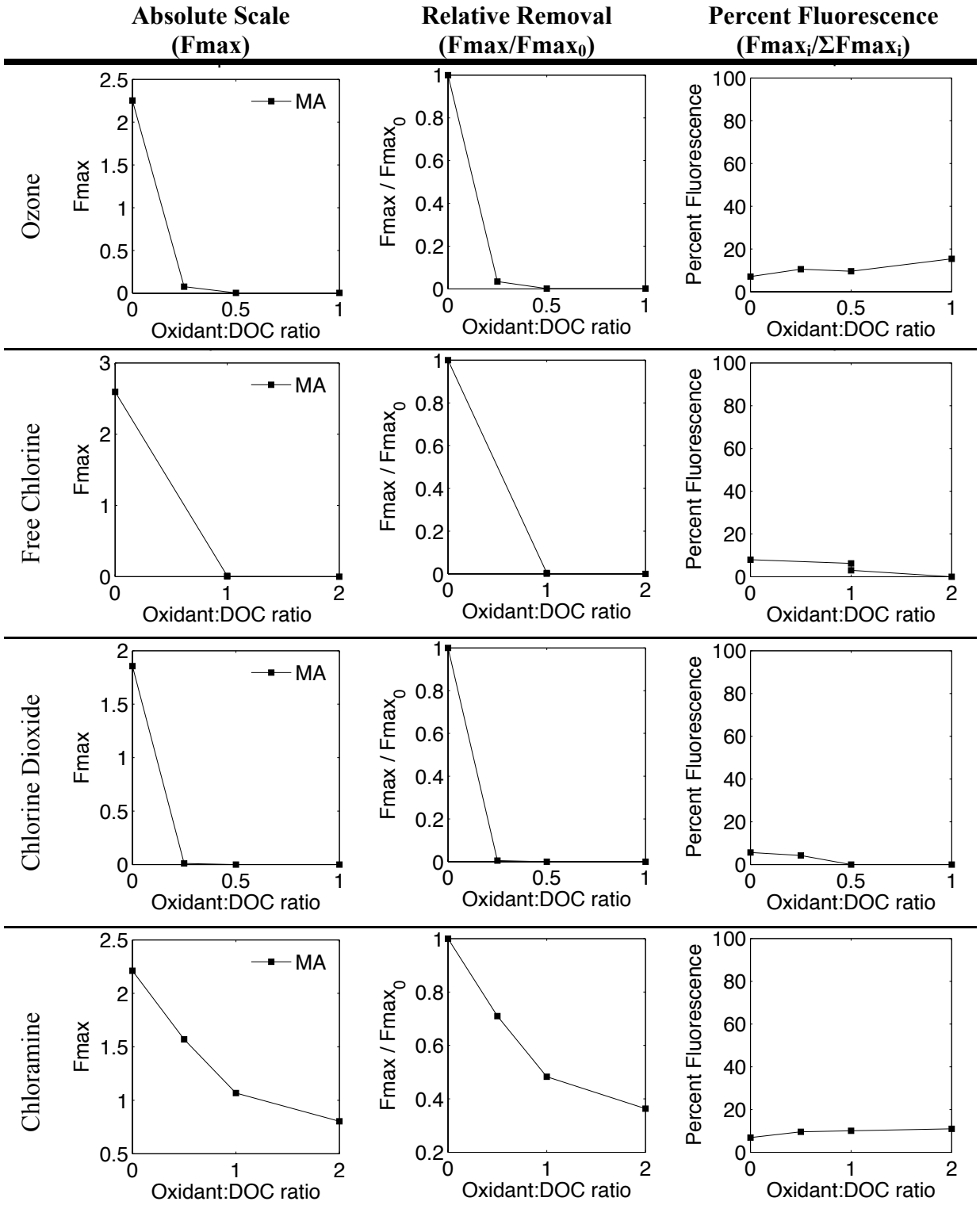

Figure B.25. Component P6 as a function of oxidant dose for all four oxidants evaluated. Data presented on an absolute scale, relative to the initial component Fmax and relative to the sum of all components.

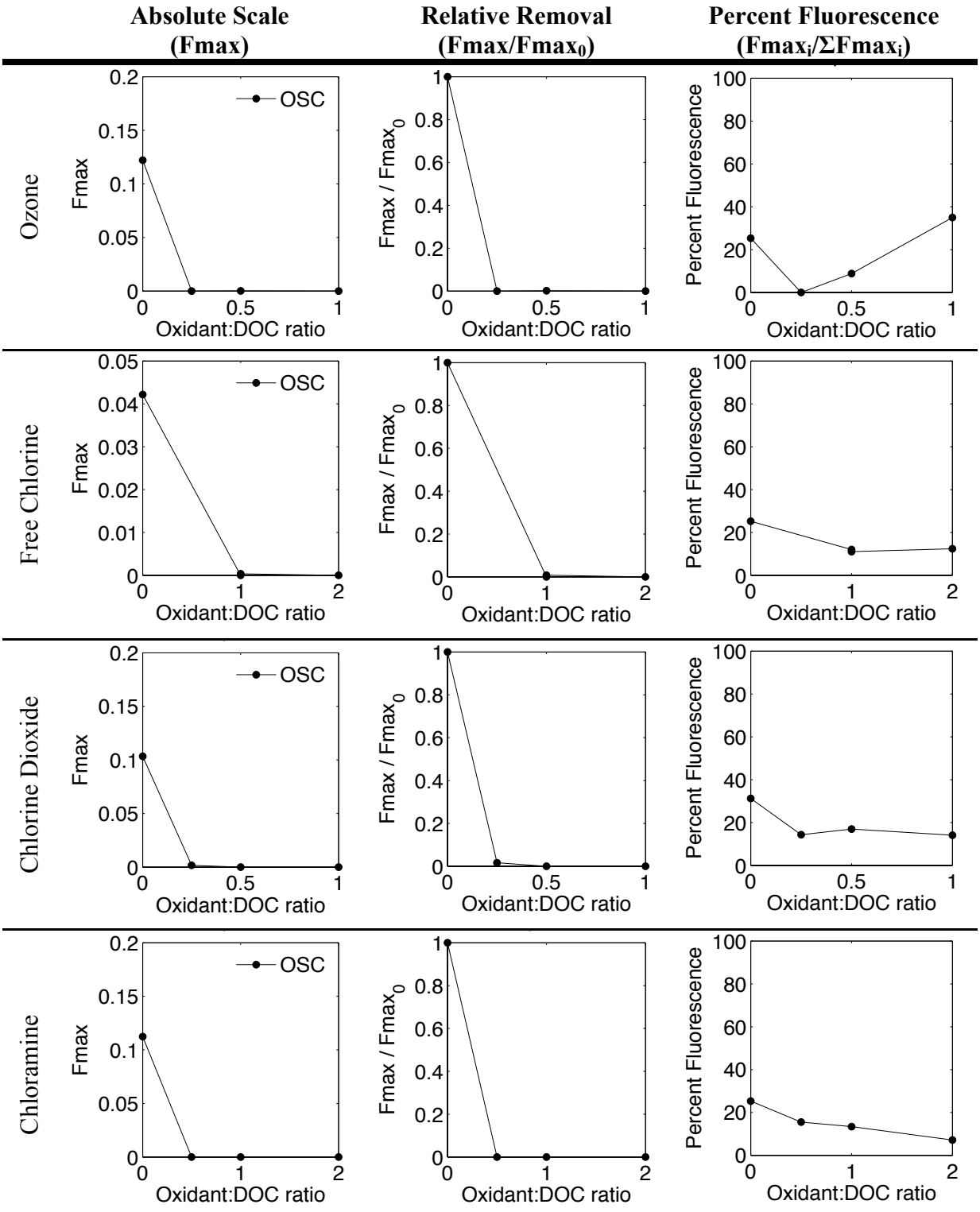

Figure B.26. Component P7 as a function of oxidant dose for all four oxidants evaluated. Data presented on an absolute scale, relative to the initial component Fmax and relative to the sum of all components.

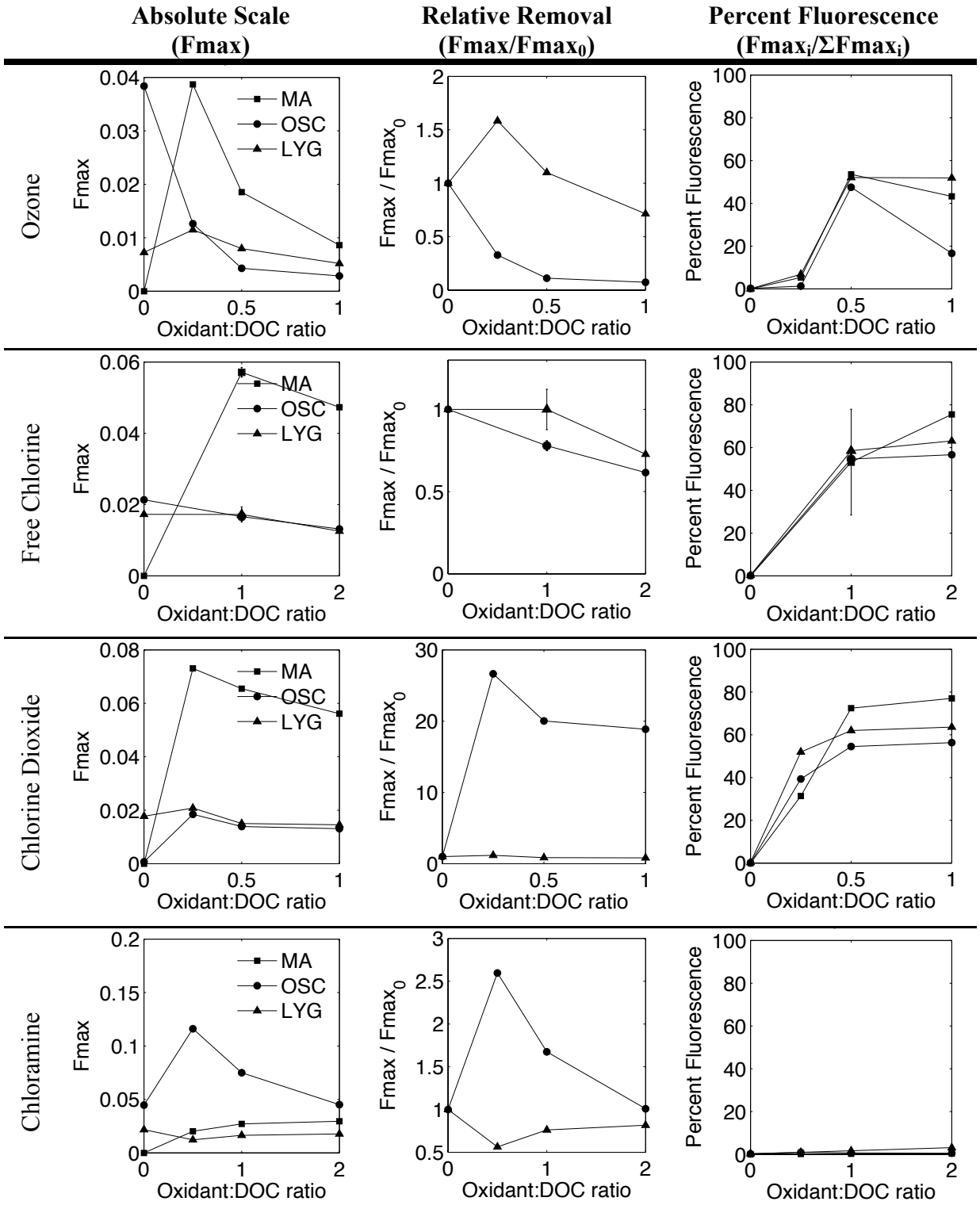

Figure B.27. Component P8 as a function of oxidant dose for all four oxidants evaluated. Data presented on an absolute scale, relative to the initial component Fmax and relative to the sum of all components.

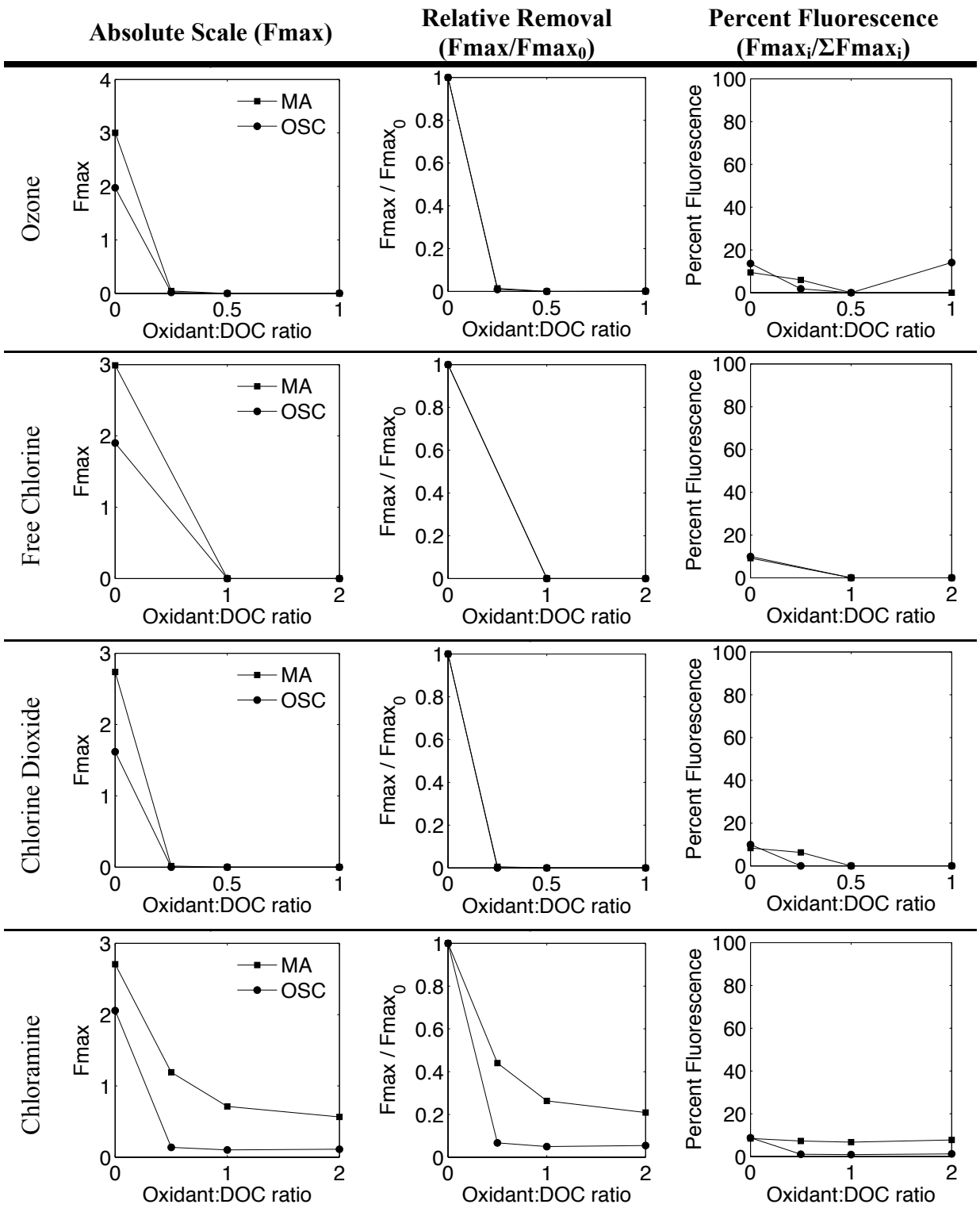

Figure B.28. Component P9 as a function of oxidant dose for all four oxidants evaluated. Data presented on an absolute scale, relative to the initial component Fmax and relative to the sum of all components.

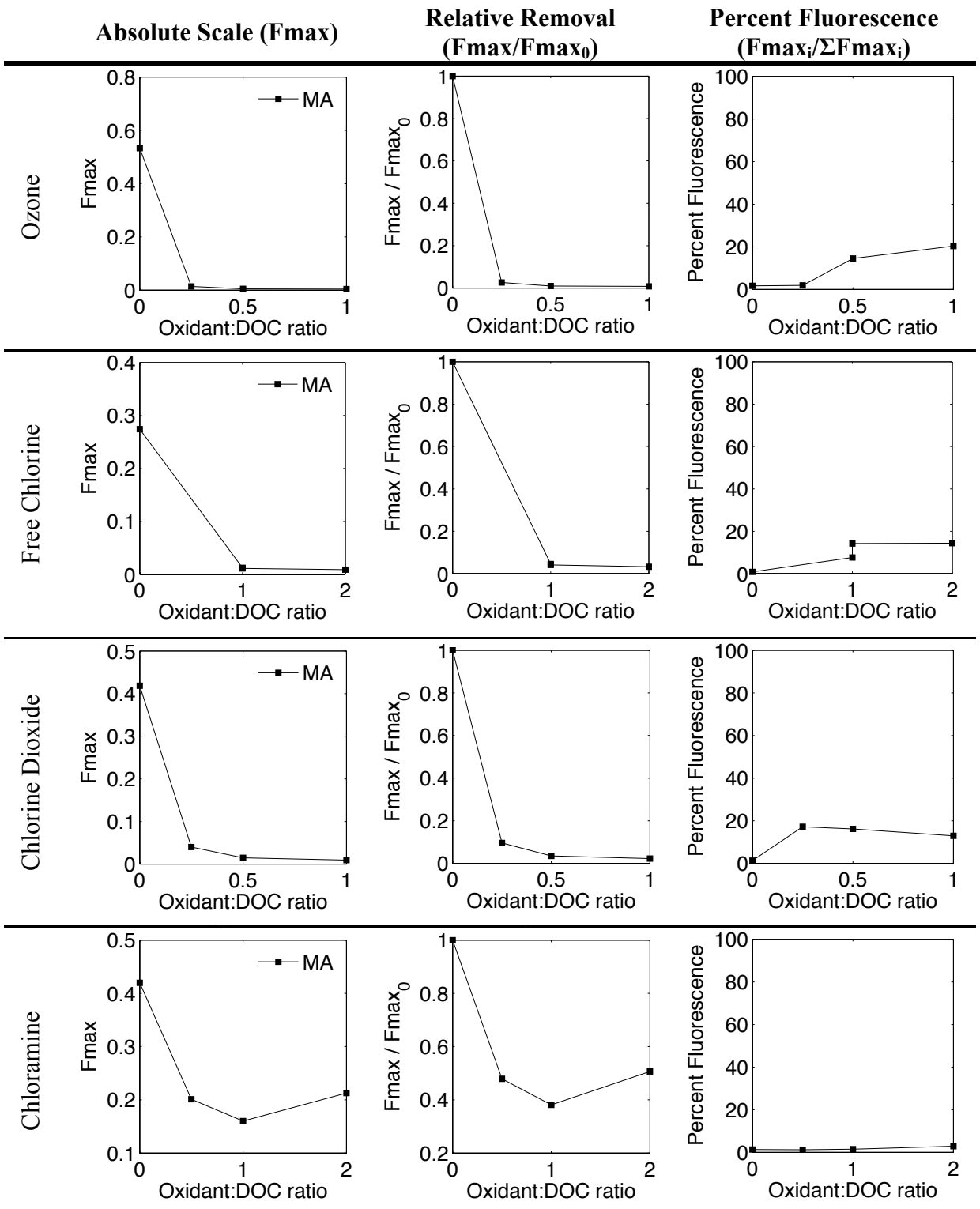

Figure B.29. Component P10 as a function of oxidant dose for all four oxidants evaluated. Data presented on an absolute scale, relative to the initial component Fmax and relative to the sum of all components.

Appendix C Supplementary Information for Chapter 6

C.1 Protein Peak Response

For MA exposed to ozone, the relative change in Peak P intensity followed a pattern similar to FDOM. Figure C.1 shows that Peak P intensity decreased with increasing ozone dose but to a lesser degree than CRW. This difference could be inferred as IOM release based on the previous discussion, but is not an ideal approach for rapid monitoring. Oxidation by chlorine dioxide could not conclusively detect IOM release based on an intensity increase, because the uncertainty between duplicates is too large and not statistically significantly different from 1 ($p=0.53$). For free chlorine and chloramine oxidation, Peak P increased for at least one dose and then decreased to a level below the CRW control. These results were unusual. If all the Peak P fluorescing IOM released is oxidized and loses its fluorescence signature, then it would be expected that the Peak P fluorescence would decrease to the same level as background CRW DOM at the same oxidant dose. The observed intensity below the CRW controls could be an indication of quenching. Past work found that when isolated IOM is spiked into CRW, the observed increase in Peak P intensity is less than what is predicted by specific peak intensities indicating a quenching of the fluorescence emission (Korak et al., 2014c). The observed fluorescence below the levels predicted for CRW controls may also be due to quenching mechanism between released IOM and CRW DOM.

The relative change in Peak P intensity was less sensitive to OSC cell oxidation compared to FDOM intensity. Even though Peak P has a higher specific fluorescence intensity compared to FDOM, Peak P intensity only exhibited a small 5-10% increase during chloramine oxidation (Figure C.1). There was no difference in Peak P intensity during free chlorine oxidation compared to CRW. For ozone oxidation, Peak P decreased to a lesser extent than CRW, which could be inferred as IOM contributing fluorescent material to the dissolved phase. There

was no difference in Peak P decrease for chlorine dioxide concentration at the lowest cell concentration tested (1,400 cell/mL). At the higher cell concentration (2,800 cell/mL), Peak P decrease exceeded that of CRW, which may be an indication of quenching interactions between background DOM and IOM in addition to intensity reduction due to oxidation.

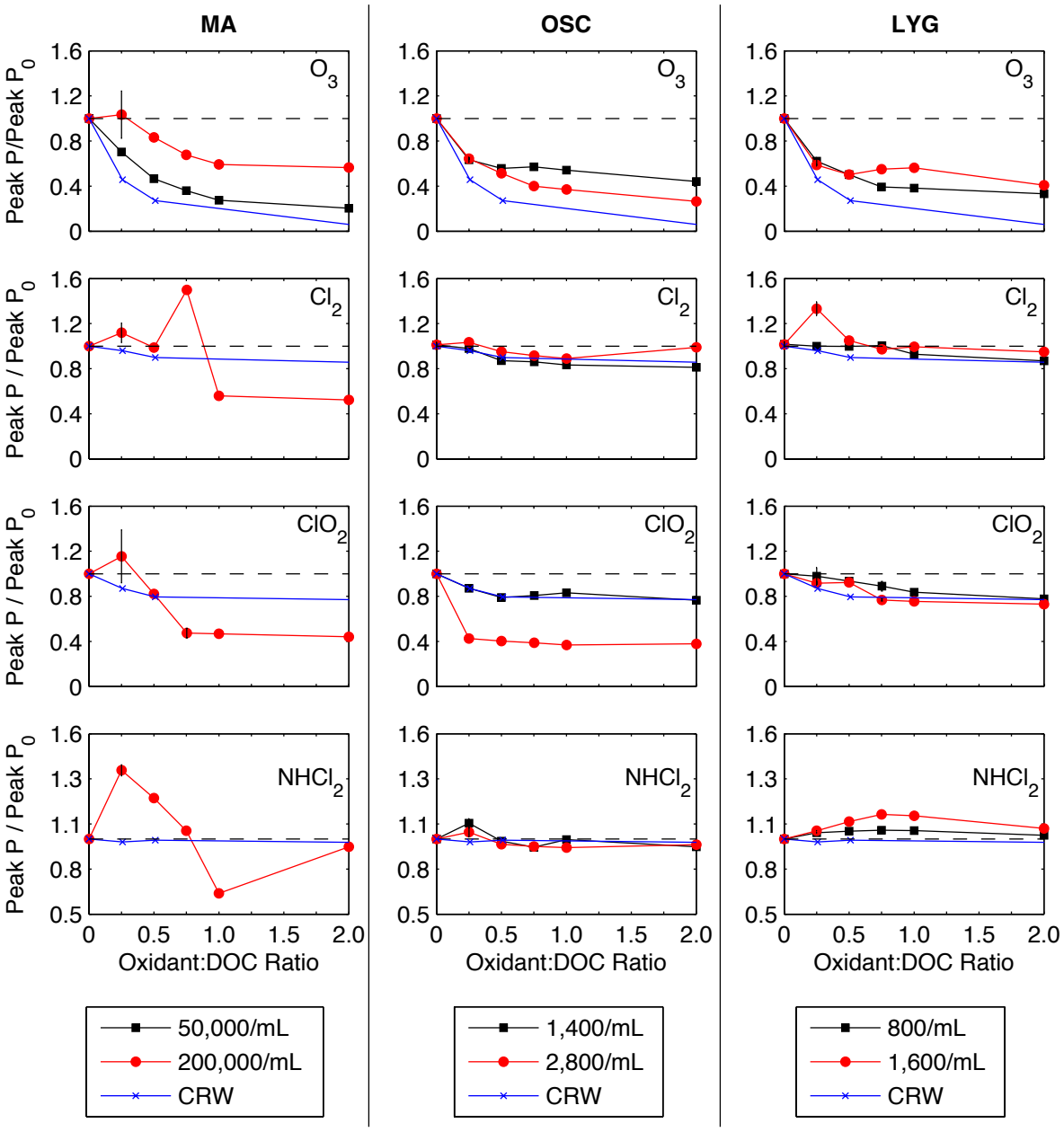

Figure C.1 Peak P response as a function of oxidant:DOC ratio for cells from three cyanobacteria species (MA, OSC, and LYG) suspended in CRW and four oxidants (ozone, free chlorine, chlorine dioxide and chloramine).

Lastly, LYG showed similar trends with respect to Peak P response as a function of oxidant dose as shown in Figure C.1. For ozone, Peak P intensity decreased but to a lesser extent compared CRW, which could be inferred as IOM release. A similar trend was observed for chlorine dioxide oxidation except that there was a smaller difference between the CRW control studies and both cell concentrations. During free chlorine oxidation at 1,600 cell/mL, Peak P intensity increased by 30% at the lowest oxidant dose ratio (0.25) and decreased with higher doses. At 800 cells/mL, no increase was observed. Chloramine oxidation led to an increase in Peak P intensity that was greater than the increase observed for CRW alone. There was also a greater increase for the higher cell concentration compared to the low, which could be an indication of increased IOM in the dissolved phase.

Even though each of the isolated IOM samples had a strong fluorescence signal in the protein-like region, this region performed poorly as an indicator of IOM release. IOM oxidation studies found that Peak P intensity decreases with increased exposure to ozone, free chlorine, and chlorine dioxide (Korak et al., 2014c). Following Peak P during cell oxidation studies demonstrates that the intensity increases more than 30% on only 3 of the 12 tests. In the case of MA, the decrease below CRW levels suggests that there are non-ideal quenching interactions that complicate applying Peak P as a surrogate for IOM release. Replicates also demonstrated that Peak P shows more variability compared to FDOM and FI.

C.2 Pigment Region EEMs from Cell Oxidation Studies

C.2.1 Microcystis

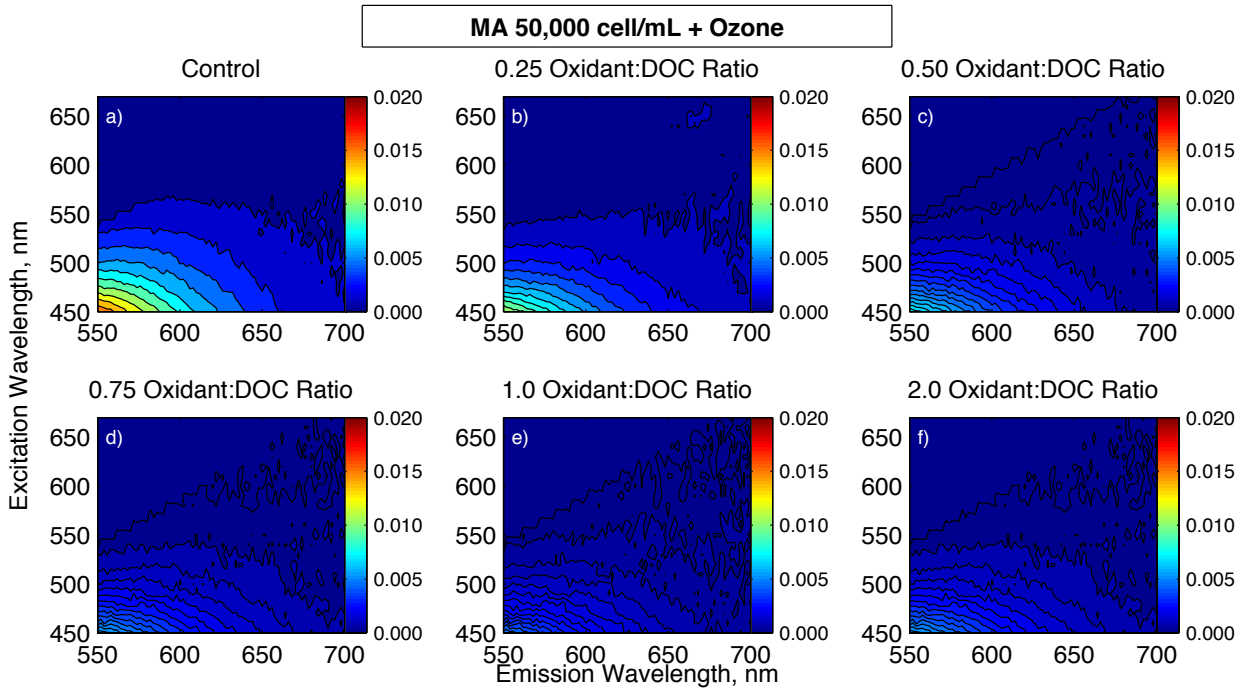

Figure C.2 EEMs of MA cell oxidation in CRW by ozone at 50,000 cells/mL

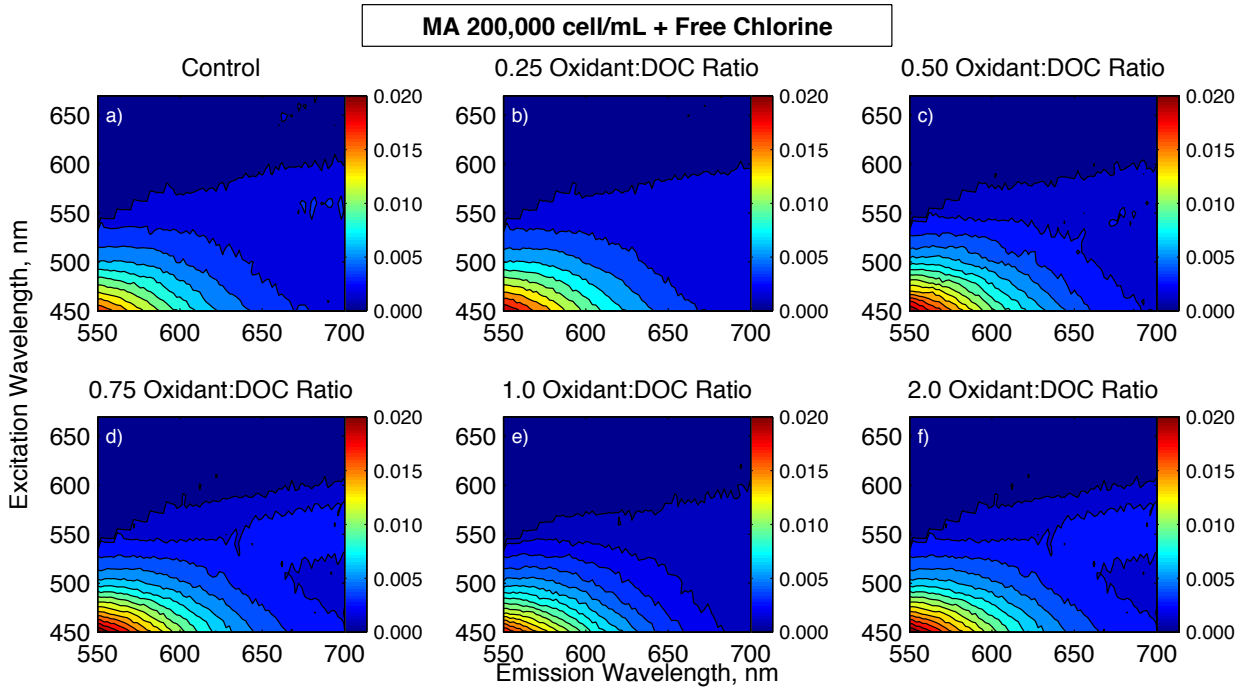

Figure C.3 EEMs of MA oxidation by free chlorine at 200,000 cells/mL

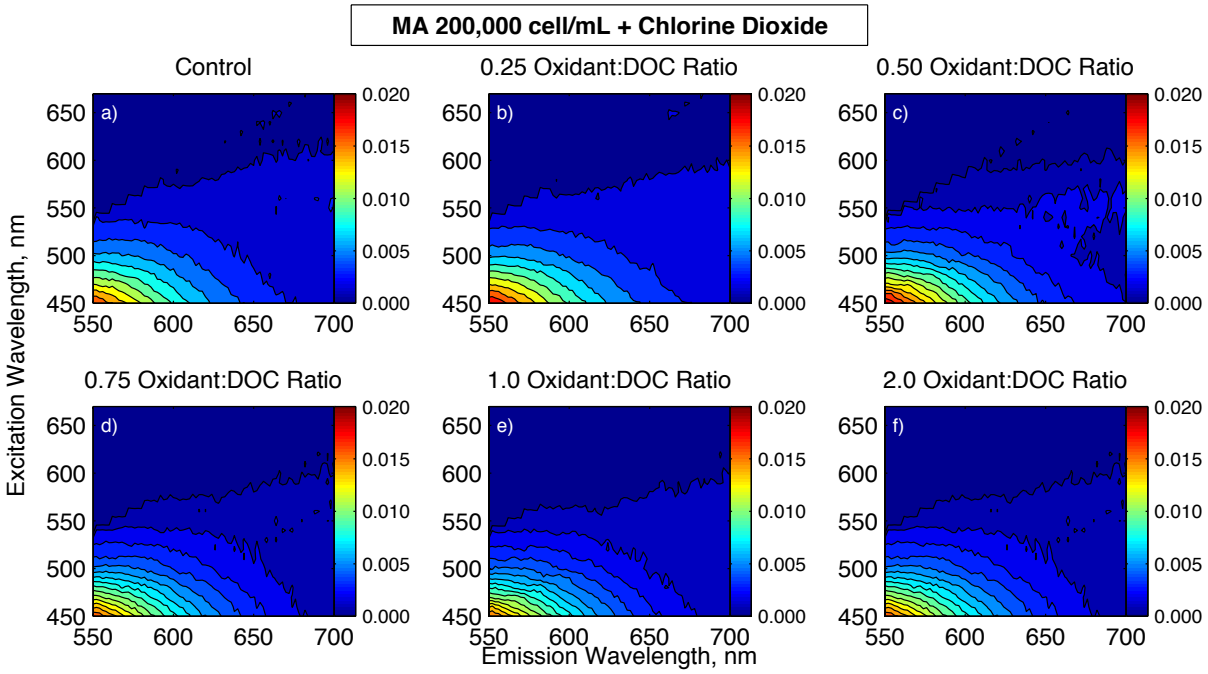

Figure C.4 EEMs of MA cell oxidation in CRW by chlorine dioxide at 200,000 cells/mL

C.2.2 Oscillatoria

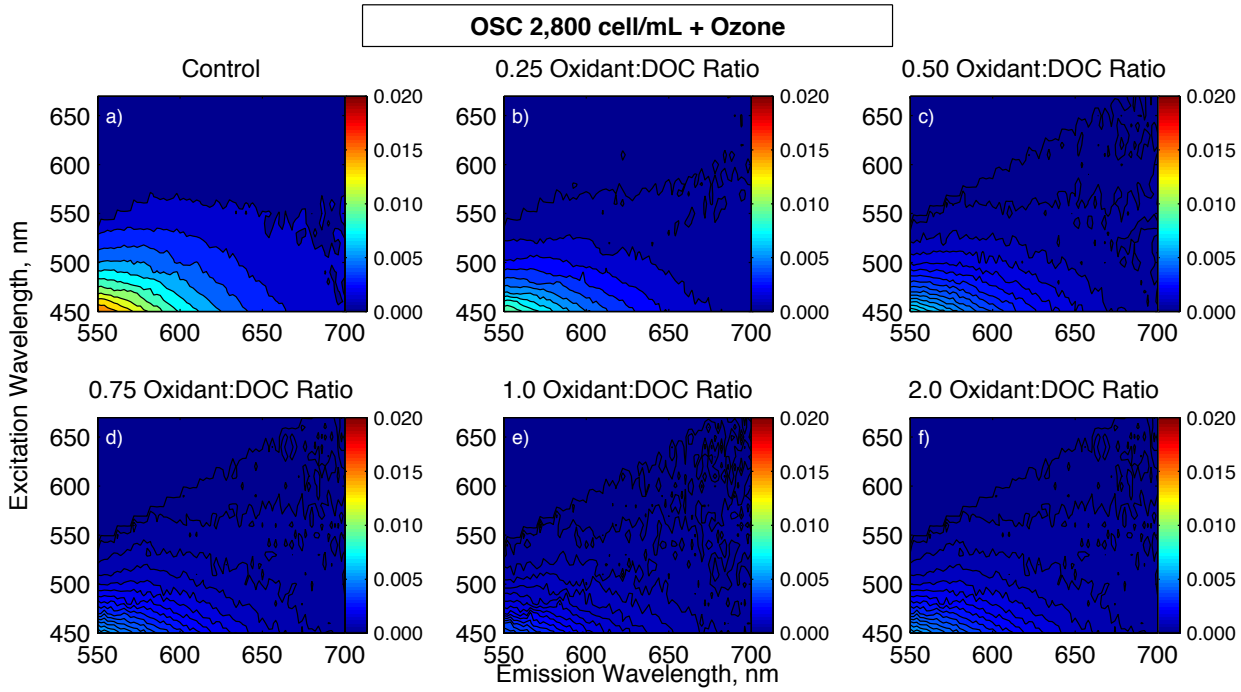

Figure C.5 EEMs of OSC cell oxidation in CRW by ozone at 2,800 cells/mL

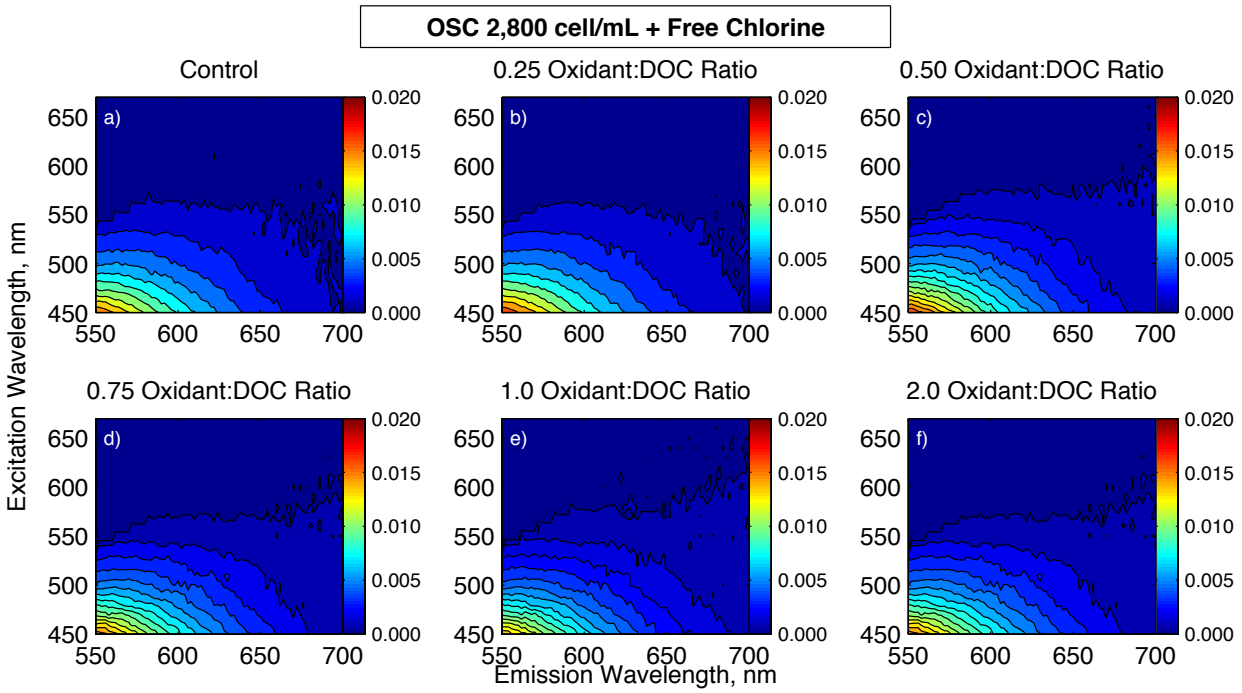

Figure C.6 EEMs of OSC cell oxidation in CRW by free chlorine at 2,800 cells/mL

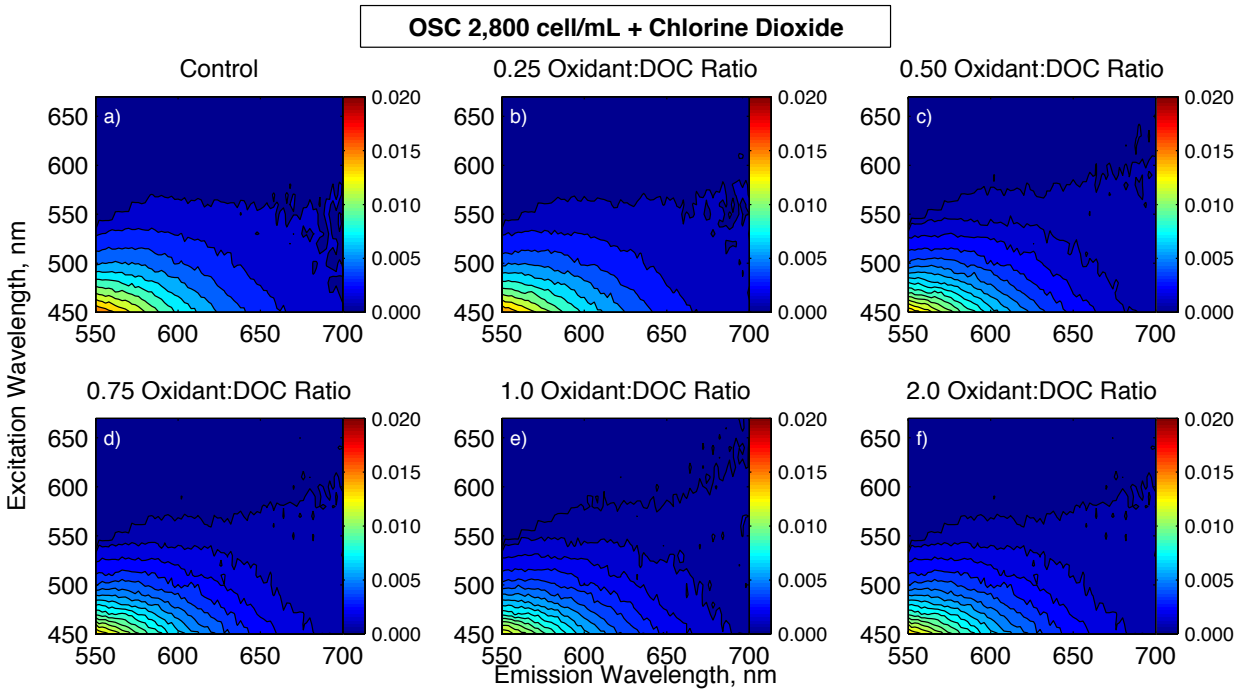

Figure C.7 EEMs of OSC cell oxidation in CRW by chlorine dioxide at 2,800 cells/mL

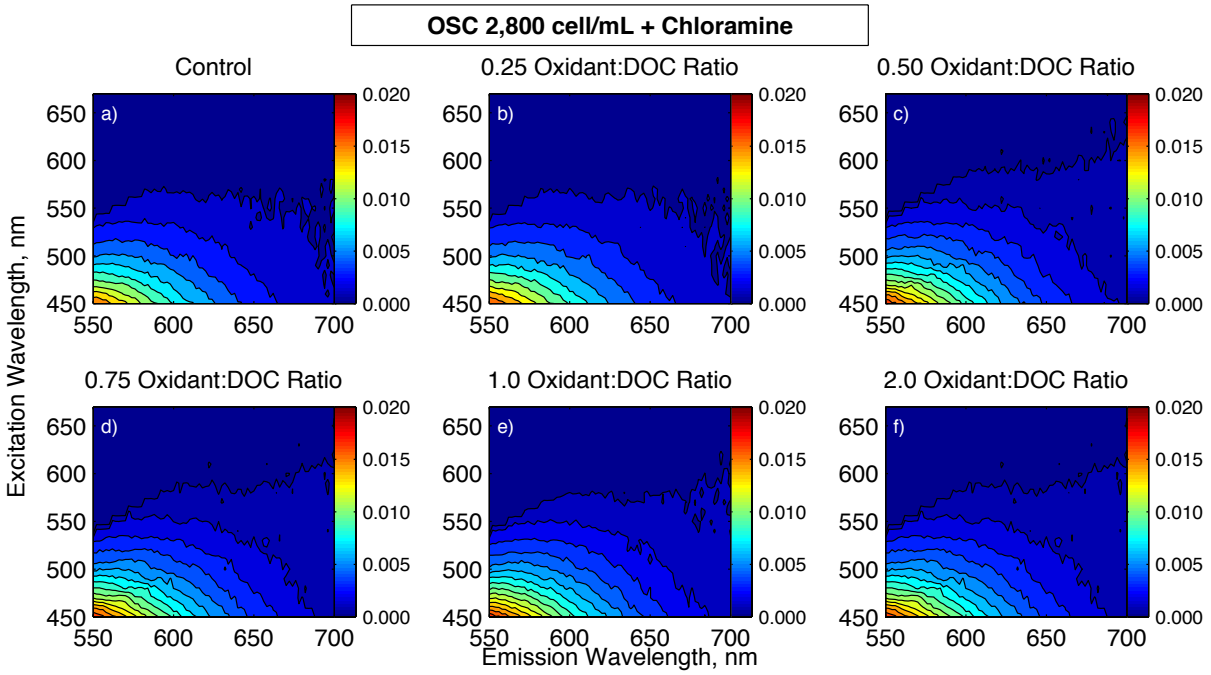

Figure C.8 EEMs of OSC cell oxidation in CRW by chloramine at 2,800 cells/mL

C.2.3 Lyngbya

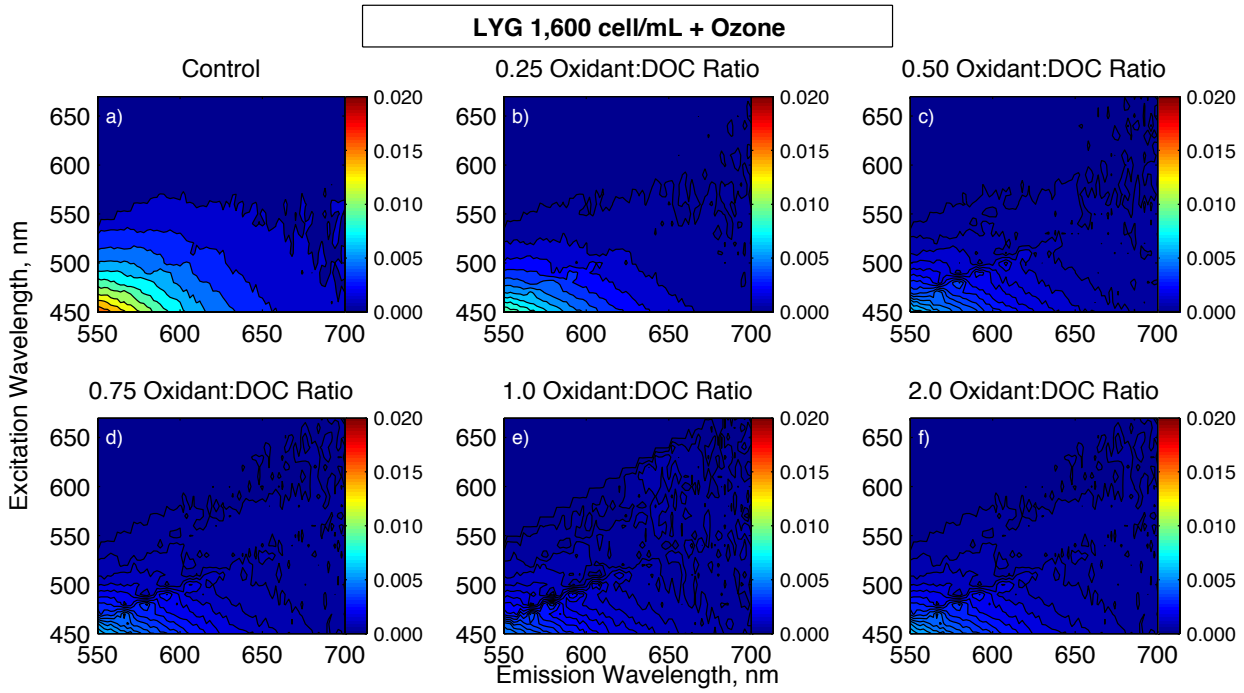

Figure C.9 EEMs of LYG cell oxidation in CRW by ozone at 1,600 cells/mL

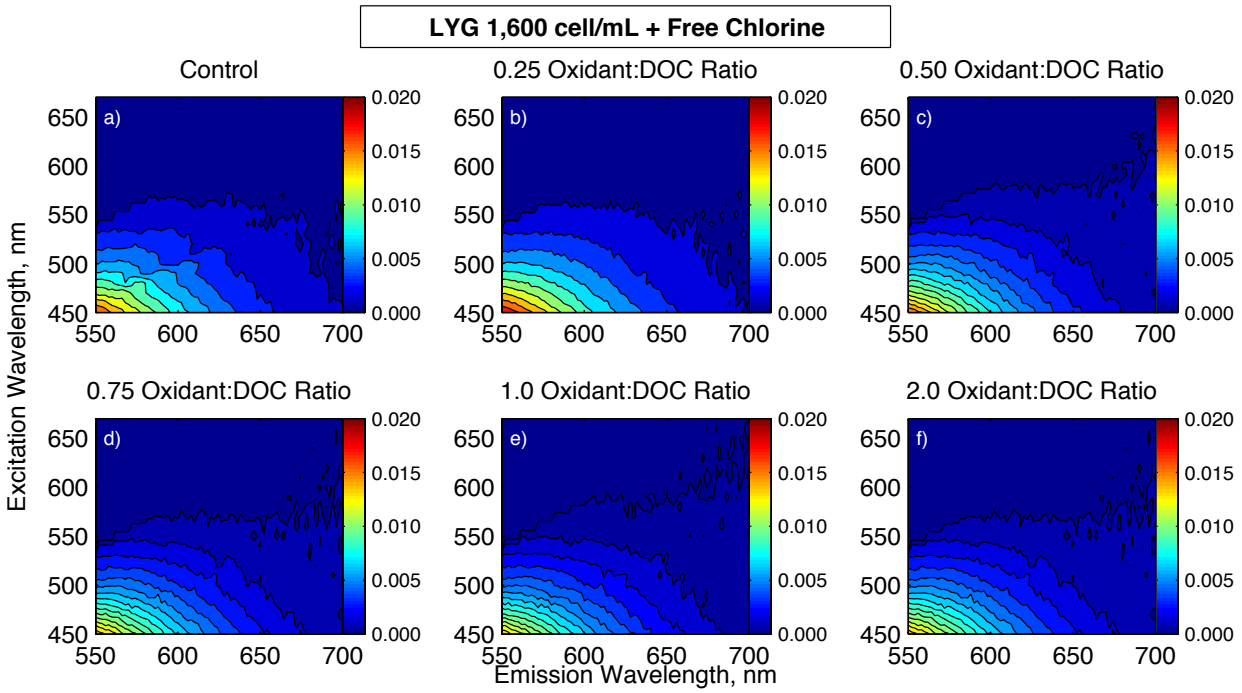

Figure C.10 EEMs of LYG cell oxidation in CRW by free chlorine at 1,600 cells/mL

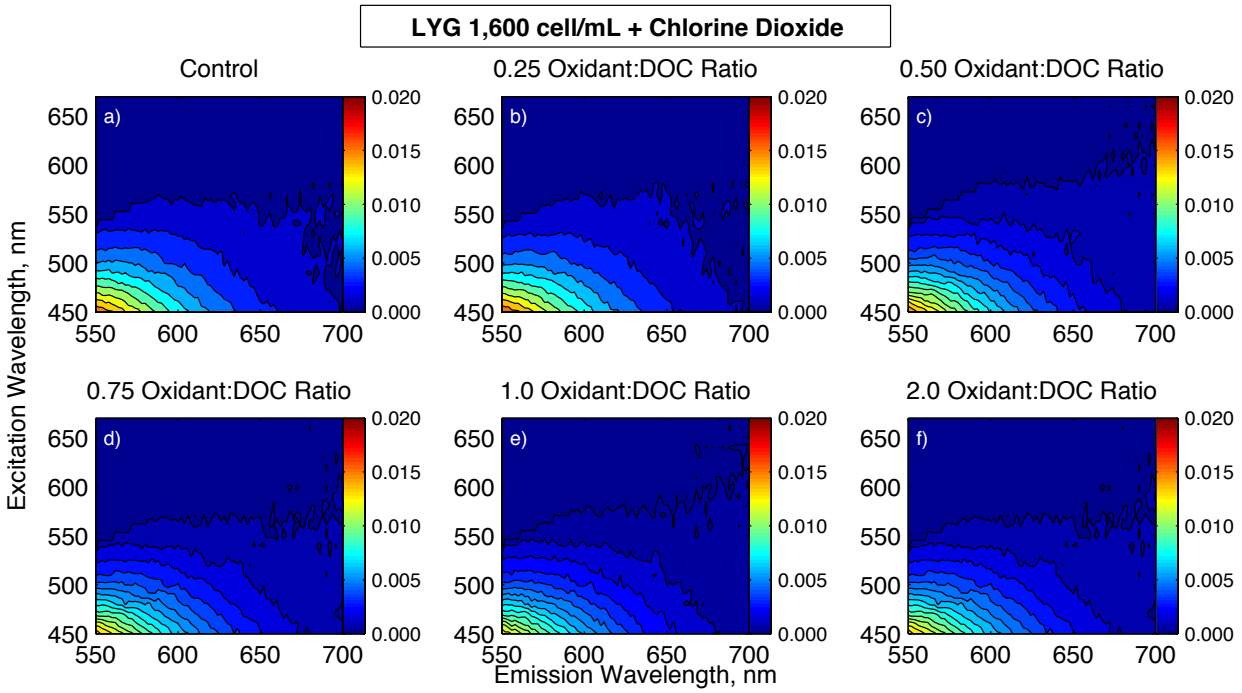

Figure C.11 EEMs of LYG cell oxidation in CRW by chlorine dioxide at 1,600 cells/mL

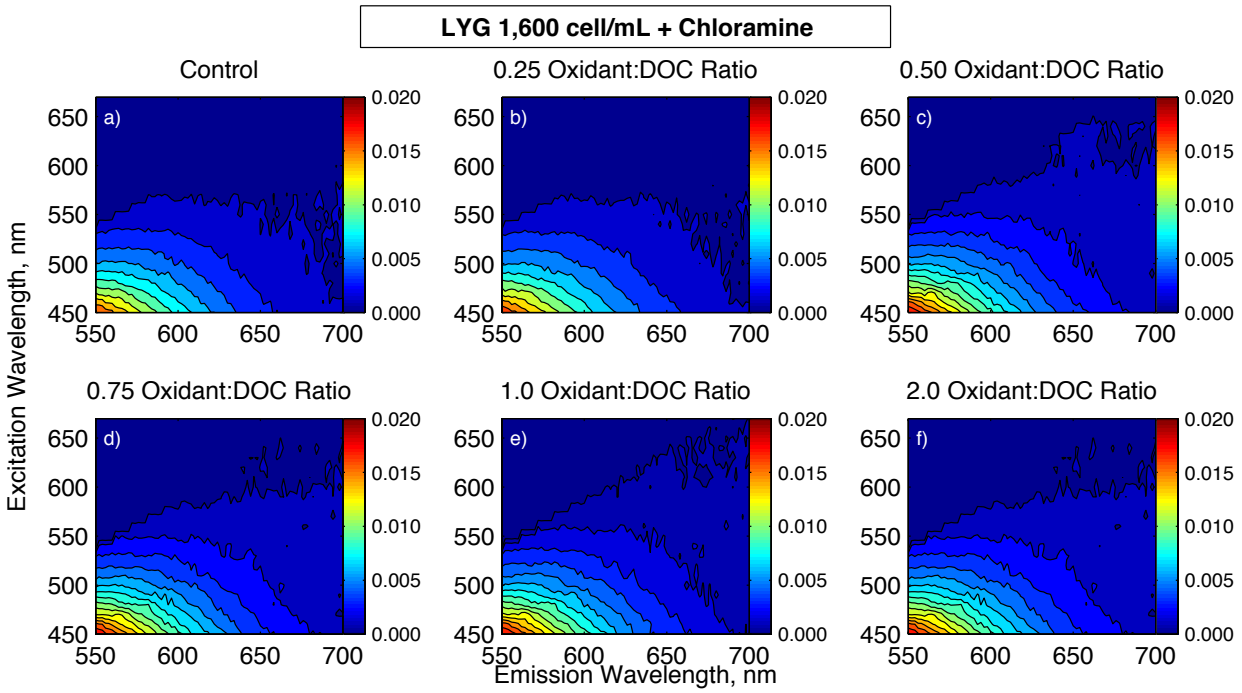

Figure C.12 EEMs of LYG cell oxidation in CRW by chloramine at 1,600 cells/mL